



On Multi Body Systems Simulation in Product Design

Petri Makkonen

**Stockholm 1999
Doctoral Thesis
Department of Machine Design
Royal Institute of Technology, KTH
SE-100 44 Stockholm, Sweden**

Abstract

The aim of this thesis is to provide a basis for efficient modelling and software use in simulation driven product development. The capabilities of modern commercial computer software for design are analysed experimentally and qualitatively. An integrated simulation model for design of mechanical systems, based on four different "simulation views" is proposed: An integrated CAE (Computer Aided Engineering) model using Solid Geometry (CAD), Finite Element Modelling (FEM), Multi Body Systems Modelling (MBS) and Dynamic System Simulation utilising Block System Modelling tools is presented. A theoretical design process model for simulation driven design based on the theory of product chromosome is introduced.

This thesis comprises a summary and six papers. Paper A presents the general framework and a distributed model for simulation based on CAD, FEM, MBS and Block Systems modelling.

Paper B outlines a framework to integrate all these models into MBS simulation for performance prediction and optimisation of mechanical systems, using a modular approach. This methodology has been applied to design of industrial robots of parallel robot type. During the development process, from concept design to detail design, models have been refined from kinematic to dynamic and to elastodynamic models, finally including joint backlash. A method for analysing the kinematic Jacobian by using MBS simulation is presented. Motor torque requirements are studied by varying major robot geometry parameters, in dimensionless form for generality. The robot TCP (Tool Center Point) path in time space, predicted from elastodynamic model simulations, has been transformed to the frequency space by Fourier analysis. By comparison of this result with linear (modal) eigen frequency analysis from the elastodynamic MBS model, internal model validation is obtained.

Paper C presents a study of joint backlash. An impact model for joint clearance, utilised in paper B, has been developed and compared to a simplified spring-damper model. The impact model was found to predict contact loss over a wider range of rotational speed than the spring-damper model. Increased joint bearing stiffness was found to widen the speed region of chaotic behaviour, due to loss of contact, while increased damping will reduce the chaotic range. The impact model was found to have stable under- and overcritical speed ranges, around the loss of contact region. The undercritical limit depends on the gravitational load on the clearance joint.

Papers D and E give examples of the distributed simulation model approach proposed in paper A. Paper D presents simulation and optimisation of linear servo drives for a 3-axis gantry robot, using block systems modelling. The specified kinematic behaviour is simulated with multi body modelling, while drive systems and control system are modelled using a block system model for each drive. The block system model has been used for optimisation of the transmission and motor selection. Paper E presents an approach for re-using CAD geometry for multi body modelling of a rock drilling rig boom.

Paper F presents synthesis methods for mechanical systems. Joint and part number synthesis is performed using the Grüber and Euler equations. The synthesis is continued by applying the theory of generative grammar, from which the grammatical rules of planar mechanisms have been formulated. An example of topological synthesis of mechanisms utilising this grammar is presented. Finally, dimensional synthesis of the mechanism is carried out by utilising non-linear programming with addition of a penalty function to avoid singularities.

Keywords: Design, Simulation, Optimisation, Control Systems, Modelling, Computer Aided Design, Computer Aided Engineering, Multi Body Systems, Finite Element Method, Backslash, Clearance, Industrial Robots, Parallel Robots.

List of papers

This thesis treats user-adapted and efficient modelling and performance simulation in product design. It consists of a summary and six papers.

Paper A

Makkonen, P.,

Integrated CAD Methodology for Simulation Driven Product Development,

Presented at the OST-95 conference on Machine Design, in Oulu, Finland, May 1995.

Paper B

Makkonen, P.,

Framework for Modular Multi Body Systems model for Kinematic and Elastic Dynamic Simulation of Parallel Robots,

Submitted for publication as a shortened version at the ICED-99 Conference in August 1999, Munich, Germany.

Paper C

Makkonen, P.,

On the development of a planar clearance joint model for Multi Body Systems simulation,

Internal Report 98/1, Department of Machine Design, Engineering Design, November, 1998.

Paper D

Makkonen, P. and Persson, J.-G.,

Optimisation of a servo system: the design of control, transmission and motor selection,

Internal Report 95/3, Department of Machine Design, Engineering Design, November, 1995.

Paper E

Makkonen, P.,

Product Development and Performance Optimisation of Rock Drill Boomers,

Presented at the OST-96 conference on Machine Design, in Stockholm, Sweden, May 1996.

Paper F

Makkonen, P. and Persson, J.-G.,

Configuration and Dimensional Synthesis in Mechanical Design: an Application for Planar Mechanisms,

Presented at 43rd CIRP General Assembly, Singapore, August 1994.

1. Introduction

1.1 Background

When designing mechanical systems, the dynamic behaviour is often difficult to foresee intuitively just from the major design parameters, e.g. from manufacturing drawings and bill of materials. In general, there is no possibility to synthesise a new product concept directly from the specified functional and performance requirements. The design process will then be iterative, one or several concept solutions that should meet the specified requirements are proposed by the designer and must then be analysed and verified, to determine if the specified functional requirements are satisfied. If not, the concept has to be modified or completely redesigned. In this iterative design synthesis-analysis loop, analysis for verification of product performance could be carried out in many different ways, e.g. by isolated functional rig tests in the laboratory, by complete prototype testing, by rough calculations or by mathematical modelling and computer simulation at varying degree of detail.

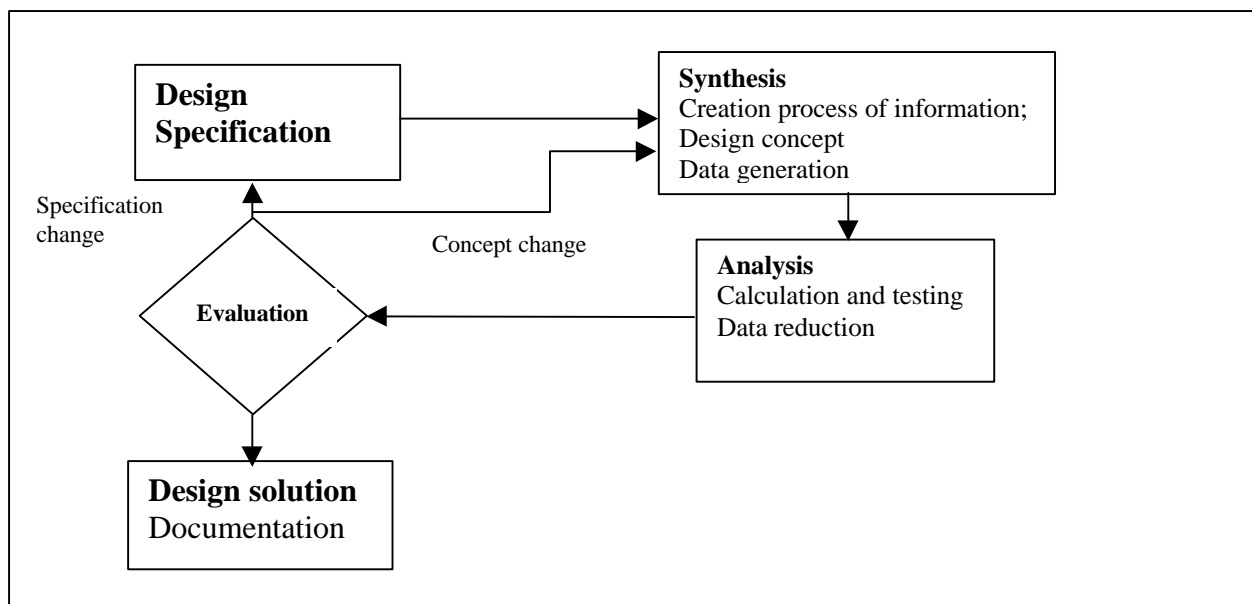


Fig 1. *Synthesis and analysis loop in design.*

Traditionally, prototype testing has been the predominating method for analysis and verification of product performance. Manufacturing of hardware prototypes and laboratory testing is however, in most cases, very time consuming and expensive. Hardware prototypes also suffer from the problem that the design parameter values, like geometry and configuration, main dimensions and materials are relatively fixed. The product concept can then be evaluated only for one set of parameter values at a time, i.e. in one point in the design parameter space. If the products performance does not meet the specification, the hardware parameters contributing to the non feasible performance must be identified and varied until a satisfactory solution has been obtained. For each parameter change, the design has to be changed and the prototype must be modified.

Mathematical modelling and computer simulation of product concepts and detail design solutions, for prediction of product properties and performance, has been used since the mid-sixties. At that time, time-consuming programming and debugging of product specific code, usually in FORTRAN, had to be developed. For this reason, simulation was most often not considered an alternative for evaluation during the design of new products. Computer simulation was then used primarily for

refinement and optimisation of mature, "static" and long-life product families. It is not until the last decade, since the introduction of advanced generalised software packages for CAE (Computer Aided Engineering) and of high-performance work stations, that simulation has proved to be a powerful tool in new product design. The possibilities for rapid development of product specific and product family specific parametrised models has then simplified modelling work. There is now a considerable potential for shortening the cycle time during design iterations. By speeding up the synthesis-analysis loop by means of powerful computerised analysis tools, computer simulation could now be used also during the early conceptual design phase, for quick evaluation, modification and optimisation of design concepts.

Current general CAE software packages are however very complex, and it is not obvious for the designer or for an industrial corporation how to fully utilise the potential of these new tools. Several important questions are still under discussion in industry, e.g. whether an integrated environment or a distributed simulation with communication between different types of simulation software should be preferred, if simple geometry models should be created directly in the simulation software or if a CAD solid model always should be used as a master model for all analyses etc. There is obviously a need for a systematic approach in modelling and simulation. The use of simulation software should be different during the various design phases for a product development project. Design theory and product development models from design research have an obvious potential and should be used as a basis for an improved and efficient methodology and approach to modelling and simulation in the design of mechanical products. The optimal combination of simulation and physical prototype testing is another important issue in industry. Simulation results should be utilised to minimise testing effort and to concentrate the expensive testing to the most relevant cases. Test results on the other hand, should be used to improve mathematical models of basic or product specific phenomena and to incorporate empirical knowledge in the simulation models.

This situation in industry, concerning the potential - that is still far from fully utilised - for modelling and simulation as a tool for efficient and rapid development of mechanical products, formed the basis for this PhD project at the Department of Machine Design at KTH.

1.2 Scientific approach

The objective of this thesis work is to study how multi body systems simulation should be efficiently used in product development. Multi body systems simulation is a modelling technique closely related to other similar modelling techniques in Computer Aided Engineering (CAE). A study of the relative strengths and weaknesses of these methodologies is then motivated, to determine the most feasible modelling methodology for different problem areas. Multi Body Systems simulation software have interfaces to modelling techniques which enable the use of co-simulation or model transfer. The potential of model integration and model transfer to other software will then be studied. The level of model detailing varies during a product development project. The question is then, how large and complex systems can be represented approximately, and how models can later be upgraded to more accurate representations. The scalability of models is also closely related to how large models are integrated into small ones. These are just some of the research questions, which should be answered.

The research hypothesis for this project has been, that based on existing design theory and process models for product development, a methodology could be developed for efficient and rapid modelling and simulation during design of mechanical systems, utilising current commercially available CAE software. The intention has been to evaluate the applicability of different modelling tools, for the different phases during a design project. During synthesis of concept solutions, rapid

modelling of relatively simple models, for quick and rough evaluation of major parameters' influence on product performance, will be required. During detail design, more detailed models, e.g. for verifying simulations, for establishing a test programme for physical prototype testing, or for optimisation of the product, would be required.

These goals motivated the use of a case study approach. Product examples from different phases of product development should be studied as well as the level of detailing. The following subtasks were formulated:

- Experience gathering and establishment of research background
- Literature survey of simulation and modelling
- Industrial case studies and analysis of cases
- Development of a framework for multi body systems simulation
- Development of methods for subsystem modelling

The experience gathering and establishment of research background comprised evaluation of software products and purchasing of software. The chosen software was I-DEAS from SDRC Inc. for CAD geometry modelling and FEM analysis; ADAMS from Mechanical Dynamics Inc. for multi body systems analysis. The author attended courses given by both software suppliers. For the development of block system models, Matlab/Simulink from MathWorks Inc. was used. Literature surveys were carried out continuously during the research project. They were conducted within the following fields: Synthesis and analysis of mechanisms, robotics in general, parallel and gantry robots, simulation of elasticity with multi body systems and finite element method, and finally, modelling of clearance joints. The results of the literature survey are reported according to the problem area, in the papers and in the summary part of this thesis.

Based on literature studies on design theory, a process model, Integrated Simulation Driven Design Process, has been formulated. This approach has then been implemented in industry and the methodology has been applied to industrial product development projects. A methodology for synthesis of planar mechanisms has also been outlined, as one separate initial study during the theoretical phase of this research project. Rigid body modelling by means of MBS (Multi Body Systems) software has constituted the backbone for simulations in this work. For detailed modelling of mechanical systems to simulate the products dynamic behaviour, generic methods for incorporation of elasticity and joint backlash into the MBS models have been developed. Drive system and control system modelling by the block system approach has also been utilised in combination with rigid body modelling, for one specific robot application.

1.3 Contribution

As part of the simulation process methodology, original contributions are presented, concerning:

- Framework for kinematic and elastodynamic simulation of multi body systems
- A method to compute the Jacobian matrix for a robot system, by means of MBS simulation
- A modelling approach for representing elastic structural parts as beam elements and lumped masses in MBS models
- A generic contact model of impact type for representing backlash in a clearance joint
- A method for comparative internal multi body system model consistency validation using eigen frequency analysis and fourier analysis of time plane simulation results
- A method for developing a formal grammar for mechanism synthesis of planar mechanisms using graph theory and number synthesis equations

A number of applications within the field of robotics have also been carried out. The findings from the process implementation and from the product development cases can be seen as a verification of the methodology approach. The author spent considerable time with ABB Robotics in Västerås, with simulations during the development of their parallel type 3-axis pick-and-place robot DELTA, now commercialised as "Picker". In this project, the authors approach to elasticity and joint backlash in MBS modelling, was applied. Other robot applications were the 3-axis Porta 100 gantry robot family at ABB Production Development (now a product within ABB Robotics) and a rock drilling rig boom at Atlas Copco Rock Drills in Örebro. These three industrial applications did represent different product types, different market situations and different phases in the product development process.

In the DELTA project, kinematic and rigid dynamic analysis was carried out for parameter studies of various concept variants. The analysis was then refined by incorporating the authors models for elasticity and joint backlash for improved performance prediction.

The gantry robot represents a modular product family for customised design, where simulation will contribute to dimensioning e.g. of motors and drive system, to meet a specific customers requirements. The product family modelling of mechanical system, drive system and control system then represents an important tool for tendering as well as in design.

In the drilling rig boom project, a detailed solid geometry model was already available and the task was to use this model for kinematic and dynamic analysis.

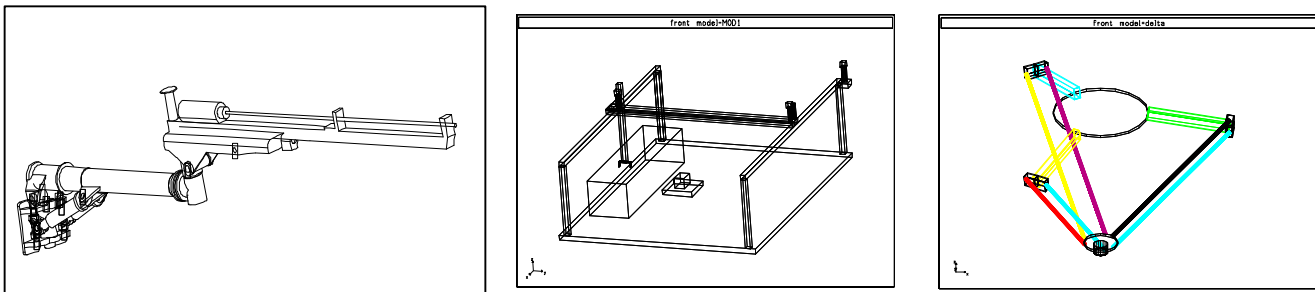


Fig 2. a) Rock Drill Boomer.

b) Porta100 gantry robot.

c) DELTA robot.

1.4 Outline of the thesis

This thesis combines the appended papers and discusses the results described in the papers. Chapter 2 concentrates on computer simulation models in product development. Chapter 2.1 discusses the difference between distributed and integrated modelling approaches, chapter 2.2 the synthesis of product and component models related to the product chromosome model of Andreassen (1992). Chapter 2.3 presents the synthesis of planar mechanisms by utilising graph theory and number synthesis. Chapter 3 deals with the incorporation of elasticity and contact phenomena to multi body simulation. Chapter 3.1 discusses elasticity simulation using elasticity submacros. It presents also model validation utilising time and frequency plane analysis. Chapter 3.2 presents a literature study on joint clearance models and the development of a new impact type clearance model for revolute and spherical joints. As a demonstration, the developed model was used for simulation of DELTA robot elasticity. Chapter 4 introduces the case studies described in the six papers.

Paper A presents an approach to integrate the distributed use of the simulation tools, CAD, FEM, multi body systems simulation and block systems simulation, and is thus presented first. Paper B presents an approach to integrate all simulation models into MBS simulation. The submodels which are used in the paper are the joint clearance model described in paper C and the elastic beam model described in appendix A. Papers D and E are examples of the integrated use of simulation tools. Paper D presents the simulation of a gantry robot drive and control system, using block systems simulation and MBS. Paper E presents the approach of modelling the multi body dynamics of a rock drill boom using CAD and FEM. The last paper, F, presents the principles of systematic mechanism synthesis.

2. Design theory and computer simulation models in product development

2.1 Background and prerequisites

One of the fundamental problems in mechanical design is that the designer can only manipulate the defining attributes of the design, Mortensen (1995). This fact is a consequence of system theory, Klir (1967). The attributes which define a system must thus be distinguished from the attributes which describe its behaviour. The defining attributes are designated as characteristics (German: Merkmale) and the attributes which are related to behaviour, as properties (German: Eigenschaften) by Andreasen (1994). Characteristics like dimensions, geometry, material and surface quality related to a machine part can be affected directly, as well characteristics related to the complete product i.e. the structure or assembly order. However, each property of the product can be derived only after its defining characteristics have been determined. Properties relevant for a robot are e.g. work space, load capacity, structural stiffness and lifetime. To design a product that satisfies the expectations of the products properties, i.e. the performance specification, the designer must use physical prototypes or models for simulation. However, models always consider only part of the defining or behavioural attributes of the design object. E.g. assembly drawings contain only the structure and geometry of the product. This implies, that the modelling is a process, that filters the observed facts, according to a theory by Tomiyama (1989). A model holds also "private" attributes that do not belong to the model, Buur & Andreasen (1989). A hydraulic diagram describes the flow and component structure of a hydraulic system, but it is drawn on paper and it has no functional properties (figure 3.).

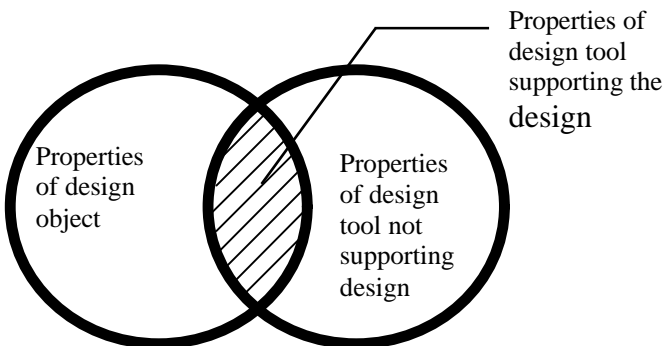


Fig 3. Properties of a design tool.

Thus, any theory used for modelling of the design object filters its own projection of the products properties. These projections are called viewpoints of the product. In figure 3, the coverage of design object properties is shown with CAD, FEM and MBS models as examples. Such a model system is possible to implement with either a distributed or an integrated modelling approach.

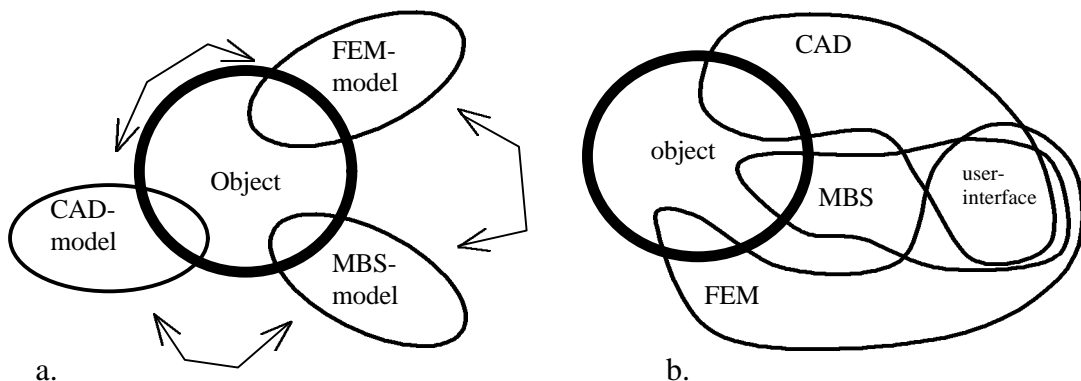


Fig. 4. a. Distributed approach of modelling. b. Integrated modelling approach.

The distributed approach is implemented with separate modelling programs, while with an integrated approach, one program includes all model aspects. The distributed approach requires parameter transfer either manually or by software, while in an integrated approach all parameters are given in the same program. The conclusion is, that integrated programs easily become large, complex and monolithic, with an increasing amount of properties and features not belonging to or representing the object.

2.2 Product synthesis

2.2.1 Computational design models

Finger and Dixon (1989) classify design process models as *prescriptive*, *descriptive* or *computational* models. This thesis concentrates on prescriptive and computational models.

In contrary to the design of mechanisms, the automation of conceptual design of product families and component layouts with automatic, non-human interactive design loops in general machine design is still impossible, and will remain so for a long time in the future. This is due to the difficulty to generate abstractions of spatial relationships of a design concept's functional units (known as organs according to Andreasen (1994)) without loosing the validity of their function due the laws of kinematics and geometry.

However, in energy-transforming systems, spatial relations are often secondary design restrictions enabling the use of energy flow models. This has been discussed by Ulrich and Seering (1989) and by Prabhu (1990). The use of bond graphs is discussed by Malmquist (1994), the use of block systems models in paper **D** of this thesis. In order to treat spatial relations defining mechanical and kinematical functions together with energy-transforming functions, Malmquist suggests combination of the bond graph representation with shape representation. In such an approach, kinematical building boxes can be used, Kota and Chiou (1992). Van Griethuysen (1992) suggests a reversible design process to maintain the functional validity of a design solution representation at different levels of abstraction. The same approach has been applied in the synthesis of planar mechanisms, Makkonen (1993) and in Paper **F**. The conclusion is, that automated design synthesis requires control and monitoring of the functional validity of design models at different abstraction levels.

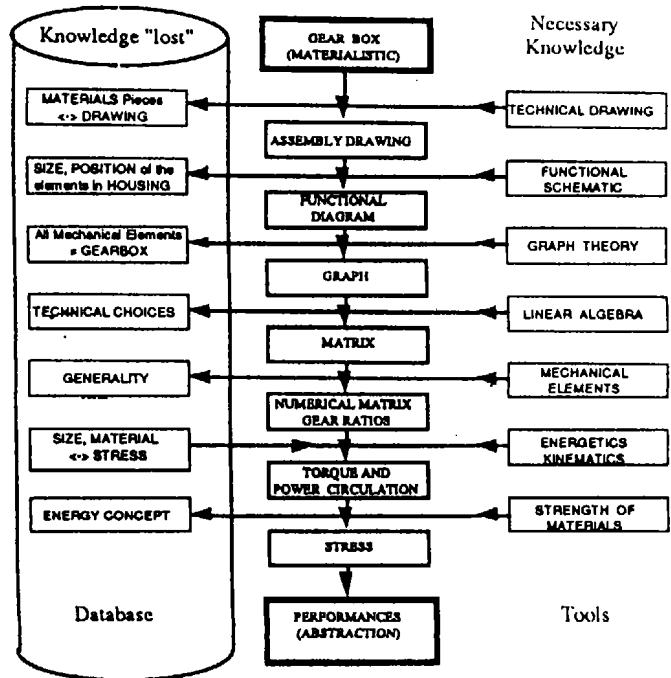


Fig. 5. Loss of information in the synthesis-analysis loop of transmission design, van Griethuysen (1992).

2.2.2 Descriptive design models

If the computational maintenance of functional validity is impossible, only intuitive, human interactive design is feasible. These design theories are merely descriptive, Hubka and Eder (1988), providing guidelines and design process descriptions. Pahl & Beitz (1984) and several other authors have written design guidelines, i.e. descriptions of sequences of design activities in a design project and examples of right and wrong detail solutions. Based on extensive analysis of successful products and failures, Suh (1988) suggests axiomatic design principles. According to Suh, two axioms should be used as general criteria for good design solutions. The first axiom, the *independency axiom*, states that any design should have an independent solution for each function. The second axiom, the *information axiom*, states that any design solution should have a minimal information content, e.g. minimum amount of means or parts implementing the function, minimum amount of dimensions and minimum amount of tolerancing information etc. Suh's *independency axiom* corresponds to the statement of *clarity* by Pahl & Beitz, Suh's *information axiom* corresponds to the statement of *simplicity* by Pahl & Beitz. The process-oriented models have been criticised for their sequentiality and for their formalisation of the design procedure. Designers creativity is characterised by recursivity, iteration and abstraction, which are restricted by the design process, Malmquist (1993).

2.2.3 Prescriptive design models

For the design of machine systems, the Theory of Domains according to Andreasen (1980) models the causality relations of a product in four domains. The definition of the functional requirements of a machine system is a consequence of the process which it is designed to implement. The elements of the process are realised by technical functions which order the organs that implement the functions. Some of the implementing organs order new functions which will require an iterative function-organ structure. The organs are implemented by machine parts. The Theory of Domains describes the design process as a navigation process within all four domains: process, function, organ and part structure. The sequence can be mapped, but not prescribed.

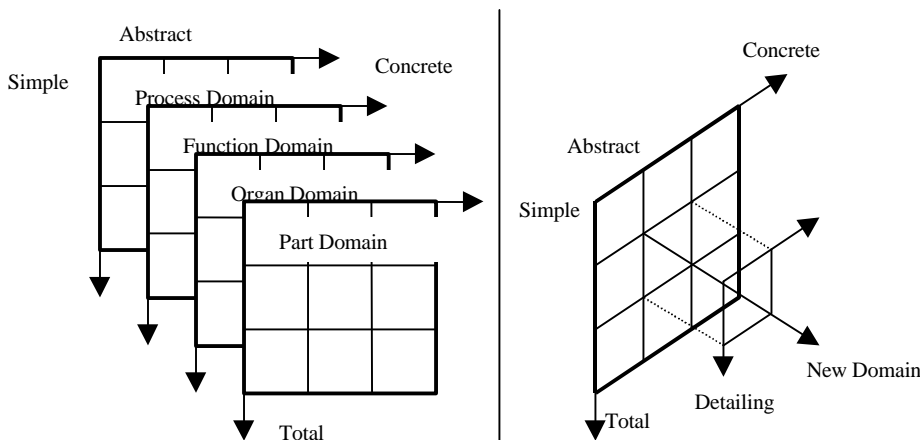


Fig. 6. Theory of Domains. Andreasen, 1980.

If the causality flows from the different domains are traced during the design process, a connection graph describing the chain of decisions for generating the solutions is obtained. Such a model is called a product chromosome model by Ferreira (1990) and Andreasen (1992). According to Aasland (1995), the chromosome model is a *constitutional model* defining the product, the life

phase system model and the life phase systems. It describes the product, and the products configuration modifications through different life phases.

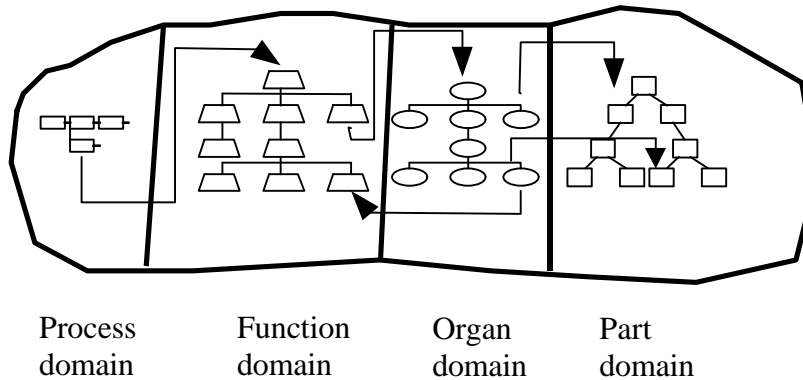


Fig. 7. Product chromosome model with it's causality relations.

As an example, the configuration of a computer will change between transport and customer use. The constitutional model is thus a life phase neutral model and a base for other models, usually implementable with a PDM¹-tool. Simulation models are *property models*. A property model, Aasland (1995), describes how characteristics create properties of the artefact. A simulation model has two categories of characteristics, *product characteristics* as dimensions and motor power and *behaviour characteristics* as drive cycle. The output properties of a simulation model is the simulated behaviour i.e. representing the product properties. The simulated properties are verified with a relevant case, from the properties of a physical prototype. Thus a PDM-model organised as product chromosome offers a life phase and simulation model neutral function-means structure, product property and behaviour parameters. The PDM-model thus maps the causalities of the simulation models and their parameters.

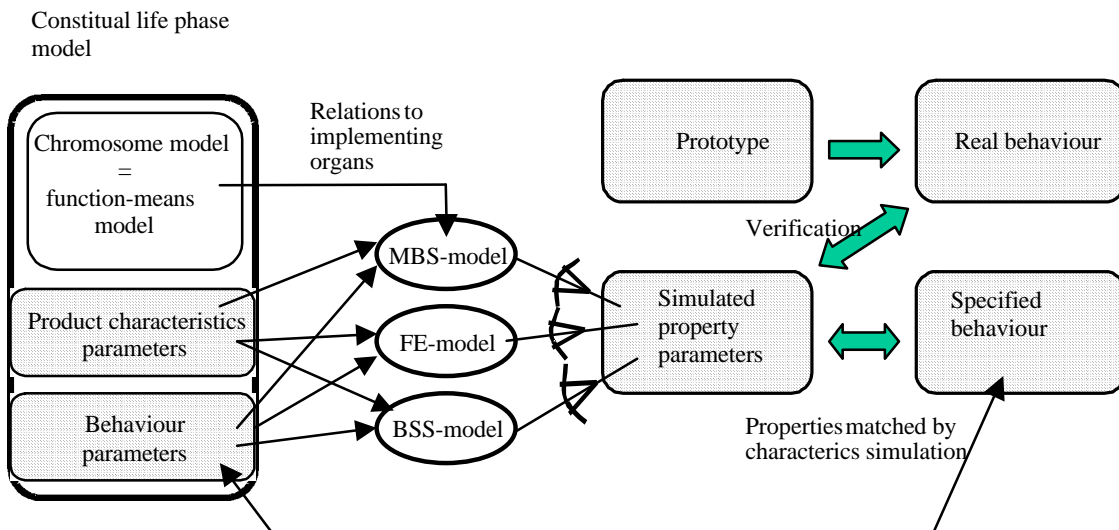


Fig. 8. Product chromosome model as life phase system model related to multibody, finite element and block system simulation models.

¹ PDM = Product Data Management.

This framework is suitable for many CAE applications. Alulib by Skanaluminium, Alulib (1992), is an example of chromosome model based software. It is a static browser software for demonstration of design solutions for aluminium profiles, where the designer can browse solutions based on dispositions at different domain levels. As a static browser, it is however not a parametrised model, as compared to the model in figure 8. In Paper A an approach is presented to map the domain model to the source parameters of design, *customer requirements* and *manufacturing constraints* of the manufacturing process. The customer requirements are usually more devoted to the process and function domains than manufacturing, which is directed to part design and assembly considerations, thus part and organ domains, Figure 9. Also, different CAE tools are mapped on corresponding domains: The process and function domains are preferably modelled by the block systems approach while mechanical organs are modelled with multi body simulation. The part domain is modelled by CAD solid geometry and finite element models.

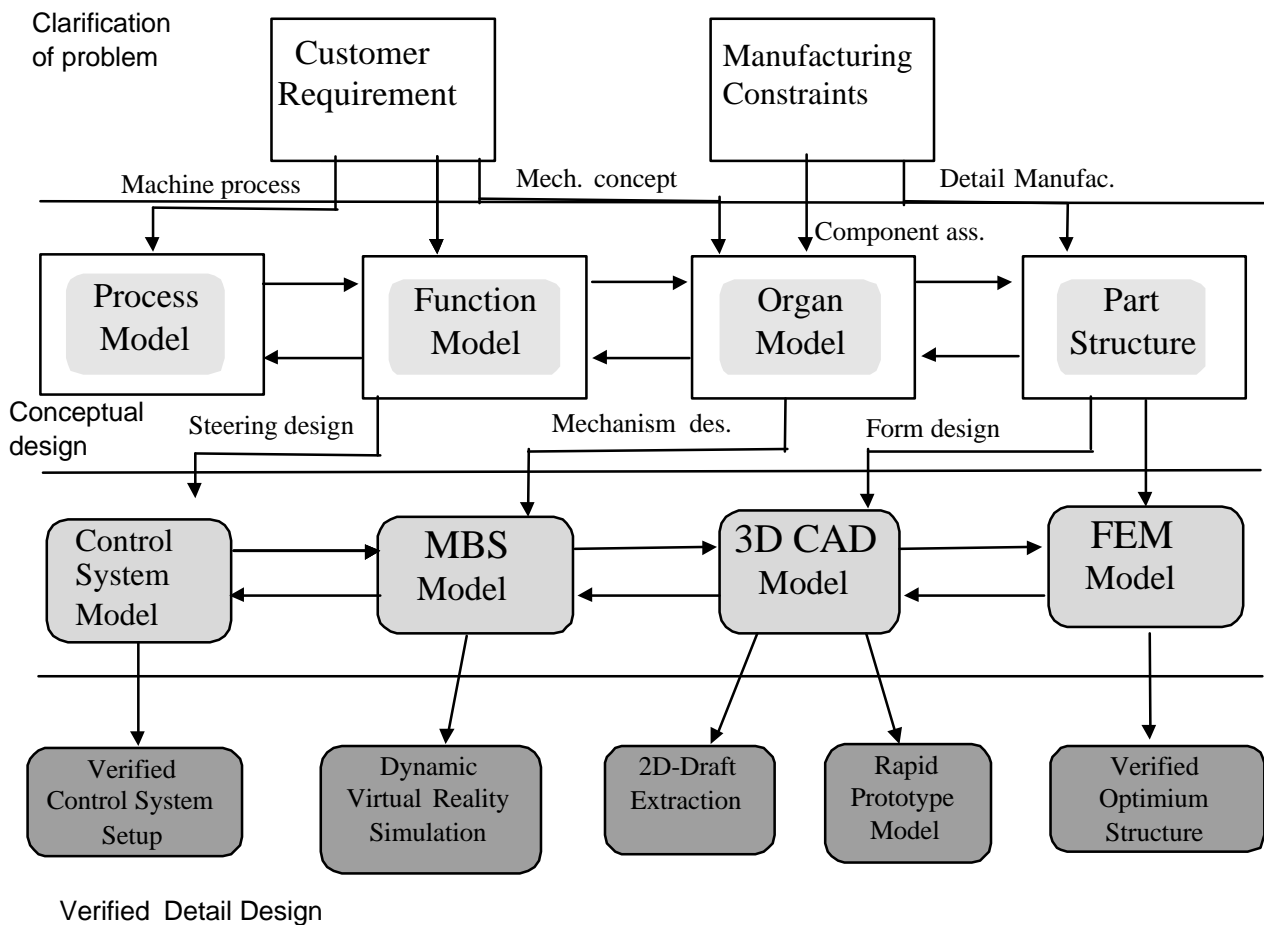


Fig. 9. Integrated Simulation Driven Design Process, from paper A.

The model parameters have a unique distribution inside the modelling elements of each software tool. Depending of the element structure of the modelling tools, the parameters from the design domains are distributed to the different element structure levels in the simulation model, figure 10. An MBS-element implements a dynamic function i.e. it is a dynamic organ. According to Artobolevski (1961), each production machine consists of separate subsystems: drive machinery, transmission, work machinery and optionally a controlling function. Equivalently, an MBS-organ consists of *drive element*, *drive chain*, *tool part* and *feedback element*. The *drive element* is

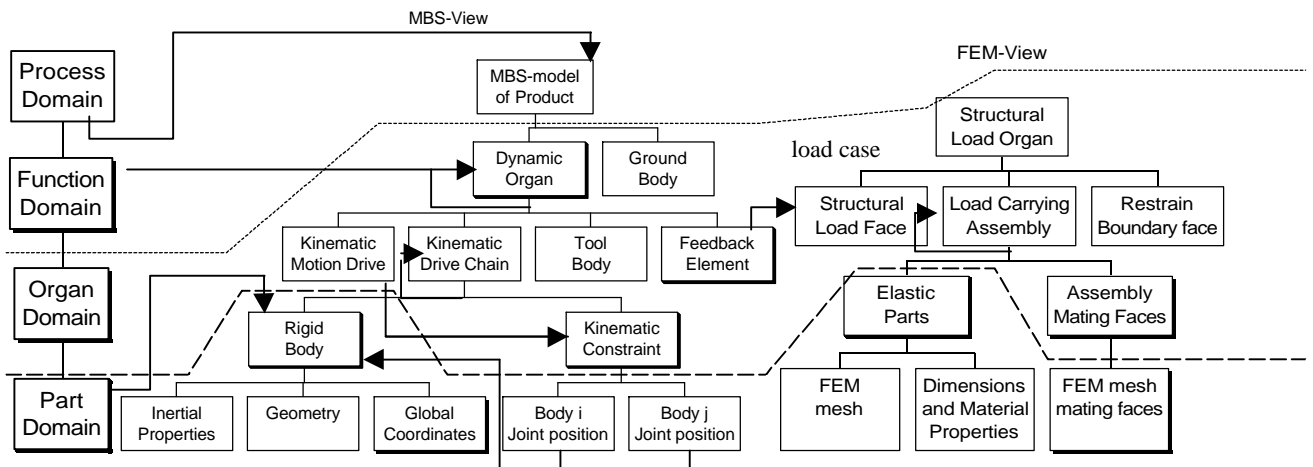


Fig 10. An example of chromosome framework related to MBS and FEM model views. The shadowed boxes are multiple instances.

related to a *kinematic constraint* creating a motion. The kinematic chain is recursively defined, at the innermost level as a *kinematic constraint*. The *rigid body* includes *inertial properties*, *geometric shape representation* and location and velocity related to the ground body. An FE-model consists of *structural load organs* consisting of *load face*, *load carrying assembly* and *restraining face*. Each load carrying assembly is a recursive structure including *elastic parts* and *mating faces*, Sellgren and Drogou (1998). A mating face is defined as an object located on a geometric face.

3. Synthesis of mechanism systems

3.1 Synthesis methods for mechanism design

In the domain of mechanism and robot design, the laws of kinematics and dynamics are governing the design. A taxonomy of mechanism design activities is shown in table 1., Olson et al (1985). The main phases of mechanism design consist of problem definition, mechanism type synthesis and dimensional synthesis. The topological and functional requirements are defined during the problem definition phase. In the type synthesis phase, the number of joints and parts are defined, the kinematic chains are enumerated and input, ground and output parts are assigned. Finally, in dimensional synthesis the mechanism link length optimisation is performed.

The topologic-dimensional synthesis of mechanisms includes the following tasks:

- Number synthesis of planar mechanisms joint and part numbers
- Development of topological graphs of joint and link systems
- Definition of sub chain structures inside the topological graph
- Determination of input, output and ground links
- Initial dimensioning using constraint equation satisfaction for locking conditions
- Definition of optimisation criteria for the coupler curve
- Non-linear programming with penalty functions for singularities

Table 1. Systematic mechanism design, Olson (1985).

I. Problem Definition	A. Topological Requirements 1. Nature of motion (planar or spatial) 2. Degree of freedom (number of inputs)
	B. Functional requirements 1. Number of distinct outputs 2. Task to be accomplished by each output 3. Complexity of each task
	C: Constraints 1. Dimensional constraints 2. Inertial constraints
II. Type synthesis	A. Topological synthesis 1. Enumeration of basic kinematic chains satisfying topological requirements. 2. Enumeration of "basic mechanisms" derivable from each basic chain, by assigning the ground link.
	B. Topological analysis 1. Determined type of freedom (if d.o.f. is greater than one) and distinct ways of applying input(s). 2. Identify possible output(s) to satisfy functional requirements. 3. Assign joint types based on specified inputs and functional requirements. 4. Evaluate each mechanism based on functional requirements.
III. Dimensional synthesis	A. Kinematic synthesis - For a given type of mechanism, determine dimensions based on functional requirements. B. Kinematic analysis - Evaluate mechanism based on dimensional constraints and kinematic (static criteria). C. Dynamic Analysis - Evaluate mechanism based on inertial constraints (kinetostatics, kineto-elastodynamics, time response etc).

3.2 Type synthesis of mechanisms

In the early stage of mechanism design, different linkage configurations are to be considered to achieve a concept that satisfies the functional requirements of the mechanism. At this stage, it is helpful to have charts of all possible kinematic chains up to the required number of links and degrees of freedom. The systematic enumeration of planar kinematic chains has been a subject of

many studies for a long time. The existing methods employed for structural synthesis of kinematic chains with simpler joints have been based on intuition and ingenuity, Soni (1971). Some approaches are based on graph theory, e.g. Woo (1967) and Dobrjansky and Freudenstein (1987) for instance. The approach based on Assur groups utilises Assur's theory of kinematic joint pair *dyads*, e.g. Manolescu (1964). The catalogues of planar kinematic chains with up to 10 links have been developed by means of computer programs and published in literature. However, when the number of links in kinematic chains increases to more than 10 links, it becomes very difficult to synthesise and identify all possible chains by inspection without making mistakes. Kiper and Schian (1976) developed a computer program to synthesise chains up to 12 links with one degree of freedom resulting in 6856 kinematic chains. Mruthyunjaya (1984) developed a computer program, based on transformation of binary pairs for structural synthesis and analysis of simple-jointed kinematic chains with up to 10 links and three degrees of freedom. Sohn and Freudenstein (1986) have used the concept of dual graphs of kinematic chains to establish the enumeration of planar linkages with up to 11 links and two degrees of freedom. Tuttle, Peterson and Titus (1988) had an approach to utilise the symmetry group theory to generate kinematic chains by performing the contraction and expansion operation on a base structure and synthesised kinematic chains with 10 links and three degrees of freedom.

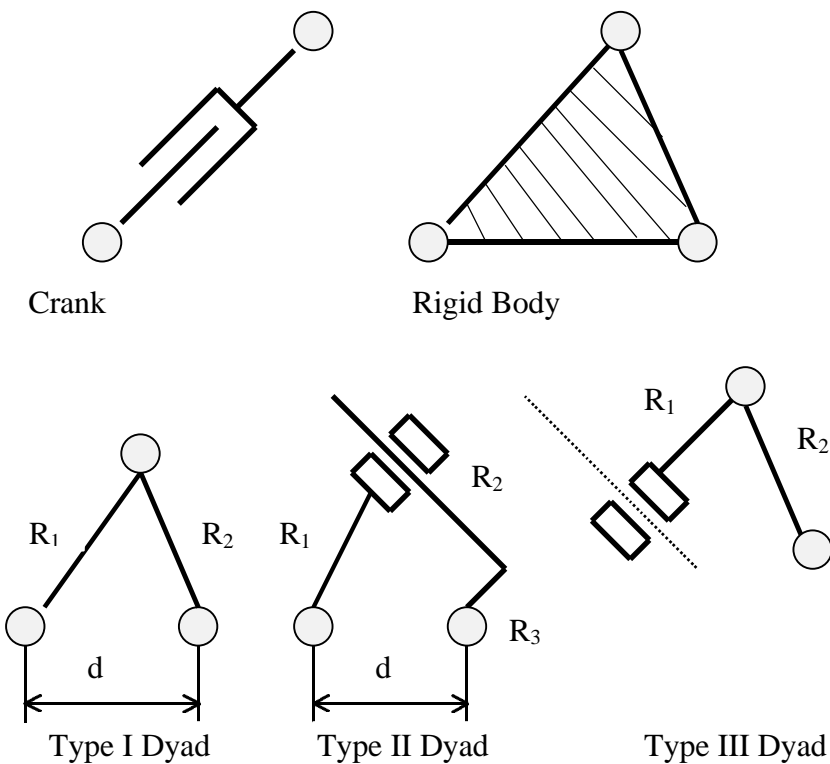


Fig. 11. Assur Groups of Dyads.

by using graph theory and number synthesis. The number synthesis is divided into the following essential steps:

- Generation of graphs up to the desired degree of complexity
- Labelling the edges of each graph in non-isomorphic ways
- Assigning ground, input and output link locations.

The number synthesis of joint and part numbers are developed using the equalities between the joint and part number and number of kinematic loops in a planar mechanism. Freudenstein and Vucina (1991) have used graph theory and number synthesis to develop part and joint number variants for eight windscreens wiper mechanism concepts. These variants are then subject to dimensional optimisation of the wiper sweep area with respect to the windscreens area.

The basic idea in graph theoretic mechanism synthesis is to consider the kinematic structure and function as independent in the initial design stage. The kinematic structures are then generated

The derivation of number synthesis rules is based on basic equations of graph theory and mechanism degree of freedom. The global degree of freedom of a spatial mechanism system is given by the Kutzbach equation

$$F = (6 - k)P - \sum_{i=1}^5 i \cdot n_i \quad (1)$$

where

F = the mechanism system degree-of-freedom

k = the number of constrained degrees of freedom common to all parts

P = the number of parts (ground included)

n_i = the number of kinematic pairs (joints) restricting i degrees of freedom

For planar mechanisms ($k=3$), the Kutzbach equation is reduced to the Grübler equation (2). Initially all parts have three degrees of freedom, the ground part is fixed, and the system's degree of freedom is restricted by first and second degree of freedom joints.

$$F = 3(P - 1) - 2n_1 - n_2 \quad (2)$$

where

n_1 = the number of kinematic pairs of 1st degree (rotation or translation only),

n_2 = the number of kinematic pairs of 2nd degree (combined rotation and translation).

There are three types of possible joints in a plane system: rotation and translation joints restrict two degrees and translation-rotational joints restrict one degree of freedom, see figure 12.

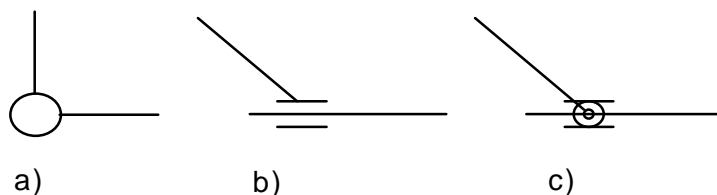
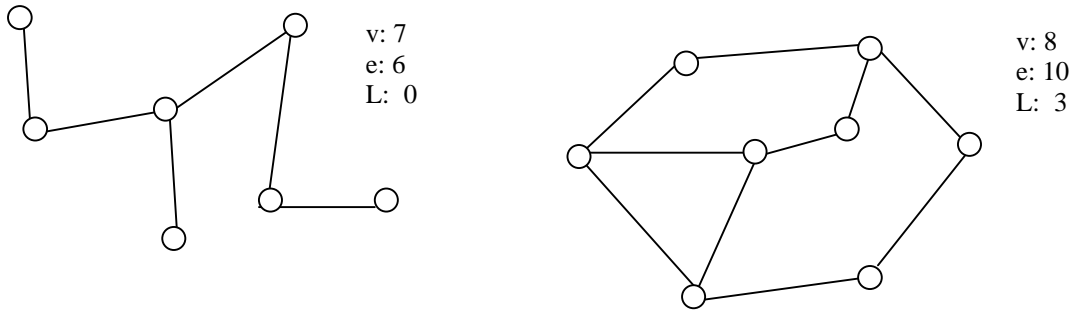


Fig. 12. a) Rotation joint. b) Translation joint. c) Translation-rotational joint.

We apply the following statements of graph theory:

- Each *edge* connects two *vertices*.
- *Vertices* may be connected by *edges*. An *edge* is said to be *incident* at a vertex if the vertex is the endpoint of that edge.
- The *degree of a vertex* is the number of edges incident at that vertex.
- A *circuit* is a closed path, in which each vertex is traversed exactly once.
- Two or more graphs are *isomorphic* if there is a one-to-one correspondence between their edges and vertices which preserves incidence.
- A *tree* is a sub graph of a connected graph containing all of its vertices and no circuits.

**Fig. 13. a)** a tree graph.**b)** graph with three loops.

From the statements above we can derive the basic equations of graph theory to be applied to mechanism synthesis:

For any graph, let

e = number of edges,

v = number of vertices,

L = number of independent loops,

v_i = number of vertices of degree i .

Then from the statements above we obtain:

$$e_{tree} = v - 1 \quad (3)$$

$$L = e - v + 1 \quad (4)$$

$$2 \cdot e = \sum i \cdot v_i \quad (5)$$

Moreover, all planar graphs fulfil the Euler equation:

$$v - e + a = 2 \quad (6)$$

where a is the number of areas.

Any planar mechanism can then be topologically represented as a graph as follows: The *topological graph* of a mechanism is a graph where vertices correspond to links (or parts) and the edge connections correspond to the joint connection of links. From the basic structural equations of graphs, eq. (3) - (5), and from the Grubler equation (2), when the system global degree-of-freedom, $F = 1$, we obtain:

$$L = j - l + 1 \quad (7)$$

$$2 \cdot j = \sum i \cdot l_i \quad (8)$$

where

j = number of joints in the mechanism ($j = n_1 + n_2$),

l = number of links ($l = P$),

l_i = number of links with i joints.

For a mechanism, assigning $F = 1$ in equation (1) gives:

$$3P - 4 - 2n_1 - n_2 = 0 \quad (9)$$

Equation (7) could also be written:

$$L = n_1 + n_2 - P + 1 \quad (10)$$

Equation (10) gives the quantity of loops in a planar mechanism with one degree of freedom. By using integer programming of equation (9) and the subsidiary condition that all parameters are non-negative, we can calculate the following component number combinations for planar mechanisms.

Assuming that the mechanisms are assembled only from binary (P_2) and ternary (P_3) parts (parts having two respectively three joints belonging to the part), we get:

$$P = P_2 + P_3 \quad (11)$$

and

$$2\sum n_i = 2P_2 + 3P_3 \quad (12)$$

The number combinations for loop, joint and part numbers for possible mechanism configurations are now calculated using integer programming:

L	n_1	n_2	P	P_2	P_3	
1	4	0	4	4	0	
1	2	1	3	3	0	
2	7	0	6	4	2	
2	5	1	5	3	2	
...	

The synthesis of joint, loop and part numbers is followed by the generation of graph structure of a mechanism system. The abstraction of substructures in a graph can be performed in various ways, e.g. by using Franke's notation, Olson, Erdman and Riley (1985). By using Franke's notation, the generation of mechanism variants is performed in two phases. In the first phase substructures are abstracted by defining the order of loops and locations of multiple joint parts in the graph structure. In the second phase, for each graph, the parts of input and output are defined and thus the mechanism is topologically defined.

Franke's notation includes abstractions to represent binary part kinematical chains and multiple joint links. Consider the mechanism in figure 14. It is a 12-part, 16-joint planar mechanism with revolute joints only. According to Franke's notation each part connected with at least three kinematic pairs, is represented with a circle.

The number inside the circle indicates the number of kinematic pairs of that part. Each circle has as many lines connected to it as the part has kinematic pairs. This is called the valency number of the part. Each line represents a chain of binary parts, and the number assigned to the line shows the number of binary parts. By using equations (2) - (10), it can be shown, that the number of circle marked parts added with the sum of numbers on the lines is equal to the number of parts in the mechanism. Also, the sum of the numbers in the circles and twice the sum of numbers on the lines is equal to twice the number of joints.

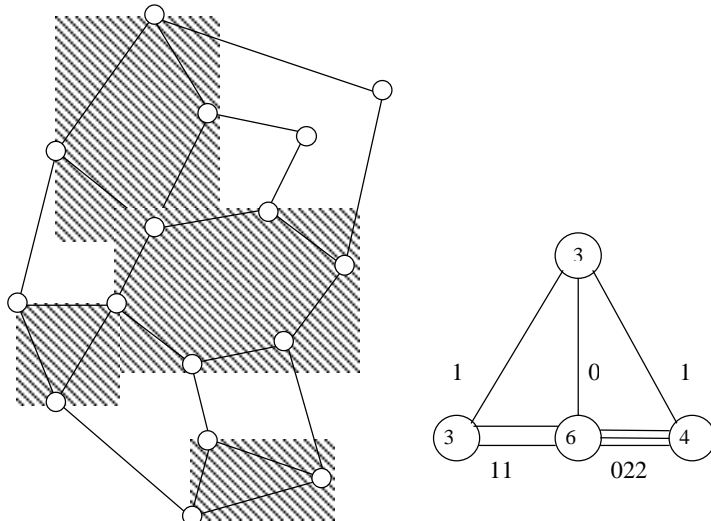


Fig. 14. Franke's notation of a 12-part mechanism, Päärti, (1989).

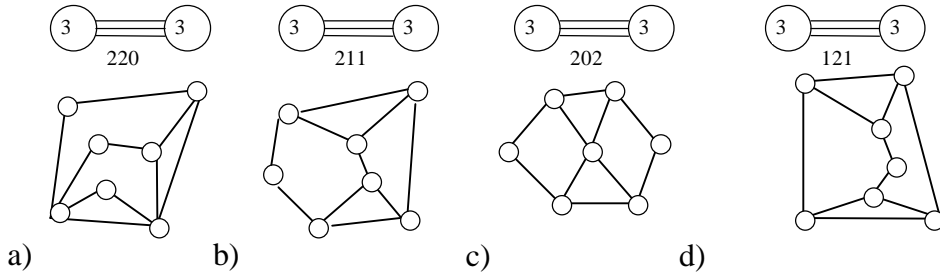


Fig. 15. Topological variants of six-part mechanisms.

Let us demonstrate Franke's notation for the second last number synthesis case of eq. (13). Since $P=6$, $P_2=4$, $P_3=2$, $n_1=7$, $L=2$, we get two circles due to two ternary parts, both having three lines connected to them, due to the two independent loops. Also, the sum of line numbers must be four, due to the number of binary parts. Since for each adequate kinematic chain (Franke's line) there is minimum zero and maximum two parts, we can derive four unique line number variants (220, 221, 112 and 121) of the mechanism. Thus we can derive alternative kinematic representations for topologies, figure 15. The last part of a mechanism topology definition is the assignment of input, output and ground link.

3.3 Locking conditions of mechanism singularities

Topological mechanism synthesis results in a unique description of the mechanism structure. However, it doesn't include any information of the dimensioning of the mechanism. The locking conditions and singularities of a mechanism are complex functions of each topology and the dimensional parameters. Therefore, arbitrary mechanisms must avoid locking conditions to function properly. General conditions for arbitrary topologies are very difficult to derive. For link mechanisms with revolute joints it is however possible to identify fourbar sub mechanisms in the kinematic structure. This doesn't ensure mechanisms completely free of singularities, however it contributes to the selection of link lengths, if the causality flow from input link to output link in the structure is followed.

Fourbar mechanisms can be classified according to their link lengths into three categories: double-cranks, rocker-cranks and double-rocker mechanisms. Based on this categorisation and the order of link lengths, Barker (1985) has published a complete classification of fourbar mechanisms, into 14 categories. In this categorisation the mechanisms are proposed to be named according the main type e.g. Grashof, and operation of input, coupler and output link (Table 2.).

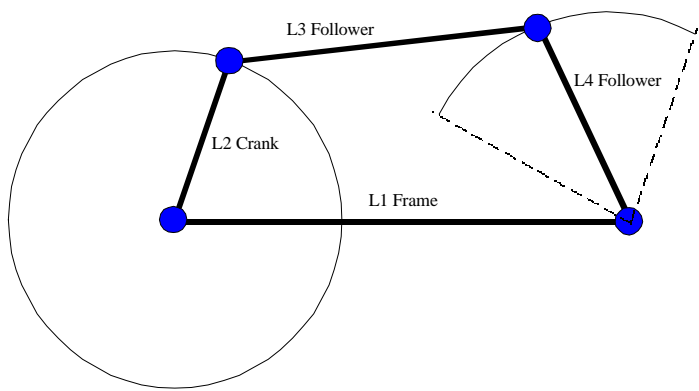


Fig 16. A crank-rocker type of fourbar mechanism.

In figure 16 a fourbar mechanism is shown having the following links, Päärti (1989):

- L1 = Frame length
- L2 = Crank length
- L3 = Coupler length
- L4 = Follower length

The classification of a fourbar mechanism is based on the length of the links:

- s = the length of the shortest link
- l = the length of the longest link
- p,q = the length of the intermediate links

According to Grashof, a fourbar mechanism has at least one revolving link, i.e. crank, when

$$s + l < p + q \quad (14)$$

This class of mechanisms is called Grashof-mechanisms. A fourbar mechanism can't rotate at all, thus all links are rockers when

$$s + l > p + q \quad (15)$$

If the equality

$$s + l = p + q \quad (16)$$

applies, the mechanism is a change-point fourbar, thus both cranks can rotate.

Table 2. Complete classification of fourbar mechanisms, Päärtti (1989).

Number	$(s+l) \otimes (p+q)$	Characteristic bar length	Class	Proposed name	Symbol	
	\otimes	Category				
1	<	Grashof	frame, $L_1 = s$	1	Grashof crank-crank-crank	GCCC
2	<	Grashof	input, $L_2 = s$	2	Grashof crank-rocker-rocker	GCRR
3	<	Grashof	coupler, $L_3 = s$	3	Grashof rocker-crank-rocker	GRCR
4	<	Grashof	output, $L_4 = s$	4	Grashof crank-crank-crack	GCCC
5	>	non-Grashof	frame, $L_1 = s$	1	Class 1 rocker-rocker-rocker	RRR1
6	<	non-Grashof	input, $L_2 = s$	2	Class 2 rocker-rocker-rocker	RRR2
7	<	non-Grashof	coupler, $L_3 = s$	3	Class 3 rocker-rocker-rocker	RRR3
8	<	non-Grashof	output, $L_4 = s$	4	Class 4 rocker-rocker-rocker	RRR4
9	=	change point	frame, $L_1 = s$	1	change point crank-crack-crack	CPCCC
10	=	change point	input, $L_2 = s$	2	change point crank-rocker-rocker	CPCRR
11	=	change point	coupler, $L_3 = s$	3	change point rocker-crank-rocker	CPRCR
12	=	change point	output, $L_4 = s$	4	change point rocker-rocker-crack	CPRRC
13		change point	two equal pairs	5	double change point	CP2X
14		change point	$L_1 = L_2 = L_3 = L_4$	6	triple change point	CP3X

To enable computerised dimensional synthesis, it is compulsory to select feasible initial dimensions for a mechanism that guarantees its function and then create an initial coupler curve, even if it is not optimised for the functional requirements. In paper F, the fourbar mechanism synthesis program assumes initial conditions to accomplish crank-type input (mechanisms 1,2,4,9 and 10 in table 2). During the optimisation, crank-type input requirements are maintained by non-linear programming of dimensions using penalty functions for singularities.

3.4 Dimensional optimisation

The purpose of dimensional optimisation is to find a dimension combination for a given topology, that satisfies the desired couple curve as closely as possible without violating the boundary conditions. In paper F, for dimensioning of a mechanism, optimisation utilising the gradient method, has been applied. The least square error function to be minimised during optimisation, is given in eq (17).

$$f(\bar{x}) = \sum_{i=1}^m \left(a |\bar{p}_o(i) - \bar{p}_t(i)|^2 + b (\mathbf{a}_o(i) - \mathbf{a}_t(i))^2 \right) \quad (17)$$

where

\bar{p}_t = trial path point vector,

\bar{p}_o = object path point vector,

\mathbf{a}_t = trial path angle vector for the tool,

\mathbf{a}_o = object path angle vector for the tool,

a = path deviation weight (zero in function optimisation),

b = tool angle deviation weight (zero in path optimisation),

m = number of path points.

The function is given in a kinematically bounded form. This leads to the synchronised bounded optimisation for the path, i.e. the kinematic position and speed difference as a function of time between trial and object point should be as small as possible. To the error function f , a penalty function g is added to handle the subsidiary conditions, i.e. acceptance of positive dimensions only and limited accelerations etc.

$$g(x) > 0 \quad (18)$$

so that the complete objective function can be on the form:

$$F(\bar{x}) = f(\bar{x}) + k \ln \frac{1}{g(x)} \quad (19)$$

The optimisation can be carried out, using the classical gradient method:

$$\bar{x}_{i+1} = \bar{x}_i - k \nabla F(\bar{x}_i) \quad (20)$$

4. Rigid body modelling and Multi Body Systems simulation

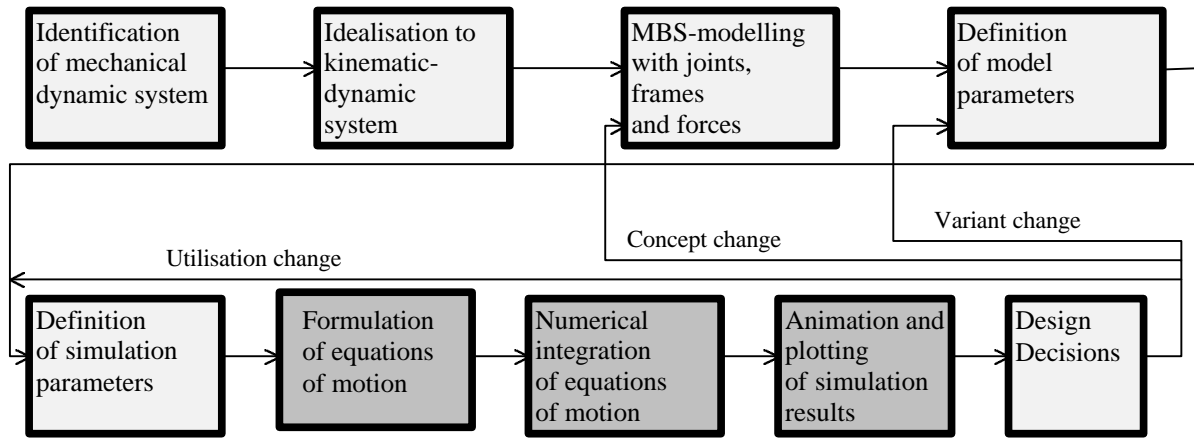


Fig. 17. Simulation process based on multi body simulation. The lighter boxes represent human activities while the dark ones represent tasks performed by the computer.

Multi body systems simulation is a method to analyse real world mechanical systems, applying a systematic procedure, multi body systems modelling. *Multi body systems modelling* is a formalism to idealise a mechanical system to a discrete model consisting of *rigid bodies*, *kinematical constraints* and *constitutive relation elements*. Each part of the real system is idealised with one free six degree of freedom coordinate system known as rigid body or *frame*, having a mass, mass centre and inertia tensor related to it. In every multi body system, there is one fixed, inertial frame designated as ground part, to which the position of the other coordinate systems are related at the initial configuration of the system. A kinematical constraint is an ideal massless, non-elastic motion restriction defining an inter-relational motion restriction between two separate coordinate systems i.e. bodies, at defined points on each body. Various types of such elements exist enabling free rotation, translation, screw motion etc. For such a constraint, a kinematical motion generator can be specified, which defines the motion of the constraint's free coordinate as a function of time. A constitutive relation element is a massless element transmitting the force between two distinct points of two different bodies. The force vector can be any function of position, speed, acceleration or other relevant characteristics of the model, describing any kind of external physical force acting on the body. When necessary, the reactive component acting on the opposite frame can be neglected.

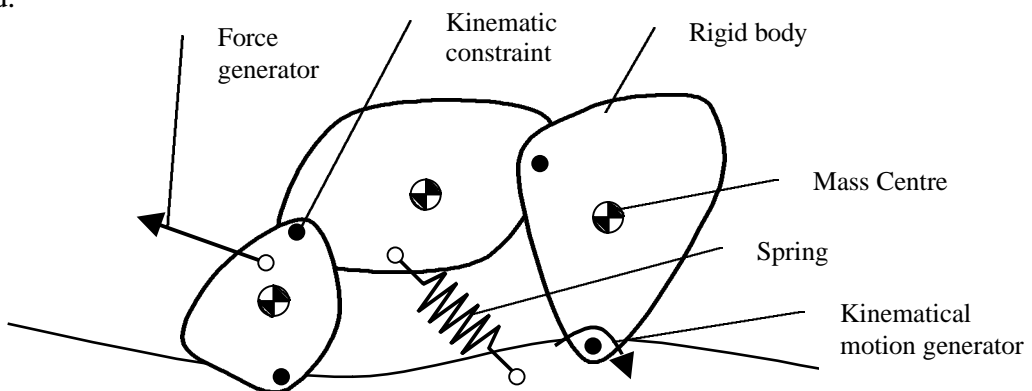


Figure 18. An example of a multi body system.

Multi body systems analysis is a systematic procedure to formulate automatically a multi body system. The method for derivation of the equations of motion is dependent of how the coordinates of the mechanism system are represented. In maximal or absolute coordinate system representation, the equations for each body's six Cartesian coordinates and Euler angles are derived. The kinematic constraints are then treated as constraining equations. With minimal, relative or joint coordinate approach, only as many equations are derived as the system has free joint coordinates. The former method has the advantage that the dynamical formulation of the equations of motion is straightforward, since the kinematical constraints between different bodies can be introduced into the dynamical formulation by using a set of nonlinear algebraic constraint equations. Moreover, this approach allows easy additions of complex force functions and constraint equations. The latter method requires systematics to represent the joint coordinates e.g. according to the Denavit-Hartenberg method, Denavit and Hartenberg (1955), so that the dynamic equations will be expressed in terms of the system degree of freedom. For many applications, this approach leads to a complex recursive formulation based on closure equations of kinematic loops. Also, the incorporation of driving functions or constraint equations in the recursive formulation is difficult. This approach is, however, more desirable in some applications due to a minimum set of coordinates. In both approaches, the motion equations are solved after the initial conditions are specified, using numerical integration. As a result, the position, velocity and acceleration history of the bodies are obtained as well as the internal forces acting in the system. By using an MBS program, the need for building and testing prototypes can be reduced significantly. Such techniques are often referred to as virtual prototyping, figure 18.

In this thesis work, the commercial software package ADAMS from Mechanical Dynamics Inc., has been utilised, ADAMS (1998). During conceptual design, simple geometries can be generated in ADAMS. For detail design, solid geometry CAD models can be imported. For a first evaluation of design concepts, a kinematical analysis is performed, giving position, velocities and accelerations as results. With definition of part masses and inertia, rigid body dynamics can be calculated, giving forces and torque required for a specified motion. These forces can be transferred to a FEM-program, for off-line calculation of stresses and elastic deflection of a part. For refined dynamic analysis, elastic properties of mechanism parts, as well as joint backlash can be incorporated in the MBS model.

5. Elasticity and contact phenomena in rigid body modelling

5.1 Modelling of structural elasticity

The modelling of elasticity is divided into two main categories: The first category of modelling is based on rigid body systems, where the elasticity is represented as constitutive relations between lumped rigid bodies. The second category uses elastic body systems, where the elasticity is modelled as a rigid frame superimposed by the elastic mode shape functions describing the displacement field, Sorge, Bremer and Pfeiffer (1992). Pure rigid body systems model the elasticity either as rigid body pairs coupled with an elastic element, Fertis (1973), Amrouche (1992), or the elastic system is replaced by a combination of rigid bodies and springs, Huston (1982), Rauh (1987). The condensed rigid body approach discretises a finite element structure to a set of rigid bodies and to force-deformation relations, according to an appropriate distribution method, e.g. Shabana (1985). For instance, ADAMS software, ADAMS/FEA, (1994), condenses the sparse finite element mass and stiffness matrices of the original structure to n discretised master nodes (rigid bodies with six degrees of freedom each). The condensation produces $6n \times 6n$ mass and stiffness matrices that are completely dense. The translation of stiffness matrices is a straightforward procedure. However, the condensation of mass matrices is based on lumping, thus only the three moments of inertia of each master node are translated, while the inertia couplings between the nodes are not translated. The drawback is that natural frequencies are not accurately preserved. However, large deflections maintain the accuracy better due to superposition of rotations.

Elastic body systems can be described as a superposition of the mode shapes from finite element modal analysis to the rigid body, Hale and Meirovich (1980). A state variable is assigned to each mode shape, and the relative amplitude of each mode is calculated during the time analysis. The total deformation of the body is achieved by linear superposition of the mode amplitudes during each time step. The natural frequencies are modelled more accurate than in the condensation approach, while large deformations are not allowed.

The above models are used only to achieve accuracy in prediction of the systems motion in multibody simulation. A detailed analysis of a particular body under stress is restricted, since multi body theories treat the body basically as rigid. Thus calculation and visualisation of stress fields is usually impossible. In the reversed sequence the external load field is calculated using multibody software, and the loads are incorporated to the finite element analysis, Jahnke, Popp and Dirr (1992).

Paper **B** presents an approach, where the elasticity of linkage bars in a parallel robot is modelled using $n+1$ rigid bodies and n constitutive relations between each rigid body pair. The n rigid bodies are distributed equally in length between the end points and the part mass m_r is distributed as follows: A lumped mass m_r/n is associated to the $n-1$ intermediate bodies. The mass $m_r/2n$ is added to the two end bodies. The inertia tensor J_r is lumped equally to the $n-1$ intermediate frames, of element length L_r/n . The constitutive relations between the elements are 6×6 force-deformation relations. The force-deformation relation is considered to be a massless Timoshenko beam, described in paper **B** and in Appendix **A**.

A certain degree of approximation of the elastic multi body system is desirable in modelling the system, for computational efficiency. However, approximation may result in inaccurate or false

results. Liou and Patra (1994) have considered the factors affecting the accuracy of dynamical FE-analysis. Here we consider some of the factors concerning MBS simulation accuracy when including elasticity as presented in paper **B**.

Mass discretisation of elastic beams. If a beam-type structural part is modelled as a single massless beam element, the inertia and Coriolis effects along the continuous beam must be separately treated. In paper **B**, beam structures are instead modelled as discrete chains of rigid bodies and massless beam elements. Thus the mass is discretised along the beam and the Coriolis and inertia effects are included in the MBS solution due to the inertia forces acting at the intermediate bodies. The residual error due to mass discretisation is small, if the mechanism is not too flexible, Sung et al (1986).

Vibration response. Vibration analysis of a mechanism is a very time consuming process. The most time devastating is dynamic vibration analysis (including joint backlash models) in the time plane. This type of analysis is required only when the dynamical path compliance of the mechanism is to be analysed, and it is not suitable for parametric studies due to the numerical effort. In many cases it is however not necessary to find the system's vibration response in the time plane. When the bar structures of a mechanism are designed, the designer usually needs just to know the approximate natural frequencies and amplitudes of the system. However, different lengths, cross sections and materials need to be considered, addressing the need for fast parametric analysis. Therefore, quasi-static eigen mode analysis can be used as an approximation of time plane vibration analysis. For deciding whether quasi-static or vibration analysis is to be performed, Sanders and Tesar (1978) suggest that with an "enough stiff mechanism" quasi-static analysis may be used. Their criterion for stiffness is that the first natural frequency w must be twenty times higher than the angular speed of the mechanism input w_i , to use the quasi-static analysis, thus $w/w_i > 20$. In figure 19, the mechanism drive frequency (first peak at less than 10 Hz) and first natural frequency (about 70 Hz) are shown in the diagram from the Fast Fourier Transform (FFT)-analysis of time plane simulation results.

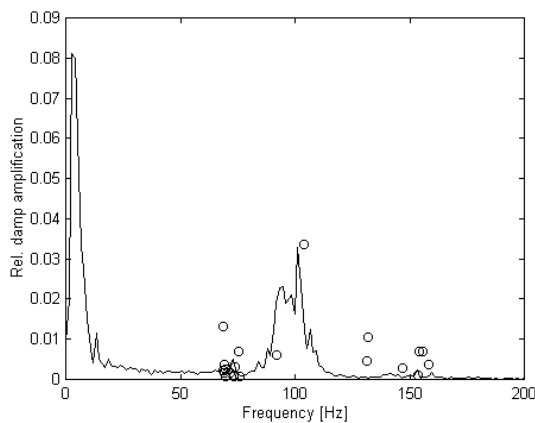


Fig. 19. The peaks of crank input frequency and mechanism eigen frequency, from FFT-analysis (curve). The rigid-elastic eigen modes are from linear analysis of the MBS-model (circles).

Variation of system natural frequency. It is known, that for static conditions, the eigen frequency of a mechanism system varies with different postures, Turcic, Midha and Bosnik (1983). An analysis of this phenomena is shown in paper **B**, see figure 20. Experimental studies have shown, Liou and Erdman (1988), that the natural frequency of each individual link dominates the system natural frequency. Thus, in certain cases natural frequencies of a system can be predicted if the eigen frequencies of individual links are known.

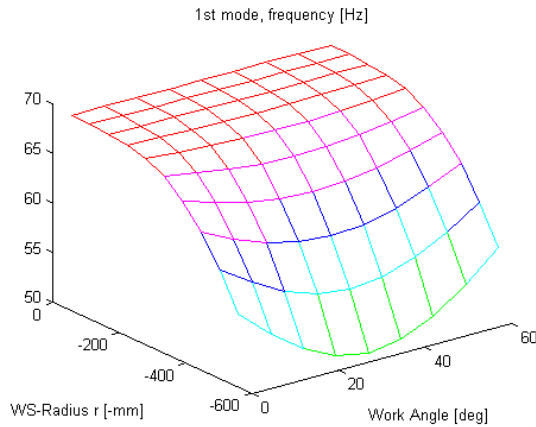


Fig 20. Variation of the DELTA-robot's 1st natural frequency as a function of the TCP position.

Time step. In time plane analysis, Bathe (1982) suggests an approach based on the first few harmonics of the major excitation. Assume, that major excitation is given with input angular frequency w . The step size is to be adjusted so that N times higher modes are included in the sampling. Also, the sampling rate must be S times the highest frequency. The maximum time step Δt will then be, assuming Sanders and Tesar's criterion:

$$\Delta t \leq \frac{2p}{20NSw} \quad (21)$$

Shock and impact loads are initiated from joint clearance contacts, for instance. Clearance impacts introduce longitudinal shock waves. The shock limits the length of the time step according to the Courant condition, Liou and Patra (1994). According to this condition, the maximum time step is the traversal time for the shock wave over one rigid body pair. The time step is thus depending of the body pair characteristic length δ and the wave speed, which depends of the beam materials modulus of elasticity E and density ρ :

$$\Delta t = \frac{d}{\sqrt{E/\rho}} \quad (22)$$

Model validation based on frequency analysis. As previously discussed, the length of the time step in time plane integration has influence on the accuracy of the analysis. The time step should be short enough to include the response of relevant physical modes in the simulation, but long enough to maintain efficiency of integration. Liou and Patra (1994) suggest the validation of FEM-models based on Fast Fourier Transformation (FFT). This approach can be applied also for MBS-analysis. The required time step can be determined, if the frequency response of the system is known. The frequency response is determined, if some characteristic displacement data from the MBS-simulation, e.g. the TCP path, is Fourier transformed. If the FFT data indicates the existence of very high frequencies together with low frequency behaviour, the problem is ill-conditioned. This requires a very short time step. To solve such problems, in some MBS codes, stiff-integrators are available, ADAMS (1998). In most cases however, the response is similar to that of fig. 19, having an interval of dominating frequencies. Usually the FFT-response has a dominating low frequency due to the driving speed of the mechanism. The higher mode peaks represent the eigen frequencies of the mechanism. Thus the highest peak frequency indicates the limit of the time step.

Another validation method, which is proposed as an original contribution of paper **B**, is the consistency verification between linear eigen mode analysis and Fourier transformation of time plane simulation. Assuming that the frequency response from the FFT of simulated mechanism displacement is time invariant enough, the linear eigen mode analysis should give modal frequencies and amplitudes that correspond to a certain degree to the FFT frequency amplification, figure. 19. Due to the kinematic constraint of input cranks, no eigen modes of input frequencies are however obtained from the analysis.

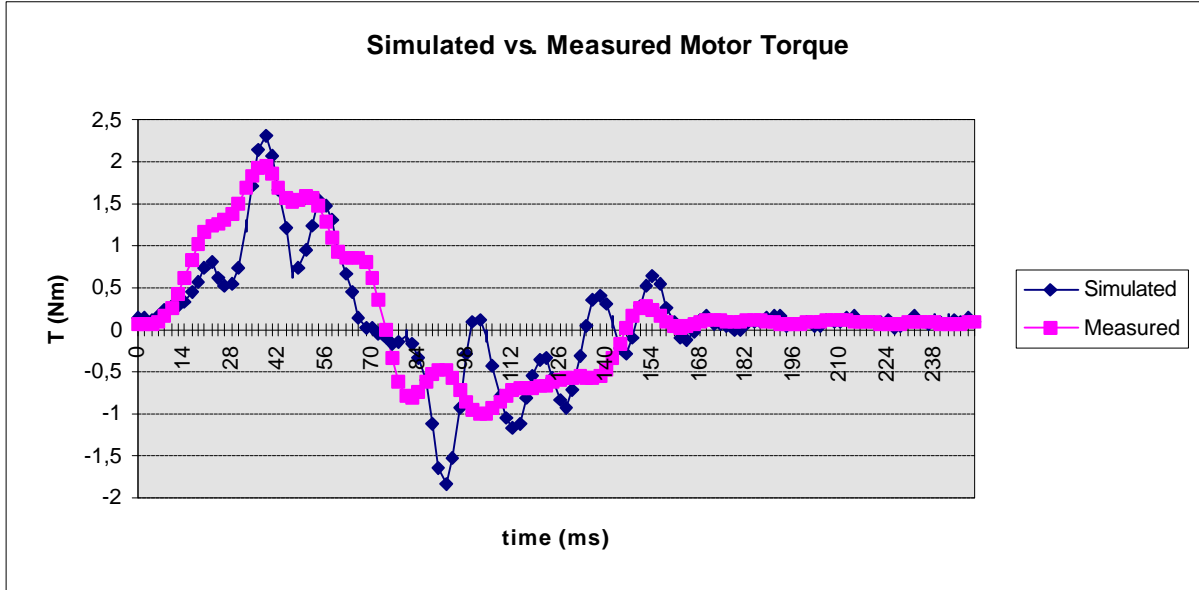


Fig. 21. Simulated vs. measured load of one motor in the DELTA robot.

Model validation based on time plane analysis. A common method for MBS-model validation is the excitation and observation of mechanism actuators. The mechanism actuator's accelerations, velocities or displacements are recorded as a function of time when the actuators are performing an arbitrary cycle. The load (e.g. motor current or hydraulic pressure) is recorded as a function of time, and the loads are compared to the loads obtained from simulation, fig. 21. The numerical computation of the time derivative of measurement data (acceleration, velocity or position time history) will influence the verification accuracy. For the case illustrated in fig. 21, the simulations were performed using measured motor speed history, which will decrease the accuracy of motor inertia estimation due to the numerical derivation. The acceleration history is the best to use, as it reflects directly the inertia, and no numerical derivation is then needed.

5.2 Modelling of joint clearance

Multi body system simulation is based on the assumption, that mechanisms are modelled with kinematic ideal joints without friction and clearance. In real world, however, joints always include friction and clearance. In radial bearings, friction is acting tangentially and the clearance impacts radially. The joint friction models which are used in multi body models, ADAMS (1998), are based on Coulomb friction. Modified models of dry friction assume that the friction force F_m is velocity dependent:

$$F_m = m F_k(v) \quad (23)$$

where F is normal load and the static friction coefficient is m . The dimensionless velocity dependent friction function $k(v)$ describes the curve fitting to measurements of dry friction sliding. In literature, different approximations for the function k are available. More detailed models include lubrication conditions and clearance variation due to temperature variation, like calculation programs for bearings based on standardised procedures for hydrodynamic lubrication. Due to their complexity, they can only be used off-line to compute parameters for multi body friction models. In papers **B** and **C**, the bearing modelling has been concentrated to clearance modelling and friction has not been included. In paper **D**, a one dimensional model with Coulomb dry friction is used.

Clearance is an unavoidable property of a journal bearing. A journal bearing comprises two principal elements, the journal and the sleeve. Due to manufacturing tolerances and to ensure adequate function as revolute joint, the radius of the bush must be larger than the pin radius. This introduces the difference between the bush and pin radius, known as clearance, e.g. Seneviratne, Earles and Fenner (1996). By using pre-tensioning, the clearance may be diminished. This however leads to stiffness hysteresis. In rolling contact bearings, the support forces are distributed over extremely small contact areas of line or point contact character. This reduces the friction force of the contact, but also increases the elasticity influence of the contact. Pre-tensioning in journal bearings increases the friction and wear. Tolerance based pre-tensioning has a short life time, while spring based pre-tensioning has not. Still, it has the disadvantage, that contact loss is achieved if the joint has a load above the pre-tensioning limit. The spring pre-tensioning principle for double ball joints of the DELTA parallel robot is shown in figure 22. A similar arrangement can be applied for single ball joints and journal bearings.

The existence of clearance may result in contact loss when the support force is zero. The pin moves relative to the bush and impacts back to contact when the free movement limit is reached. This leads to impact vibration reducing the systems performance by generating high forces causing a possible bearing failure or increasing fatigue. The bearing wear may increase and grow the clearance with self-cultivating effect. Also, in addition to increasing compliance error, noise and vibrations of the mechanism belong to the unwanted phenomena.

According to a literature review, the models of clearance fall into four different categories (Seneviratne, 1985), see figure 23:

- Zero clearance approach: the contact loss and magnitude is predicted from zero clearance analysis.
- Massless link approach: the bearing surfaces are assumed to be rigid and their centre distance is modelled as massless link of constant length.
- Spring damper approach: the bearing surfaces are assumed visco-elastic and they are modelled as a spring damper system.
- Impact model approach: the bearing elements are modelled as two impacting bodies, with a contact force-displacement function.

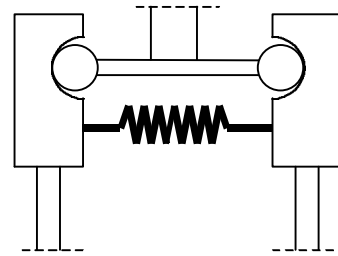


Fig. 22. Principle for ball joint pre-tensioning of the DELTA robot lower arms.

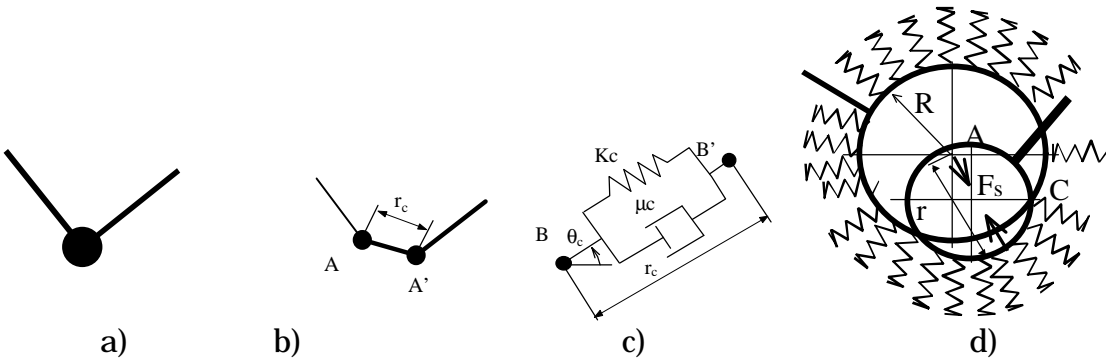


Fig. 23. Schematic representation of model principles of a) Zero clearance b) Massless link c) Spring damper d) Impact model

Besides these categories, the clearance modelling is characterised from the features of the type of the application:

- Linkage mechanism: Slider crank, four bar, five bar, idealised joint, other mechanism
- Damping: non-existent, viscous, Coulomb, direction related (radial/tangential/uniaxial)
- Clearance joint number in the model: single, multiple
- Links: rigid or elastic

Zero clearance analysis is easy to perform and suitable for multi body analysis requiring only to study the reaction force in the joint. Earles and Wu (1977) carried out an extensive experimental programme to predict the magnitude of the impact force F_{imp} .

$$F_{imp} = C_b (C_m^\Delta - 1) \ln(\dot{\theta}/R) \quad (24)$$

where C_b and C_m are constants of the bearing, Δ is the clearance, $\dot{\theta}$ is the angular speed of the bearing support force, and R is the bearing support force. Due to non-existence of negative support force it was motivated to form a criteria, "contact will be maintained if $\dot{\theta}/R > 1$ rad/Ns". Additional experimental evidence for this criteria has been provided by Earles and Killicay (1980) and Fawcett and Grant (1979), reporting good agreement with the criterion. However, the boundary value for the loss of contact varied between one and three. Also, the dimensionality of the constant one, implies existence of a "natural constant" of clearance, and theoretical efforts to cast this into a dimensionless form has failed. Haines (1979) reports that with very high values, up to $\dot{\theta}/R = 200$ rad/Ns contact losses have not been observed. This clearly degrades the prediction potential of the zero-clearance model.

In the *massless link* approach, clearance is modelled by adding an extra link for describing the distance between pin and bush centres. This adds an extra degree of freedom to the system. This attempt to explain clearance in mechanisms assumes that the complex behaviour of the mechanism is primarily due to the introduction of this extra freedom. Thus it assumes that the bearing contact surfaces are rigid, and the contact is maintained as long as a compressive force in the massless link is not observed. The model also neglects tangential friction. This means, that for the condition of combined radial and tangential compression of the link, the angular speed $\dot{\theta}$ of the massless link can increase significantly. In reality, the radial compression would introduce contact loss instead of increase in angular speed and thus Seneviratne and Earles (1992) have used the chaotic change of $\dot{\theta}$ position as a criteria that contact loss has occurred. The introduction of an extra degree of freedom

to the model requires the specification of two initial conditions, the angle $\dot{\theta}_0$ and the angular speed $\ddot{\theta}_0$ of the massless joint. This is obtained by assuming it to be the same as the angular position γ_0 and speed $\dot{\gamma}_0$ of the support force from the zero-clearance analysis. Assuming that the tangential friction of the joint can be neglected and that the joint is initially in contact, the massless-link model can predict the contact loss when it occurs for the first time. The assumption of a single-mode model (always in contact) makes it unable to predict what happens after the contact is lost. Thus, the massless link model is restricted to analysis only for checking that contact loss doesn't occur.

In the *spring damper* approach the clearance is modelled by coupling a spring damper unit between the journal bearing centre and the shaft centre. The bearing support force is assumed to be zero, when the distance difference r between the centres equals the clearance distance r_c , thus

$$F_s = K(r - r_c) + C\dot{r} \quad (25)$$

where F_s is the bearing support force, K is the bearing stiffness and C is the bearing damping factor. The model has two degrees of freedom, an additional degree of freedom r compared to the massless link model. Thus, in this model the geometrical loss of contact can be observed. The radial degree of freedom introduces an initial value problem, where the initial angular position $\dot{\theta}_0$ and speed $\ddot{\theta}_0$ are obtained from zero clearance analysis. The initial radial position r_0 and velocity \dot{r}_0 is

$$r_0 = \frac{F_{t0}}{K} + r_c \quad (26)$$

$$\dot{r}_0 = \frac{d}{dt} \left(\frac{F_{t0}}{K} + r_c \right) = \frac{\ddot{F}_{t0}}{K} \quad (27)$$

where F_{t0} is the bearing force at $t=0$ from the zero-clearance analysis.

In the *impact model* approach, the clearance is modelled as two impacting bodies. The contact impact is modelled either according to the principle of impulse conservation using e.g. an assumed coefficient of restitution, or with contact elasticity as a function of penetration depth. The principle of impulse conservation is numerically faster and suitable for simulating particles. The treatment of continuum body collision requires the modelling of energy transformation between translatory kinetic energy and impulse moment energy, due to the fact that contact forces usually not intersect the mass centre of a continuum body. In the contact elasticity model, the bearing force is a function of penetration depth $r-r_c$. The complete function is as follows,

$$F_s = \Pi(r - r_c) \{ K(r - r_c)^e - S(r, r_c, 0, r_c + d, 1)C\dot{r} \} \quad (28)$$

where Π is a Heaviside function, e is the material elasticity exponent ($e=1$ is used here) and d the penetration depth. To prevent discontinuity at the moment when contact is remade, the damping coefficient is a cubic step function S of the penetration. The damping is assumed to zero in contact, and saturates to C , at a predefined penetration d . This characteristic depth is selected to be 1.2 μm in paper C. The function $S(x)$ is a smoothing cubic spline polynomial as follows:

$$S(x, x_0, h_0, x_1, h_1) = \begin{cases} h_0 : x \leq x_0 \\ h_0 + (h_1 - h_0) \left[\frac{(x - x_0)}{(x_1 - x_0)} \right]^3 : x_0 < x < x_1 \\ h_1 : x \geq x_1 \end{cases} \quad (29)$$

The difference as compared to the spring-damper model is that in contact-loss mode, the negative, contact remaking force doesn't exist due to the Heaviside function factor $\Pi(r-r_c)$. Thus, it is assumed that the model has a greater tendency to predict contact-loss behaviour than has the spring-damper model.

Experimental results in literature. A model verification was tried, based on measurements reported in the literature, of a crank-counter-rocker type four bar test mechanism, having a clearance joint at the coupler rocker joint. This mechanism is described in Seneviratne, Earles and Fenner (1996) and parameters are given in paper C. The test rig was operated with a variable speed motor with a speed range of 200 – 400 r/min. The clearance in the test mechanism was 100 μm . Seneviratne, Earles and Fenner (1996) described that with this test rig, the regular, in-contact behaviour was observed until 255 r/min. No over-critical, stable contact remaking speed was observed until 400 r/min. In this model, however, an additional spring of stiffness $k = 671 \text{ N/m}$ was added to the rocker arm, without the description of spring fixation parameters, thus a reproductive simulation could not be performed. Simulations with impact and mlsd (Mass Less Spring Damper) models showed contact loss at 94 r/min and 130 r/min respectively, indicating large differences in contact loss limit, which needs to be explained.

Zero-gravity limit. Due to the fact, that the tensioning spring provided an additional load to the rocker arm in the same direction as the gravitational load, it was reasonable to assume that negative, gravity exceeding acceleration caused contact loss. Thus, zero-clearance analysis without a tensioning spring and with normal gravity was performed. With Seneviratne's and Earles' (1992) model, a sequence of analyses was performed, under and over 99.7 r/min, without the additional spring load. As verified by control calculations, analysis with speeds less than 99.7 r/min showed that gravity pre-tensioned the clearance joint and that the acceleration never changed its direction with respect to gravity. When the speed was increased over 99.7 r/min, an oscillating vertical acceleration was observed. A hypothesis was formulated, that the oscillating, gravity pre-tension exceeding acceleration was one of the factors that caused contact loss. An additional confirmation was given by Seneviratne and Earles (1992) massless link mechanism, which persisted to have regular behaviour until 116 r/min, while over the limit of 119 r/min the model started to oscillate in a chaotic way. This limit was far from the 255 r/min limit, reported by Seneviratne, Earles and Fenner (1996), but near the 99.7 r/min limit. They also compared this result to the analytic criteria $\mathfrak{g}/R > 1$ of Earles and Seneviratne (1990), which predicted contact at a speed of 106 r/min, and definite contact loss at 123 r/min.

Massless link vs. impact model. Since the model with additional spring load according to Seneviratne, Earles and Fenner (1996) could not be reproduced, a comparison between the spring-damper link and the impact model was performed using the Seneviratne, Earles and Fenner (1996) model without additional spring load. The contact loss limits were analysed with respect to variation of rotational speed and the elasticity of the bearing joint. The actual parameter values are reported in paper C. The contact loss was detected by observing the contact force. The simulations were performed with rotational speed within the range 0-400 r/min. Within this range, under- and overcritical stable areas were observed. The results have been summarised in table 3.

Table 3. Contact loss limit of impact and massless spring damper models.

Model	K_c [N/m]	μ_c [Ns/m]	Lower limit regular- chaotic [r/min]	Upper limit chaotic- regular [r/min]
impact	10^8	3000	92 - 94	205 - 208
impact	10^7	3000	110 - 130	150 - 160
impact	10^6	3000	120 - 140	140 - 150
impact	10^8	0	97 - 100	205 - 210
mlsd	10^8	3000	100 - 130	150 - 160
mlsd	10^7	3000	120 - 130	130 - 140
mlsd	10^8	0	102 - 106	N/A

When using as a reference case stiffness value $K_c=10^8$ N/m and damping $m=3000$ Ns/m, the impact model predicts the lower limit for contact loss to 92 r/min. Compared to the mlsd model, the limits between regular and chaotic behaviour are sharper for the impact model. Nevertheless, when the bearing stiffness is reduced as compared to the reference case stiffness, the limits become unsharp even in the impact model. As expected, lower stiffness will reduce the chaotic regime in both models. This finding is consistent with Seneviratne, Earles and Fenner (1996). In general, the impact model tends to predict contact loss over a wider rotational speed range than does the spring-damper model, making the impact model more inclined for prediction of contact loss. When the reference case is compared to damping-free behaviour, the contact loss region is more narrow, which is also expected. However, an over-critical stable speed region for the mass-less spring-damper model can't be observed. Currently, a test rig is under construction that will be used to study the contact loss limit speed experimentally.

5.3 Application of an impact type clearance joint model in MBS simulation of the DELTA parallel robot

The impact model developed was applied to the MBS-model of the DELTA parallel robot. The impact model was in this case modified to a three dimensional model of a spherical joint to represent the joints of the ends of the lower bars of the robot. The joint contact force equations were the same as in the planar joint model, i.e. according to equations (28) and (29).

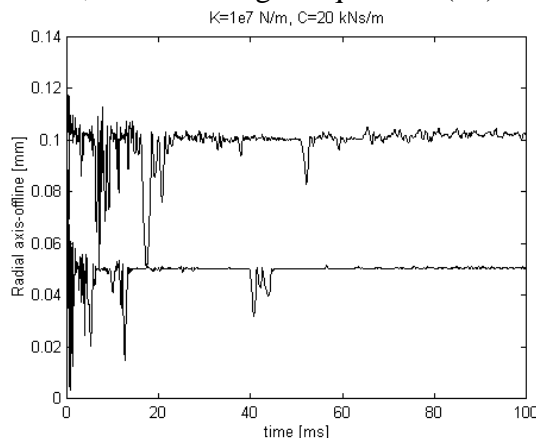


Fig. 24. Time history of radial difference between ball house and ball centres, with clearance 50 mm and 100 mm, respectively.

Representative stiffness and damping values $K_r=1\times 10^7$ N/m and $m=2\times 10^4$ Ns/m were used as reference. The kinematical spherical joints of the DELTA robot were replaced with submodels of clearance joints using representative clearance values of 50 μm and 100 μm . The simulations were conducted for a 400 mm long path with a 100 ms cycle time under continuously increasing and decreasing acceleration, at the middle of the work space. The time step of the “gear stiff” integrator was initially 1.0 μs , and the maximum limit was set to 200 μs . At start, the balls were assumed to be in loss of contact at the middle position, i.e. at maximum clearance distance.

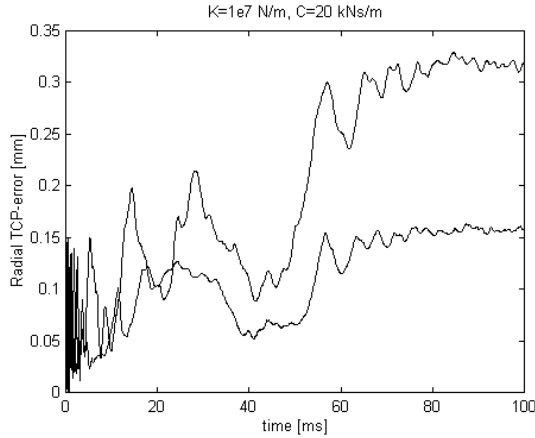


Fig 25. Time history of cumulative clearance error at TCP path, clearance 0.05 and 0.01 mm.

The analysis of contact force angular directions showed convergence to a fix angle confirming the phenomena shown in figure 25, that cumulative clearance error of a mechanism tends to increase when external tensioning forces of joints have the same direction. A series of simulations using clearance from 50 μm up to 1.0 mm were carried out using a joint stiffness of $K_r=1\times 10^8$ N/m and damping of $m=2\times 10^4$ Ns/m. The results indicate, that the relative time of contact maintained increases steadily the smaller the clearance is, with an anomaly of very low relative contact loss time at 0.4 mm. The impact force damps out from the initial value of about 1.2×10^4 N, to saturate at a coarse level of 500 N, independent of the clearance.

When the clearance was maintained at a level of 0.1 mm with damping $m=2\times 10^4$ Ns/m, the stiffness was varied from $K_r=2\times 10^7$ N/m to $K_r=10^8$ N/m. The contact was best maintained at $K_r=6\times 10^7$ N/m, while with lower values more vibration *at contact* was observed due to lower stiffness. The bearing contact impact force however increased with stiffness.

6. Summary of Papers

Paper A: Integrated CAD Methodology for Simulation Driven Product Development

Paper A presents a model for software organisation in simulation driven design. It outlines the development of a Computer Aided Engineering procedure. Based on characteristics of the most common categories of CAE tools for mechanical design, like Computer Aided Design, Multi Body System simulation, Finite Element Modelling and Block System Simulation tools, a framework for simulation driven design is presented. This product model is called Integrated Simulation System, ISS. The goal with ISS is to introduce a simulation environment, offering transparent viewpoints based on the domain familiar model languages.

According to Klir (1967) a system can be distinguished by defining and behavioural attributes. While the designer can only manipulate the defining characteristics, the use of simulation tools can shorten the time lag to observation of system behaviour, given that the selected model can observe that property. The defining characteristics and the property classes of the model categories are mapped to the framework. This is done in order to identify to which activities of the design process each model viewpoint suits best. The selected model of design process domains was the general procedural model of the design process by Hubka and Eder (1988), classifying the entity relations of design to process, function, organ and part domains. The different model categories were found to match well on these design domains enabling the dynamic implementation of the chromosome model of Andreasen (1992) and Ferreira (1990).

The empirical part of this work is a simulation of gantry robot kinematics with a multi body systems simulation software. The kinematics has been programmed by using a set of piece-wise fuzzy functions. Finally the multi view model (ISS) has been demonstrated for the gantry robot case, including a discrete block system model of drive and control systems.

Paper B: Framework for Modular Multi Body System model for Kinematic and Elastic Dynamic Simulation of Parallel Robots.

Paper B presents a framework for multi body system simulation utilisation in industrial product development projects. When high-speed and high accuracy is needed, the modelling should also include elastic and contact mechanical phenomena. The detail level of the simulation increases, and the dynamical properties complex dependence of the defining parameters makes intuitive design impossible. Thus optimisation of a complex product requires detailed mathematical modelling. This framework is subject to several requirements. The performance measures must represent both kinematic, dynamic and non-linear properties of a mechanical system, and they must be defined independently from the concept, to ensure unpartial evaluation. It follows that specification is uncoupled from the design concept. In design it is common that MBS-analysts and CAD-designers work together. Therefore it is important that a natural sequence of mechanical design activities is supported² and modelling of different problem views is possible with one master model, not to mention other requirements. This framework was implemented in industry and was applied to the development of the DELTA series of parallel robots.

² Park (1995) discusses robot design as an activity not concentrated only on one problem level, but considering several aspects as kinematics, isotropy, dexterity, work space, dynamic properties and so on.

Paper B begins with a comparative discussion of specification space definitions for robots. Joint and work space definitions of Khatib (1996) and work cycle space definitions of others e.g. Rajan (1985) or Ono and Teramoto (1993) are discussed and compared. During preliminary design a specification based on simple formalism is often the best. This paper uses a sequential linear vertical/horizontal pick-and-place sequence inside the work space boundary. The limits of the work space boundary is solved by using joint force relaxation and dynamic analysis. The free-angle restrictions caused by joint geometries were modelled by using joint force relaxation. Also, for analysis of the variation of the kinematic Jacobian along a given robot trajectory, an original contribution was made. By successively applying unit force components to the TCP, a series of quasistatic multi body analyses for a given trajectory are computed. The kinematic Jacobian is calculated from the joint torque response in each point of the robot trajectory. As a result from this procedure, many important forward and inverse kinematics related characteristics of the trajectory can be analysed: isotropy, condition number, minimum and maximum singular value. In the analysis of robots dynamical properties, joint and operation space form of motion equations are compared, Park (1995), Khatib (1996). However, no simple method to compute the mass matrix properties with an MBS code was found without tedious unit acceleration operations in all orthogonal directions for an arbitrary trajectory. Therefore, ordinary scalar properties related to a dynamical trajectory like mean, rms and maximum torque, joint maximum and rms velocities were selected to be more suitable as performance measures during the early product development phase of robot design.

The basic hypothesis in **paper B** is the acceptance that modern high-quality commercial multi body codes are already established. Thus, the research was concentrated to utilisation of those codes for faster modelling of applications than by development of completely new codes from scratch. This addresses the need of developing a multi disciplinary framework model applicable to ordinary MBS-codes. The requirements of *modularity* and *transparency* of model viewpoints speaks for a single model language, preferably the software's own command language. Generic modelling, Kjellander (1995), using macro programming in MBS model language is more advantageous than imperative programming, Hyvönen and Seppänen (1985). Macro programming and parametrisation

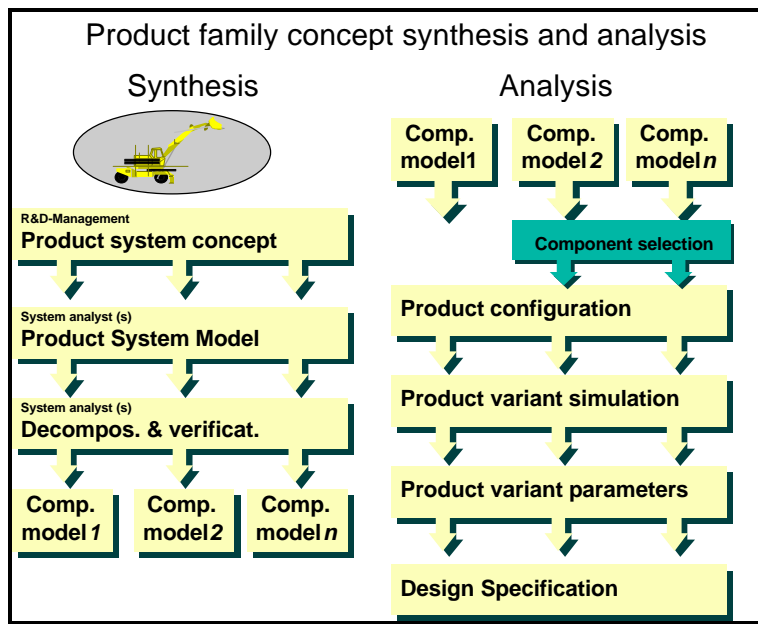


Fig. 26. Product model decomposition with MBS-modelling.

of a model command file is a key factor to develop a hierachic, variometric and generic model of components, which can be re-configured and -parametrised to represent all kind of configurations of a certain product family.

The last part of paper **B** concentrates on the simulation of an elastic model of the DELTA robot. The elastic beam model is a series of coupled rigid bodies having Timosenko beams as connecting elements, Natrayanaswami et al. (1974). The Timosenko beam model includes shear deformations, of importance for short beams. The complete derivation of the beam stiffness matrix is shown in appendix **A**, as well as the expressions for asymmetric correction factors for uneven shear stress over the beam cross section. The elasticity of gears was modelled as a linear visco-elastic coupling between motor and mass with the gear mass reduced to the mechanism. A brief analysis showed the gear eigenfrequency to be as high as 500 Hz, and thus not limiting the control of the mechanism. The lower beam structure of six bars supporting the TCP-plate showed however to be critical for the application. With most materials the first eigenfrequency mode was maintained at 70 Hz, at the middle of the work space. Studies at the work space boundary limits showed that outside of the 300 mm radius from the midpoint the eigenfrequency started to continuously decrease towards 50 Hz at the work space boundary. Another design problem identified, was the TCP-plates sensitiviness for rotational vibrations at 100 Hz due to transversal and longnitudinal vibration of the lower beams. These two unwanted features can be reduced by linkage cross section design. Finally, Paper **B** presents a spatial generalisation of the planar clearance joint of paper **C**. The clearance contact model was applied to the ball joints of the DELTA robot. While in the real design, the clearance is pre-tensioned by springs, in this modelling, the clearance in the lower ball elements was assumed to be 50 and 100 μm . The simulations including the clearance model showed that diminishing clearance and stiffness of joints will decrease the vibration amplitude of the TCP.

Paper C: On the development of a planar clearance joint model for Multi Body Systems simulation

Mechanical clearance is an unwanted but usually unavoidable property of a journal bearing or a mechanism joint, to ensure lubrication and correct function of the bearing element. During operation, clearance is subject to contact loss leading to impacts and increased joint deterioration, which can even be a self-cultivating mechanism, Seneviratne (1985). The dynamics of clearance joints is difficult to model, and many models e.g. Dubowsky (1974) have been developed for simulating the behaviour on component level. Approaches that are suitable for studies at the level of mechanism system are relevant for multi body simulation. In general, they are however primitive. Earles and Wu (1975) suggest, based on extensive experimentation, a method to predict contact loss in a four bar mechanism. Their criterion is, that loss of contact occurs when the angular speed of the bearing support force is large, compared to the length of the force vector in a zero clearance analysis. However, contradictory examples were reported by Haines (1979). Earles and Wu (1973) incorporated a fixed length clearance by including an additional mass-less link representing the distance between centres of bearing pin and bush. To include also the mode of contact loss, Seneviratne (1996) replaced the mass-less link with a mass-less spring-damper element.

Paper **C** presents an enhancement to the spring-damper model. The proposed impact model is a two mode (contact/loss of contact) model, where the contact is modelled as a Winkler-model (bearing bush is modelled as a radial spring-pillow) when in contact. The contact remaking pulling force doesn't exist as in the spring-damper model, thus larger inclination to contact loss behaviour than with a spring-damper model is expected. The model is verified against a four bar test model and experimental data from Seneviratne et al. (1996). The impact model was found to have the same kind of qualitative behaviour as the spring-damper model of Seneviratne. Chaotic behaviour is

observed between 94 and 205 r/min with a stiff bearing. Lower stiffness will reduce and smoothen the boundary. However, the lower boundary differs much from Seneviratne et al. (1996). One reason for this is that the external spring load used by Seneviratne is not described in a reproducible way. Better agreement is obtained with the results from Seneviratne and Earles (1992), which predict contact loss at 110 r/min with the previously mentioned conservative mass-less link model. The follower arrangement is also slightly different. An interesting finding observed during this research phase was, that vertical acceleration around 90 r/min is near zero-g with gravity included. This happens close to the observed lower chaotic boundary of 94 r/min, and can be one of the explaining factors for contact loss at that speed. When the vertical acceleration approaches zero the horizontal component still exists. None of the researches have considered the effects of radial friction, which should be a inclining factor for the lower contact loss limit. The discussion of friction influence is speculative, but addressing which factors should be included in future research.

Paper D: Optimisation a of servo system: the design of control, transmission and motor selection

In paper **D** a linear servo system transmission has been modelled and optimised. A gantry robot for handling of parcels, with three independent linear axes, was studied as an application. First, the kinematics and dynamics for an uncoupled, single axis system is derived and the principles for cycle time minimisation is shown, based on the assumption that the payload restricts the maximum allowed acceleration. Properties of electric motors, mainly DC motors, are discussed, and a simple mathematical model is derived. Finally, servo system design is discussed and a discrete block system submodel based on a total system simulation model comprising *motor model*, *mechanism model* and *control model* for the gantry robot system is presented.

The kinematic simulations presented in paper **A** were based on the assumption, that the proposed gantry robot configuration could achieve the *specified kinematics*. The simulation model which is presented in paper **D**, gave the *dynamic* performance with different motor size, transmission ratio and kinematic path configurations. The block system model results can be transferred back to the MBS model of the mechanical system in order to visualise the combined three dimensional simulations of the gantry robot.

Related to this thesis, the objective of paper **D** is to show, that properties of a product belong to different type of classes. Each class of properties should be modelled with the most suitable tool, to express one specific view of the product. The view selected in paper **D** is *dynamic system modelling by means of block representation*, which means, that the physical relationships are modelled and represented by discrete function blocks, and the relations between the blocks are defined by connections. The use of *block scheme*³ as a metaphor to represent the model of a dynamic system gives an intuitive description of the module structure and interrelations for the designer.

Paper E: Product Development and Performance Optimisation of Rock Drill Boomers

Paper **E** presents an alternative approach to multi body modelling as compared to papers **A**, **B** and **D**. A hydraulic rock drilling rig boom was studied as application. In paper **E**, the product model is transferred to the MBS program by creating a kinematic model file of the mechanism in CAD-software. To add visualisation, the geometry of movable frames of the robot is transferred as IGES

³**Block scheme** is a representation of a system where the elements are described and represented by function blocks in a plane and their relations are represented in form of connected lines. **Schema** is (in the philosophy of Kant) a rule or principle that enables the understanding to unify experience.

files part by part to the MBS-model. In frames where elasticity is needed, the geometry is transferred to a FEM-program, and then utilised as geometric boundary to define the FEM mesh. Very complex geometries are difficult to mesh, and therefore the geometry must be idealised not to include all irrelevant details leading to large, heterogenous and distorted meshes. Idealisation is sometimes required also for MBS visualisation reasons. The FEM mesh is then condensed to superelements to reduce the number of nodes in the FEM model, to some tens or hundreds in the MBS model. The reduced mesh is converted from FEM nodes and stiffness matrix, to MBS-frames and stiffness matrix. Finally, an elastic MBS model is obtained. The transfer process, especially for rigid models, can be automated with macro programming. For instance, the hydraulic drilling boom model can be converted to a rigid multi body model in a few minutes by means of pre-recorded macro routines. However, the loop from the definition of CAD model parameters to MBS model results is cumbersome, and it can be recommended only when a CAD-geometry already exists. In the development of new products, during conceptual design, the approach of paper E is not recommended.

Paper F: Configuration and Dimensional Synthesis in Mechanical Design: an Application for Planar Mechanisms

Design synthesis of machines and robots is traditionally a difficult and intuitive process. Computer support for synthesis has few general approaches. Main categories are databases of solution principles like TRIZ, Altschuller and Altov (1996) for general problem solving or the Alulib library for solution principles of aluminium profiles. However, within very restricted problem areas design rules can be modelled. Paper F presents an approach for automatic synthesis of planar mechanisms. The topological synthesis is modelled from Grüblers equation of a mechanisms degrees of freedom and from Eulers equation for numbers of kinematical loops in a mechanism, Freudenstein and Vucina (1991). As original contribution, by using the topological equations, a generative grammar for planar mechanisms is derived. This gives initial candidates for mechanism concepts, which then are subject to mechanism dimensional optimisation. To overcome the requirements of locking conditions, i.e. singularities due to dimensioning, a penalty function optimisation is used combined with the gradient method. The method for mechanism optimisation in this paper has been verified by two computer programs. For topological synthesis, a FORTRAN program was developed, which takes as input the link adjacency matrix of the initial topology. As output, the program writes the model file for the initial mechanism to ADAMS multi body program. ADAMS simulations are used in each iteration during the optimisation.

Appendix A: Derivation of the stiffness matrix for beam elements in MBS models

The assumptions for modelling of elasticity by massless beam elements, as well as the Timosenko beam model, accounting for shear deformation, are presented. Further, definitions of the shear stress asymmetric correction factors and the derivation of the beam element stiffness matrix are presented in detail.

7. Conclusions

In this thesis the use of multi body simulation as an essential part of the design process of mechanical systems, has been treated. Several different conceptual approaches to use multi body systems simulation as part of the product development process have been studied:

- Comparison of CAE modelling approaches in product development concerning CAD, FEM, MBS and block system modelling (paper A).
- Multi body simulation of industrial robots based on a modular, submodel integrated approach (paper B).
- Development of a joint clearance submodel to be used in multi body simulation (paper C).
- Multi body simulation based on off-line block system simulation of an uncoupled drive design (paper D).
- Multi body simulation based on CAD-geometry modelling (paper E).
- Synthesis of planar mechanisms for multi body simulation (paper F).

During the thesis work, a modular framework for the analysis and optimisation of a robots kinematic, dynamical, elastic and clearance properties has been developed. For this approach, different operation space definitions were compared for design specification, and the work cycle space was found to be the simplest one for concept analysis of robots. For the analysis of kinematic properties, an original method for evaluation of the kinematic Jacobian in multi body analysis was developed. For the analysis of a robots work space, a joint submodel for elasticity simulation of beams was derived and utilised for a parallel robot eigen frequency analysis. For model internal consistency validation, a method for comparing FFT of time plane simulation results to eigen mode solution of linear analysis was presented. An impact clearance model for a mechanism joint was developed and compared to other clearance models for joints presented in the literature. Using these results, a model for spherical and rotational clearance joints was developed and utilised in modelling of a parallel robot.

An alternative method for the use of multi body analysis is the utilisation of CAD geometry to build MBS models. By using CAD-geometry, also FE-mesh pre-processing can be utilised and imported to MBS-models. This approach has been utilised in the modelling of a hydraulic rock drilling rig boom. Control system models can be divided into several block system models, and the behaviour can be imported to an MBS-model. This approach has been applied to modelling of the uncoupled drive systems of a 3-axis gantry robot.

Findings

1. The selection of modelling tool for the simulation task is dependent of the actual design phase during product development. In conceptual design, modelling work utilising a parametrised MBS model is usually a faster way to model, due to the fact that geometries have not yet been designed in detail. The re-use of CAD-geometry for MBS model use is judged to be a feasible method in the analysis of established products, when most of the detail design has already been carried out. The need to import FE-structures is motivated if very complex geometries need to be analysed, e.g. vehicle bodies. The inverse approach, i.e. export of load cases from MBS simulation results, to study component design with FE-analysis is more often needed. For simple geometries elasticity can be represented in MBS models by coarse mass discretisation and chains of beam elements.

2. If a simple mechanical system can be modelled as block system model, e.g. in case of uncoupled drives, it is not motivated to use hybrid simulation (block systems simulation coupled to MBS).
3. The analysis of design concepts for three dimensional mechanisms can be semi-automated by definition of macro routines for performance specification and analysis of simulated performance, for different multi body model concepts.
4. For the application of planar mechanism design, the utilisation of graph theory enables systematic derivation of conceptual models. By utilising graph theory, the equations for degree of freedom and generative grammar, an original contribution to derive a grammar for synthesis of planar mechanisms was performed.
5. The persistent use of macro techniques and parametrisation is essential for effective MBS-modelling. They are the only two modelling technical prerequisites for component modelling to generate any possible product family configuration.
6. For the development of high-precision mechanisms, clearance free joint design has been a common principle. However, the non-linear contact mechanics related to clearance can not be avoided. The level of MBS-software is currently mature enough to facilitate inclusion of simple models for clearance, e.g. for joints and transmissions, to be integrated in MBS-models of precision mechanisms with reasonable numerical efficiency and computing time.

8. References

- Aasland, K., 1995. *Design methodology and product models*, Proceedings from Produktmodeller '95 conference, April 25-26, 1995, Linköping. pp. 49-59.
- ADAMS/FEA, 1994. *ADAMS/Finite Element Analysis Reference Manual*, Version 8.0, Mechanical Dynamics Inc., Ann Arbor, Michigan, 236 p.
- ADAMS, 1998. *ADAMS/Solver reference manual*, Version 9.1, Mechanical Dynamics, Inc., Ann Arbor, Michigan.
- Altshuller, G. and Altov, H., 1996. *And Suddenly the Inventor Appeared – TRIZ, the Theory of Inventive Problem Solving*, Technical Innovation Center Inc., Worcester, MA.
- Alulib, 1992. Skanaluminium, Oslo, 1992.
- Amirouche, F. M. L., 1992. *Computational methods in Multi Body Dynamics*, Prentice-Hall Inc., Englewood Cliffs, New Jersey, 478 p.
- Andersson, K., 1995. *NUTEK-ansökan 1995 - Projekt: Användaranpassad och effektiviserad funktionsmodellering och simulering vid produktkonstruktion*, Department of Machine Design, Engineering Design, KTH, Stockholm.
- Andreasen, M. M., 1980. *Syntesemetoder på systemgrundlag*, PhD thesis, Lund University, Lund.
- Andreasen, M. M., 1992. *The theory of Domains*, Technical Report, Institute for Engineering Design, Technical University of Denmark, Lyngby.
- Andreasen, M. M., 1994. *Modelling - The language of the designer*, Journal of Engineering Design, Vol. 5, No 2.
- Artobolewski, I., 1961. *The Theory of Mechanisms and Machines*, In Estonian: Mehhanismide ja Masinate Teooria, Estonian State Library, Tallin.
- Barker, C. R., 1985. *A complete classification of planar four-bar linkages*, Machines and Mechanisms Theory, Vol. 20, no. 6, pp. 535-554.
- Bathe, K. J., 1982. *Finite Element Procedures in Engineering Analysis*, Prentice-Hall, Englewood Cliffs, New Jersey.
- Blundell, M. V., Phillips, B. D. A. and Mackie, A., 1996. *The Role of Multibody Systems Analysis in Vehicle Design*, Journal of Engineering Design, Vol. 7, No. 4, 1996.
- Buur, J. and Andreasen, M. M., 1989. *Design models in mechatronic product development*, Design Studies, Vol 10, No. 2.
- Denavit, J. and Hartenberg, R. S., 1955. *A kinematic notation for lower-pair mechanisms based on matrices*, ASME Journal of Applied Mechanics, Vol. 2., no. 2, pp. 215-221.

Dobrjansky, L. and Freudenstein, F., 1967. *Some applications of graph theory to structural analysis of mechanisms*, Transactions ASME, Journal of Engineering Indices, Vol 89B, pp. 153-158.

Dubowsky, S., 1974. *On predicting the dynamic effects of clearances in planar mechanisms*, Transactions ASME, Journal of Engineering Indices, Vol. 96B.

Earles, S. W. E. and Killicay, O., 1980. *A design criterion for maintaining contact at plain bearings*, Proceedings, Institution of Mechanical Engineers, Vol 194, pp. 249-258.

Earles, S. W. E. and Wu, C. L. S., 1973. *Motion analysis of rigid Langrangian mechanics and digital computation*, Mechanisms (Proceedings, Institution of Mechanical Engineers), London, pp. 83-89.

Earles, S.W.E. and Wu, C.L.S., 1975. *Predicting the occurrence of contact and impact at bearing from zero-clearance analysis*, Proceedings of the 7th World Congress in Machines and Mechanisms Theory, IFToMM, Newcastle.

Earles, S. W. E. and Wu, C. L. S., 1977. *Determination of contact loss at a bearing of a linkage mechanism*, Transactions ASME, Journal of Mechanical Engineering Indices, Vol 97B, pp. 347-353.

Earles, S. W. E. and Seneviratne, L. D., 1990. *Design guidelines for predicting contact loss in revolute joints of planar linkage mechanisms*, Journal of Mechanical Engineering Science, Institution of Mechanical Engineers, London. Vol 204c, pp. 9-18.

Fawcett, J. N. and Grant, S. J., 1979. *Effects of clearance at the coupler-rocker bearing of a four bar linkage*, Mechanisms and Machines Theory, Vol 14(2) pp. 99-110.

Ferreirinha, P. et al., 1990. *TEKLA, A Language for Developing Knowledge Based Design Systems*, Proceedings of ICED 1990, Dubrownik, Heurista, Zürich.

Fertis, D. G., 1973. *Dynamics and Vibration of Structures*, Wiley, New York.

Finger, S. and Dixon, J. R., 1989. *A Review of Research in Mechanical Engineering Design. Part I: Descriptive, Prescriptive and Computer-Based Models of Design Processes*, Research in Engineering Design, 1(1), pp. 51-67.

Freudenstein, F. and Vucina, D., 1991. *An application of Graph Theory and Nonlinear Programming to the kinematic synthesis of mechanisms*, The Journal of Mechanisms and Machines Theory, Vol 26, pp. 553-563.

Van Griethuysen, J. P., 1992. *The Constructive-Deductive Design Approach – Application to Power Transmissions*, CIRP Annals, Manufacturing Technology, Vol. 41/1, pp. 169-172.

Haines, R. S., 1979. *Survey: Two-dimensional motion and impact at revolute joints*, Machines and Mechanisms Theory, Vol 15., pp. 361-370.

Hale, A. L. and Meirovitch, L., 1980. *A general substructure synthesis method for dynamic simulation of complex structures*, Journal of Sound and Vibrations, Vol 69, pp. 209-326.

Hubka, V. and Eder, W. E., 1988. *Theory of Technical Systems*, Springer-Verlag, Berlin, Heidelberg.

Huston, R. L., 1982. *Multibody Dynamics: Analysis of Flexibility Effects*, Proceedings of the 9th U.S. National Congress of Applied Mechanics.

Hyvönen, J. and Seppänen J., 1985. *Lisp world II: Programming Methods and –systems*, In Finnish: Lispmaailma II: Ohjelmointimenetelmät ja –järjestelmät, Kirjayhtymä, Helsinki.

Jahnke, M., Popp K. and Dirr, B., 1992. *Approximate analysis of flexible parts in Multibody systems using the finite element method*, In: W. Schiehlen (ed.), Advanced Multibody System Dynamics, Netherlands, Kluwer Academic Publishers, pp. 237-256.

Khatib, O., 1996. *Inertial Properties in Robotic Manipulation: An Object-Level Framework*, Int. Journal of Robotics Research, February 1, 1996, pp. 19-36.

Kiper, G. and Schian, D., 1976. *Collection of Gruebler Kinematic Linkages with up to Twelve Links*, In German. Verein Deutsche Industri, VDI-Z, Vol. 117, pp. 283-288.

Kjellander, J., 1995. *Produktmodeller i Skapandefasen*, Proceedings Produktmodeller-95, April 25-26, 1995, Linköping, pp. 121-128.

Klir J. and Valach, M., 1967. *Cybernetic modelling*, Iliffe Books, London.

Kota, S. and Chiou, S.-J., 1992. *Conceptual Design of Mechanisms Based on Computational Synthesis and Simulation of Kinematical Building Blocks*, AI EDAM, 6(2), pp. 95-109.

Liou, F. W. and Erdman, A. G., 1988. *Analysis of a high-speed flexible four-bar linkage*, Journal of Acoustics, Stress, & Reliability Design, Vol 111, pp. 35-47

Liou, F. W. and Patra, A. K., 1994. *An advisory system for the analysis and design of deformable beam-type multi-body systems*, Mechanisms and Machines Theory, Vol 29., No. 8, pp. 1205-1218.

Makkonen, P., 1993. *PLASMA - a Mechanism Synthesis Program*, Masters Thesis, Faculty of Mechanical Engineering, Helsinki University of Technology.

Makkonen, P., 1994. *Study of software tools*. In Swedish: Studie av programvaruverktyg, Internal report 94/3, Engineering Design, Department of Machine Design, KTH, Stockholm.

Makkonen, P. and Persson, J.-G., 1994. *Configuration and Dimensional Synthesis in Mechanical Design: an Application for Planar Mechanisms*, 43rd CIRP General Assembly, Singapore, Annals of the CIRP, Vol. 43/1/1994.

Makkonen, P., 1995. *An Effectivised Method for Mechanism Design: - an Application for the Design of Packing Machines*, Proceedings Produktmodeller-95, April 25-26, Linköping.

Malmquist, J., 1993. *Towards Computational Design Methods for Conceptual and Parametric Design*, PhD thesis, Machine and Vehicle Design, Chalmers University of Technology, Gothenburg.

Manolescu, N. I., 1964. Revue Romaine Sci. Tech. Ser. Mec. Appl., Vol 9., pp. 1263-1313.

Mortensen, N. H., 1995. *Linking Product and Product Life Modelling to Design Theory*, Produktmodeller '95 conference, April 25-26, Linköping, ISBN 91-7871-541-5.

- Mortensen, N. H., Svendsen, K.-H. and Hansen, C. T., 1993. *På vej mod en "Designer's Workbench*, Konstruktionsdag '93, Instituttet for Konstruktionsteknik, Danmarks Tekniske Højskole, Lyngby.
- Mruthyunjaya, T. S., 1984. *A computerised methodology for structural synthesis of kinematic chains*, Mechanisms and Machines Theory, Vol. 19, pp. 487-530.
- Natrayanaswami, R. and Adelman, H. M., 1974. *Inclusion of Transverse Shear deformation in Finite Element Formulations*, AIAA Jnl, Vol 12., No 11, pp. 1613-1614.
- Olson, D. G., Erdman, A. G. and Riley, D. R., 1985. *A systematic procedure for type synthesis of mechanisms with litterature review*, Mechanism and Machines Theory, Vol 20, no. 4, pp. 285-295.
- Ono, K. and Teramoto, T., 1993. *Minimum-Time Trajectory Planning for Multi-Degree-of-Freedom System under Average Heat Generation Restriction*, Robotics, Mechatronics and Manufacturing Systems, T. Takamori and K. Tsuchiya (Editors), Elsevier Science Publishers B. V. (North-Holland).
- Pahl, G. and Beitz, W., 1984. *Engineering Design - a systematic approach*, Springer Verlag, The Design Council, Berlin, London.
- Park, F. C., 1995. *Optimal Robot Design and Differential Geometry*, ASME Journal of Mechanisms, Transmissions and Automation in Design, Special 50th Anniversary Design Issue, Vol 117, June 1995, pp. 87 - 93.
- Prabhu, D. R., 1990. *Generation of Topology and Configuration of Power Specified Systems: A Methodology for design Automation*, PhD-thesis, Cornell University, Ithaca, NY, USA.
- Päärnä, A., 1989. *On the computer aided mechanism synthesis of robots, manipulators and 4-bar mechanisms*, PhD thesis, Acta Universitas Ouluensis, Series C Technica, Vol. 50, Oulu University, Department of Mechanical Engineering.
- Rajan, V. T., 1985. *Minimum time trajectory planning*, Proc. IEEE International Conference in Robotics Automation, pp. 759-764.
- Rauh, J., 1987. *Ein Beitrag zur Modellierung elastischer Balkensystem*, Fochr. Ber. VDI-Z, 18(37).
- Sanders, J. R. and Tesar, D., 1978. *The analytic and experimental evaluation of vibratory oscillations in realistically proportioned mechanisms*, Journal of Mechanical Design, Vol. 100, pp. 762-768.
- Sellgren, U., 1995. *Simulation driven design - A functional view of the design process*, Licentiate thesis, Machine Elements, Department of Machine Design, KTH, Stockholm.
- Sellgren U. and Drogou R., 1998. *Behavior Modeling in Mechanical Engineering – A Modular Approach*, Engineering with Computers Vol. 14. pp.185-196.
- Seneviratne, L. D., 1985. *A design criterion for maintaining contact at revolute joint with clearance*, PhD thesis, University of London.

Seneviratne, L. D. and Earles, S. W. E., 1992. *Chaotic behaviour exhibited during contact loss in a clearance joint of a four-bar mechanism*, Mechanisms and Machines Theory, Vol 27, No 3 pp. 307-321.

Seneviratne, L. D., Earles, S. W. E. and Fenner, D. N., 1996. *Analysis of a four-bar mechanism with a radially compliant clearance joint*, Institution of Mechanical Engineers, Journal of Mechanical Engineering Science, Proceedings, Part C., Vol 210, No C3, pp. 215-223.

Shabana, A. A., 1985. *Substructure Synthesis Methods for Dynamic Analysis of Multi-Body Systems*, Computers & Structures, Vol. 20, No. 4, pp. 737-744.

Sohn, W. J. and Freudenstein, F., 1986. *Application of Dual Graphs to Automatic Generation of the Kinematic Structures of Mechanisms*, Transactions ASME, Journal of Automation in Design, Vol. 108, pp. 392-398.

Soni, A. H., 1971. *Coupler coquates of eighth link mechanisms with ternary and quadternary links*, Transactions ASME, Journal of Engineering Indices, Vol. 93B, pp. 231-238.

Sorge, K., Bremer, H. and Pfeiffer F., 1992. *Multi-Body Systems with Rigid-Elastic Subsystems*, In: W. Schielen (ed.), Advanced Multibody System Dynamics, Kluwer Academic Publishers, the Netherlands, pp. 195-215.

Suh, N. P., 1988. *The Principles of Design*, Oxford University Press.

Sung, C. K. and Thompson, S. B., 1986. *Survey of Finite Element Techniques for Mechanism Design*, Mechanisms and Machines Theory, Vol 21. pp. 121-133.

Tomiyama, T., et al., 1989. *Metamodel: A Key to Intelligent CAD Systems, Research in Engineering Design*, (1989) 1: 19-34, Springer-Verlag, New York.

Turcic, D. A., Midha, A. and Bosnik, J. R., 1983. *Dynamic Analysis of Elastic Mechanism systems, PartII: applications and experimental results*, ASME Paper No. 83-WA/DSC-38.

Tuttle, E. R., Peterson, S. W. and Titus, J., 1988. *Enumeration of basic kinematic chains using the theory of finite groups*, ASME-American Society of Mechanical Engineers, Design Engineering Division DE v 15-1 PT1 September 25-28 1988, pp. 165-172.

Ulrich, K. T. and Seering, W. P., 1989. *Synthesis of Schematic Descriptions in Mechanical design*, Research in Engineering Design, Vol. 1, No. 1., pp. 3-18.

Woo, L. S., 1967. *Type synthesis of plane mechanisms*, Transactions ASME, Journal of Engineering Indices, Vol. 89B, pp. 159-172.

Zeid, I., 1991. *CAD/CAM Theory and Practice*, Department of Mechanical Engineering, Northeastern University, Mc-Graw Hill, ISBN 0-07-112901-4, Singapore.

Thesis context

1. INTRODUCTION.....	1
1.1 BACKGROUND	1
1.2 SCIENTIFIC APPROACH	2
1.3 CONTRIBUTION	3
1.4 OUTLINE OF THE THESIS.....	4
2. DESIGN THEORY AND COMPUTER SIMULATION MODELS IN PRODUCT DEVELOPMENT	6
2.1 BACKGROUND AND PREREQUISITES	6
2.2 PRODUCT SYNTHESIS	7
2.2.1 Computational design models.....	7
2.2.2 Descriptive design models	8
2.2.3 Prescriptive design models	8
3. SYNTHESIS OF MECHANISM SYSTEMS.....	12
3.1 SYNTHESIS METHODS FOR MECHANISM DESIGN.....	12
3.2 TYPE SYNTHESIS OF MECHANISMS	12
3.3 LOCKING CONDITIONS OF MECHANISM SINGULARITIES	17
3.4 DIMENSIONAL OPTIMISATION.....	19
4. RIGID BODY MODELLING AND MULTI BODY SYSTEMS SIMULATION.....	21
5. ELASTICITY AND CONTACT PHENOMENA IN RIGID BODY MODELLING	23
5.1 MODELLING OF STRUCTURAL ELASTICITY.....	23
5.2 MODELLING OF JOINT CLEARANCE	26
5.3 APPLICATION OF AN IMPACT TYPE CLEARANCE JOINT MODEL IN MBS SIMULATION OF THE DELTA PARALLEL ROBOT	31
6. SUMMARY OF PAPERS	33
<i>Paper A: Integrated CAD Methodology for Simulation Driven Product Development.....</i>	33
<i>Paper B: Framework for Modular Multi Body System model for Kinematic and Elastic Dynamic simulation of parallel robots.</i>	33
<i>Paper C: On the development of a planar clearance joint model for Multi Body System simulation</i>	35
<i>Paper D: Optimisation of servo systems: the design of control, transmission and motor selection.....</i>	36
<i>Paper E: Product Development and Performance Optimisation of Rock Drill Boomers.....</i>	36
<i>Paper F: Configuration and dimensional synthesis in mechanical design: an application for planar mechanisms</i>	37
7. CONCLUSIONS	38
8. REFERENCES.....	40

Integrated CAD Methodology for Simulation Driven Product Development

Petri Makkonen

petri@damek.kth.se

Royal Institute of Technology - KTH

1. Introduction

During the last decade, Computer Aided Design has changed much. The design modelling has largely altered from 2D draft modelling to 3D volume geometry models in mechanical industry. This is mainly due to the rapid development in computer performance and world wide competing software vendors who have developed high quality solid geometry modelers, which are fully parametrised, and thus contribute to easy and efficient modelling, parameter variation, component cataloguing and so on. Taking a 3D solid model as a base for the product model contributes integrated simulation: Finite Element Analysis (FEA) can be executed quickly with the aid of automatic mesh generation algorithms. FEA is also used for analysis of many different physical effects: Structural analysis, thermal deflections, vibrations, magnetic fields for instance. FEA can also be used for structural synthesis in mass optimisation. Multi Body Systems (MBS) analysis is used in the analysis of dynamic mechanical systems. ADAMS (Automatic Dynamic Analysis of Mechanic Systems) is perhaps the most used software for MBS-analysis.

The above mentioned development and the potential of these new simulation software tools addresses to several research questions: Which potential do they offer and how can they be utilised in most efficient way during the product development process. An interesting question is, what kind of emerging potential the concurrent and integrated use of different softwares and product models can offer for the product development process.

The aim of this paper is to discuss the properties of the above mentioned softwares and of the potential and possibilities in the integrated use of these softwares. Based on this introduction, an object oriented model for design process is presented. According to this model, a design methodology is presented, which utilises four different kind of simulation models concurrently. The models are: *parametrised solid geometry model*, *multibody systems simulation model*, *finite element structural analysis model* and *control systems simulation model*. A model for the simulation environment is presented which is expected considerably speed-up the design of dynamic mechatronic products or robots and manufacturing systems. The test case presents an inverse kinematic simulation model for a three axis gantry robot and the optimisation of robot design including servo motor and control system design.

2. Product design process

During decades number of design process models have been introduced. [Finger and Dixon] divide them to *prescriptive*, *descriptive* and *computational models*. An other classification of contributions to the field of design science can be described according to figure 1 [Hubka].

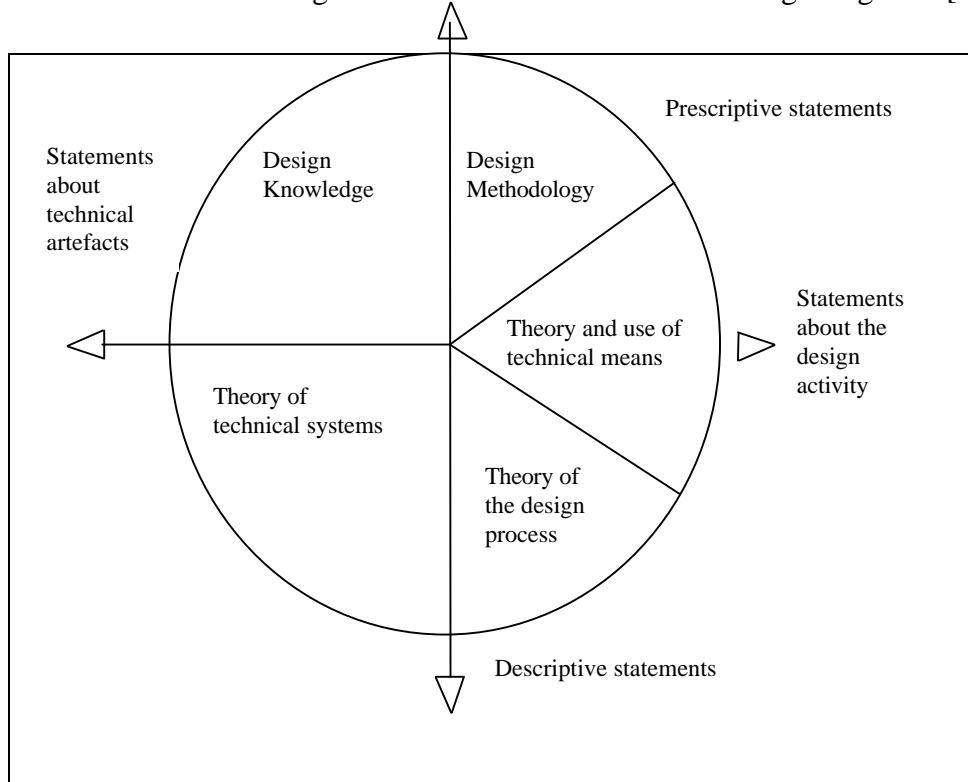


Fig. 1. The structure of contributions to design science. From [Hubka and Eder]

Prescriptive models of the design process provide instructions on how the designer should proceed in order to obtain a good design solution. A large number of process-orientated prescriptive models have been presented in the literature, for instance by Hubka and Eder, Adreasen, Pahl & Beitz, VDI2221, Ullman, Koller and Roth, not to mention other researchers contributions. While terminology and contents are varying, some common elements can be pointed out: The design process is generally viewed as a process in which an abstract problem formulation in terms of a "need" is successively transformed and concretised into a detailed manufacturable product description. The descriptive models of the design process derive their statements from physical laws and from the observation of properties and interrelations in machines. This view to machine design is very old: In 1875, one of the founders of mechanical engineering, Releaux, formulated a number of ideas about the various disciplines involved in mechanical engineering, and divided it to four domains:

- the study of machinery in general
- the special or theoretical study of machinery
- the study of machine design
- the study of pure mechanisms

In the study of machine design, the analytical and dimensioning approach has been dominant, but from the 1960's genuine theories about processes of synthesis in machine design have been

developed. Hubka, for instance, describes the machine design process based on systems theory: machines are seen as systems formed of parts and components and their interrelations. From this viewpoint the theory of technical systems is formed from four elements: [Andreasen]

- *Process structure* describes the input and output state of the operand and the state of partial processes as *transformation functions*.
- *Function structure* shows the *effects of purpose functions* that are needed in the machine to create the desired transformation of the operand.
- *Organ structure* is composed of the organs that are the function carriers of the technical system. Each organ realises one or more functions in the function structure through some physical effect.
- *Part structure* implement the organs and thus - via the process of assembly - implement the machine.

We have no possibility to go deeper into Hubka's theory in this paper, but some important notes should be made: [van Griethuysen] has described the reasons why synthesis is much more difficult than analysis: during analysis, information is irreversibly lost, which is demonstrated in fig 2.

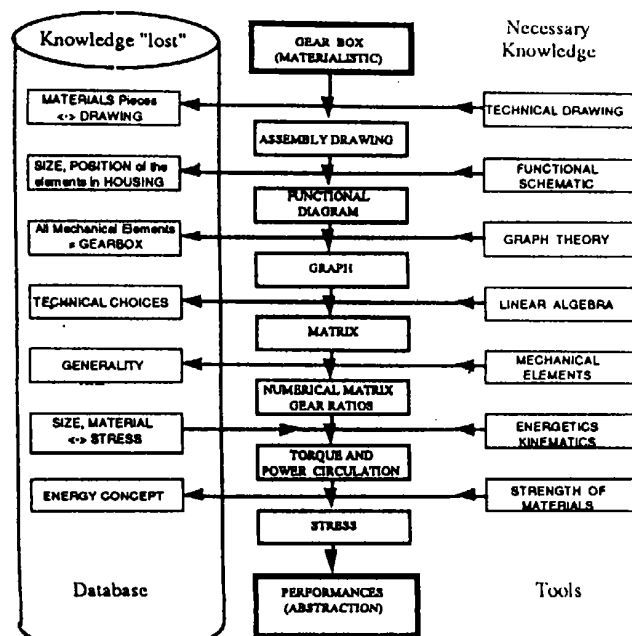


fig. 2 Loss of information in synthesis-analysis loop of transmission design. [Griethuysen]

When a mechanical system is designed much information must be created which has to be related to other information in the model in a consistent way. Complex constraining conditions of the design must be fulfilled, but during the analysis the constraining conditions are lost.

However, if the restrictions are mapped by a descriptive theory which models also the constraining conditions, the information of product topology is not lost and the product can be reconfigured. In the domain of mechanisms [Makkonen] has succeeded reconfiguring planar mechanisms by the use of graph theory.

According to industrial practice, the synthesis task is much restricted by the manufacturing technology and by other history in product families etc. The designers conceptual problem solving can be greatly aided, if the product model supports *manufacture feature modelling*. The CAD-system should support the designer by offering him parametrised feature catalogues of the factory's manufacturing system. However, the creativity in engineering design of machinery lies much in the search of topological conceptual solutions.

3. Object oriented model for the development of robotic products

The design process applied to robotic products, or more generally, products whose functional behaviour are characterised by complex dynamics, needs several different viewpoints, from conceptual design to a functionally verified product model which is used to produce the manufacturing data. For simulation of product behaviour, the most important properties of the product are its kinematic structure, geometry, inertia, structural stiffness, motor characteristics and control system performance. These properties define the dynamic behaviour of the product. These properties are nevertheless strongly coupled, since the geometry affects kinematics, inertia and structural stiffness. Together with motor characteristics and control system strategy these properties are affecting the dynamic performance of the product. Therefore a natural approach is to use the geometry model as a master model, which propagates its object (part) structure and attributes (data) to other models. The first model which should be propagated is then the Multi Body System Simulation (MBS) model which together with the Control System Model (CSM) can simulate the product dynamics. After having analysed the dynamic performance, the results of load history of the product can be propagated to the Finite Element Analysis (FEA) which can be used to optimise the structural properties. This in turn affects again on the dynamic performance which requires MBS and CMS simulation. After some zigzagging between models the system converges (hopefully) towards an optimum design. That design can be propagated back to the Geometry Model (CAD).

It is important to notice, that these models should not be of the level of detail. The geometry model is the most detailed level, since this is used also in the last phase of design, when the manufacturing data is produced, but the FEM and MBS models can be simplified and should concentrate on the most important organs and parts of the design.

An other important aspect is to couple this set of models to a pragmatic methodical model of the product development process. Since simulation results from the different models must be exchanged, the models can be used simultaneously and thus this product development methodology supports *concurrency*. As many different fields of expertise will be required for the different types of modelling the concurrency is supported even more, different specialists are allowed to work concurrently by contributing to the product design with tools familiar for them.

In time, the product development process can be divided in a sequence of activities. Hubka and Pahl & Beitz separate the product development process roughly into the following activities:

1. Elaboration of the assigned problem
2. Conceptual design
3. Laying out - Embodiment design

4. Detail design

While Pahl & Beitz's model doesn't explicitly couple knowledge of machine design theory to the different phases of the design process, Hubka's *General Procedural Model of the Design Process* (GPMDP) is integrated from two other aspects. Firstly, the different aspects to machine design (the theory of Domains) are integrated into the design process. The process structure, function structure, organ structure and component structure are modelled in the different phases of design and thus the *causality relations* are understood in a much better way. Secondly, GPMDP allows the integration of theories and knowledge of special domains of machine design, like shipbuilding or robotics design. In this way Hubka's GPMDP represents better the requirements on decent theories for engineering design:

"It is better to have a naive theory of sophisticated knowledge, than to have a sophisticated theory of naive knowledge."

In this paper we adopt and modify the Hubka's *General Procedural Model of the Design Process* to structure the time scale of the *Integrated Simulation Driven Design Process* (ISDDP). In figure 3. a schematic representation of an object oriented model of ISDDP is represented. In this case, the ISSDP approach is applied to robot design. The special knowledge of robot design is integrated to the design process while at the same time the process model contributes to *concurrent engineering* with different simultaneous simulation models and Hubka's GPMDP with elaboration, conceptual design, embodiment design and detail design.

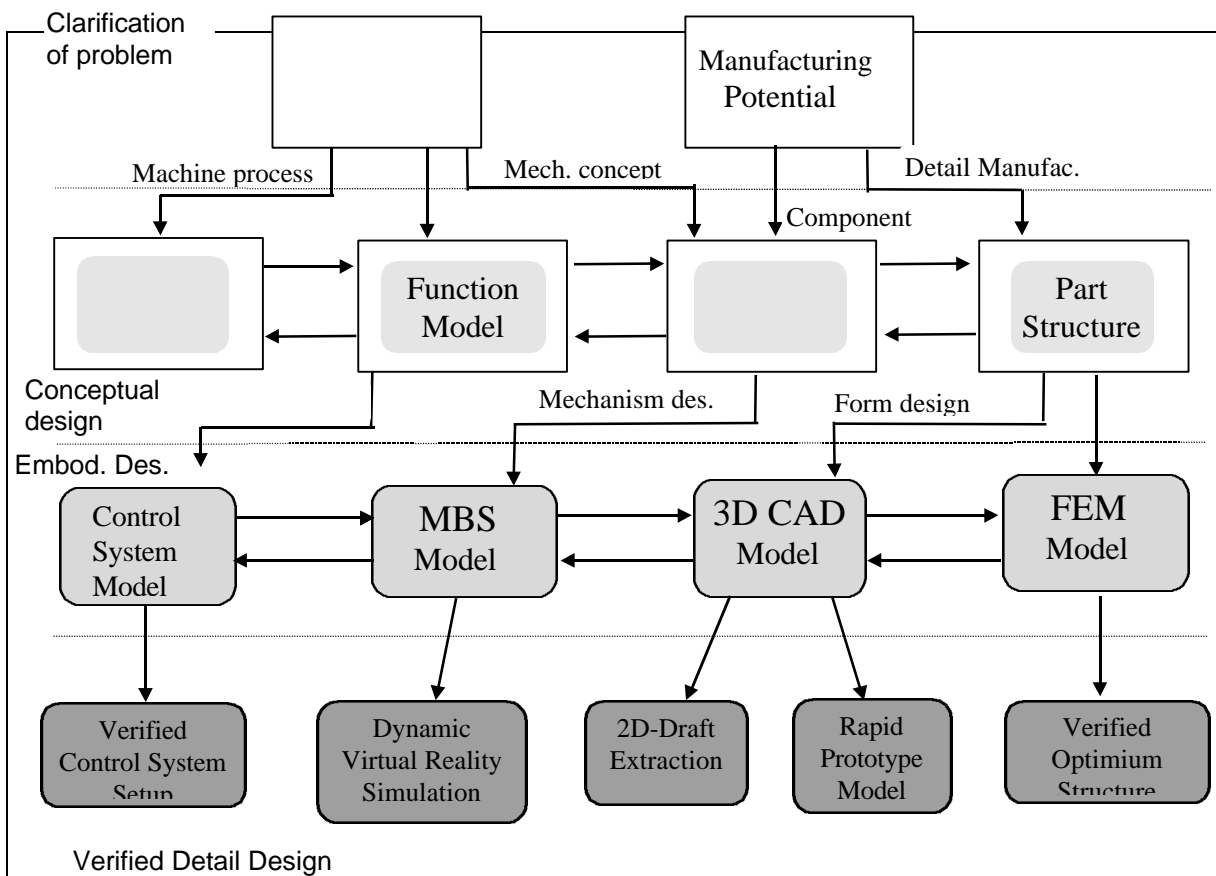


Fig. 3. *Integrated Simulation Driven Design Process*.

4. Integrated Simulation Environment for Product Development

The *Integrated Simulation Driven Design Process* approach could be used for establishing a computer aided simulation environment, as central part of the design process. The design modelling begins in MCAE-software e.g. IDEAS, where a parametrised 3D-Solid model is developed. By utilising component libraries and application software to represent the different viewpoints of the Theory of Domains, a solid structure is constructed for the product. This will be the master model of the product. By using assembly application software, the products assembly structure is modelled, and the kinematic/dynamic simulation model can be built. This model is transferred to ADAMS mechanisms simulation software to simulate the dynamic performance of the design. With control systems simulation software, like Simulink in MATLAB, a control system simulation model is built and linearised in MATLAB. The steering matrixes are transported to ADAMS, and the functional behaviour of the integrated mechanism-control system model can be simulated. A special FORTRAN application subroutine package CONSUB, which has been developed in this research project, integrates various simulation subroutines to the system. There are subroutines for interactive kinematic simulation (*Virtual Reality Testing*) for robot systems and a non-linear control systems integration software for Simulink, which is still under development. By using optimisation and Design-of-Experiments functions in ADAMS, design changes must be propagated to the Master Model. During the dynamic simulation, the structural forces are solved, and they can be modelled with IDEAS or ANSYS FEM simulation software for stress and flexural analysis. Research on modular FEM simulation with IDEAS is carried out at KTH for UVA grinding machines [Sellgren]. In Figure 4, a model for computer aided Integrated Simulation System (ISS), is presented. This system is partly implemented, and still under development.

Integrated Simulation System

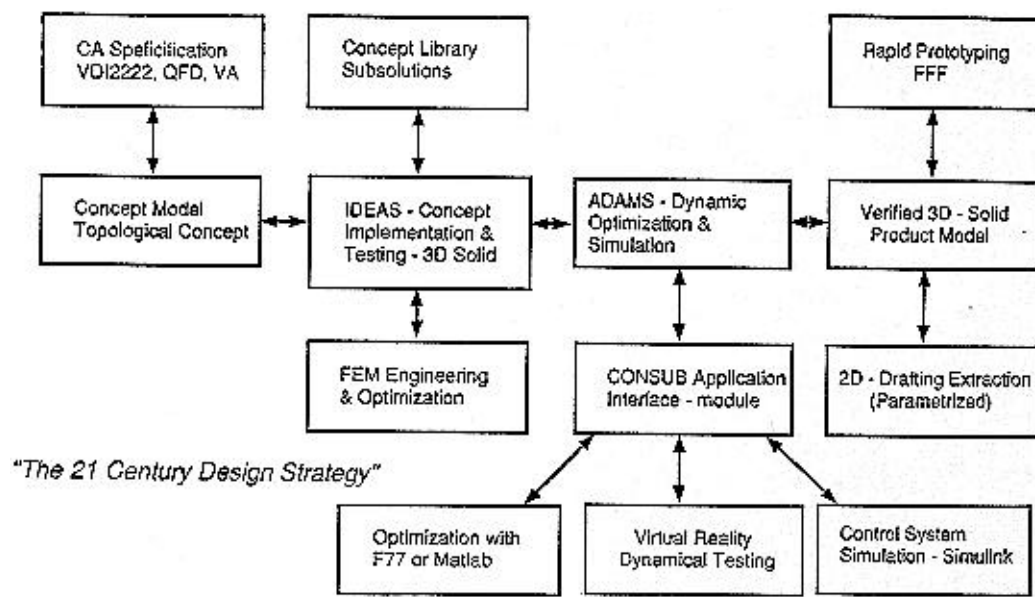


Fig. 4. Integrated Simulation System for industrial robot design.

5. ADAMS Dynamic Systems Simulation Software

ADAMS supports the designer for many different types of analysis. The appropriate analysis is much dependent of the total degree of freedom of the system to be analyzed. The degree of freedom for a mechanism is defined by Kuzhbach's equation (1):

$$\begin{Bmatrix} F_2^e \\ F_3^e \end{Bmatrix} = \begin{bmatrix} K_{22}^{II} & K_{23}^{II} \\ K_{32}^{II} & K_{33}^{II} \end{bmatrix} \begin{Bmatrix} x_2 \\ 0 \end{Bmatrix} \quad (1)$$

Where F = Systems total degree of freedom.

Z = General degree of freedom for each part. (6=spatial, 3=planar mechanism).

N = Number of bodies in the system (ground included).

n_i = Number of parts having i degrees constraints.

If F is greater than zero, the system is underconstrained, i.e. a dynamic system. If F is zero the system is a mechanism, and if F is less than zero, the system is overconstrained. If an overconstrained system can still move kinematically, ADAMS simulates it, required that the constraints are redundant and they can be removed.

Depending on the design task, the designer can do following analysis:

- *Static analysis* determines a state for the system in which all of the internal and external forces are balanced in the absence of any system motions or internal forces. It determines which external forces are required to keep the system static in the given configuration, and which internal forces it causes.
- *Quasi-Static Analysis* (Kinetostatic analysis) is a sequence of static analyses performed for different configurations of the system. Typically it is used to determine the static balance of the system in different positions.
- *Kinematic Analysis* allows the user to analyse a fully kinematically determined system (a mechanism, by definition). The path curves, displacements, velocities and accelerations at any point of interest can be determined for a mechanical device. If the masses and inertia properties are defined, ADAMS calculates the internal and constrained forces in the mechanism. Quasi-Inverse kinematics can be carried out from kinematic analysis by requesting the external forces and torque on the axles of motions. ADAMS determines the required forces and torques to implement the motion.
- *Dynamic Analysis* provides the time-history solution for all displacements, velocities, accelerations and internal forces in a mechanical system driven by a set of external forces and excitations. The analysed system cannot be kinematically determined, it simulates systems, that have several degrees of freedom.
- *Linear Analysis* is done by separate package ADAMS/Linear, which performs a linearisation of the mechanical system in a given configuration point. The analysis gives as a results the standard state equation matrixes.
- *Transient Analysis* selects automatically the appropriate simulation type for a mechanism system. If the system has zero degree of freedom, then a kinematic analysis is performed. If the system has more than zero degrees of freedom, a dynamic analysis is performed.

The numerical stability of ADAMS is high and the results are in most cases very reliable. The reason for this is, that ADAMS checks the changes of each simulation step. If great changes are observed ADAMS starts a complex algorithm, which corrects the simulation errors and

reduces the step size. Comparing the average experiences for instance to MATLAB/Simulink-system, the numerical stability is adjusted in a much more automatic way, and the user doesn't need to stress of numerical algorithms stability so much as in MATLAB/Simulink.

ADAMS offers also tools for the design studies and optimisation. The Design-Of-Experiments-option offers a multi-factorial analysis with parameter variation. Thus ADAMS can produce results from changing values of design parameters, and gives the designer an estimation of the designs sensitivity to design parameters. The optimisation-option allows the user to define an arbitrary objective function, which ADAMS tries to minimise or maximize by finding the optimum values of the design parameters.

6. Case study: Gantry robot drive configuration design

ABB Production Development produces manufacturing systems. One major product is the gantry robot model 100. Each unit is modified according to various customer performance requirement specifications. A dynamic simulation model was developed which simulates the operation of the robot in two ways: Firstly, an inverse kinematic analysis is executed to simulate forces acting on the pay-load, as well as on robot motors and transmission system. A CAD-model is illustrated in figure 5.

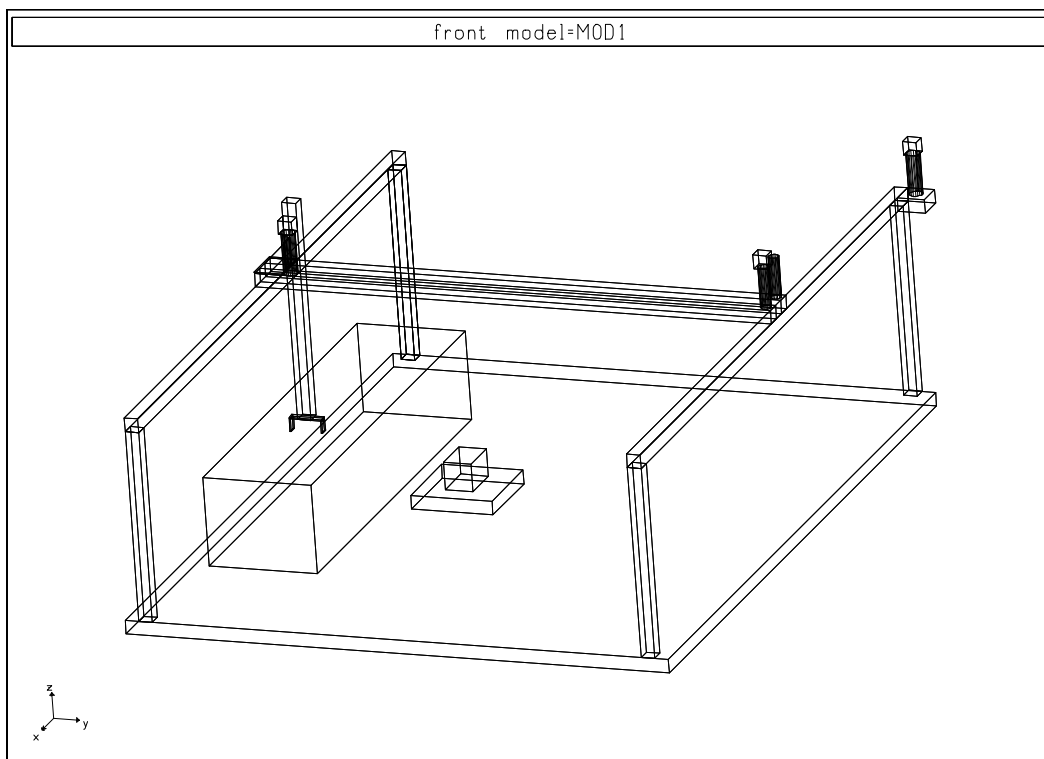


Fig. 5. Geometry model of the ABB robot.

The kinematic path was programmed using a fuzzy logic approach. The path was modeled separately for each axis X, Y and Z. The sequence of path-movements are activated as a sum of single path-axis-profiles, which are activated and deactivated by multiplying them with fuzzy activation functions having value 1 when activated and 0 when deactivated. Equation 2. describes the total kinematic function:

$$\mathbf{x}(t) = \sum_{i=1}^n \mathbf{s}_i(t) f_i(t) g_i(t) \quad (2)$$

Where

- $x(t)$ = total kinematic equation
- $x_i(t)$ = ith kinematic profile
- $s_i(t)$ = ith profile
- $f_i(t)$ = Activation time for i:th function
- $g_i(t)$ = Deactivation time for i:th function

One example of a fuzzy logic function of this type is given below:

```

! Funktionerna, som definierar robotsystemets kinematik. PM950503
constraint modify motion_generator &
motion_name = MOT_X_1 &
function =
"HAVSIN(TIME,0,0,0.05,250)*STEP(TIME,0,0,0.01,1)*STEP(TIME,0.04,1,0.06,0)", &
" +250*STEP(TIME,0.04,0,0.06,1)*STEP(TIME,0.54,1,0.56,0)", &
" +HAVSIN(TIME,0.55,250,0.82,-700)*STEP(TIME,0.54,0,0.56,1)", &
" *STEP(TIME,0.81,1,0.83,0)", &
" +HAVSIN(TIME,0.82,-700,1.05,0)*STEP(TIME,0.81,0,0.83,1)", &
" *STEP(TIME,1.04,1,1.06,0)"

```

The ideal path profile function should be obtained from double time integration of a linearly increasing acceleration / deceleration profile as shown in figure 6. A separate FORTRAN subroutine function is currently under development to describe the integral function which can be called from ADAMS.

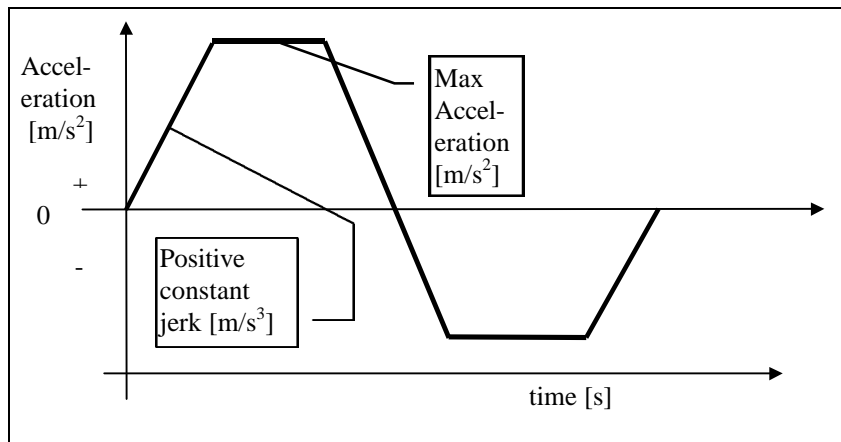


Fig. 6. Ideal jerk restricted acceleration profile

After having created the dynamic model of a robot, and having simulated it's inverse kinematics, robot path profiles, motors and transmissions can be optimized. ADAMS system can be used to calculate and plot position, velocities , hodographs, accelerations, etc. In figure 7. a velocity profile is shown.

Fig. 7. Velocity profile of the robots axis.

The next phase of the development project is to create a motor and control system simulation model by using a control systems simulation software, e.g. MATLAB/Simulink. This model is transferred to ADAMS, while the mechanism model is reconstructed from the CAD-model. The results from dynamic analysis are then FEM-analysed for stresses and deflections. In figure 8. a planned model for an integrated simulation system is shown. It combines the *motor torque control* model from Simulink with the *MBS-model* of ADAMS, which interacts with the *CAD master model* and exports it's geometry and stresses to the ANSYS *FEM-model*.

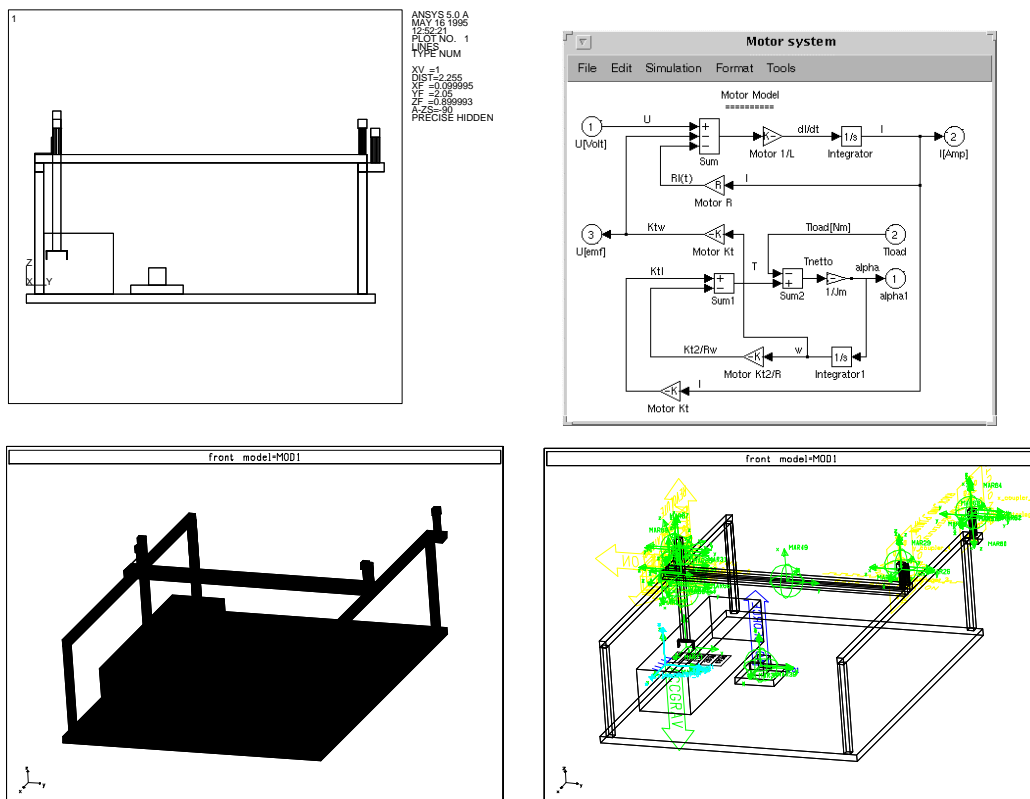


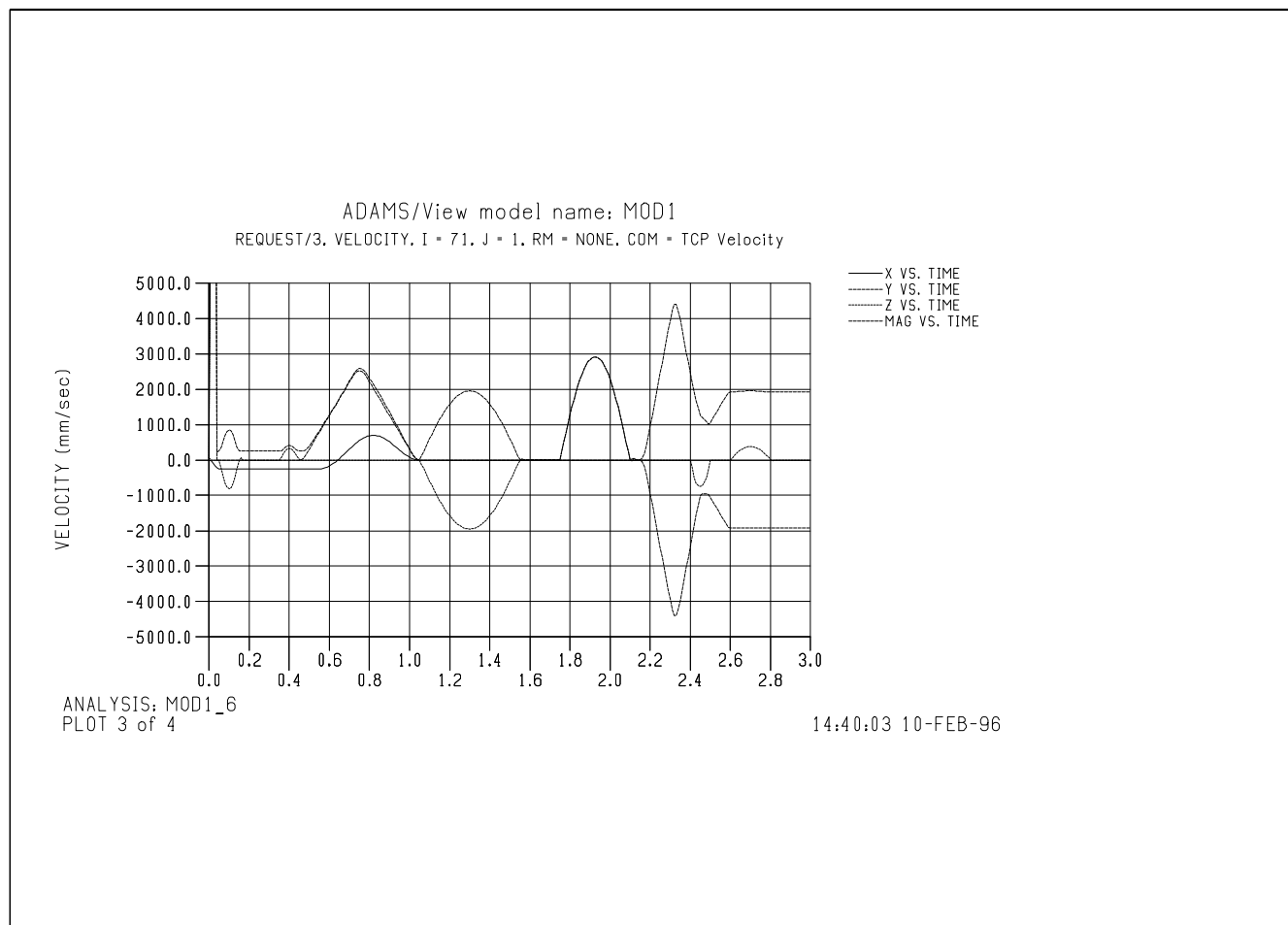
Fig. 8. Integrated Simulation System model (ISS) for a portal robot.

7. Discussion

There is yet a lot to do in this research project, but preliminary results from integrated simulation have given promising results. The industrial response to the project has been positive, and we plan to continue by integrating the control systems model to an MBS-model.

8. References

1. Andreasen, M. M., The theory of Domains. Technical report, Institute for Engineering Design, Technical University of Denmark, 1992.
2. Finger, S. and Dixon, J. R., A Review of Research in Mechanical Engineering Design. Part I: Descriptive, Prescriptive and Computer-Based Models of Design Processes. *Research in Engineering Design*, 1(1):51-67, 1989.
3. van Griethuysen, J.-P., The Constructive-Deductive Design Approach - Application to Power Transmissions, *CIRP Annals, Manufacturing Technology*, Vol 41/1, pp 169-172., 1992.
4. Hubka, V. and Eder, W. E., Theory of Technical Systems. Springer-Verlag, Berlin, Heidelberg, 1988.
5. Makkonen, P., PLASMA - A Mechanism Synthesis Program. Masters Thesis, Helsinki University of Technology, 1993.
6. Pahl, G. and Beitz, W., Engineering Design. Springer-Verlag, Berlin, Heidelberg, 1984.
7. Sellgren, U., Functional Views of Product Models. *Produktmodeller '95*, 25.-26.4.1995, Linköping. ISBN 91-7871-541-5.



Framework for Modular Multi Body Systems Model for Kinematic and Elastic Dynamic Simulation of Parallel Robots

Petri Makkonen

Department of Machine Design, Engineering Design
Royal Institute of Technology, KTH

List of Symbols

A	Area of cross section	R	Radius of bearing eye
b	Work cycle path length parameter	r	Radius of bearing pin, Cartesian coord. vector of TCP
C	System damping matrix	\mathbf{dr}	Infinitesimal vector displacement of TCP
$C_i(q)$	Joint damp coupling matrix	r_A	Vector position of rigid beam end A
$c_i(q)$	Position dependent coupling matrix	r_B	Vector position of rigid beam end B
$c(q, \dot{\varphi})$	Damping vector function of joints	$r(q)$	TCP path of kinematic/dynamic model
C_{max}	Damping of bearing contact	$r_e(q)$	TCP path of elastic model
D_{tcp}	Work tool plate diameter	$\dot{\mathbf{r}}$	TCP velocity in Cartesian coordinates
D_{base}	Base plate diameter	$\ddot{\mathbf{r}}$	TCP acceleration in Cartesian coordinates
d	Distance between pin and journal axes, damping ratio between matrixes	$r^{-1}(r(t))$	Inverse kinematic function
d.o.f.	Mechanical degree of freedom	S	Relative reachability index in angular space, static surface moment
e	Material elasticity exponent	s	Spline polynomials
E	Modulus of elasticity	T	Torque, kinetic energy, time interval
F	TCP Cartesian force and torque vector	TCP	Tool Center Point
F_s	Bearing support force	t	Time, cycle time
$f()$	Trajectory movement function	U	Orthonormal base matrix for manipulability ellipsoid
$g(q)$	Gravity force vector function on joints	u_i	Eigenvectors of $J(q)$
h	Work cycle trajectory heighth	u	Vector of displacements in elastic system
h_{tcp}	Height of TCP plate	\dot{u}	Vector of velocities in elastic system
I	Quadratic surface moment, unit matrix	\ddot{u}	Vector of accelerations in elastic system
J	Moment of inertia	\ddot{u}_r	Vector of accelerations in rigid system
J_m	Rigid structure inertia	x, y, z	Cartesian coordinates
$J(q)$	Jacobian of TCP with respect to joints	z	Transmission reduction ratio
J_{ij}	Element ij of Jacobian matrix	\mathbf{Da}	Angular displacement around x-axis
\mathfrak{J}	Joint space	\mathbf{Db}	Angular displacement around y-axis
K	Position dependent stiffness matrix	\mathbf{Dc}	Angular displacement around z-axis
K_g	Gear angular elasticity	e	Joint bearing penetration
K	Jacobian matrix condition number	q	TCP space angle area
l_u	Upper link length	z	Asymmetric shear stress correction factor
l_v	Lower link length	k	Beam shear deformation contribution
$l_{y,z}$	Beam cross section local width in z resp. y direction	$L(r)$	Kinetic energy matrix
L	Beam element length	I	Eigenvalues
M	Mass matrix, beam moment over cross section	$\mathbf{m}(r, \dot{\varphi})$	Centrifugal and coriolis force vector
$M(q)$	mass matrix (n x n) in joint space	\mathbf{f}	TCP orientation vector
m	Mass, number of joint coordinates	Π	Heaviside function
m_i	Mass of i th rigid body in model	p	Dimensionless geometry parameters
m_{ij}	ij th element of mass matrix	t	Joint actuator torque vector
m_r	Mass of original rigid body	t_m	Joint actuator torque matrix
N	Normal force in beam cross section	j	Shaft rotation position
n	Number of TCP coordinates, number of elastic beam elements	\dot{j}	Shaft rotation velocity
P	Power	\ddot{j}	Shaft rotation acceleration
$p(r)$	Gravity vector	c	TCP location vector
q	Joint coordinate position vector	w	Motor angular velocity
$\dot{\varphi}$	joint (angular) velocity	Indices:	
$\ddot{\varphi}$	joint (angular) acceleration	a	Motor shaft
$\ddot{\varphi}_e$	joint velocity error vector	$amax$	Maximum value of all motors
q_{min}	Joint coordinate minimum limit	e	Elastic path
q_{max}	Joint coordinate maximum limit	g	Motor air gap
Dq	Joint displacement length where stopper torque changes from zero to maximum	m	Mechanism (robot joint) shaft
dq	Infinitesimal vector displacement of joints	min, max	Minimum resp. maximum value during cycle
\mathfrak{R}	Work space	l_u	Lower resp. upper link
		TCP	Tool Center Point

Abstract

Multi body system simulation is used for modelling and simulation of all kinds of mechanisms, robots and other mechanical systems, which are characterised by their dynamical behavior. When such devices are designed for requirements of high-speed and high accuracy the modelling obligates to include elastic and contact mechanical phenomena. The complexity of simulation increases, and careful consideration is required, to maintain simulation activities integrated to the phases of the product development process with minimum effort spent. The study in this paper presents as an example some of the design parameters of the parallel robot DELTA and it's most characterising performance measures in kinematic, dynamic, elastodynamic and contact mechanical sense. The selection of coordinate space representation for requirement specification is discussed in joint, work and work cycle space. The kinematic Jacobian is discussed, and a method for calculating it with multi body system software by utilising unit force method is shown. Based on the considerations of property driven design, a framework for an elastodynamic and contact mechanical multi body simulation is outlined. The modelling of beam structure elasticity and contact problems of ball joints are shown. Finally, as an example of the methodology, the simulation of dexterity, kinematic isotropy and actuator's load sensitivity of main dimensions is demonstrated, as also the elasticity properties dependence of linkage material and cross-section parameters. The simulation of path accuracy has also been shown. This proposed methodology is implementable with most of the commercial numerical three dimensional multi body systems software, independent of brand.

1. Introduction

The objective of this paper is to present a framework for the use of multi body system (MBS) simulation to support design decision making based on performance in an industrial product development project of parallel robots. The framework describes a product concept independent MBS metamodel for the analysis of kinematic, dynamic and elastodynamic properties as a function of design parameters.

Some of the most common performance measures in the literature for robots are presented. The characterisation of performance measures and the selection of coordinates, Khatib (1995) is discussed to identify the measures applicability for the presented modelling approach.

The results show some of the details of the simulation methodology. First the kinematic inverse and work space analysis is presented, then dynamic work cycle analysis of actuator loads and finally, simulation of eigen frequency variation in different postures within the workspace.

2. On the characteristics and performance measures of robots

2.1 Mechanical performance measures of robots

The main parameters of a robot related to mechanical structures are according to Rivin (1987):

- Payload
- Mobility, i.e. degree of freedom, singularities
- Workspace (volume, shape, degree of redundancy, positioning and orientation volume)
- Accuracy and repeatability of positioning in various locations and load conditions
- Structural stiffness, masses, damping coefficients and natural frequencies
- Economy (cost, reliability, maintainability, etc.)

Most of the parameters above e.g. maximum payload, accelerations and accuracy are interrelated and dependent on TCP instant velocity and position in workspace. However, definitions and test procedures for the measures are not yet completely established enabling valid comparative analysis between different design concepts.

The dynamical performance of a manipulator depends strongly on the inertia and acceleration characteristics of the end effector. Much research effort has been placed on developing performance measures depending on different operation space definitions, like joint space or work space, e.g. Khatib (1996). Much research has been directed to identifying and quantifying certain measures to achieve some "optimisation" definition. These definitions lack however the criteria for a useful measure: It should be formulated so, that it reflects the intrinsic properties of the mechanism. It should also be invariant of the selection of coordinate system, enabling comparison between different concepts, and account for the non-linearity of the configuration space, Park (1995). The computational effort for achieving the measure should be reasonable, though many reports don't consider the numerical costs of predicting these measures.

One of the objectives in this paper is to identify a method to describe the specifying geometric and material related characteristics of robots in a modular way, so that different model levels and viewpoints maintain transparency. A specific goal is to describe the specifications for performance measure analysis suitable for general purpose MBS-formalism that are numerically inexpensive, but still representative enough to describe the different operation and load conditions. Therefore, when suitable measures to study the dexterity and agility with numerical MBS are selected, the way of representing the coordinate space and the locality vs. globality of the measures must be considered.

2.2 Coordinate space representations

It is quite obvious, that reachability and agility of the Tool Center Point (TCP) are some of the most important characteristics related to robot mechanisms work space. It is common, that the work space volume is divided into two components, *reachable* and *dexterous* work space volume e.g. Kumar and Waldron (1981). The reachable work space includes all the points reachable by the end effector, while the dexterous workspace is restricted to the space reachable with any arbitrary orientation of the TCP. The angular reach at the given point P in workspace is called reachability index S, the ratio between space angle area \mathbf{q} of all possible angles of TCP at point P and the space angle of a sphere.

$$S = \frac{\mathbf{q}}{4\pi} \quad (1)$$

2.3 Kinematic Jacobian

The direct kinematic solution defines a robot's position in Cartesian space as a function of generalised coordinates. The generalised coordinates are the arbitrarily selected complete set of lengths, angles and other scalar quantities, that uniquely define the instant configuration of a mechanical system. In robotics, the generalised coordinates are usually represented by a coordinate vector \mathbf{q} , which defines the positions of independent joints, i.e. the actuator positions.

Since the actuator coordinates define the complete configuration of the robot, all coordinates of every part of the robot are a function of the joint coordinate vector \mathbf{q} . Thus the Cartesian coordinates of the TCP in ground frame can be written as a function of \mathbf{q} :

$$\underset{nx1}{r} = r(\underset{mx1}{q}) \quad (2)$$

The TCP vector r defines the position of the TCP. Its dimension n is equal to the robots degree of freedom. The vector \mathbf{q} includes the joint coordinates, where m is the number of actuators¹. For a 3 d.o.f. positioning robot r is a of size (3x1) $\mathbf{c} = (x,y,z)^T$. A complete 6 d.o.f. robot has the r -vector size (6x1) consisting of both position vector $\mathbf{c} = (x,y,z)^T$ and orientation vector $\mathbf{f} = (\mathbf{f}_1, \mathbf{f}_2, \mathbf{f}_3)^T$ represented in some appropriate coordinate system, i.e. using the Euler angles method.

The robots TCP's kinematic sensitivity of actuator movements is determined by the vector derivative, the Jacobian. Writing equation (2) in component form gives:

¹ To be kinematically actuator determined, all robots must have $m \geq n$. For ordinary robots $m = n$, i.e. there are as many actuators as the robot has degrees of freedom. In actuator redundant robots, $m > n$, in order to enhance performance i.e. to avoid singularities.

$$\begin{aligned} r_1 &= r_1(q_1, q_2, \dots, q_m) \\ r_2 &= r_2(q_1, q_2, \dots, q_m) \\ &\dots \\ r_n &= r_n(q_1, q_2, \dots, q_m) \end{aligned} \quad (3)$$

To calculate the time derivates of r_i expressed in q_j , we use the chain rule of derivation, and write the derivative in matrix form:

$$\left[\begin{array}{c} \dot{r}_1 \\ \dot{r}_2 \\ \dots \\ \dot{r}_n \end{array} \right] = \left[\begin{array}{cccc} \frac{\partial r_1}{\partial q_1} & \frac{\partial r_1}{\partial q_2} & \dots & \frac{\partial r_1}{\partial q_m} \\ \frac{\partial r_2}{\partial q_1} & \frac{\partial r_2}{\partial q_2} & \dots & \frac{\partial r_2}{\partial q_m} \\ \dots & \dots & \dots & \dots \\ \frac{\partial r_n}{\partial q_1} & \frac{\partial r_n}{\partial q_2} & \dots & \frac{\partial r_n}{\partial q_m} \end{array} \right] \left[\begin{array}{c} \dot{q}_1 \\ \dot{q}_2 \\ \dots \\ \dot{q}_m \end{array} \right] \quad (4)$$

or in a more compact vector form:

$$\dot{\mathbf{r}} = J(\mathbf{q}) \dot{\mathbf{q}} \quad (5)$$

Equation (5) is usually written:

$$\dot{\mathbf{r}} = J(\mathbf{q}) \dot{\mathbf{q}} \quad (6)$$

$J(\mathbf{q})$ is called the Jacobian matrix where each element is defined as:

$$J_{ij} = \frac{\partial r_i}{\partial q_j}, \quad i = 1 \dots n, j = 1 \dots m \quad (7)$$

From (6) we get the relation between TCP position and joint coordinates for an infinitesimal displacement:

$$\dot{\mathbf{r}} = J(\mathbf{q}) \dot{\mathbf{q}} \quad (8)$$

2.4 The Kinematic Jacobian in Force Domain

The kinematic reachability (dexterity) of a robot arm requires that the kinematic workspace has no singular points, where the robot can loose one or more degrees of freedom. In the neighborhood of singular points the actions of the manipulator are not well conditioned, and the linear transformation (5) becomes non-invertible. There exist two main categories of singularities, Craig (1989):

- All manipulators have a **workspace boundary singularity** when the robot is fully stretched out or folded back on itself

• **Workspace interior singularities** may occur away from the boundaries inside the workspace generally caused by two or several lining up links.

The variation of the Jacobian in the robot work space is an important performance characteristics not only for invertability; many important performance

characteristics are related to it like *isotropy*, *condition number*, *minimum singular value*. Thus it is important to be able to analyze the Jacobian in work space. Multi body systems software have weak support tools for this kind of analysis, but by using the principle of virtual work the Jacobian can be easily computed by MBS software, when applying the following analysis method:

Assuming no external static load (zero gravity conditions) and no inertia load, i.e. a quasistatic approach, the principle of virtual work requires that there is an energy balance between the work performed in joint space compared to work performed in work space. Thus the energy must be the same in any set of generalised coordinates. We get the dot products relation:

$$\mathbf{F} \cdot \mathbf{dx} = \mathbf{t} \cdot \mathbf{dq} \quad (9)$$

where \mathbf{F} is a Cartesian force-torque vector acting at the TCP, \mathbf{dx} is the Cartesian displacement of TCP, \mathbf{dq} is the displacement in joint coordinates and \mathbf{t} is the joint torque vector. In matrix form the equality becomes:

$$\mathbf{F}^T \mathbf{dx} = \mathbf{t}^T \mathbf{dq} \quad (10)$$

From eq. (4) we get:

$$\mathbf{dx} = \frac{\partial \mathbf{x}}{\partial q} \mathbf{dq} \quad (11)$$

Substituting eq. (11) in to eq. (10) we may write

$$\mathbf{F}^T \frac{\partial \mathbf{x}}{\partial q} \mathbf{dq} = \mathbf{t}^T \mathbf{dq} \quad (12)$$

This must hold for all \mathbf{dq} , and thus we get the joint force vector as a function of the TCP force vector

$$\mathbf{F}^T J(q) = \mathbf{t}^T \quad (13)$$

or by transposing:

$$\mathbf{t} = J(q)^T \mathbf{F} \quad (14)$$

By applying now the principle of unit forces, we assume, that in a subsequent series of n analyses, where n is the degree of freedom of the robot, an orthogonal series of unit forces are acting on each of the TCP's coordinates, subsequently. The system of forces defines then a matrix equation, where the force vector \mathbf{F} is replaced by a matrix of unit forces, i.e. unit matrix \mathbf{I} , and \mathbf{t}_m is a matrix composed of the calculated joint force vectors:

$$\mathbf{t}_m = [\mathbf{t}_1, \mathbf{t}_2, \dots, \mathbf{t}_n] = J(q)^T \mathbf{I} = J(q)^T \quad (15)$$

Thus, in MBS-analysis the joint force system response during a series of quasistatic analyses under TCP unit force equals the kinematic Jacobian of the robot. This important property will be utilized for evaluation of the DELTA robot concept, chapter 4.2.2.

2.5 Workspace kinematics

The kinematic methods to analyse dexterity allow to study the work space volume, kinematic accuracy, static force response and singularities in work space. For any robot mechanism, the coordinates r of the robots tool center point in the work space \mathfrak{R} are functions² of joint space \mathfrak{J} coordinates q .

$$r = r(q) \quad (2)$$

Salisbury and Craig (1982) considered the dexterity of articulated hands as a function of how an infinitesimal displacement in joint coordinates changes the tool center point coordinates. Derivating (2) in time defines the Jacobian of TCP to joint coordinates q , describing the TCP's velocity as a function of joint velocities

$$\dot{r} = \frac{\partial r}{\partial q} \dot{q} = J(q) \dot{q} \quad (16) \quad (5,6)$$

Assuming, that the joint velocity error vector \dot{q}_e in \mathfrak{J} is restricted by a hypersphere

$$|\dot{q}_e| = \sqrt{\sum_{i=1}^m \dot{q}_{ei}^2} \leq 1 \quad (17)$$

the kinematical error in \mathfrak{R} will be a hyperellipsoid, *manipulability ellipsoid*, first described by Yoshikawa (1985).

$$\dot{q}_e^T J(q) \dot{q}_e \leq 1 \quad (18)$$

The orthonormal base U which columns u represent the principal axes of the ellipsoid is obtained using singular value decomposition:

$$(J(q) - II)u = 0 \quad (19)$$

The orthonormal base U is a matrix composed of the eigenvectors u_i as columns. The principal axes of the ellipsoid will be the eigenvectors u_1, u_2, \dots, u_n , where u_i is the i th column vector of U . The length of the ellipsoid principal axes are $r_i = \sqrt{1/I_i}$, where I_i are the eigen values of $J(q)$. In the points near of repeating positioning this ellipsoid should be as

² This direct kinematic function can be developed arbitrarily or using a systematic procedure. As well known, one of the most common methods is the Denavit-Hartenbergs method, Denavit and Hartenberg (1955).

spherical as possible, indicating no distortion in the velocity map, while the main axis of the ellipsoid should preferably be oriented in picking direction. The distortion of the ellipsoid is the ratio between the longest and shortest principal axes i.e. the ratio between I_{\max} and I_{\min} . This is according to matrix theory the *condition number*, the ratio between the largest and smallest eigenvalue of the matrix $J(q)$. At the most accurate posture the ratio has its minimum value, one. The kinematic singularities are interpreted as loss of the robots ability to move into a certain direction in a singular position. In that position some of the Jacobian's values have become zero, indicating the minimum singular value of the Jacobian as design criteria. An infinitely large singular value (zero in the inverse Jacobian) indicates, that the mechanism is singular for inverse movement, i.e. infinite joint forces would be required to move the TCP.

2.6 Joint space dynamics

The dynamical equations of motion of a manipulator are most often expressed in joint space. Using the Lagrangian formulation of motion, Lind (1994) presents the derivation following closely to Lee (1982), Tourassis and Kircanski (1985) and Vukobratovic and Stepanenko (1985), leading to the matrix form (for simplification, the viscous terms of friction are neglected here):

$$M(q)\ddot{q} + c(q, \dot{q}) + g(q) = \dot{t} \quad (20)$$

The inertial properties of the mass matrix $M(q)$, ($n \times n$) are related to the systems kinetic energy:

$$T = \frac{1}{2} \dot{q}^T M(q) \dot{q} \quad (21)$$

The inertia matrix is always symmetric and positive definite. The symmetry is caused by Newton's third law, the action-reaction principle, while the positive definite property implies that it is non-singular and that it can be inverted to M^{-1} , which is also a positive definite form. Thus the direct kinematical problem can be solved by rewriting eq. (20) as

$$\dot{q}^T M(q)^{-1} (\dot{t} - c(q, \dot{q}) - g(q)) \quad (22)$$

The diagonal elements m_{ii} of $M(q)$ indicate the efficient inertia of link i to joint i while the off-diagonal elements represent the coefficients of the reaction torque (force) of actuator i to the acceleration of joint j , Lind (1994).

The centrifugal and coriolis vector forces $c(q, \dot{q})$ are defined by the coupling matrix $C_i(q)$

$$C_i(q) = \begin{bmatrix} q^T c_1(q) q \\ \dots \\ q^T c_n(q) q \end{bmatrix} \quad (23)$$

$c_i(q)$ is a position q dependent ($n \times n$) coupling matrix for the reaction force on joint i indicating the coefficient of the centrifugal force due to velocity of link j at the diagonal elements, and the coefficient of coriolis force due to the velocity of links j and m , according to Lind (1994). The dimension of the coriolis matrix $C_i(q)$ is very large, ($n^2 \times 1$), and thus very time consuming to calculate. However, in very high speed robots the coriolis terms are dominating.

2.7 Work space dynamics

In the operation space approach the dynamic response of the end effector is of interest. Khatib (1990) presents an approach where the coordinate frame is attached to the end effector, the TCP, instead of representing the dynamics in joint coordinates. When the robot is kinematically non-redundant (i.e. $n = m$)³, the work space excludes the kinematic redundancy. The joint space equations of dynamics (20) can then be converted to the work space coordinates where the end effector is subjected to operational forces F . The equation of motion is then

$$\Lambda(r) \ddot{q} + \mathbf{m}(r, \dot{q}) + p(r) = F \quad (24)$$

where $\Lambda(r)$ is the inertia energy matrix, $\mathbf{m}(r, \dot{q})$ the centrifugal and coriolis force vector and $p(r)$ the gravity force vector defined in the coordinates of the operating space. The energy matrix describes the inertial properties of the manipulator in work space point r . There exists an identity between the quadratic forms for kinetic energy in the joint space (21) and in the operation space

$$T = \frac{1}{2} \dot{q}^T M(q) \dot{q} = \frac{1}{2} \dot{q}^T \Lambda(r) \dot{q} \quad (25)$$

We get, by substituting the joint space coordinates in (25) by (6), the relationship between joint and work space coordinate energy matrices:

$$\Lambda(r) = J(q)^{-T} M(q) J^{-1}(q) \quad (26)$$

For the matrix $\Lambda(r)$ applies corresponding properties as for the joint coordinate mass matrix. The diagonal elements Λ_{pp} describe the coefficient of inertia of coordinate r_p , while the off-diagonal

³ While Khatib (1990) presents the properties concerning redundant robots, here only the non-redundant robots are discussed. Thus the dependence between joint and work space coordinates is simplified and properties of pseudo kinematic matrices are not regarded.

elements I_{pq} are the coefficients of reaction force or torque of coordinate r_p to the acceleration of r_q . Also this inertia matrix is symmetric and positive definite allowing to formulate the direct dynamic equations for the acceleration of TCP in work space coordinates.

$$\ddot{\mathbf{r}} = \Lambda^{-1}(r)(F - \mathbf{m}(r, \dot{\mathbf{r}}) - p(r)) \quad (27)$$

The operational space equations of motion describe the dynamic response of the manipulators work tool when the operational force is applied. Since robots are usually controlled by joint actuator forces, this is inconvenient. Remembering the force domain relation of the kinematic jacobian

$$\mathbf{t} = J(q)^T F \quad (14)$$

we get

$$\ddot{\mathbf{r}} = \Lambda^{-1}(r)(J(q)^{-T} - \mathbf{m}(r, \dot{\mathbf{r}}) - p(r)) \quad (28)$$

2.8 Work Cycle Space

In previous sections we have presented methods to study the performance measures of a robot related to joint and work space descriptions. It could be noticed, that these measures require solving of different kind of jacobians. Some of them, like the kinematic jacobian in the force domain, are relatively simple to evaluate, while others, related to dynamics, require tedious unit acceleration operations in each configuration point when numerical MBS software is used. A third configuration space for performance study is the work cycle space. The use of work cycle is intuitive for a designer and numerically cheap to analyse compared to joint or work space analysis, while it requires, that the selected cycles are representative enough for describing the intended use.

For a pick-and-place robot the minimisation of work cycle time is one of the most important requirements to achieve increased productivity. In the past, much effort has been spent to optimise minimum-time trajectories under various restrictions, like maximum-minimum input torque e.g. Rajan (1985), and Ozaki, Yamamoto, Mohri, (1987), or average heat generation restriction, Ono and Teramoto, (1993). The maximum work cycle performance is solved by constrained optimisation using a suitable parametric description of the work path form, like an Hermite polynomial expression. This kind of optimisation gives the fastest profile form, but has also the drawback that the profile's start- and endpoints are predefined and a change in them requires new optimisation.

In the preliminary evaluation of new designs, however, a relatively simple description of the work cycle is preferable. In our case a characteristic work cycle in the workspace was defined representing a typical pick-

and place work cycle in the cartesian space shown in figure 1:

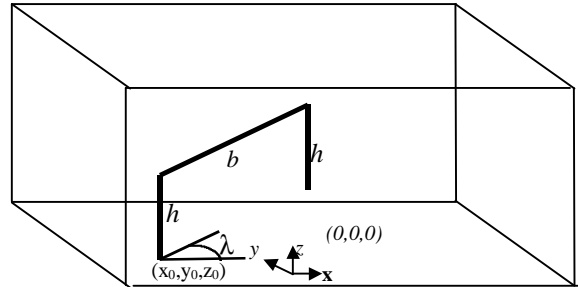


Fig. 1. Characteristic work cycle

The trajectory for the TCP is a typical pick-and-place sequence beginning from the work space point (x_0, y_0, z_0) , including vertical rise h , horizontal movement of length b , vertical sink h and a corresponding return sequence. Let the trajectory be divided into these six sections. The kinematical definition of the trajectory is given by the matrix equation (29):

$$\begin{bmatrix} x_r \\ y_r \\ z_r \end{bmatrix} = \begin{bmatrix} x_0 \\ y_0 \\ z_0 \end{bmatrix} + \begin{bmatrix} 0 & \cos I & 0 & 0 & -\cos I & 0 \\ 0 & \sin I & 0 & 0 & -\sin I & 0 \\ 1 & 0 & -1 & 1 & 0 & -1 \end{bmatrix} \begin{bmatrix} f_1(t, t_1, a_{\max}, h) \\ f_2(t, t_2, a_{\max}, b) \\ f_3(t, t_3, a_{\max}, h) \\ f_4(t, t_4, a_{\max}, h) \\ f_5(t, t_5, a_{\max}, b) \\ f_6(t, t_6, a_{\max}, h) \end{bmatrix} \quad (29)$$

where the travelling time is the difference between the path's corner points passing times t_i . Half of the travelling time is accelerated and half decelerated with a_{\max} :

$$T_i = t_{i+1} - t_i = \sqrt{4s/a_{\max}} \quad (30)$$

The section movement functions $f(t, t_i, a_{\max}, s)$ are acceleration restricted:

$$f_i(t, t_i, a_{\max}, s) = \int_{t_i}^t a_{\max} \min \left| t - t_i, t_i + \sqrt{\frac{4s}{a_{\max}}} - t \right| dt \quad (31)$$

The path section function is a simple double ramp function with constant acceleration at the first half and constant deceleration at the second half of the path. The ramp function can be easily changed to more complex ramp functions as presented in Makkonen (1995).

2.9 Kinematic simulation

The simulation of a work cycle path, described in chapter 2.8, requires solving the inverse kinematic problem

$$q(t) = r^{-1}(r(t)) \quad (32)$$

However, most of the numerical MBS-software are capable to solve only direct kinematic problems (2) straight forward. A method to obtain an inverse

kinematic analysis described by Elliott (1995), is the adding of a dummy positioner mechanism to the robot model, which has its own joint coordinate system configured exactly in the work-space coordinates, e.g. $\mathbf{c} = (x, y, z)^T$ and $\mathbf{f} = (f_1, f_2, f_3)^T$. The tool center point (TCP) of the robot is fixed together with the TCP of the positioner mechanism. The kinematic degree of freedom (d.o.f.) equals that of the original robot. The positioner mechanism has a greater dexterity than the robot, usually ideally infinite. A direct kinematic analysis is performed using the work-space coordinates $r(t)$ as input for the joint coordinate system of the positioner mechanism. The time-function response $q(t)$ of (2), is recorded by a FORTRAN subroutine. This is the inverse kinematic response of the TCP path, eq. (31). The direct kinematic analysis is then performed by releasing the positioner mechanism from the robot's TCP, and performing a direct kinematic analysis of the robot by using $q(t)$ as joint input for the robot.

2.10 Dynamic simulation

The dynamic simulation of the work cycle is a simple straight forward procedure, where the inverse kinematic response $q(t)$ during time $t=[0..T]$ is used to solve the load of the actuators by using eq (33).

$$\mathbf{t}(t) = M(q(t))\dot{\mathbf{q}} + c(q(t), \dot{q}(t)) + g(q(t)) \quad (33)$$

The analysis gives the motor torque requirement $\mathbf{t}(t)$, which can be post-processed off-line from the MBS-analysis to get important performance measures like absolute maximum actuator torque for each motor

$$t_{\max} = \max_{t=0..T} |\mathbf{t}(t)| \quad (34)$$

and average heat generation restriction for each motor

$$t_{rms} = \max_{t=0..T} \left| \frac{1}{T} \int_0^T t^2(t) dt \right| \quad (35)$$

In symmetrical parallel structures the motors have equal size, thus the torque load of all motors are restricted by:

$$t_{a\max} = \max_{i=1..j} |\mathbf{t}_{i\max}| \quad (36)$$

where j is the total number of actuators. We assume, that the mechanism arms are driven by a transmission with a kinematic reduction ratio z . The power balance assuming no friction gives:

$$T_g \dot{\mathbf{q}}_a = J_a \dot{\mathbf{q}}_a \dot{\mathbf{q}}_a + J_m \dot{\mathbf{q}}_m \dot{\mathbf{q}}_m + T_m \dot{\mathbf{q}}_m \quad (37)$$

The shaft speeds of the motor and mechanism are related by the transmission ratio:

$$\dot{\mathbf{q}}_a = z \dot{\mathbf{q}}_m \quad (38)$$

From (34), (35) and (38) we derive some of the motor load characteristics, which can be analysed off-line after the simulation. The maximum motor load during a cycle depends on transmission ratio and the acceleration of the mechanism shaft

$$T_{g\max} = \max \left| \frac{1}{z} \left((J_a z^2 + J_m) \dot{\mathbf{q}}_m(t) + T_m(t) \right) \right| \quad (39)$$

The mean temperature rise of the coils is restricted by the RMS-torque

$$T_{g\max} = \frac{1}{T} \sqrt{\int_0^T \left[\frac{1}{z} \left((J_a z^2 + J_m) \dot{\mathbf{q}}_m(t) + T_m(t) \right) \right]^2 dt} \quad (40)$$

The maximum power is

$$P_{g\max} = \max \left[\left| ((J_a z^2 + J_m) \dot{\mathbf{q}}_m(t) + T_m(t)) \dot{\mathbf{q}}_m(t) \right| \right] \quad (41)$$

and the RMS mean power is

$$P_{ms} = \frac{1}{T} \sqrt{\int_0^T \left[\left(\frac{1}{z} \left((J_a z^2 + J_m) \dot{\mathbf{q}}_m(t) + T_m(t) \right) \dot{\mathbf{q}}_m(t) \right) \right]^2 dt} \quad (42)$$

3. Framework for an elastodynamic simulation model

3.1 Multi Body Systems simulation

Multi body systems (MBS) simulation is perhaps one of the best known computer based analysis methodologies to study the dynamical behavior of any mechanical system independent from the application. It became established as a tool for engineering analysis during the 1980ies in a similar manner as the growth of finite element analysis (FEM) during the previous decade. Several computer programs are available commercially, the most widely used is ADAMS from Mechanical Dynamics Inc., Blundell, Phillips and Mackie (1996).

3.2 Elasticity Modelling in Multibody Systems

In the analysis of light weight structures like satellites or very fast robots, or when high precision of simulations is demanded, the elasticity of bodies must often be accounted for, Sorge, Bremer and Pfeiffer (1992). Traditional rigid body dynamics offers an insufficient solution since no coupling between the rigid body motion and the elastic deformations is given. In the elastodynamic simulation of mechanical systems, both FEM and MBS are used, while both of the methodologies must be modified.

The finite element simulation in mechanism analysis is implemented as a Cartesian coordinate approach for the substructures, where the system's

kinematics is modeled entirely as finite element d.o.f. in the joints. The modelling of kinematics requires an adequate formalism to describe the finite rotations due to their non-additivity. Geradin (1992) describes the kinematic topology in implicit form using transformation of the sets of degrees of freedom (d.o.f.) from the local to global frame. The joint behavior and drive constraints are defined in the element frame using an appropriate set of lagrangian multipliers. Finally, the system equations of motion are deducted by calculating the total internal energy of the system by summing the effects of strain, kinetic and dissipation energy of the elements and solving the variational equation describing the energy balance between the internal and external virtual work restricted by the kinematic constraints.

According to Geradin (1992), in the holonomic case, this leads to dynamic-algebraic equations (DAE). This method has been implemented in MECANO software, Cardona et al. (1988), which utilises a larger FEM package SAMCEF. The MECANO solves the multibody dynamics of the FEM model and includes an element library containing rigid and elastic bodies, rigid and elastic joints of different types, active elements and so on. The application of the Finite Element Method to mechanism simulation encounters some problems when large deformation is considered: firstly, the dimensional size of the problem tends to rise and secondly, the computational efficiency decreases since the global element matrices must be updated for each step when the configuration of the system changes.

The modelling of elasticity in Multi-Body systems can be based on several approaches, divided into two main categories: Pure rigid body systems (**i.-iii.** below), where the elasticity is represented by constitutive relations between the bodies, or: Elastic body systems (**iv.** and **v.**), where the elasticity is modeled as a combination of a rigid frame superposed by the elastic shape functions describing the displacement field influence. At least the following approaches are found in the literature: Shabana (1985), Sorge, Bremer and Pfeiffer (1992):

i. Rigid Body Pairs model the elasticity between two points of interest in a structure undergoing large motions. In a general 3D case, the elasticity is modeled as a six d.o.f. beam element between two node frames. The element shape functions are derived using e.g. Timoshenko beam theory, Fertis (1973), Amiroche (1992), ADAMS (1994).

ii. The elastic system is represented by a combination of rigid bodies and springs or other frame pair element functions of class **i.** above, Huston (1982), Rauh (1987). The shape functions are distributed as nodal element pairs enabling non-linear inertia-variant elastic deformation of a multi body system using linear displacement functions between node frames.

iii. Condensed rigid elastic body structure models discretise the elastic body to a set of rigid frames. The

mass of the elastic body is divided according to an appropriate distribution method on the node frames. The shape function, such as assumed for instance in Raleigh-Ritz method, spans over the entire body leading to a linear inertia-invariant elastic multi body system, Shabana (1985). Due to the node frame mass distribution, dynamic stiffening by external force fields is included as in class **ii.** methods above. The mass, stiffness and damping matrices can be obtained also using Finite Element Modelling; Sorge, Bremer and Pfeiffer (1992), while usually the large dimensionality of the model must be reduced using superelement reduction. The selected master nodes of the FE-model define the rigid node frames of the rigid body model, ADAMS/FEA (1994).

iv. Elastic mode shape body models can be achieved by describing body deformation with a set of mode shape function or mode shape vectors, Hale and Meirovich (1980). The shape vectors can be obtained using finite element method or experimentally by modal analysis.

v. The above mentioned methods regard rough modelling of elastic properties, to achieve sufficient accuracy in the multi body simulation. Thus detailed analysis of a particular body is limited, e.g. calculation and visualisation of stresses is usually not possible. Detailed structure analysis requires reversing the FEA/MBS sequence: Firstly, the external load field is calculated for a given body using multi body simulation, then the structural stress analysis is performed with finite element analysis software. Jahnke, Popp and Dirr (1992) present an approach, where a symbolic MBS code NEWEUL generates the equations of motion of the examined body and the numerical calculation of motion and forces is performed with NEWSIM. The load history is read into a general purpose finite element code SOLVIA, having user supplied subroutines for the calculation of load case history. The presented method is applicable for any general purpose MBS capable to solve constraint forces and acceleration in arbitrary point and any FEM code for non-linear dynamic analysis.

According to Liou and Erdman (1988), independent of how the elastodynamic multi body system is modeled, the result is always a set of coupled non-linear equations of the form:

$$\mathbf{M}\ddot{\mathbf{x}} + \mathbf{C}\dot{\mathbf{x}} + \mathbf{K}\mathbf{x} = \mathbf{F} - \mathbf{M}_p\ddot{\mathbf{u}}_p - \mathbf{M}_c\dot{\mathbf{u}}_c - \mathbf{M}_a\mathbf{u} \quad (43)$$

where

\mathbf{M} = system mass matrix

\mathbf{M}_c = Coriolis mass matrix of the system

\mathbf{M}_a = normal or tangential matrix of the system

\mathbf{K} = system stiffness matrix

\mathbf{C} = system damping matrix

\mathbf{u} =vector of elastic nodal displacements in local frames

$\dot{\mathbf{u}}$ =vector of elastic nodal velocities in local frames

$\ddot{\mathbf{u}}$ =vector of elastic nodal accelerations in local frames

$\ddot{\mathbf{a}}$ = vector of rigid body accelerations in global frame
 \mathbf{F} = Vector of external forces acting on the system

Each time the system changes its posture, the mass and stiffness matrices must be updated, since they are functions of both time and displacements. The right hand side of the equation represents the inertial forces due the motion of the system, while the left hand side represents the forces due the constitutive relations due to internal motions of the system.

3.3 Modelling principles

According to Blundell, Phillips and Mackie (1996), the selection of an MBS-code for industrial use requires the evaluation of the following software properties: generality of use, modelling capability, ability for different analysis modes, and pre- and post-processing capacity. It is well known, that product development of robots requires simultaneous balancing between the requirements of different problem domains. As modern high quality MBS-codes exist and there is a need for general purpose simulation models enabling ease of model development and ability to simulate several problem categories in dynamics with one simulation system, it is reasonable to develop a multiview simulation model which is *modular, transparent and generic*. Since all modelling

work is based on the specific model language of the used software tool, the principle of generic modelling causes *macro programming* to be much more advantageous than traditional imperative statement programming. Macro programming enables the abstraction of the MBS-tools model language, which is called an *abstracted model* of the model (command) language, Hyvönen and Seppänen (1985). Thus, independent of the specific software used, *component model sub macros* can be developed fast by re-using and parametrising command files of the created model. The parametrisation of a model can be variometric (dimensional) or structural (generic) by character, thus not describing a specific model but the method or procedure how to create it, Kjellander (1995). Instead of developing simulation models from scratch for each project separately, the analysis group of a design department re-use design information for analysis of new product variants. The modelling and simulation of a large system, a product family for instance, will be a two phase activity of synthesis (the creation and decomposition of a thought system's model of its components into a component library) and analysis (combination of the library components to a new concept and analysis and optimisation of the concept's parameters both at system and component level), see figure 2:

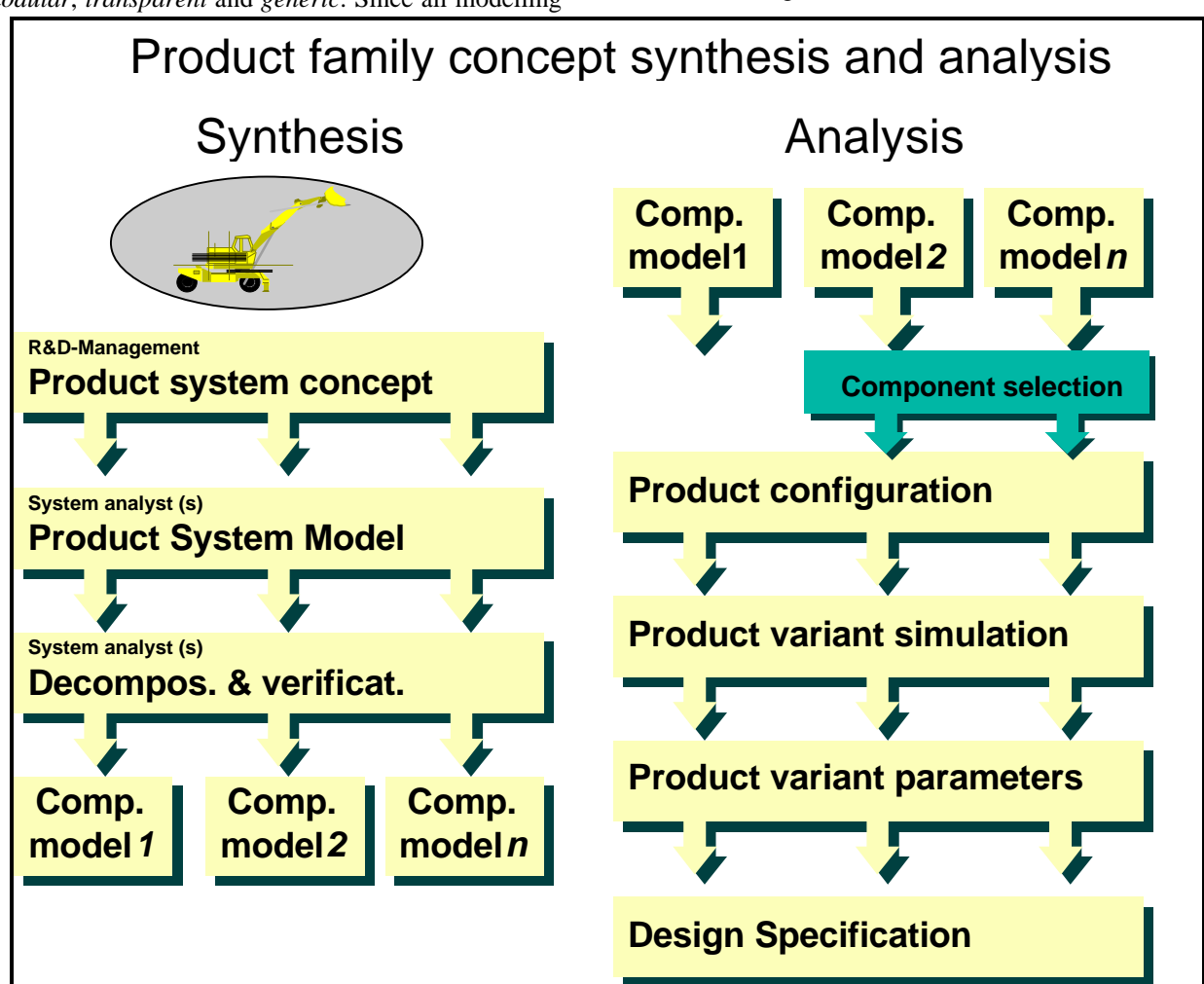


Fig. 2. Synthesis and analysis of a product model.

A general purpose MBS-simulation model is able to predict several kinds of kinematic and dynamic properties, given that a suitable sequence of analyses is written. The library of different analysis procedures helps the designer to concentrate separately, as independently as possible, on each problem domain of robot design, e.g. work space, motor load, eigenfrequency and so on. The reference model introduces the problem specific submodels and corresponding analysis procedures in the natural

sequence of robot design. The simulation work process is shown in figure 3. The figure shows, that a mechanical system, which is created using rigid bodies (marked with fixed lines), can be partly changed to elastic structures, shown with dotted lines. The same principle applies to all other model views: The generative algorithms replace the old submodels and create the new submodel modules, with a user selected set of design parameters.

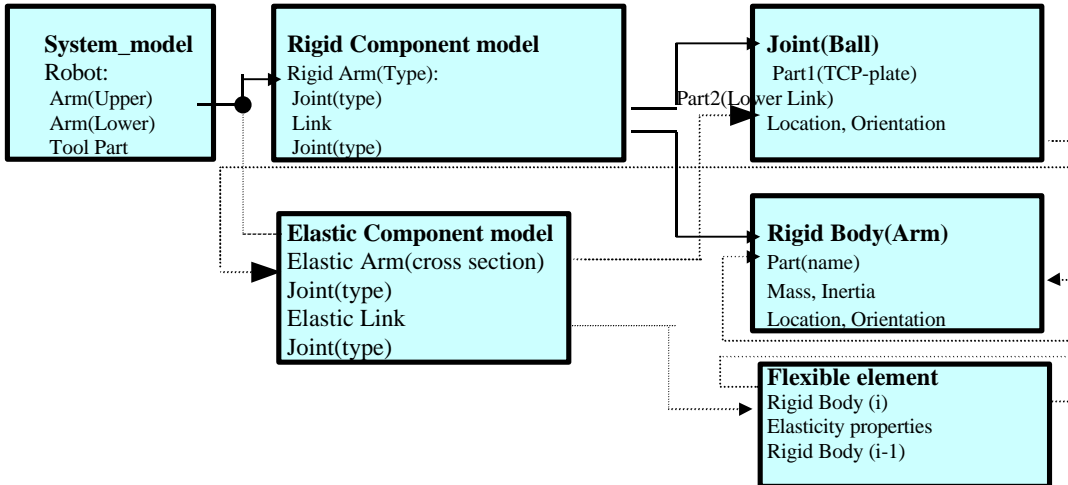


Fig. 3. Example of a part of the generative model structure

The analyses and design attributes are categorised according to the problem categories: e.g. the linkage length parameter group determines the dexterity of work space with kinematic work space analysis, while the cross section and materials selection parameter group defines the link masses by means of dynamic

work cycle analysis. The complete isolation of problem domains is naturally impossible; e.g. the profile parameters determine also eigenfrequencies and stiffness properties, questions to be answered by the model for linear analysis of eigenfrequencies.

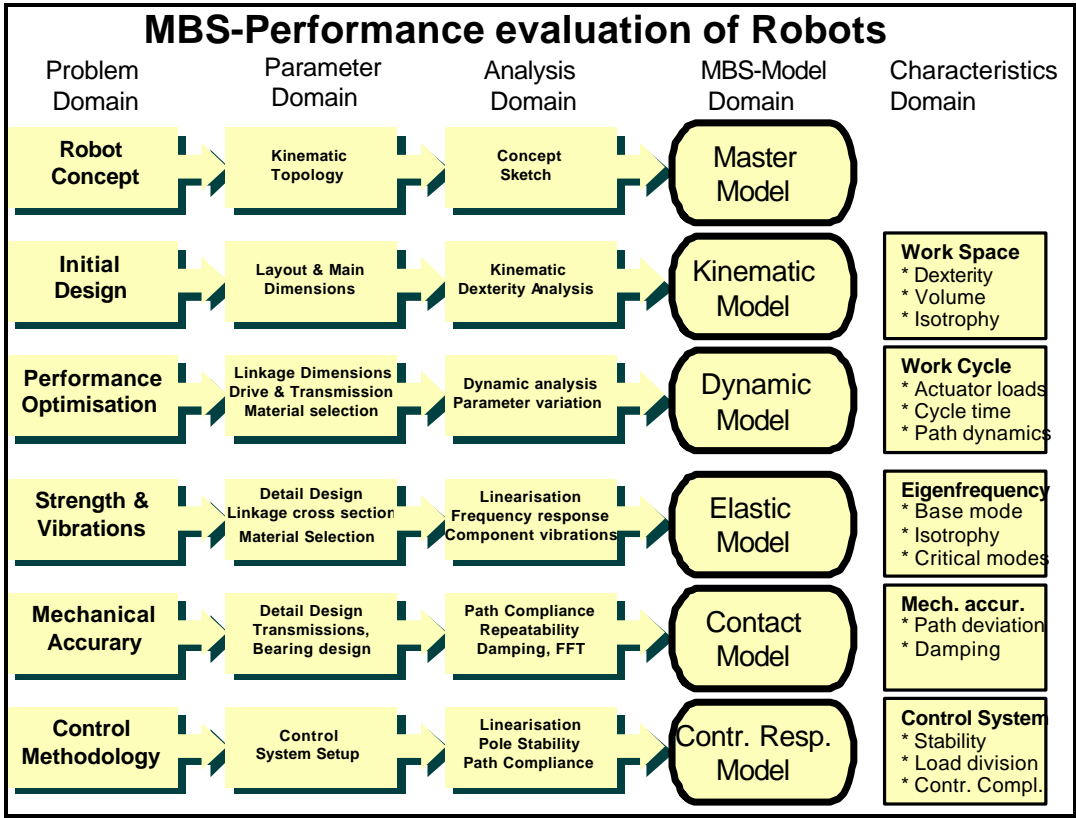


Fig. 4. The progress of simulation activities during product development

When a new modelling methodology is presented, it can be accepted only when it is verified. However, when a very complicated model is to be verified over its entire parameter space, complete experimental verification is virtually impossible, since it would require far too many experiments due to the model's large parameter space and dimensionality. Therefore, in many research projects the verification of the total model has been performed with just one configuration leaving unclear how the model works with other configurations. Keskinen (1994), has used the following assumptions for model verification.

- A verification is considered to be valid alone, independent of if it is based on experiments or if it is theoretically derived.
- When all submodels, their interfaces, numerical stability and the model topology is verified, then also the total model is assumed to be correct, given that one total system verification is shown to be correct.

3.4 Model framework example

As an application example for the simulation procedure proposed in this paper, we show the model structure of a three degree of freedom parallel robot DELTA presented by Clavel (1989). The model framework presented in this paper is developed for the use of a commercial numerical MBS-algorithm, and it is implemented using ADAMS 8.2 multi body software including the ADAMS/View, ADAMS/Solver and ADAMS/Linear modules.

The DELTA robot has been developed for high-speed picking applications, like manipulation of chocolate pralines to consumer packages. The high speed is achieved due to the following characteristics of the robot: very light and stiff structure, all motors installed on the fixed base plane and finally, all motors are attending to the movement of the traveling plate thus driving the load. The structure of the robot is shown in fig 5.

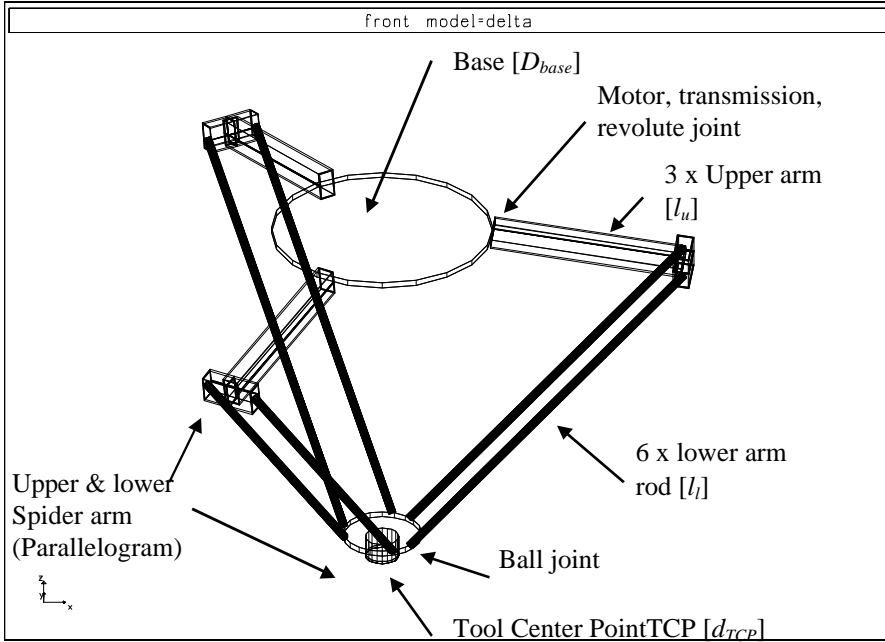


Fig. 5. The DELTA robot and its main dimensions.

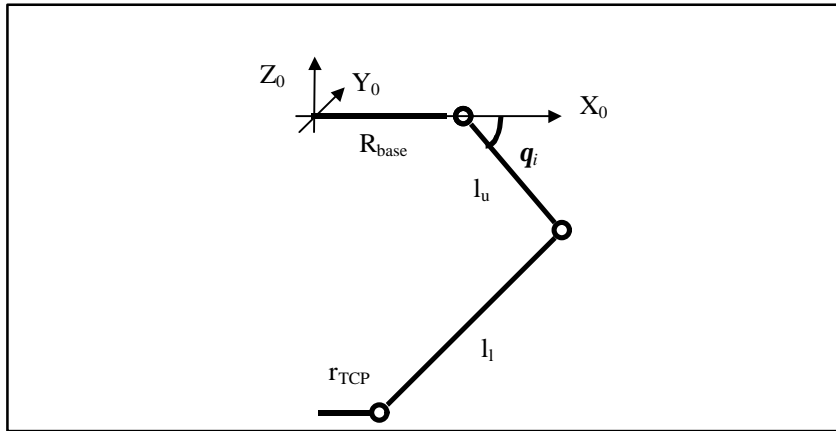


Fig. 6. The dimension parameters of the DELTA robot

In figure 6. the main dimensions of the DELTA robot are defined. Pierrot, Dauchez and Fournier (1991) have shown, that that this set of parameters is optimal in which the actuated variables and traveling plate position can be directly correlated without any use of non-actuated variables. They derive also a compact analytical model for direct and inverse kinematics.

The simulation methodology presented in this paper is not restricted to model one robot concept. It is a general approach to model robot concepts, parallel or

serial, and to evaluate different concepts with concept invariant performance criteria. Figure 7. shows the general structure of the simulation framework. By using only one parametrised master model, four different models for each model view can be automatically generated.

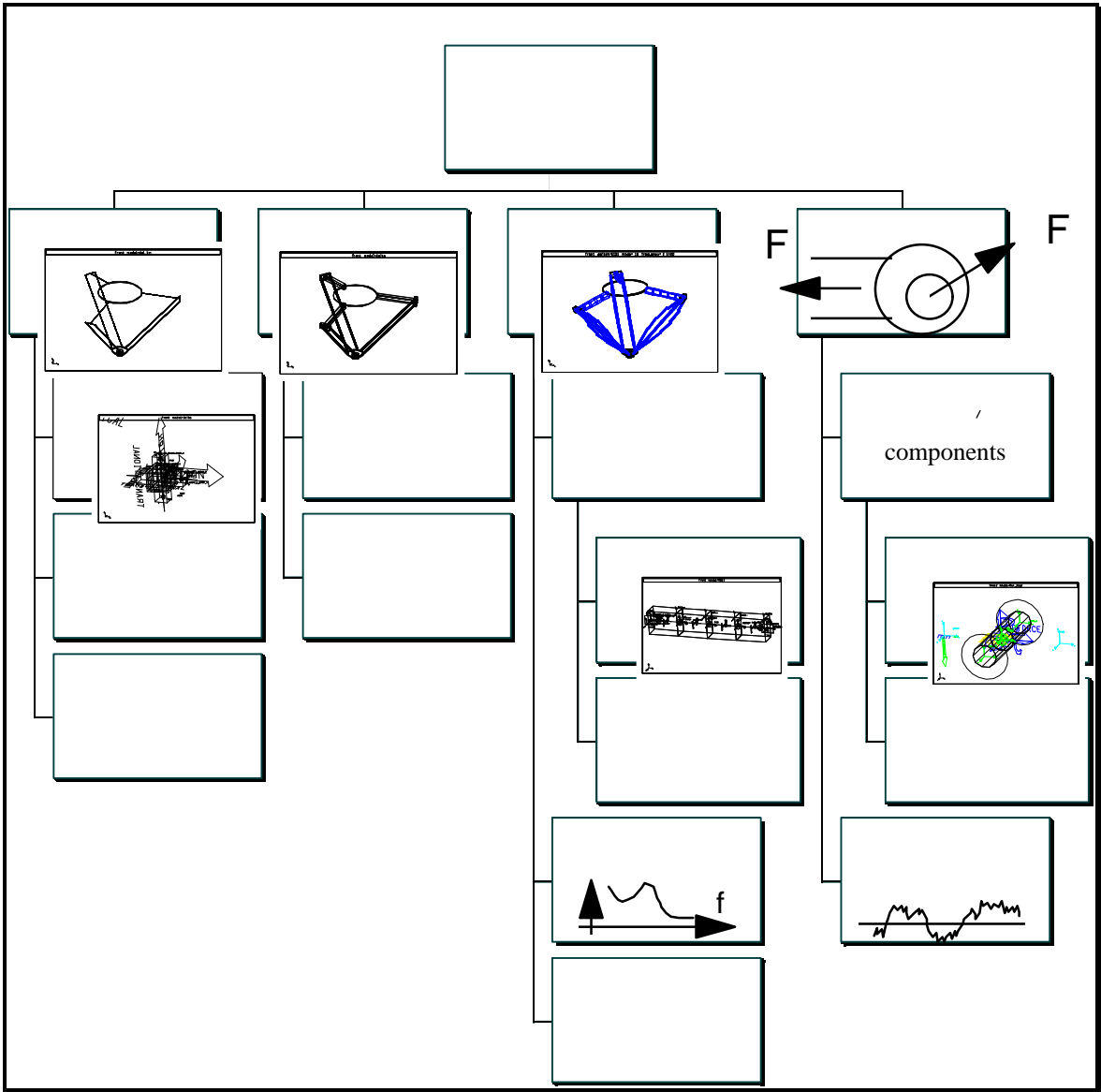


Fig. 7. The framework of generic submodels and analysis macros.

The methodology requires, that the master model is created transparently with interchangeable component structure by using generative programming, Kjellander (1995).

3.5. Modelling elastic beams

In this paper only two types of elastic components are considered: cantilever beams and gear boxes. The beams are considered to meet the following basic assumptions:

- The cross sections remain undeformed and plane under load (Euler-Bernoulli hypothesis).
- Uniform cross section.
- Linear elasticity, thus Hooke's law is applicable.
- Forces and moments at the beam end points are considered linearly dependent on the relative displacement and velocities between the beam end points.
- All six flexibility degrees of freedom are considered, i.e: neutral axis tension/compression;

torsion; transverse displacement in two directions; and angular displacement in two transverse directions.

- In the rigid beam form, the mass m_r and inertia tensor J_r of the total beam length L_r is lumped in the middle frame between the end points, and all three frames are locked kinematically together to form one rigid beam.

- The beam element is considered massless.
- The elastic and inertial properties of each element remain time invariant.
- Large elastic deflections of the structure are accounted for, due to the MBS approach with relative displacement of local frames.
- All damping effects of the beam vibrations can be represented by equivalent linear viscous damping, acting between frame pairs.

For an elastic structural component of beam type, length L_r , the component is divided into n equal length massless beam elements, according to the assumptions above. The total mass m_r and the inertia tensor J_r of

the component are lumped and distributed to the MBS frames as follows: A lumped mass m_r/n is associated to the $n-1$ intermediate frames. The mass $m_r/(2n)$ is added to the $n-1$ intermediate frames, of element length L_r/n .

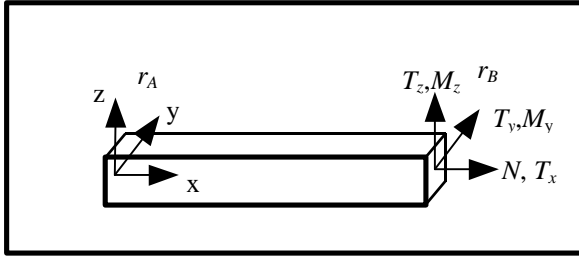


Fig 8. Beam frames and load case.

The deformation relation has also structural damping, and is thus of the form

$$F = K \mathbf{D}\mathbf{r} + C d\mathbf{D}\mathbf{r}/dt \quad (44)$$

where the damping matrix is proportional to the stiffness matrix

$$C = dK \quad (45)$$

In FEM (Finite Element Modelling), the elasticity of a full (six nodal d.o.f.) 3D beam is usually represented by a 12 x 12 stiffness matrix. The 12 x 12 matrix gives the relation between each of the six force and moment components at the two beam end points and the six displacement components at the two end points. However, for elastic beam elements in an MBS model, a 6 x 6 stiffness matrix representation is used instead. This 6 x 6 matrix gives the relation between each of the six forces and moments at beam end point i with respect to the six displacement components at beam end point j . The opposite beam end point j is located at the origo of the beam element frame. The x-axis of the beam frame j defines the centroidal axis of the undeformed beam. The y-axis and z-axis of the j frame represent the principal cross section axes of the undeformed beam, fig 9a. All deformation components at end point i are expressed in the j -frame which is fixed to and moving with the beam end point j . All deflection components at beam end point j are then equal to zero, expressed in frame j .

Fig.9a. Massless beam element

It is well known, Sundström (1988) for instance, that in short beam elements with cross section height h and span l , for $l/h < 5.0$, the beam shear forces have significant contribution to the beam deflection. It can be significant also for thin-walled cross sections and for composite and sandwich structures. Therefore, Timoshenko beam theory has been applied, Adelman

and Natrayanaswami (1974). The constitutive relation between frame r_j forces and the relative deformation vector is given by (46)

$$\begin{bmatrix} N \\ T_y \\ T_z \\ M_n \\ M_y \\ M_z \end{bmatrix} = K \begin{bmatrix} \Delta x \\ \Delta y \\ \Delta z \\ \Delta a \\ \Delta b \\ \Delta c \end{bmatrix} \quad (46)$$

where K is a 6x6 matrix, as discussed:

$$K = \begin{bmatrix} \frac{EA}{L} & 0 & 0 & 0 & 0 & 0 \\ 0 & \frac{12EI_z}{L^3(1+k_y)} & 0 & 0 & 0 & -\frac{6EI_z}{L^2(1+k_y)} \\ 0 & 0 & \frac{12EI_y}{L^3(1+k_z)} & 0 & \frac{6EI_y}{L^2(1+k_z)} & 0 \\ 0 & 0 & 0 & \frac{GI_x}{L} & 0 & 0 \\ 0 & 0 & \frac{6EI_y}{L^2(1+k_z)} & 0 & \frac{EI_y(4+k_z)}{(1+k_z)} & 0 \\ 0 & -\frac{6EI_z}{L^2(1+k_y)} & 0 & 0 & 0 & \frac{EI_z(4+k_y)}{(1+k_y)} \end{bmatrix}$$

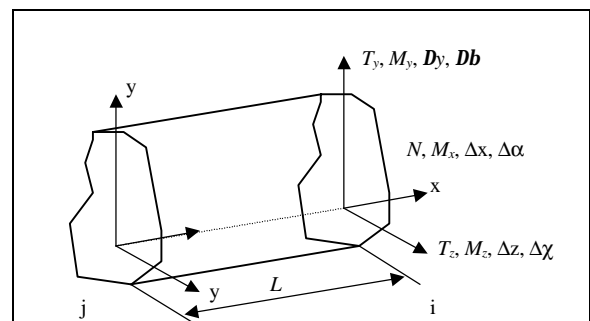
and where the factors \mathbf{k} account for shear deformation:

$$\mathbf{k} = \frac{12V EI}{GA}; \quad k_y = \frac{12V_y EI_z}{GA}; \quad k_z = \frac{12V_z EI_y}{GA} \quad (47)$$

This form of the beam stiffness matrix is also used in ADAMS (1994). The asymmetric correction factors V_y and V_z that account for uneven shear stress over the beam cross section are expressed by eq. (48) and (49). For a solid rectangular section, the asymmetric correction factor is $\zeta=6/5=1.2$. For a solid circular profile $\zeta=10/9=1.11$. For a thin-walled pipe-section $\zeta=2.0$. For derivation of the Timoshenko beam stiffness matrix, see Makkonen and Persson (1998).

$$z_y = \frac{A}{I_z} \int_A \frac{S_z(y)^2}{l_z(y)^2} dA \quad (48)$$

$$z_z = \frac{A}{I_y} \int_A \frac{S_y(z)^2}{l_y(z)^2} dA \quad (49)$$



In figure 9b., we see an example of a beam which has been generated with the macro subroutine for a short flexible beam with rectangular cross section.

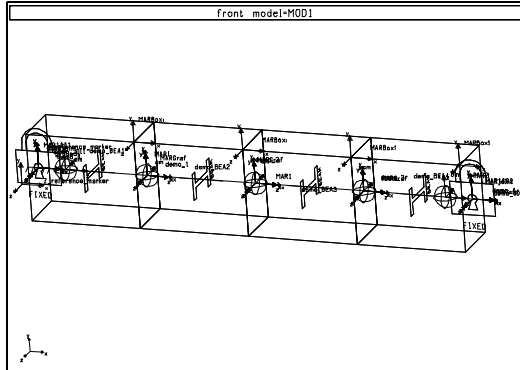


Fig. 9b. MBS-model of a flexible beam structure.

3.6 Gear elasticity

Each of the three actuator shaft gears are modeled as a simple one d.o.f. system, where the free coordinate replaces the connection with a linear visco-elastic coupling between the actuator and mechanism shaft. The constitutive relation is

$$T_g = k_g (\mathbf{j}_a - \mathbf{j}_m) - c_a (\dot{\mathbf{j}}_a - \dot{\mathbf{j}}_m) \quad (50)$$

This submodel is similar to the gear model presented in Makkonen (1995). An enhanced gear model including clearance and non-linear stiffness is currently under development at KTH, dept. of Machine Design.

3.7 Modelling of joint clearance and elasticity

Modelling of contact problems in multi body dynamics is a relatively new research area and the use of contact models is still not well established. The first approach was to analyse the problem with a kinematic model based on zero-clearance and predict the contact loss to begin when the joint force was negative, Earles and Wu (1975). The results were however far non-conservative, and could not predict contact loss. Seneviratne (1985) presented a model for simulation of a planar four bar mechanism by representing the clearance with a mass-less link, having length equal to clearance distance. The conceptual weakness of the model is thus the assumption that the clearance distance is always at maximum and contact is continuously maintained. Seneviratne, Earles and Fenner (1996) presented a model, where the clearance is represented by a spring-damper element. So far, this was conceptually the most accurate description. However, the element was assumed to be linear thus having always positive contact re-establishing force and thus a non-conservative model for predicting loss of contact. Makkonen (1998) presents a planar impact model for the clearance of a journal bearing. This

model has a linear visco-elastic support force when contact is established and no support force exists during contact loss. Hahn (1994) presents a constraint stabilisation method for multi body analysis of several 3D joints, verified in one-dimensional space.

Here a clearance joint model is presented, which is a three dimensional generalisation of the model of Makkonen (1998). The contact force is a function of the contact depth penetration e .

$$e = d - R + r \quad (51)$$

The dimension parameters are shown in figure 10:

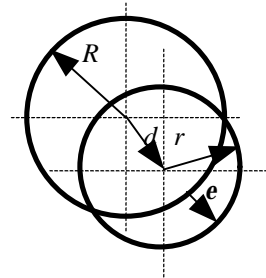


Fig. 10. Dimension parameters of contact depth.

The contact force is assumed to follow a linear force-penetration law when in contact. The contact is detected by a Heaviside function $P(e)$, which has the value zero when contact is lost, else one when e is positive thus contact is established. To prevent discontinuity in damping force at contact, the damping force is multiplied with a cubic step function of the penetration. At zero penetration the damping coefficient is zero while saturating to the maximum of m_r , at a predefined maximum e_r , describing the thickness of the lubrication film. The force function is thus

$$F_s = \Pi(e) \{ K_r e^e - S(e, 0, 0, e_r, 1) m_r \} \quad (52)$$

where the damping function $S(x)$ is a cubic spline polynomial as follows:

$$S(x, x_0, h_0, x_1, h_1) = \begin{cases} h_0: x \leq x_0 \\ h_0 + (h_1 - h_0) \left[\frac{(x - x_0)}{(x_1 - x_0)} \right]^3: x_0 < x < x_1 \\ h_1: x \geq x_1 \end{cases} \quad (53)$$

The material parameters of the contact force function are the bearing elasticity K_r , material damping m_r and the progressivity e . Keskinen (1994) mentions the non-applicability of the classical Hertzian contact theory due to the assumption of considerable radial clearance and logarithmic dependence of compression. He also shows five different contact element configuration related phenomena which usually are not modeled due to local

elastic effects: sleeve elasticity, ring deflection, eccentric eye, bend of pin and elasticity of ball bearing rolling elements. An approximation of the progressivity properties for a journal bearing are given by Rivin (1987), which can be obtained off-line for metallic ball joints, eq. (54) and are valid for a range of average surface pressure

$$p_a = \frac{F_s}{pR^2} < 7.5 \text{ MPa} \quad (54)$$

where the progressivity parameters have been modified to be valid for a ball joint:

$$K_r = C_0 \frac{E_1 E_2}{E_1 + E_2} \frac{pR^2}{\sqrt{2(R-r)}}, \quad e = 3/2 \quad (55)$$

and $C_0=132.25 \text{ m}^{-1}$ is a dimensional constant. For heavy loaded joints Rivin suggests progressivity $e=5/2$ for an average pressure between 7.5 MPa and 25 Mpa. Steel data give however far too high estimates, and boundary lubrication has not been considered. Seneviratne (1996) gives for a typical $\phi 25 \times 25 \text{ mm}$ journal bearing a stiffness of $K_r = 2 \times 10^8 \text{ N/m}$, based on FEM-analysis.

4. Simulation examples

4.1 Model

The kinematical, dynamical and elasto-dynamical behavior of a parallel robot "DELTA" was investigated. The model was built using ADAMS/View 8.2 preprocessor and with elasticity and simulation support macro codes developed by the author. See fig 5. in chapter 3.4 for parameter definitions.

- Upper links:

$$E_u = 1.60 \times 10^{10} \text{ N/m}^2 \quad A_u = 3.04 \times 10^{-4} \text{ m}^2$$

$$L_u = 0.35 \text{ m} \quad r_u = 1600 \text{ kg/m}^3$$

$$I_u = 1.79 \times 10^{-6} \text{ m}^4 \quad D_{base} = 0.4 \text{ m}$$

$$m_u = 0.17 \text{ kg}$$

- Lower Links

$$E_l = 1.60 \times 10^{10} \text{ N/m}^2 \quad A_l = 4.08 \times 10^{-5} \text{ m}^2$$

$$l_l = 0.75 \text{ m} \quad r_l = 1600 \text{ kg/m}^3$$

$$I_l = 1.79 \times 10^{-6} \text{ m}^4 \quad m_l = 0.049 \text{ kg}$$

- Work Tool

$$D_{TCP} = 0.1 \text{ m} \quad h_{TCP} = 0.014 \text{ m}$$

$$m_{TCP} = 0.414 \text{ kg} \quad r_{TCP} = 2640 \text{ kg/m}^3$$

4.2 Kinematic simulation

4.2.1 Analysis of work space

The reachable work space is most conveniently analysed by relaxating the actuators from motor torque and by applying an external load, e.g. a tension force from a spring, on the TCP, forcing the robot mechanism to follow an extreme path limiting the work space. The extreme boundary is solved by letting

the spring rotate around the outer side of the work space. The robot's TCP follows then the boundary of the work space. The sequence of balance positions is calculated using kinematic quasistatic analysis. However, the tests showed the method to be in many arbitrary cases numerically unstable. A more reliable, and for design purposes enough accurate method was to use force relaxation with dynamic analysis. A numerically stable process was achieved by applying velocity related overcritical damping, eq. (56). At the TCP is thus applied a kinematically controlled tensioning vector force of form:

$$\begin{bmatrix} F_x \\ F_y \\ F_z \end{bmatrix} = \begin{bmatrix} k_x r \cos(\omega t) - c_x \dot{x} \\ k_y r \sin(\omega t) - c_y \dot{y} \\ k_z(z_0 - \Delta z \operatorname{int}(\omega t / 2p)) - c_z \dot{z} \end{bmatrix} \quad (56)$$

Many contributions to kinematic theories don't consider the influence of geometrical design to the restrictions of joint coordinate space. Here the coordinate restrictions are modeled in joint space by defining restrictions caused by geometry and internal collisions. These restrictions are modeled as elastic joint coordinate stoppers describing the "hysteresis" functions of each joint with piece-wise cubic spline polynomials being of form (57):

$$\begin{aligned} \mathbf{t}_{ri} = & s(q_i, q_{i \min} - \Delta q_i, t_{i \max}, q_{i \min}, 0) \quad (57) \\ & + s(q_i, q_{i \max}, 0, q_{i \max} + \Delta q, t_{i \max}) \end{aligned}$$

In figure 11., a work space dexterity analysis is performed using the tensioning vector equation (56). The stepwise screw motion of TCP in z-axis shows the limits of workspace in each xy-plane.

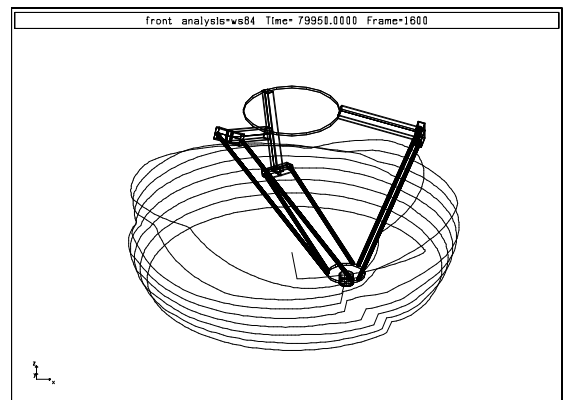


Fig.11. Dexterity analysis of DELTA with TCP path

4.2.2 Kinematic isotropy

As indicated by equations (14) and (15), the jacobian matrix $J(q(t))$ as a function of kinematic path $q(t)$ can be easily calculated by analysing the force response of a subsequent series of kinematic simulations. Thus by applying a suitable kinematic path the kinematic isotropy of the robot can be studied. Kurtz and Hayward (1992) and Park (1995) consider

the performance measures of the kinematic Jacobian. According to Klein and Blaho (1987), the condition number $k(J)$ should be the preferred index since it has direct physical significance due to the relations of Craig and Salisbury (1982):

$$\frac{\|dr\|}{\|r\|} \leq k(J) \frac{\|dq\|}{\|q\|} \quad (58)$$

$$\frac{\|dF\|}{\|F\|} \leq k(J) \frac{\|dt\|}{\|t\|} \quad (59)$$

(58) shows the amplification of relative errors going from joints to TCP, $k(J)$ thus being a performance measure when selecting sensors and actuators, Kurtz and Hayward (1992). The condition number varies from one (isotropy) to infinity (singularity).

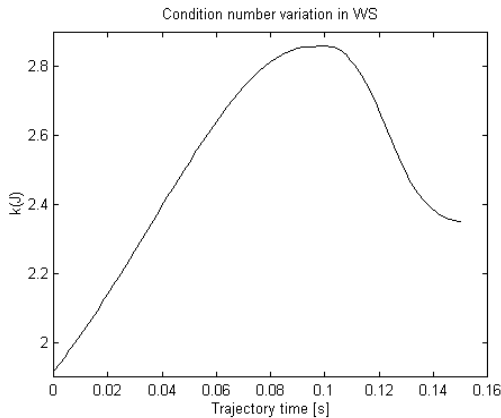


Fig 12. Condition number variation over time for a radially traversing path

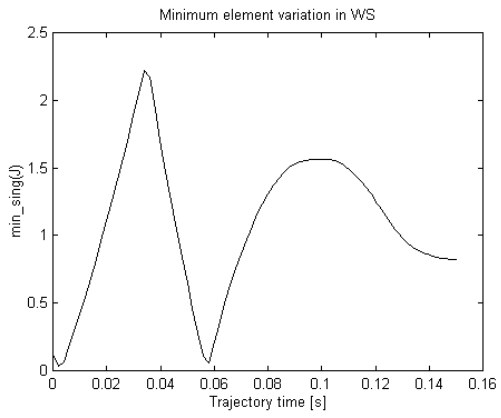


Fig. 13. Minimum singular value variation

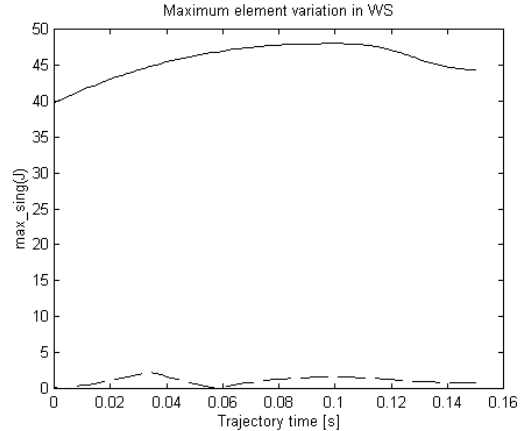


Fig. 14. Maximum singular value with minimum value at the same scale.

In kinematically singular points the manipulator is unable to be moved kinematically forward i.e. from joints to TCP due to some singular value being infinite, or kinematically backward i.e. from TCP to joints due to some singular value equal to zero. This suggest the minimum and maximum singular value as another possible measure for local dexterity.

The figures 12, 13 and 14. above demonstrate the discussed measures variation along one radial path of DELTA. Note that the X-axis represents time, not a radial coordinate. The figures show, that the condition number varies quite much over the work space, and in maximum the isotropy is distorted by having the largest principal axis almost three times the shortest principal axis of the manipulability ellipsoid. The largest singular value does not vary much indicating good forward kinematics, while the great variation in minimum value and near zero values predict near singularities of the inverse kinematics.

4.3 Dynamic simulation

The performance measures presented here are based mainly on the derivations presented in chapter 2.10. Dimensionless analysis is a practical way to study a design solutions performance sensitivity to design parameters.

Fig 15. shows the motor load parameters dependence from the ratio of upper and lower links at the middle of the workspace, for a representative work cycle.

$$p_1 = \frac{l_u}{l_l} \quad (60)$$

The equivalent work space volume is approximated linearly by keeping constant linear dependence

$$l_u + 1.5l_l = 1.505[m] \quad (61)$$

The largest value of each performance value is scaled to one.

The results indicate, that when the link length ratio increases almost all measures decrease (even in

decreasing pace) except maximum upper arm torque and mechanism power. At the ratio $p_l=0.63$ the maximum motor torque is at minimum.

The second dimensionless geometry parameter (fig 16.) is the relative diameter difference between the upper and lower plate with respect to the lower link length, Pierrot, Dauchez and Fournier (1991).

$$p_2 = \frac{R - r}{l_l} \quad (62)$$

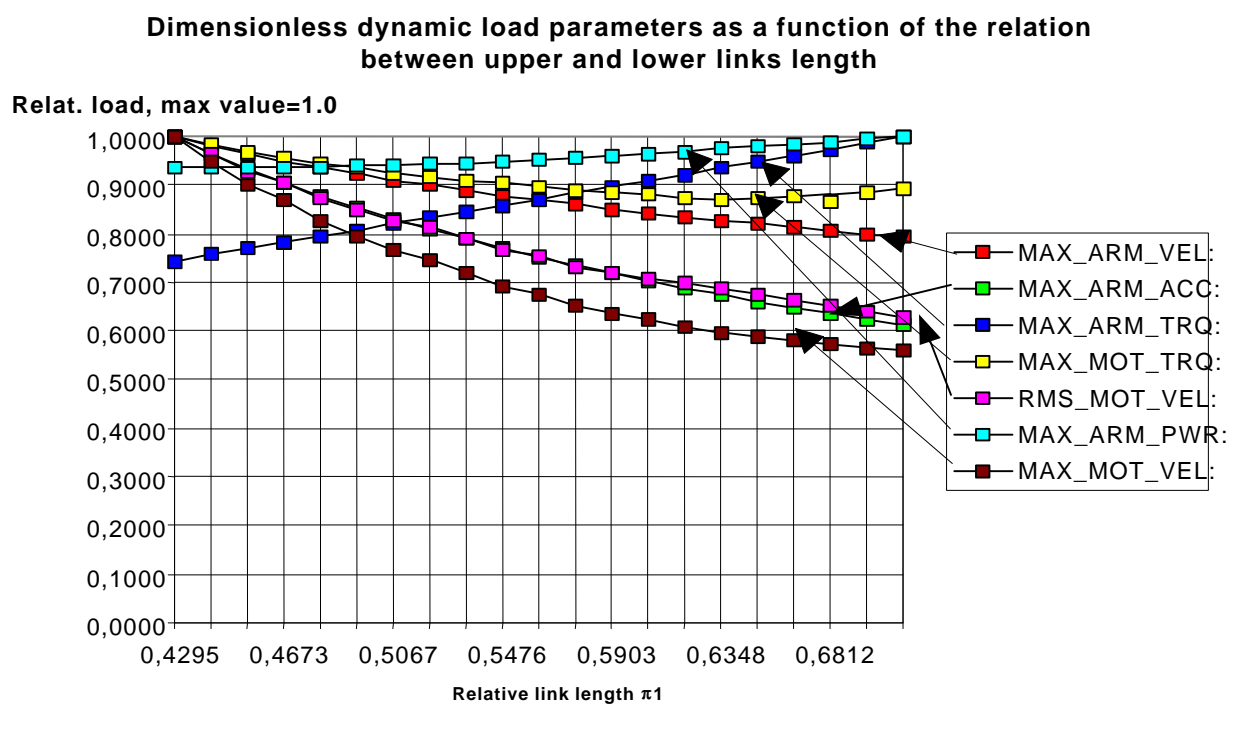


Fig. 15. Relative motor load variation in the middle of work space.

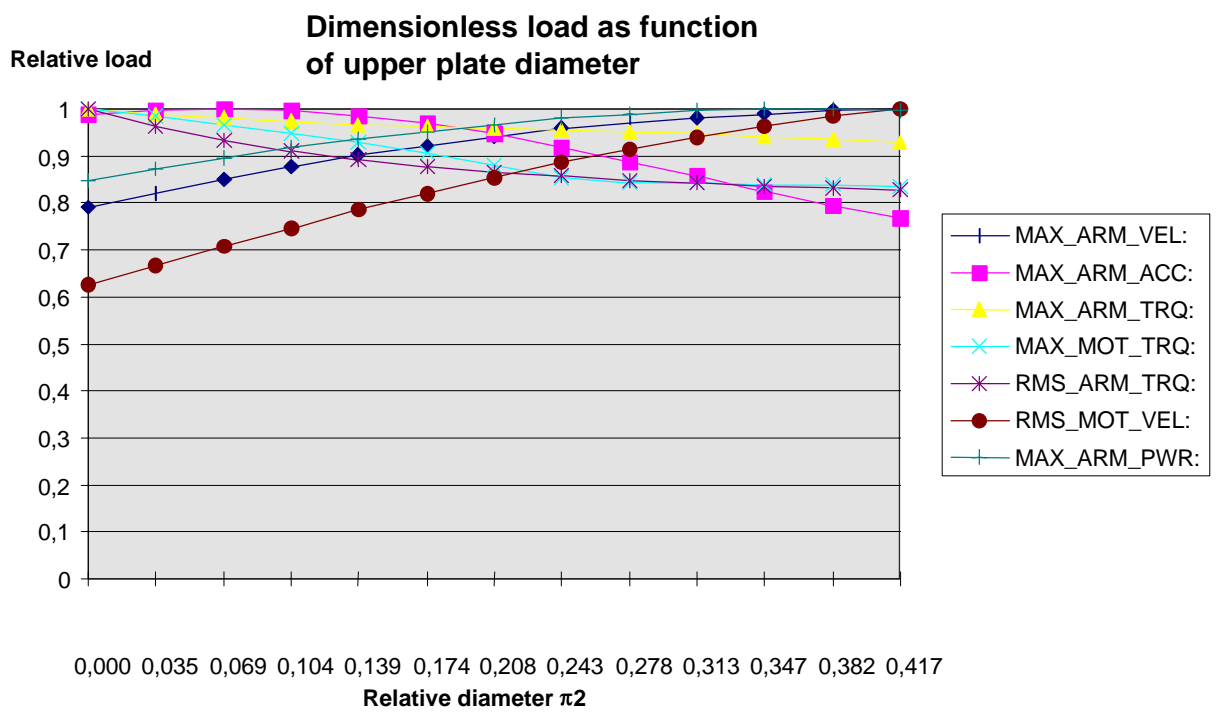
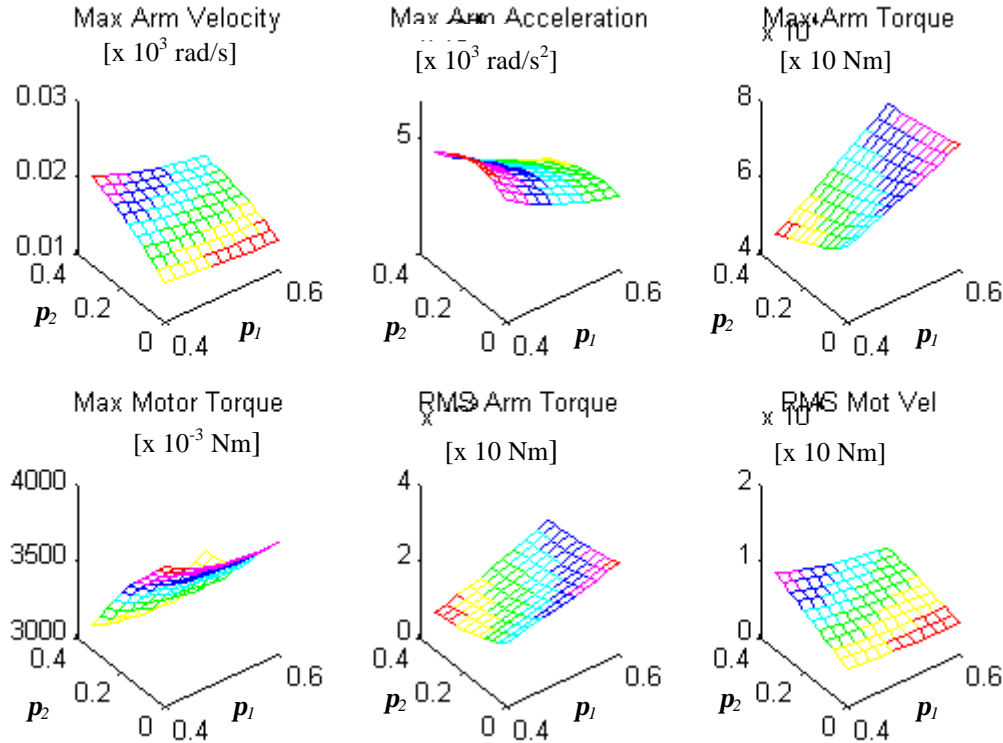


Fig. 16. Upper plate diameter effect on load parameters

Figures 15 and 16 describe well each parameter's load sensitivity. However, the diagrams don't describe the order of relative importance of the parameters. This question is answered only by knowing the allowed

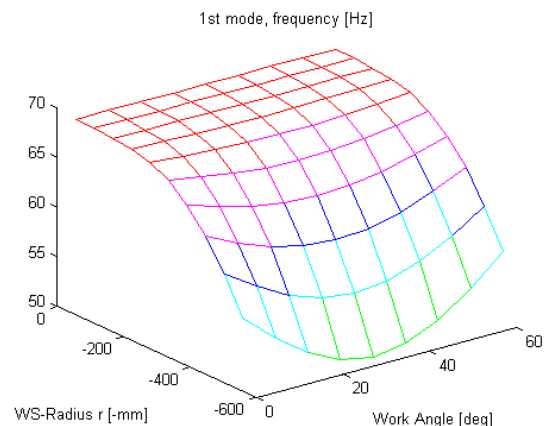
maximum load profile. These restrictions come from factors outside the multi body modelling, mainly from detail design decisions, and they are not handled here.

**Fig. 17.** A summary of the load sensitivity to dimensionless geometry parameter variations for the DELTA robot.

4.4 Elastodynamic simulation

4.4.1 Frequency analysis

To obtain very short cycle times with a high-speed, deformation passive control system, a mechanism with very high modal frequency must be designed. It has been reported that the system natural frequency varies with different posture positions e.g. Turcic, Midha and Bosnik (1983). The work space variation of DELTA is symmetric in 60 degrees sectors (Fig. 18.).

**Fig 18.** Eigenfrequency variation over the workspace, in TCP's polar work space coordinates.

Static conditions in modal analysis give more conservative frequency values and are numerically faster to solve than analysis under dynamic conditions. Variation of the linkage parameters show some of the sensitivity to link cross section dimensioning and link material selection. Composite material is used for the links. 0-fiber has only longitudinal fiber direction, while 90/45/0-fiber has corresponding angle (degrees) of fiber directions, thus longitudinal, diagonal and transverse fiber directions (Table 1).

Table 1. Material and cross section profile geometry influence on structural stiffness. =upper link \emptyset =lower link. Frequencies are calculated at TCP position (0,0,-650).

Profile type	Material	E(GPa) G(GPa)	ρ (kg/m ³)	Freq (Hz)
50x30x2 \emptyset 14x1	90/45/0-fib. 0-fiber	100/40 250/3	1600 1600	69.71
50x30x2 \emptyset 14x1	0-fiber 0-fiber	250/ 3 250/3	1600 1600	66.19
50x30x2 \emptyset 14x1	Alumin. 0-fiber	70/26 250/3	2700 1600	69.65
50x30x2 \emptyset 16x1	90/45/0-fib. 0-fiber	100/40 250/3	1600 1600	80.88
50x30x2 \emptyset 14x2	90/45/0-fib. 0-fiber	100/40 250/3	1600 1600	66.61

4.4.2 Time plane analysis

Time plane analysis of the elastodynamic model is a time consuming process. It's use is motivated only for certain problem categories, like path accuracy and vibration analysis. The results are obtained faster, if the inverse analysis in chapter 2.9 is performed from the kinematic model. Mechanical accuracy is then obtained by computing the path difference between the elastic dynamic path and the ideal kinematic path.

$$\mathbf{d}\mathbf{r}(t) = |\mathbf{r}_e(q(t)) - \mathbf{r}(q(t))| \quad (63)$$

If an MBS-code enables both dynamic and linear analysis (i.e. eigenmode analysis by MBS-system linearisation), they can be used complementing each other, when the elastodynamic properties of a mechanical system are to be analysed. Liou and Patra (1994) present the idea of internal model validation by concerning displacement time history data from FEA output with Fourier transformation, and comparing this result with frequency domain analysis. A similar approach can be obtained in MBS simulation when the path vibration (eq. 63) of the flexible model is converted with FFT and compared to results of modal analysis.

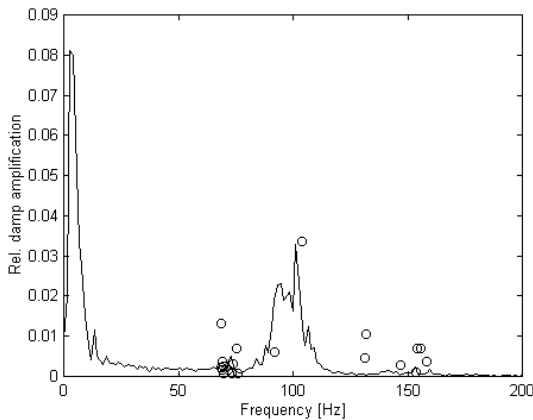


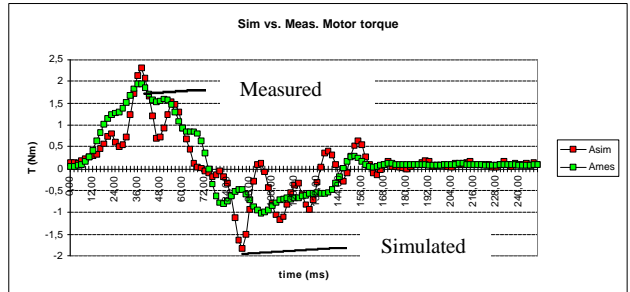
Fig.19. Frequency response of the 20 lowest rigid body modes (circles), $t=500$ ms, of the elastic models

dynamic linearisation, compared to FFT analysis of path vibration (curve), $t=200..600$ ms.

The low frequency variation peak under 10 Hz in figure 19., comes from path geometry, and must be rejected. The first modes of the robot are found at 70 Hz due to transverse vibrations of upper beams, while the highest amplification (lowest damping) is found at the frequency of 100 Hz due to transverse vibration of lower beams. These modes match quite well with the FFT analysis, as do also higher modes due to various bending vibrations.

4.5 Model verification

The model was verified by recording experimentally the motor air gap torque of the robot on a point-to-point cycle. The parameters are given in chapter 4.1, except for link length $l_1=800$ mm. The measured torque profiles were compared to a simulated cycle. In figure 20, the motor torque of motor 1 is shown. The oscillations of the simulated case are due to low resolution numerical derivation of the motor torque, to calculate estimates for motor



inertial torque due to shaft acceleration.

Fig. 20. Simulated and measured torque of motor 1.

4.6 Non-linear simulation

The most demanding type of analysis handled in this paper is dynamic analysis of a model including elasticity and joint clearance, in the time domain. When the bearing stiffness increases and free clearance is decreased, the frequency of vibrations increases. The time step of the integrator must then be shortened. When prestressed joints are used, free clearance is lost, and the impacts due to *loss of contact*, Seneviratne (1985), diminish and the clearance is observed as decreased elasticity, Rivin (1987).

The clearance was modeled using the clearance submodels described by eq. 52-53. Instead of Rivin's model, eq. 55-56, arbitrary values $K_c=1\times 10^7$ N/m and $m_c=2\times 10^4$ Ns/m were used as reference. The kinematical spherical joints of the DELTA robot were replaced with submodels of clearance joints using clearance values of 50 μm and 100 μm , arbitrarily. The simulations were conducted at a 400 mm long

path for a 100 ms cycle time under continuously increasing and decreasing acceleration, at the middle of the work space.

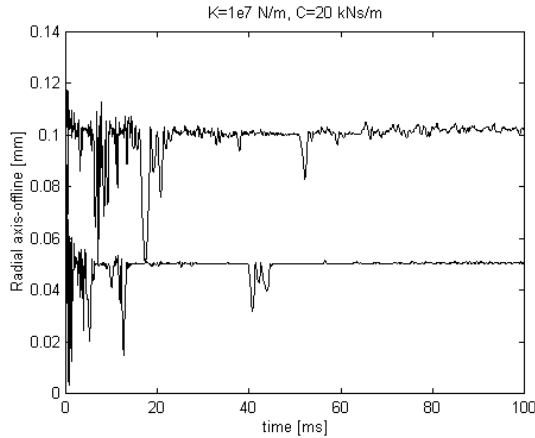


Fig. 21. Time history of axial difference between ball house and ball centers, clearance 0.05 and 0.1 mm, respectively.

The time step of the “gear stiff” integrator was initially set to 1.0 μ s, and the maximum limit was set to 200 μ s. Initially, the balls were assumed to be in loss of contact, at middle position, i.e. at maximum clearance distance.

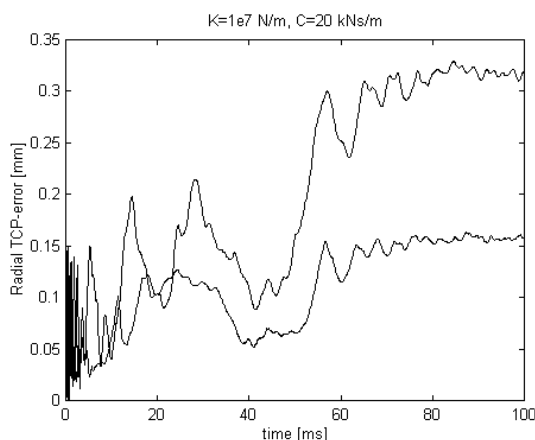


Fig 22. Time history of cumulative clearance error at TCP path, clearance 0.05 and 0.01 mm.

The analysis of contact force angular directions showed convergence to a fix angle confirming the phenomena shown in figure 20, that cumulative clearance error of a mechanism tends to increase when external joint forces have the same direction. A series of simulations using clearance values from 50 μ m up to 1.0 mm were carried out using joint elasticity of 1×10^8 N/m and damping of 2×10^4 Ns/m. The results indicate, that the relative time of contact maintained increases steadily the smaller the clearance is, with an anomaly of very low relative contact loss time at 0.4 mm. The impacts damp out from the initial value of about 1.2×10^4 N, to saturate at a coarse level of 500 N independent of the clearance.

When the clearance was maintained at a level of 0.1 mm with damping 2×10^4 Ns/m, elasticity was varied from 2×10^7 N/m to 1×10^8 N/m. The contact was best maintained at 6×10^7 N/m, while with lower values more vibration *at contact* was observed due to lower elasticity. Bearing contact impact force, however, increased the larger the stiffness was.

4.7 Numerics and CPU-times

The CPU-time requirements were examined by running a 100 ms long radial simulation cycle. The models were created using ADAMS 8.2 software. The dynamic equations were solved using a variable time-step, variable polynomial degree (1-6), Gear-stiff integrator with a maximum of 25 prediction iterations allowed per time step. The computer used was Sun Ultra 30. Dynamical, elastic and clearance analyses were performed (No. 1-5) with varying bearing stiffness of the clearance models. Also, the combined analyses with both clearance and elasticity (No. 6) were evaluated.

Table 2. CPU-time variation of the model simulations.

N.	Model	K N/m	Cumul. Iterat.	Steps	Integ. order	CPU- time (s)
1	Dyn.	-	387	100	-	6.7
2	Dyn.	-	3001	1000	-	7.5
3	Elast.	-	2575	2001	1-4	67.0
4	Clear.	10^8	40740	5021	1-2	76.8
5	Clear.	10^7	21913	5041	1-2	19.2
6	Cl+El.	10^7	313440	50437	1-5	5432.3

The numerical work increases when elasticity or clearance is simulated, with factors of 40 to 60. Combined clearance and flexibility analysis is very time consuming, indicating that separated studies of these phenomena will save considerable time, in parametric studies for instance. However, combined model studies are of importance for final verification purposes.

5. Conclusions

A simulation methodology is presented for evaluation of mechanical design decisions influence on the kinematic and dynamic performance of a robot. The methodology comprises model decomposition to component models and model configuration to different dynamic problem domains during the product life cycle. Implementation using macro techniques enables the use of highly developed commercial software instead of spending time on developing specific MBS solvers. Moreover, macro use allows model abstraction describing procedures for model

creation. By re-use of macros a number of concept variants can easily be generated.

The use of simulation models is restricted by the solving time and by the reliability of the results. While the generation of a system model by means of macro techniques is fast, the time to achieve results can vary very much because of following reasons:

- 1) The more detailed a model is, the more time must be spent on defining the parameters, based on measurements or theoretical engineering reasoning.
- 2) Due to non-linearities and discontinuities in local models, the time step of integration and hence the total solution time can vary some decades as compared to pure kinematic models.
- 3) Parameter variation studies often require overnight simulations, while giving good knowledge of the parameter sensitivity.

Despite some analysis activities are time consuming, the time spent on MBS simulation is not lost. The methodology forces designers to explicitly answer questions on mechanical function or design parameter values. If some of the parameters are unknown, they should be surveyed by parameter studies. By working out the parameters systematically during the sequence of a product development project with model views tailored to different phases of the project, the quality of design increases and the probability of malfunctions due to design errors will decrease.

6. Acknowledgments

The author wants to acknowledge NUTEK and ABB Robotics Products for the financial support and for industrial problem setting. Prof. Jan-Gunnar Persson supervised the work and spent much effort on discussing the modelling as well as on editing the paper. Prof. Sören Andersson, Prof. Bernie Roth, Dr. Kjell Andersson, MSc. Jesper Brauer and MSc. Priidu Pukk gave delightful comments.

7. References

- ADAMS, 1994. ADAMS/Solver Reference Manual, Version 8.0, Mechanical Dynamics Inc., Ann Arbor, Michigan.
- ADAMS/FEA, 1994. ADAMS/Finite Element Analysis Reference Manual, Version 8.0, Mechanical Dynamics Inc., Ann Arbor, Michigan 1994, 236 p.
- Adelman, H.M. and Natrayanaswami, R., 1974. Inclusion of Transverse Shear Deformation in Finite Element Displacement Formulations, AIAA Jnl, Vol 12, No 11, 1974, pp. 1613-1614.
- Amirouche, F. M. L., 1992. Computational Methods in Multi Body Dynamics, Prentice-Hall, Inc. Eaglewood Cliffs, New Jersey, 478 p.
- Asada, H., 1982. A Geometrical Representation of Manipulator Dynamics and Its Application to Arm Design, ASME Journal of Dynamic Systems, Measurement and Control, Vol. 105, No 3, pp. 131-135 & 142.
- Blundell, M.V., Phillips, B.D.A. and Mackie, A., 1996. The Role of Multibody Systems Analysis in Vehicle Design, Journal of Engineering design, Vol. 7, No. 4, pp. 337-396.
- Cardona A., Geradin M., Granville D. and Rayemaekers V., 1988. Module d'analyse de mécanismes flexibles MECANO - Manuel d'utilisation Université de Liège, LTAS-report, Liège.
- Cardona, A., 1989. An Integrated Approach to Mechanism Analysis, PhD thesis, Université de Liège, Faculté des Sciences Appliquées, Liège.
- Clavel, R., 1989. Une nouvelle structure de manipulateur pour la robotique légère, APII 23, pp. 501-519.
- Craig, J. J., 1989. Introduction to robotics: mechanics and control, Addison-Wesley, p. 450.
- Denavit, J. and Hartenberg, R.S., 1955. A kinematic notation for lower-pair mechanisms based on matrices, Journal of Applied Mechanics, June, 1955, pp. 215-226.
- Earles, S. W. E. and Wu, C. L. S., 1975. Predicting the occurrence of contact loss at a bearing from zero-clearance analysis, Proceedings of Fourth World Congress on the Theory of Machines and Mechanisms, Newcastle.
- Elliott, A., 1995. True Inverse Kinematics Using a Dummy Positioner Mechanism, MDI Technical Bulletin TB-001003, Mechanical Dynamics, Michigan, February 1995.
- Fertis, D. G., 1973. Dynamics and Vibration of Structures, Wiley, New York.
- Gérardin M., 1992. Computational Aspects of the Finite Element Approach to Flexible Multibody Systems, In: W.Schiewlen (ed.), Advanced Multibody System Dynamics, Netherlands, Kluwer Academic Publishers, pp. 337-354.
- Hale, A. L. and Meitrovitch, L., 1980. A general substructure synthesis method for dynamic simulation of complex structures, J. Sound Vib. Vol 69, 1980, pp. 209-326.
- Hahn, H., 1994. Mathematical modelling and computer simulation of rigid body systems including spatial joints with clearance, Control Engineering and Systems Theory Group, Department of Mechanical Engineering, University of Kassel, pp. 261-267.
- Hollerbach, J.M., 1980. A Recursive Lagrangian Formulation of Manipulator Dynamics and a Comparative Study of Dynamics Formulation Complexity, IEEE transactions on Systems, Man and Cybernetics, Vol. SMC-10, No.11, November 80, pp. 730-736.
- Huston, R.L., 1982. Multibody Dynamics: Analysis of Flexibility Effects, Proc. of the 9th U.S. National Congress of Applied Mechanics.
- Hyvönen, J. and Seppänen, J., 1985. Lisp world II: Programming Methods and -systems, In Finnish: Lisp-Maailma II: Ohjelmointimenetelmät ja -järjestelmät. Kirjayhtymä, Helsinki.
- Jahnke, M., Popp K. and Dirr, B., 1992. Approximate analysis of flexible parts in multibody systems using the finite element method, In: W.Schiewlen (ed.), Advanced Multibody System Dynamics, Netherlands, Kluwer Academic Publishers, pp. 237-256.
- Keskinen, E., 1994. A Contact Dynamics Formulation for Distributed Simulation of Flexible Hydromechanical Systems, PhD-Thesis, Tampere University of Technology, Publications 134, Tampere.
- Klein, C. A. and Blaho, B. E., 1987. Dexterity measures for the design and control of kinematically redundant manipulators, Internat. Journal of Robotics Research., Vol. 6, no. 2, pp. 72-83.
- Khatib, O., 1996. Inertial Properties in Robotic Manipulation: An Object-Level Framework, Int. Journal of Robotics Research,1, February 1995, pp. 19-36.
- Kjellander, J., 1995. Produktmodeller i Skapandefasen, Proceed. Produktmodeller-95, April 25-26, Linköping, pp. 121-128.
- Kumar, A. and Waldron, K. J., 1981. The Workspaces of a Mechanical Manipulator, ASME Journal of Mechanical Design, Vol. 103, pp. 665- 672.
- Kurtz, R. and Hayward, V., 1992. Multiple-Goal Kinematic Optimisation of a Parallel Spherical Mechanism with Actuator Redundancy, IEEE Transactions on Robotics and Automation, Vol. 8, No. 5. October 1992, pp. 644-651.
- Lee, C.S.G., 1982. Robot Arm Kinematics, Dynamics and Control, IEEE, Computer, Vol. 15, No. 12, December 82, pp. 62-80.
- Liou, F.W. and Erdman, A.G., 1988. Journal of Acoustics Stress Reliability Design, 111, pp. 35-41.
- Liou, F.W. and Patra, A.K., 1994. An advisory system for the analysis and design of deformable beam-type multi-body

systems, *Mech. Mach. Theory*, Vol 29, No. 8, pp. 1205-1218.

Lind, H., 1993. A Distributed Implementation of Dynamic Control on a Direct-Drive Robot System, PhD thesis, Damek Research Group, Department of Machine Elements, The Royal Institute of Technology, Stockholm, ISSN 0282-0048.

Makkonen, P., 1995. User-adapted function simulation and performance evaluation of mechanical systems, Lic. thesis, Department of Machine Design, Engineering Design, The Royal Institute of Technology, KTH.

Makkonen, P., 1998. On the development of a planar clearance joint for Multi Body Systems Simulation, In: Makkonen, P., PhD-Thesis, Department of Machine Design, Engineering Design, Royal Institute of Technology, KTH.

Makkonen, P. and Persson, J.-G., 1999. Derivation of the stiffness matrix for beam elements in MBS models, In: Makkonen, PhD-thesis, Royal Institute of Technology, KTH.

Ono, K. and Teramoto, T., 1993. Minimum-Time Trajectory Planning for Multi-Degree-of-freedom System under Average Heat Generation Restriction, *Robotics, Mechatronics and Manufacturing Systems*, Elsevier Science Publishers B.V. pp. 197-202.

Ozaki, H., Yamamoto, M. and Mohri, A., 1987. Transactions SICE, Vol . 23, nro . 11, pp. 1199-1205.

Park, F.C., 1995. Optimal Robot Design and Differential Geometry, *ASME Journal of Mechanisms, Transmissions and Automation in Design*, Special 50th Anniversary Design Issue, Vol 117, June 1995, pp. 87 - 93.

Pierrot, F., Dauchez, P. and Fournier, A., 1991. Fast Parallel Robots, *Journal of Robotic Systems* 8(6), pp. 829-840.

Rajan, V.T., 1985. Minimum Time Trajectory Planning, Proc. IEEE Intern. Conference in Robotics Automation, pp. 759-764.

Rauh, J., 1987. Ein Beitrag zur Modellierung elastischer Balkensystem, *Fortschr. Ber. VDI-Z*, 18(37) (1987).

Rivin, E.I., 1987. Mechanical design of robots, McGraw Hill, Inc., New York.

Salisbury, J. K., and Craig, J.J., 1982. Articulated Hands: Force Control and Kinematic Issues, *Int. J. Robotics Research*, Vol 1, No 1, pp. 4-17.

Seneviratne, L. D., 1985. A design criterion for maintaining contact at revolute joint with clearance, PhD Thesis, University of London.

Seneviratne, L. D., Earles, S. W. E. and Fenner, D. N., 1996. Analysis of a four-bar mechanism with radially compliant clearance joint, *Proc. Instn. Mech. Engrs. Sci.*, London, Vol 210, No 63, pp. 215-223.

Shabana, A. A., 1985. Substructure Synthesis Methods for Dynamic Analysis of Multi-Body Systems, *Computers & Structures* Vol. 20, No. 4, pp. 737-744, 1985.

Sorge, K., Bremer, H. and Pfeiffer F., 1992. Multi-Body Systems with Rigid-Elastic Subsystems, In: W. Shielen (ed.), *Advanced Multibody System Dynamics*, Netherlands, Kluwer Academic Publishers, pp. 195 - 215.

Sundström, B., 1988. Elementary Structure Analysis, *Vibrations in Discrete Systems*, In Swedish. Fingraf AB, Södertälje.

Timoshenko, S.P. and Goodier, J.N., 1970. *Theory of elasticity*, 3rd edition. McGraw-Hill, New York. 567 p.

Tourassis, V. D. and Kircanski, N., 1985. *Scientific Fundamentals of Robotics 4, Real-Time Dynamics of Manipulation robots*, Springer-Verlag, Berlin, Heidelberg, ISBN 3-540-13072-1, ISBN 0-387-13072-1.

Turcic, D. A., Midha, A. and Bosnik, J.R., 1983. Dynamic Analysis of Elastic Mechanism Systems, ASME paper No. 83-WA/DSC-38.

Vukobratovic, M. and Stepanenko, Y., 1982. Mathematical models of General Anthropomorphic Systems, *Mathematical Biosciences*, Vol 17., 1973, pp 137-170

Waters, R.C., 1979. Mechanical Arm Control, M.I.T. Artificial Intelligence Lab, Memo 549, October 1979.

Yoshikawa, T., 1985. Manipulability of Robotic Mechanisms, *Int. J. Robotics Research*, Vol 4., No 2, pp. 3-9.

Skräp bort taget från artikkeln

Taskit paperin valmistamiseksi:

- | | |
|--|---|
| 1) Lue Keskinen | + |
| 2) Kirjoita lyhyesti välyssimuloinneista | + |
| 3) Tee materiaalitaulukot | + |
| 4) Kirjoita johtopäätökset | + |
| 5) Tee annotation list | + |
| 6) Tee 3D välysmakro | + |
| 7) Simuloi elastista rataa (KTH) | - |
| 8) Tee ratakäyra ja FFT-käyrä (KTH) | + |
| 9) Simuloi välysraataa (KTH) | + |
| 10) Kirjoita abstrakti ja johdanto | + |
| 11) Lue ja korja artikkeli | + |

¹ For addressing the need of effectivising variant design process, Prof. Eppinger, MIT, points out that variant design is far more common and gives major part of renewes in most of the industries, while projects for completely new design from scratch are less common. The objective in this paper is however to show, that even in projects for new designs macro based product modelling is reasonable, giving a simulation model for the product family right from the birth to whole life time.

2.8 Agility

To study the agility of a robot mechanism, it is not enough to study the kinematic gain of the mechanism i.e. the operation space jacobian to joint space, (For.3). It seems more reasonable to study the reaction forces or torque caused by the motion of masses. Asada (1983), presents the concept of Generalised Inertia Ellipsoid, GIE. Asada's approach is to derive the kinetic energy of the manipulator part by part, by numbering the rigid bodies from 0 to n. Thus the kinetic energy of the mechanism is

$$T = \frac{1}{2} \sum_{i=1}^n m_i v_i^T v_i + \mathbf{w}_i^T I_i \mathbf{w}_i \quad (29)$$

where, for rigid body i , m_i is I_i are the mass and inertia tensors, respectively, and v_i and \mathbf{w}_i are the Cartesian velocities with respect to the inertial frame. The velocities v_i and \mathbf{w}_i may be given by using the linear combinations of

$$\mathbf{w}_i = \sum_{j=1}^i a_j \dot{\mathbf{q}}_j, v_i = \sum_{j=1}^n (r_i^j \times a_j) \dot{\mathbf{q}}_j \quad (30)$$

where \mathbf{q}_i is joint coordinate of joint a_j is the unit vector for the direction of j th joint axis, and the r_i^j is the position vector from joint j to the center of frame i . While Asada calculates the translational and angular speed in respect to inertial system, with the equation (29), the speed can usually be generated using a general multibody program. Independent from the method, the total energy of the multi body system is given by equation (30)

$$T = \frac{1}{2} \dot{\mathbf{q}}^T H \dot{\mathbf{q}} \quad (31)$$

Where $\Theta = (\dot{\mathbf{q}}_1, \dot{\mathbf{q}}_2, \dots, \dot{\mathbf{q}}_n)^T$ is a $n \times 1$ vector, and H a $n \times n$ symmetric matrix. The kinetic energy can be calculated using any set of generalised coordinates (q_1, q_2, \dots, q_n) having equivalent correspondence to joint displacements $(\Theta_1, \Theta_2, \dots, \Theta_n)$. The total kinetic energy in generalised coordinates will then be

$$T = \frac{1}{2} \dot{\mathbf{q}}^T H \dot{\mathbf{q}} \quad (32)$$

where the matrix G is

$$G = \frac{1}{2} R^T H R \quad (33)$$

The mass and inertia discretisation gives some advantage compared to the elastic body formalism (class iv. in chapter 3.2). The model includes the rotary inertia in the distributed frames and Coriolis terms due to frame interaction affecting the right hand terms of equation (42). The mass distribution divides also the axial load in the structure due to centrifugal load causing geometric stiffening which increases the vibration frequency.

The equation for the beam's total internal energy under general load case is

$$W = \frac{1}{2} \int_0^L \frac{N(x)^2}{EA} + \frac{M_y(x)^2}{EI_y} + \frac{M_z(x)^2}{EI_z} + \mathbf{z}_z \frac{T_z(x)^2}{GA} + \mathbf{z}_y \frac{T_y(x)^2}{GA} + \frac{M_n(x)^2}{GI_x} dx \quad (46)$$

In this paper, the constitutive element is a full 6 d.o.f. relation. Let us assume, that the beam is fixed rigid from the frame r_A and connected with a 6 d.o.f. strain force relation from frame r_A to frame r_B , and the frame r_B is in rest, at the distance $(L, 0, 0)$ from frame r_A , as in figure 8. The 6x1 deformation vector Δr is the difference Δr between deformation position and orientation of frame r_b in respect to rest position of r_b .

On the development of a planar clearance joint model for Multi Body Systems simulation

Petri Makkonen
Engineering Design
Department of Machine Design
Royal Institute of Technology, KTH
Stockholm

In most multi body systems software packages, the joints of a mechanical structure are simulated by kinematical constraints of various types. In real world implementations, journal bearing joints usually require some clearance for proper function and they always have compliance and joint friction, causing loss of contact, which can lead to noise generation and joint deterioration. To predict contact loss detailed joint modelling is required, which can take into consideration the physical effects of clearance, friction and edge pressure. This paper presents a method for multi body systems simulation of planar joint clearance, where the original kinematical joint is substituted by a general constitutive force relation, positioned between the connected rigid bodies modelling the bearing house and the pin body. The force relation shown is for a radially compliant joint, but can be easily modified for translation, hooke as well as other joint types. The model is investigated by using it in a four bar mechanism application, and compared to other clearance models known from literature.

Notation

F_s	support force over bearing contact
e	material elasticity exponent
I_i	moment of inertia of link i through the centre of mass
K_c	radial stiffness for journal contact
m_i	mass of link i
r_c	length of clearance link (ML and MLSD models)
\dot{r}_c	first time derivative of r_c
\ddot{r}_c	second time derivative of r_c
r	radial distance of clearance contact point in impact model
R	radial clearance of impact model
r_i	length of link i
s_i	distance of link i 's mass centre from joint
g	orientation of F_s with respect to the mechanism base line OD
\dot{g}	first time derivative of g
q_i	orientation of link i with respect to the mechanism base line OD
\dot{q}_i	first time derivative of q_i
m	radial damping factor of clearance link
$\tilde{O}(x)$	Heaviside function being equal to one when $x>0$ and zero when $x\leq 0$

1. Introduction

Journal bearings are used for connecting moving links in mechanisms. Depending on load and bearing materials, they require little or no lubrication. They are in principle simple machine elements, relatively cheap and easy to install and maintain. Journal bearings comprise two elements: The shaft, which is a cylindrical pin, and a bearing housing being a cylindrical bushing. Usually the shaft is of ground or polished steel, while the bearing housing includes different functional layers for lubrication and absorption of contact pressure. Some radial clearance is required between bush and pin to allow the relative movement of the connected links.

During their life cycle, journal bearings are subjected to various load conditions, where some of them are particularly illconditioned leading to fatigue failure. While radial compliance leads to a line contact, the clearance allows the contact line to move freely around the bearing house. If the joint contact line is not equally longitudinally loaded over the joint bearing, the joint deteriorates unevenly. Thus it is obvious that accurate predictions of the dynamical loads and the contact pressure are important parts of the design requirements.

It is well known that loss of contact can occur in a clearance joint (7). While the joint normally transfers a force over the functional contact surfaces, sometimes the contact is lost. At that time the contact force is reduced to zero, and the pin moves freely inside the clearance area. When the contact finally is re-established, undesirable impact occurs that may cause bearing failure, e.g. due to fatigue. Noise and vibrations are transmitted throughout the mechanism structure and to the environment. Thus avoidance of loss of contact is an important design objective.

2. MBS-model for a journal bearing clearance

2.1 Current alternatives

Usually mechanisms are simulated with zero clearance models, i.e. with models having ideal infinitely stiff joints, often referred to as kinematical pairs. While this abstraction leads to a fast solvable numerical model, it is unable to predict the effects of clearance.

During the years, several approaches have been taken to simulate journal bearing clearance. They mainly fall into two categories, both being two dimensional models:

- The massless link. An additional degree of freedom is added to the model by adding an extra link with no mass, having a fixed length equal to the clearance of the joint.
- The spring-damper model. In this approach a spring-damper unit is coupled between the bearing house and shaft.

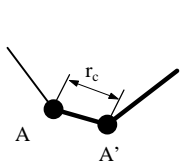


Fig 1a.

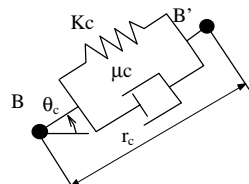


Fig 1b.

Fig. 1a). Mass-less link element between two rigid beam bodies. 1b) Spring damper element to connect two rigid parts.

2.2 The massless link (ML) model

It is considered that neglection of the bearing clearance accounts for the inability of the zero-clearance model to predict the loss of contact based simply on the condition that joint reaction force equals to zero. Earles and Wu (3) incorporated clearance to their model by representing the distance between the centers of the bearing pin and bush by a mass less link (AA' in figure 1a). This results in a mechanism having an additional degree of freedom. The resulting equations were found to be very highly non-linear and complex to solve, both in terms of software and hardware demands. Although the time domain responses of the massless link model exhibited high-frequency oscillations, the average time responses were in general similar to the zero-clearance responses.

By using results, obtained from the ML-model, Earles and Wu (4) carried out an experimental investigation and proposed the empirical criterion: contact is maintained if

$$\dot{\phi} / F < 1 \quad (1)$$

where F is the zero-clearance bearing force magnitude and $\dot{\phi}$ is the time rate of change of the orientation of bearing force \mathbf{F} . As Earles and Seneviratne state in (5), there is no immediate obvious physical or intuitive reason for the involvement of $\dot{\phi}$ in the mechanism of contact loss - other, than the fact that the parameters in the criterion are derived from the zero-clearance analysis which is not fully descriptive of the actual dynamic state of the system. The need for further studies and simulation models is underlined by the dimensional nature of the criterion. Actually, Earles and Wu are stating that there should

exist a dimensionless parameter based on actual physical conditions, that could predict loss of contact.

Also, Seneviratne and Earles have proposed an analytical theory as design criterion (8) for predicting the appearance of chaotic clearance behavior as function of rotational speed, which can be derived from zero clearance model results. The system of non-linear equations is dependent from the mechanism dimensions in a very complex way, making the method too complex for use in engineering problem solving.

2.3. The MLSD-Model

In the spring-damper model (see fig 1b) the clearance joint, B, is represented by a massless link BB' of length equal to the radial clearance, r_c . BB' has radial stiffness, K_c , and radial damping with the coefficient η_c . Seneviratne, Earles and Fenner (9), have derived the kinematical and dynamical equations of motion analytically. While the zero-clearance model requires two kinematical and two dynamical equations of motion, and the massless link approach requires four of each, the model (9) requires six equations. These equations are coupled, non-linear and have no analytical solution, thus need to be integrated numerically. The numerical values used for the model parameters are equal to the parameter values given in appendix 1. The equations for the MLSD model will be reduced to those for a massless link model when $\eta_c = \eta_{c'} = 0$. If additionally $r_c = 0$, the equations will be reduced to those for the zero-clearance model.

The models require different number of initial conditions. Since the zero-clearance model has one degree of freedom, it requires the specification of the initial conditions for the crank angle q_2 and its initial angular velocity \dot{q}_2 . The mass less-link equations have additionally one degree of freedom and require thus additionally the specification of clearance link angle q_c and its initial angular velocity \dot{q}_c . The initial values of q_c and \dot{q}_c are generally assumed to be the values of their zero-clearance counterparts: g , the orientation of the joint reaction force and \dot{g} , the angular velocity of joint reaction force, respectively.

Since the MLSD model has three degrees of freedom, it requires also definition of the clearance link length, r_c and radial velocity \dot{r}_c . Seneviratne, Earles and Fenner (9), assume the initial spring-damper length to be equal to the free length r_c plus the extension corresponding the initial joint load. The initial joint load is calculated assuming zero clearance.

Both the massless link and MLSD-model include major simplifications. In the former model, it is assumed that loss of contact never occurs. In the latter model, loss of contact could occur, but there always exists a linear relation between the clearance distance and the joint force. Thus when loss of contact is established, a stiff spring force will soon remake the contact, due to the positive contact force. This is not corresponding to physical reality, thus the model has an inclination to predict contact re-establishment more than in reality. Also, the assumption that initial values are obtained from zero-clearance analysis (9), rather than to have an initial impact due arbitrary initial values, is an oversimplified well-conditioned assumption.

2.4 Impact-model

A specific focus in this paper is the development of an impact model having zero joint force during contact loss mode. Such a model can be established by using a vector force element for the contact's internal support force.

In figure 2. a schematic figure of the impact clearance joint element is presented. It is assumed that the joint contact points are completely kinematically uncoupled. A position feedback joint active-reactive force pair is applied between the points A and C. If the joint

contact point C is inside the radius R, the joint force is assumed to be zero. If the contact point exceeds the joint clearance, contact is established and the contact force is activated.

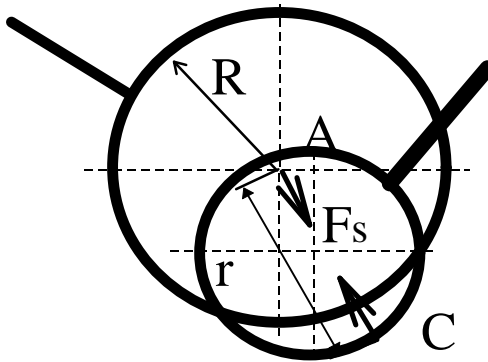


Fig 2. Contact model using vector force element definition

The position feedback control detects and activates/deactivates the bearing's internal support force during contact/contact loss. The feedback function $\Pi(r)$ is a Heaviside function having the value zero while its argument is negative and the value one while the argument is positive or zero. The Heaviside function is used to detect the contact and activating the support force. The supporting force is assumed to follow Hooke's law ($e=1$ in eq. 2), and the damping force is assumed to be proportional to the relative velocity between the parts. To prevent discontinuity in the damping force at contact, the damping coefficient is a cubic step function of the penetration. Thus, at zero penetration, the damping coefficient is always zero. The damping coefficient saturates to its maximum value C_{max} , at a predefined penetration, d . This characteristic length is selected to be about $1.2 \mu\text{m}$ in a typical bearing coating. The force function is thus:

$$F_s = \Pi(r-R) \{ K_r (r-R)^e - S(r, R, 0, R+d, 1) \mathbf{m} \} \quad (2)$$

where the function $S(x)$ is a cubic spline polynomial as follows:

$$S(x, x_0, h_0, x_1, h_1) = \begin{cases} h_0: x \leq x_0 \\ h_0 + (h_1 - h_0) \left[\frac{(x - x_0)}{(x_1 - x_0)} \right]^3: x_0 < x < x_1 \\ h_1: x \geq x_1 \end{cases} \quad (3)$$

The active/reactive force F_s is acting between the axes of bushing and pin-shaft. Thus it can be divided into components:

$$\begin{aligned} F_{sx} &= -dx/\sqrt{dx^2 + dy^2} F_s \\ F_{sy} &= -dy/\sqrt{dx^2 + dy^2} F_s \end{aligned} \quad (4)$$

where dx and dy are the coordinates of the contact point calculated from the shaft axis centre.

2.5 The operating principle selected

From these three categories of joint clearance models the impact force model is the only one, which can simulate loss of contact with zero joint force. Moreover, if the force element can also transfer torque, the model can be generalised to three dimensions. Such generalised force elements can be found in most modern MBS (multi body system) software. The basic principle for implementing the joint is to remove the existing kinematical joint from a mechanism model and change it to a general three dimensional constitutive force and torque relation having position feedback. The equations defining the forces are completely depending on the joint's idealised geometrical and contact mechanical properties and thus this method has the advantage, that it can be used not only for rotational journal bearings, but also for several other kinematic pairs, like translational, planar, screw or hooke joints. The modelling of such joints is however beyond the objectives of this work.

3. Test mechanism

The test mechanism, which dimensionally equals the test mechanism described in (8), is a crank-counter-rocker class of a four bar linkage mechanism, with a clearance bearing at the coupler-rocker joint. The dimensions and parameter values of the mechanism are given in appendix 1. The kinematical layout parameters of the simulation models are given in appendix 2. In this paper two types of simulation models are used for comparison, both with dissipative clearance joint models. The first type is with an impact joint, and the second is with an MLSD joint. The latter model is used to verify the models with simulation results presented in literature (9).

An experimental test rig having parameter values corresponding to the model is currently being constructed for later verification of the author's simulation results.

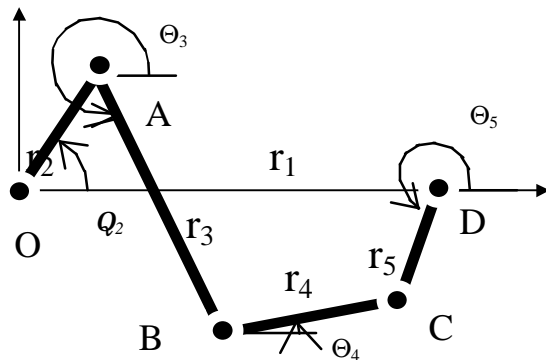


Fig 3. Fourbar test mechanism.

The plane test mechanism, which operates against gravitational load is shown schematically in figure 3. Further references are given in (9) and (10). The simulation model has an additional oscillatory fifth crank DC, which can be used to adjust the base length OC of the four bar mechanism. The crank OA is driven by a variable speed motor. In the test rig, which will be built, the distance OC is adjustable linearly. The test bearing at joint B has a radial clearance of 100 μm , consisting of a steel pin in a dry bronze bushing, of nominal diameter 25 mm and length 30 mm.

The mechanism is simulated dynamically and the crank is given an initial speed. When the mechanism is rotated freely, the crank speed depends periodically from the crank phase angle, due to the change of kinetic and potential energy of the mechanism during crank rotation. All speeds given in this paper are instantaneous speeds at the crank angle of $q_2 = 90^\circ$. The variation of rotational speed at 250 r/min is 243 - 274 r/min i.e. $\pm 6\%$.

4. Impact model results

The dynamical system was solved in ADAMS 8.2 multi body system software. The CPU time and computational effectiveness is shown in table 1. The numerical equations were solved using the Gear-stiff-integrator with a specified relative error of 5×10^6 and an absolute error of 5×10^6 . The simulated time was $t=1.25$ s, with a minimum limit of 10^3 and maximum of 10^6 simulation steps. The CPU-time was estimated from simulation runs where the rotational crank speed was 250 r/min, and in the dissipative models the radial stiffness was $K_c = 1 \times 10^8$ N/m, and without damping, i.e. $m = 0$ Ns/m, table 1.

Table 1. Computational times

Model	CPU time (s)	Iterations	Steps	Integr. order
Zero-clearance	62,01	2527	1258	2
MLSD	76,07	5118	1303	3
Impact model	523,0	55390	7439	2

As table 1 shows, the MLSD model is not much more complex than the zero clearance model and the impact model is just eight times more complex to solve. Thus both methods are well suited for modern MBS software.

For $K_c = 1 \times 10^8$ N/m, and with a critical damping value $m = 3000$ Ns/m, the mechanism was simulated over the period of $t=1.25$ s. In figure 4. the predicted resultant joint force variation over time at the clearance bearing is shown at the rotational speed of 92 r/min. After the initial shock due to start of the mechanism has been damped out, the response is regular and the contact is maintained. However, when the rotational speed is increased to 94 r/min, the contact is periodically lost. At the first revolution the contact is lost about at $q_2 = 215^\circ$ and remade at $q_2 = 365^\circ$, while at the second revolution loss occurs at $q_2 = 161^\circ$ and is remade at $q_2 = 307^\circ$, indicating non-periodicity (see figure 5.).

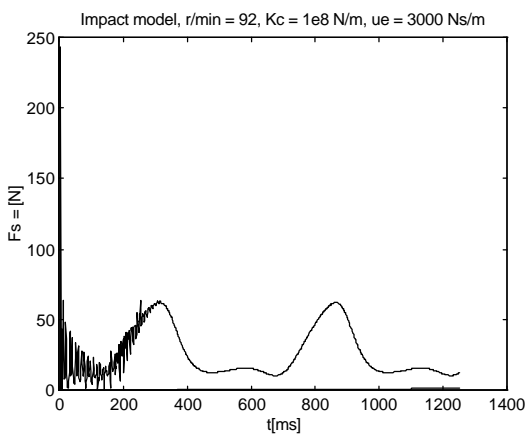


Fig 4. Predicted variation of bearing force at $\dot{q}_2 = 92$ r/min with damping.

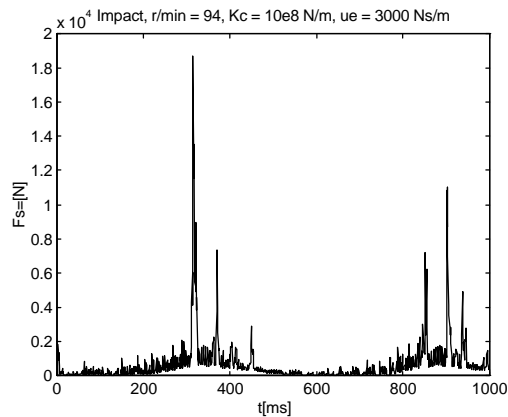


Fig 5. Predicted variation of bearing force at $\dot{\varphi}_2 = 94$ r/min with damping.

With the elasticity of the bearing $K_c = 1 \times 10^8$ N/m, and the damping $m_e = 3000$ Ns/m and when the bearing speed is incrementally increased from 94 to 205 r/min, the mechanism maintains chaotic response (fig 6). When the speed is increased up to 208 r/min (fig. 7.), the regular behavior re-occurs and the stable contact compliance is re-established, however the contact force decreases momentarily to zero as can be seen on the first and fifth cam rotation period, indicating the narrowness of the chaotic regime at over-critical rotational speed.

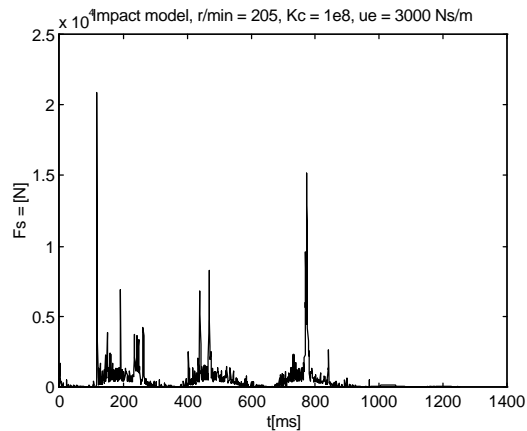


Fig 6. Predicted chaotic variation of bearing force at 205 r/min.

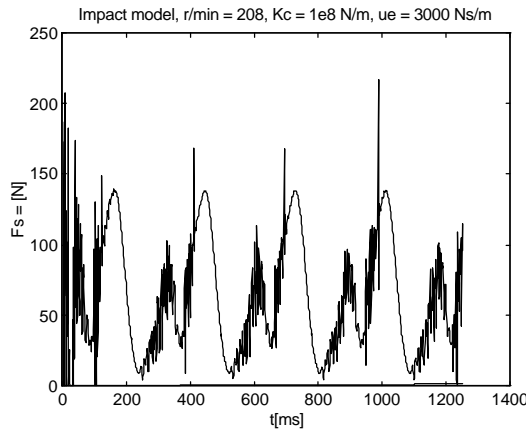


Fig 7. Predicted regular response of bearing force at 208 r/min.

In contradiction to literature (9), the lower speed limit for loss of contact was not observed at the speed of 253 r/min, but as low as 94 r/min. The reason is that in the referred simulation an external spring load was used, not reproducibly defined in the paper, increasing the speed limit significantly. In this study, simulations were performed up to 400 r/min, and no new loss of contact regime was found.

The parameter study was repeated in the lower stiffness region. For $K_c=1\times 10^7$ N/m, and the damping $m=3000$ Ns/m, the contact was maintained up to 110 r/min (fig 8). When the speed was increased up to 130 r/min, the surface contact was again lost and the behavior of the mechanism became chaotic. The chaotic behavior is however in this case quite mild, indicating the elasticity of the joint.

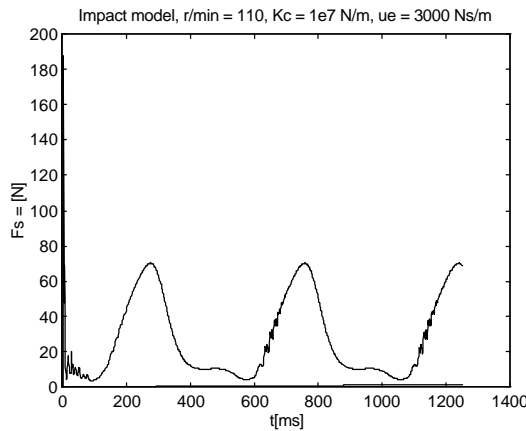


Fig 8. Predicted variation of bearing force at 110 r/min, low stiffness.

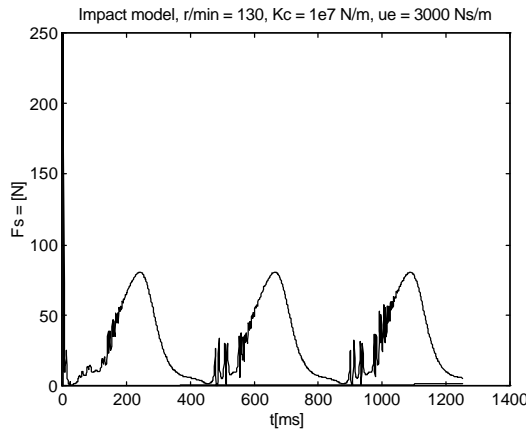


Fig 9. Predicted variation of bearing force at 130 r/min, low stiffness.

The upper boundary for the low stiffness region ($K_c = 1 \times 10^6$ N/m, and damping $m = 3000$ Ns/m) was found to be chaotic at speed of 150 r/min, while at 160 r/min stable surface contact was maintained. As for high stiffness, there was no new chaotic region found when the speed was increased to 400 r/min.

As expected, with the introduction of lower stiffness $K_c = 1 \times 10^6$ N/m, instead of $K_c = 1 \times 10^7$ N/m, the response is qualitatively similar to the case with higher bearing stiffness, but the chaotic speed region of the simulations decreases from 94 - 206 r/min to 120 - 150 r/min. Thus it is evident that the change of radial stiffness will influence the chaotic region significantly.

When the normal stiffness, $K_c = 1 \times 10^8$ N/m, is used with no damping of the bearing, the lower chaotic boundary changes from 92 r/min to 97 r/min. (fig 10 and 11.). The width of the chaotic region doesn't, however, change. The chaotic response begins at 100 r/min. This finding opposes the expectation, that increased damping diminishes the chaotic boundary and requires further investigation.

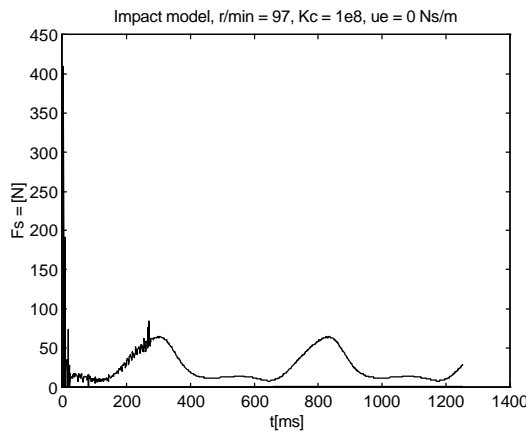


Fig 10. Regular response boundary with no damping at 97 r/min

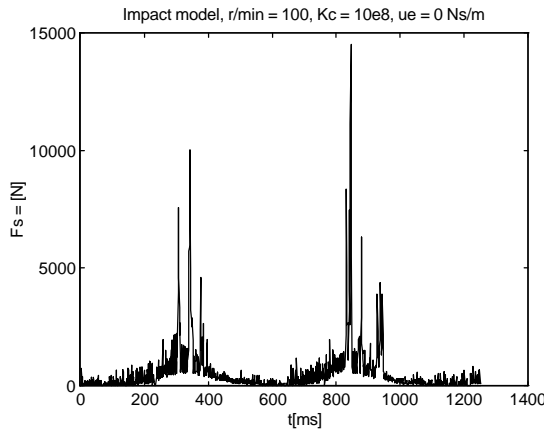


Fig. 11. Chaotic behavior with no damping at 100 r/min.

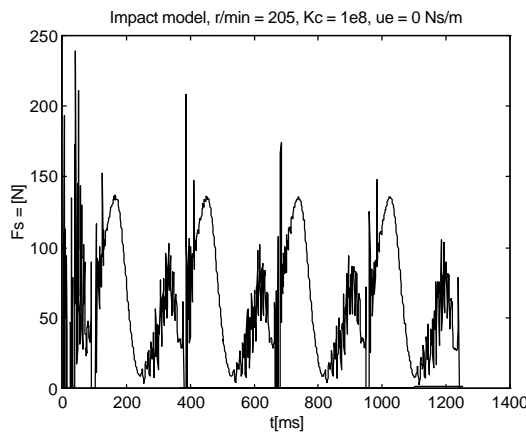


Fig. 12. Chaotic behavior with no damping at 205 r/min.

The upper speed boundary of chaos with no damping and for regular stiffness $K_c = 10^8$ N/m, was found to be 205 r/min. This transition is difficult to observe from the resultant bearing force function, merely from zero force transitions, while from the clearance distance plots it can be more clearly observed. When the speed is increased to 210 r/min, the zero force transitions disappear. (fig 12 and 13.)

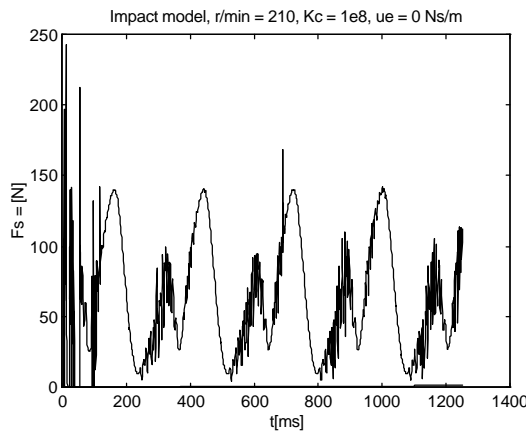


Fig. 13. Transition to regular behavior with no damping at 210 r/min.

5. Verification by comparison to the MLSD model

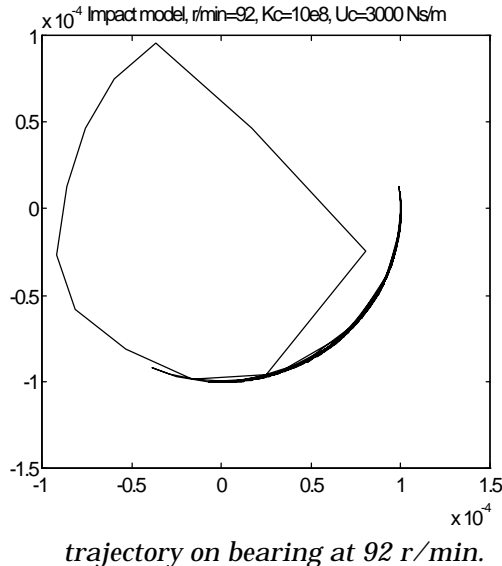
To verify the results with previous results published in literature (8), (9), simulation runs were also performed with the MLSD model. In the higher bearing stiffness region, $K_c = 1.0 \times 10^8 \text{ N/m}$, and for the damping $m = 3000 \text{ Ns/m}$, the contact is maintained up to 100 r/min. At the speed of 130 r/min, the contact is definitely lost. The chaotic behaviour is maintained up to 150 r/min, while when the speed is 160 r/min, the contact is again re-made.

For lower bearing stiffness, $K_c = 1 \times 10^7 \text{ N/m}$, and the damping $m = 3000 \text{ Ns/m}$, the contact is maintained up to 120 r/min. At the speed of 130 r/min, the contact is lost, while at 140 r/min, it is again remade.

The small changes in loss of contact regions addressed to examine how the contact area will respond for a very stiff bearing. At $K_c = 10^9 \text{ N/m}$ and damping $m = 3000 \text{ Ns/m}$, the contact regions were equal to the case of $K_c = 10^8 \text{ N/m}$ and damping $m = 3000 \text{ Ns/m}$, loss of contact was identified within the speed range 130 -150 r/min. Thus with the MLSD model, the speed region of contact loss changed less than with the impact model.

6. Contact trajectories

To clarify the behaviour of the journal's axis position trajectory relative to the bearing house axis, trajectory plots were examined. In figure 14 and 15, the pin's axis trajectory is shown, relative to the bearing house. In figure 14, the initial shock due to impact at start up is damped out. The edges on the curve indicate contact points, while numerical accuracy is low due to the long time steps during the shock. After the initial transient is damped out the regular response is indicated by an oscillating contact point between fixed angles.



trajectory on bearing at 92 r/min.

Fig 14. Predicted contact point

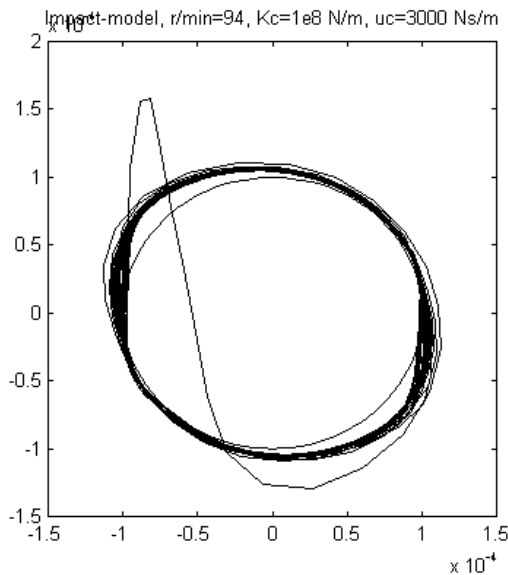


Fig 15. Predicted contact point trajectory at 94 r/min.

In figure 15, with higher speed, the initial impact is also damped out. After damping of the transient, the trajectory starts to cycle around the whole contact circumference, in a chaotic way. The inner circle indicates the clearance boundary of the contact loss area.

7. Conclusions

The usefulness of an impact clearance model has been investigated. The model's applicability for real time MBS simulation was investigated and compared to an MLSD model. The results were obtained with ADAMS 8.2 MBS software using a SUN Sparcstation 20 computer. From using this impact model the following conclusions can be made (figure 16):

- (a) the impact model predicts chaotic behavior in a wider interval of rotational speeds than does the MLSD-model.
- (b) The boundaries of unpredictable response (between regular and chaotic behavior) of the impact model with a stiff bearing $K_c = 1 \times 10^8$ N/m, is small indicating regular response outside the 92 - 208 r/min region and chaotic response inside the 94 - 205 r/min region.
- (c) With lower stiffness $K_c = 1 \times 10^7$ N/m, the chaotic region decreases (130 - 150 r/min) and also the bearing force oscillation decreases in the chaotic region due to low stiffness. However, the uncertain region increases as the regular region is outside of the 110 - 160 r/min boundaries.
- (d) With damping the chaotic regions are wider than without damping which is unexpected and will require further research.
- (e) The initial condition sensitivity was treated by letting a large transient in form of an initial impact act on the joint when the crank is started and the rest of the mechanism follows the crank. During damping out of the transient the contact is remade in an initially unpredictable angle of the bearing contact and the contact position converges to angular oscillation or will continue as a chaotic response.
- (f) The selection of time step has considerable effect on the numerical stability of the solutions. The time step should be a decade shorter than the cycle time of the elastic contact vibration, which is in most cases corresponding to around one kHz. If the detailed contact trajectory is important, more time consuming analysis is needed. However, when a large system is simulated, and only the vibration force level is of interest, variable length integrators give acceptable estimates of the level of contact force vibration.

In figure 16, regular versus chaotic responses from all analyses are shown as a function of crank rotational speed and clearance joint stiffness. When the bearing stiffness is lowered with one decade from 1×10^8 N/m to 1×10^7 N/m the width of the chaotic region decreases by 74 %.

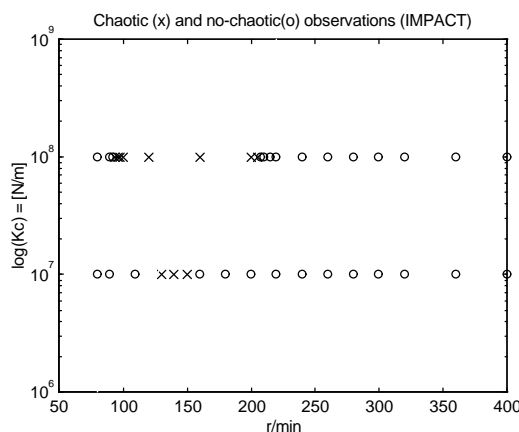


Fig 16. The observations of chaotic (x) and regular (o) response of the impact model as a function of rotational speed and elasticity with damping $m = 3000$ Ns/m

Figure 17. is similar to fig.16, but gives the response of the MLSD model. While the change of stiffness from 1×10^9 N/m to 1×10^8 N/m has very little effect on the chaotic speed region

width, the change from $1 \times 10^8 \text{ N/m}$ to $1 \times 10^7 \text{ N/m}$ will decrease the width of the chaotic region by 66 %.

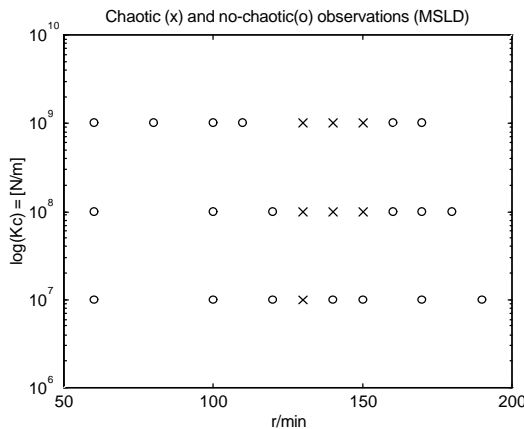


Fig 17. The observations of chaotic (x) and regular (o) response of the MLSD model as a function of rotational speed and elasticity with damping $m = 3000 \text{ Ns/m}$

8. References

- 1 Dubowsky, S. and Freudenstein, F.** Dynamic analysis of mechanical systems with clearances. *Trans. ASME, J. Engng Industry*, 1971 **93B**, 305-309.
- 2 Dubowsky, S., Prentis, J. H. and Valero R.A.** On the development of criteria for prediction of impacts in the design of high speed mechanisms with clearances. *Proceedings of Fifth World Congress on The theory of machines and mechanisms*, Montreal, Canada, 1979.
- 3 Earles, S. W. E. and Wu, C. L. S.** Motion analysis of rigid Lagrangian mechanics and digital computation. *Proc. Instn Mech Engrs, London, Mechanisms*, 1973, 83-89.
- 4 Earles, S. W. E. and Wu, C. L. S.** Predicting the occurrence of contact loss at a bearing from zero-clearance analysis. *Proceedings of Fourth World Congress on The theory of machines and mechanisms*, Newcastle, 1975.
- 5 Earles, S. W. E. and Seneviratne, L. D.** Design guidelines for predicting contact loss in revolute joints in planar linkage mechanisms. *Proc. Instn Mech Engrs, London, Part C*, 1990, 204 (C1), 9-18.
- 6 Grant S. J. and Fawcett, J. N.** Effects of clearance at the coupler rocker bearing of a four bar linkage. *Mechanisms and Machines Theory*, 1979, 14(2), 99-110.
- 7 Haines, R. S.** Two dimensional motion and impact at revolute joints. *Mechanisms and machines theory*, 1979, **15**, 361-370.
- 8 Seneviratne, L. D. and Earles, S. W. E.** Chaotic behaviour exhibited during contact loss in a clearance joint of a four bar mechanism. *Mechanisms and machines theory*, 1992, **27**, 307-321.
- 9 Seneviratne, L. D., Earles, S. W. E. and Fenner, D. N.** Analysis of a four-bar mechanism with radially compliant clearance joint. *Proc. Instn Mech Engrs Sci, London*, 1996, Vol. 210, No. 63, 215-223.
- 10 Seneviratne, L.D.** A design criterion for maintaining contact at revolute joint with clearance. PhD thesis, University of London, 1985.

Appendix 1.
Values of model parameters:

$I_2 = 0.2188 \text{ kg m}^2$, $I_3 = 0.0530 \text{ kgm}^2$,
 $I_4 = 0.2094 \text{ kgm}^2$
 $m_2 = 12.90 \text{ kg}$, $m_3 = 2.41 \text{ kg}$,
 $m_4 = 5.04 \text{ kg}$
 $r_1 = 800 \text{ mm}$, $r_3 = 100 \text{ mm}$,
 $r_4 = 390 \text{ mm}$,
 $r_4 = 580 \text{ mm}$, $r_5 = 100 \text{ mm}$, $r_c = 100 \mu\text{m}$
 $s_2 = 17.4 \text{ mm}$, $s_3 = 195 \text{ mm}$,
 $s_4 = 329 \text{ mm}$
 $q_5 = 70^\circ$, $q_2 = 90^\circ$,
 $w_2 = 80...400 \text{ r/min}$

Appendix 2.
The kinematic equations:

$$x_2 = r_2 \cos q_2 + x_1 \quad (1)$$

$$y_2 = r_2 \sin q_2 + y_1 \quad (2)$$

$$x_4 = r_5 \cos q_5 + x_1 + r_1 \quad (3)$$

$$y_4 = r_5 \sin q_5 + y_1 \quad (4)$$

$$q_3 = \arctan\left(\frac{y_4 - y_2}{x_4 - x_2}\right) \quad (5)$$

$$r_{42} = \sqrt{(x_4 - x_2)^2 + (y_4 - y_2)^2} \quad (6)$$

$$q_{42} = \arccos\left(\frac{r_3^2 + r_{42}^2 - r_4^2}{2r_3r_{42}}\right) + q_3 \quad (7)$$

$$x_3 = r_{42} \cos q_{42} + x_2 \quad (8)$$

$$y_3 = r_{42} \sin q_{42} + y_2 \quad (9)$$

Optimisation of a servo system: the design of control, transmission and motor selection

Petri Makkonen,
Jan-Gunnar Persson
Engineering Design
Department of Machine Design
Royal Institute of Technology, KTH
S-100 44 STOCKHOLM, SWEDEN

Abstract

The design of high performance and cost-effective servo systems requires optimisation. To achieve the required performance at the lowest cost will require the right selection of motor, transmission and control system. All these three aspects should be considered simultaneously during the design so that the total system fulfils the specification. Even in a simple case, in a gantry robot with linearly independent axis system, the task requires experiments and a trial and error approach. The kinematical specification can be fulfilled with high enough motor torque, but a larger motor also has greater self-inertia. By decreasing the transmission gear ratio, linear acceleration can be increased, at the cost of lower maximum speed. Yet the optimum selection of mechanical components can result in large time constants, that must be taken care of by the control system.

This paper discusses the kinematical specification of gantry robots, and shows how this specification can be utilised in optimum transmission design for each axis. After that optimisation equations for motor selection and transmission design are derived. The properties of servo motors, especially DC-motors, are discussed and a simple mathematical model is derived. Finally, servo system design is discussed and a sub model based total simulation model containing *motor model*, *mechanism model* and *control model* for servo motor systems is presented.

The motivation for this paper has been the need to improve the design process for gantry robots at ABB Production Development, and the aim is to find an modelling methodology for control system modelling by analysing a typical gantry robot.

Contents

ABSTRACT	1
CONTENTS	2
1. INTRODUCTION	3
2. KINEMATICS	4
2.1 FAST POSITIONING	4
2.2 PATH CONTROL	6
3. SELECTION OF MOTOR AND TRANSMISSION	10
3.1 MOTOR TYPES	10
3.2 DC MOTOR OPERATING CHARACTERISTICS.....	13
4. TRANSMISSION OPTIMISATION CONSIDERING SERVO MOTOR SELF-INERTIA	17
5. MECHANISM	19
6. CONTROL SYSTEM	21
6.1 AMPLIFIER	21
6.2 CONTROL DEVICE	22
6.2.1 Position control	22
6.2.2 Position-velocity cascade control.....	22
6.2.3 Force control	24
6.3 INSTRUMENTATION.....	24
7. CONTROL SYSTEM SIMULATOR	24
7.1 SIMULATION SOFTWARE.....	24
7.2 SIMULATION MODEL	24
7.3 MOTOR MODEL.....	26
7.4 MECHANISM MODEL	27
7.5 SPRING MODEL	27
7.6 CONTROL SYSTEM	27
8. MEASUREMENTS	29
8.1 TUNE UP.....	29
8.2 SIMULATION OF ABB PRODUCTION DEVELOPMENT ROBOT AXIS BEHAVIOUR	29
8.3 RESULTS	31
8.4 TAILORED MATLAB PROGRAM.....	32
8.5 MOTOR SELECTION PROGRAM.....	33
8.6 DISCUSSION.....	34
8.7 SUMMARY OF CONCLUSIONS.....	35
9. REFERENCES	36

1. Introduction

A characteristic feature of a gantry robot servo system is, that the function of each axis is independent of the other axes functions. Thus when a gantry robot servo system is to be optimised, the design optimisation problem can be reduced to design of single axis servo system. This paper concentrates on the optimisation of transmission and motor.

The dimensioning of a position servo system is a complex design task. The operation principle must be chosen and a right combination of components is then to be selected, each having many properties, which together define the operational characteristics of the total system.

One of the most common requirements for a position servo system which implements a physical movement is the need to achieve largest possible speed and accuracy, with focus on inertial constraints. Therefore this paper concentrates on the optimisation of transmission parameters and motor selection to achieve minimum work path cycle time and thus largest possible production capacity. The optimisation problem, which is presented here, is quite simple, and its solution parameters are easily transferred to the servo design. However, the solution of the problem can often significantly improve the production capacity.

The energy consumption of a servo system is mainly influenced by the following phenomena:

- Kinetic energy accumulated in moving masses
- Energy dissipation due to friction
- Elastic energy accumulated in flexible components.

The servo system's kinematic performance is restricted according specification of the product's kinematic requirements.

The kinematic performance of the servo system defines the motor selection and transmission design.

The dynamic performance requirements of the servo system defines the design of control system.

Usually the design of a servo system begins by analysis of the mechanism and with the specification of the kinematic work cycle.

2. Kinematics

2.1 Fast positioning

If the main required functional task of the servo system is positioning, the problem is usually to move the mechanism from point A to point B within a specified maximum time. The interesting question is then, how the cycle execution time should be divided between acceleration, constant speed and deceleration.

Let's show first, how the power requirement can be reduced by optimising the above mentioned times. For an ideal, frictionless device, assuming constant acceleration, the velocity profile of the movement is shown in figure 1:

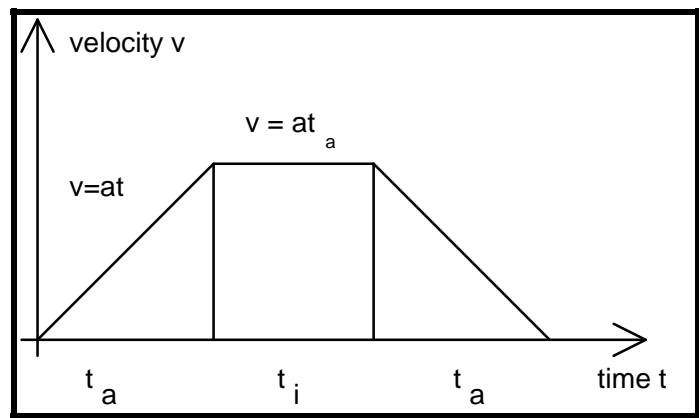


Fig 1. Velocity profile for constant acceleration, speed and deceleration.

The total distance of the movement is then:

$$s = at_a^2 + at_a t_i \quad (2.1)$$

and the elapsed total time is:

$$t = 2t_a + t_i \quad (2.2)$$

In the most elementary case we can neglect motor and transmission elasticity and motor inertia. We can then minimise the cycle time according to maximum acceptable linear acceleration and motor shaft power. We rewrite (2.1):

$$s = 2 \cdot \frac{1}{2} v t_a + v(t - 2t_a) = v(t - t_a) \quad (2.3)$$

The distance s is specified and we want to find the optimum acceleration time t_a . If the acceleration a is a restricting condition for the optimisation, the optimum acceleration time is trivially found from putting the derivate of the cycle length (2.1), (2.2) to zero:

$$\frac{ds}{dt_a} = 0 \Rightarrow t_a = \sqrt{\frac{s}{a}} = \frac{1}{2} t \quad (2.4)$$

thus half time acceleration and half time deceleration. However, the maximum motor power is limited for a specific motor size and the acceleration time t_a is then related to the acceleration a and maximum motor power P_0 :

$$t = t_a + \frac{s}{at_a} \quad (2.5)$$

$$P_0 = Fv = mav = ma^2 t_a \Rightarrow \quad (2.6)$$

$$t_a = \frac{P_0}{ma^2} \quad (2.7)$$

The total time is then:

$$t = t_a + \frac{s}{at_a} = \frac{P_0}{ma^2} + \frac{sma}{P_0} \quad (2.8)$$

$$\begin{aligned} \frac{dt}{da} = 0 &\Rightarrow a = \sqrt{\frac{2P_0^2}{m^2 s}} \quad (2.9) \\ \text{and: } t &= 3 \cdot 2^{-\frac{2}{3}} \cdot \frac{m^{\frac{1}{3}} \cdot s^{\frac{2}{3}}}{P_0^{\frac{1}{3}}} \\ t_a &= 2^{-\frac{2}{3}} \cdot \frac{m^{\frac{1}{3}} \cdot s^{\frac{2}{3}}}{P_0^{\frac{1}{3}}} \Rightarrow \frac{t_a}{t} = \frac{1}{3} \end{aligned} \quad (2.10)$$

The optimum profile in this case is 1/3 acceleration, 1/3 constant velocity and 1/3 deceleration. This kinematic profile is usually the starting point for a rough dimensioning of the servo mechanism. If the problem is to minimise the average power P_m of the motor during the work cycle, we get:

$$P_m = P \frac{t_a}{t} = \frac{ms^2}{t_a(t - t_a)^2} \cdot \frac{t_a}{t} \quad (2.11)$$

where system mass m , distance s and cycle time t are constants. This function has no zero between $0 < t_a < t/2$, but the extreme value is achieved for $t_a = 0$. An equivalent formulation, when the servo is dimensioned for the use of minimum energy:

$$E = 2 \cdot \frac{mv^2}{2} = \frac{ms^2}{(t - t_a)^2} \quad (2.12)$$

These simple examples of optimisation illustrate, that the optimum acceleration time is normally within the range $t_a = [1/3 t ; 1/2 t]$. This rough model doesn't however take in to consideration the self-inertia of the motor which is significant for high performance servo systems. The self-inertia will reduce the servo system performance particularly in servos with reduction transmission. This is the reason for the increasing use of expensive direct drive servo motors.

2.2 Path control

So far, we have considered the rough dimensioning of a positioning servo, assuming that motor inertia and mechanism friction have no influence on the motion. Kinematic path control is nevertheless a more complex optimisation task. The kinematical motion sequence between different path points should be optimised so, that minimum time is required to complete the motion sequence. Here we will present the problem in a form, which is typical for the optimisation of gantry robot installations. The servo system should be optimised according to various restrictions:

- Distance $\Delta s = s_b - s_a$, per cycle
- Maximum velocity v_{max} , which is an optimisation parameter for transmission and motor design.
- Maximum allowed acceleration a_{max} , acceptable for the payload, handled by the robot.
- Maximum allowed "jerk" (acceleration time derivative), j_{max} .

The acceleration time derivate or jerk is a performance parameter, characterising the path profile's "smoothness". Thus the time derivative is (for position coordinate x):

$$\frac{da}{dt} = \frac{d^3x}{dt^3} = j; \quad |j| \leq j_{max} \quad (2.13)$$

The jerk can typically be within the range [5; 200] m/s³, depending on the application.

The optimisation problem is then to minimise the cycle time for the path when the system moves from starting point s_0 at initial velocity v_0 to end point s_7 at final velocity v_7 , having restrictions v_{\max} , a_{\max} and j_{\max} . A profile is shown in figure 2., assuming piece-wise constant jerk, acceleration or velocity.

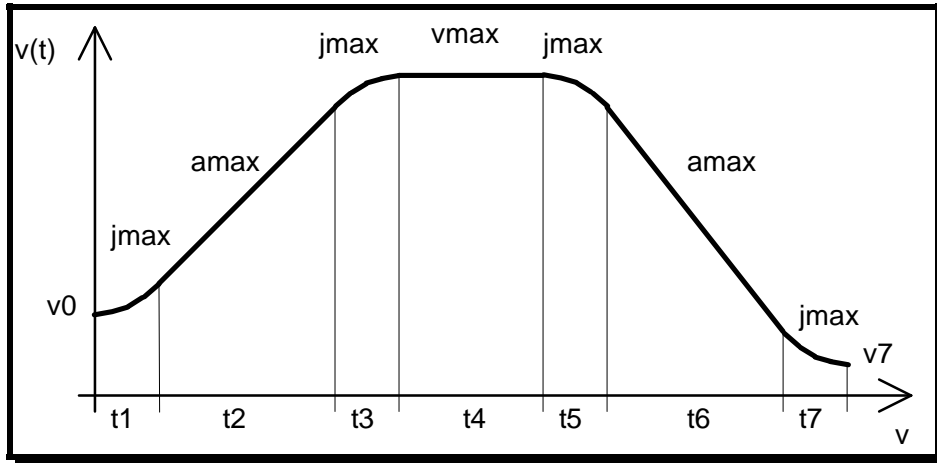


Fig 2. The time optimal kinematical path and it's restrictions.

This optimisation problem can now be formulated:

$$\begin{aligned} \min[f(t_i)] &= \sum_{i=1..7} t_i; \\ s_0 = s_a, v_0 = v_a, a_0 &= 0, \\ s_7 = s_b, v_7 = v_b, a_7 &= 0 \end{aligned} \quad (2.14)$$

The problem (2.14) is a mathematical programming problem. Assuming constant jerk j_i , the constraining equations are given in eq. (2.15):

$$\begin{aligned} s_{i+1} &= s_i + v_i t_{i+1} + \frac{1}{2} a_i t_{i+1}^2 + \frac{1}{6} j_i t_{i+1}^3 \\ v_{i+1} &= v_i + a_i t_{i+1} + \frac{1}{2} j_i t_{i+1}^2 \\ a_{i+1} &= a_i + j_i t_{i+1} \end{aligned} \quad (2.15)$$

The equations (2.15) could be developed up to time step t_7 , and then the constraints in (2.14) should be substituted to the position, velocity and acceleration equations of the seventh step. Optimum time step lengths could be calculated by Lagrange relaxation. It would require the calculation of 49 derivatives and solution of their zero points, and after that a tedious substitution back to the original relaxation formula. We will derive the solution with a simpler method. First we will list the inequalities, which have to be satisfied, and then we

derive the solution by substituting the inequalities to the kinematical equations. As a result the following algorithm for solving the optimal time step lengths is obtained.

Since $a_0 = a_3 = 0$ and $a_4 = a_7 = 0$ and if maximum jerk is always utilised, the "jerk acceleration" time must be

$$0 \leq t_i \leq \left| \frac{a_{\max}}{j_{\max}} \right|; \quad i = 1, 3, 5, 7 \quad (2.16)$$

since $j_1 = -j_3$ and $-j_5 = j_7$ the jerk times must equal in acceleration and in deceleration:

$$t_1 = t_3 \quad \text{and} \quad t_5 = t_7 \quad (2.17)$$

The constant rate acceleration time must then be

$$0 \leq t_2 \leq \frac{v_{\max} - v_0 - j_{\max} t_1^2}{a_{\max}} \quad (2.18)$$

and the constant rate deceleration must satisfy

$$0 \leq t_6 \leq \frac{v_{\max} - v_7 - j_{\max} t_5^2}{a_{\max}} \quad (2.19)$$

From the symmetry in figure 2. we can derive an equation for the path length:

$$\Delta s = s_7 - s_0 = \frac{v_0 + v_4}{2} (t_2 + 2t_1) + \frac{v_7 + v_4}{2} (t_6 + 2t_5) + v_4 t_4 \quad (2.20)$$

We derive the calculation procedure for time intervals t_i , $i=1..7$. Considering time consumption, jerk is the most restricting constraint. The next restraining is maximum allowed acceleration and maximum allowed speed. Therefore we begin by calculating the minimum allowed jerk time from (2.15):

$$\begin{aligned} a_{\max} &\geq a_2 = j_{\max} t_1; \\ a_{\max} &\geq a_6 = j_{\max} t_7 \end{aligned} \quad (2.21)$$

The minimum acceleration time is derived from (2.18) and (2.14)

$$t_2 = \min \left| \frac{v_{\max} - v_0 - j_{\max} t_1^2}{a_{\max}}, 0 \right| \quad (2.22)$$

equally from (2.19) and (2.14) we get the minimum deceleration time:

$$t_6 = \min \left| \frac{v_{\max} - v_7 - j_{\max} t_5^2}{a_{\max}}, 0 \right| \quad (2.23)$$

The time which must be consumed for constant speed is then:

$$t_4 = \frac{s_7 - s_1 - \frac{v_0 + v_{\max}}{2} (t_2 + 2t_1) - \frac{v_7 + v_{\max}}{2} (t_6 + 2t_5)}{v_{\max}} \quad (2.24)$$

If there is no need to drive with constant speed ($t_4 < 0$), the maximum speed must be redefined so, that it is achieved just momentarily:

$$v_m = \frac{s_7 - s_1 - \frac{v_0}{2} (t_2 + 2t_1) - \frac{v_7}{2} (t_6 + 2t_5)}{\frac{1}{2} (t_2 + t_6 + 4t_1)} \quad (2.25)$$

Since the maximum velocity is lowered, the acceleration and deceleration times must be recalculated

$$t_{2'} = \min \left| \frac{v_m - v_0 - j_{\max} t_1^2}{a_{\max}}, 0 \right| \quad (2.26)$$

and

$$t_{6'} = \min \left| \frac{v_m - v_7 - j_{\max} t_5^2}{a_{\max}}, 0 \right| \quad (2.27)$$

if $t_2' < 0$, the velocity difference is constraining the acceleration, and jerk time must be recalculated for acceleration:

$$t_{1'} = \sqrt{\frac{v_m - v_0}{j_{\max}}} \quad (2.28)$$

and for deceleration:

$$t_s = \sqrt{\frac{v_m - v_7}{j_{\max}}} \quad (2.29)$$

Finally, after solution of these equations, the kinematical velocity, acceleration and jerk restricted path profile can be calculated. It must be pointed out, that this algorithm assumes, that jerk, acceleration and speed are more restricting than stroke length, and that the derivation only shows the principle of the algorithm.

3. Selection of motor and transmission

3.1 Motor types

After the kinematic path function and operation sequence of the servo system has been specified, a suitable servo motor should be selected. The aim of this paper is not a comprehensive discussion of servo motors and their properties. We will take just a brief look having motor selection in our minds.

Servo motors are roughly divided in to the following groups (we are discussing servo controlled motors, characterised by feedback loop in the position (or velocity) control, which excludes stepper motors). In Table 1. a classification of the most frequently used servo motor types is presented.

Table 1. Servo motor types.

DC-Servo motors	AC-Servo motors	Conventional variable speed motors
Direct current permanent magnet motors	Synchronous AC-servo motors	Asynchronous AC-motors
Brushless DC motors (permanent magnet rotor)	Asynchronous AC-servo motors	Synchronous AC-motors

Direct Current motors are the simplest, but very efficient motors used for servo drives. They consist of a stator, rotor and a brush ring. The stator is made of permanent magnet, while the rotor has windings with two or more poles. The torque is exerted at the air gap between the rotor and stator. The switching of poles during rotation (commutation) is achieved mechanically by brushes. The motor has many advantages like high efficiency, low torque

ripple, linear torque-speed characteristics and simplicity of construction. The major drawback is that large currents are transferred through mechanical commutation. At the brush, large sparks are created because of the large inductance at rotor coils and contact resistance changes at the brush contact. The sparks cause electric disturbances and increased brush wear. The brush mechanism also increases friction losses.

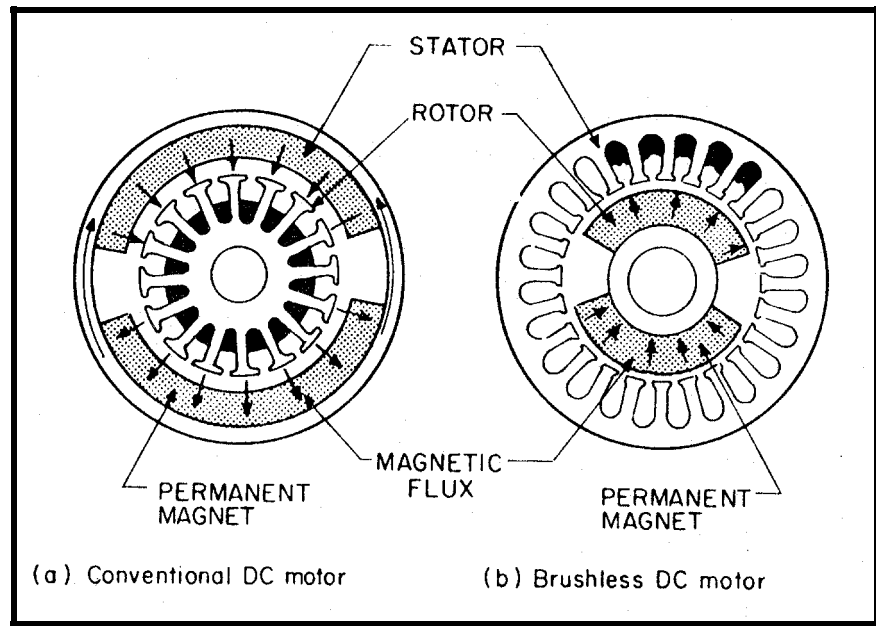


Figure 3. Principle construction of a brushless DC motor and a conventional DC motor [5].

The brushless DC motors avoids the drawbacks of mechanical commutation. The rotor of the brushless motor consists of a permanent magnets, while the stator consists of windings, see figure 3. Thus the rotor and stator are interchanged. The commutation of currents is accomplished by measuring the rotor position using a position sensor. According to the rotor position, currents are delivered to appropriate windings through electronic switching circuits.

The asynchronous AC-motor is the type of electric motor most frequently used in industry. The stator consists of windings, fed by AC and then creating a rotating field. The rotor short circuit windings or conductors create the magnet field from electromagnetic inductance. The asynchronous machine is simple and reliable. From a service point of view, it has only two bearings with sealings. It is a standard product, and it has many suppliers. The synchronous rotational speed n is determined by the supply frequency and the number of poles. The motor is always operating at subsynchronous speed, with a load dependent slip.

$$n = \frac{2 \cdot f_{AC}}{N_p} \quad (3.1)$$

where f_{AC} is the frequency of the alternating current (normally 50Hz or 60 Hz), and N_p is the number of poles. Since the number of poles can not be changed in a motor during operation, the only way to control the speed of the motor is to use a frequency converter. The price of frequency converters has become lower, and AC-servo motors are becoming more popular. The operating range of frequency converters is between 0 - 200% f_{AC} . However, the operation under 10% speed is inaccurate. Another drawback is, that AC-servos can't be locked, since they can't resist zero speed torque.

The torque of an AC-motor increases as the slip increases. The starting torque of the motor is usually 1.6..1.8 times the nominal torque, and the maximum torque is about 2.5 to 3 times the nominal torque. In frequency converter applications it must be noticed, that the "nominal" rotational speed is constantly changing. In figure 4. a typical torque curve of a AC short circuit motor is shown.

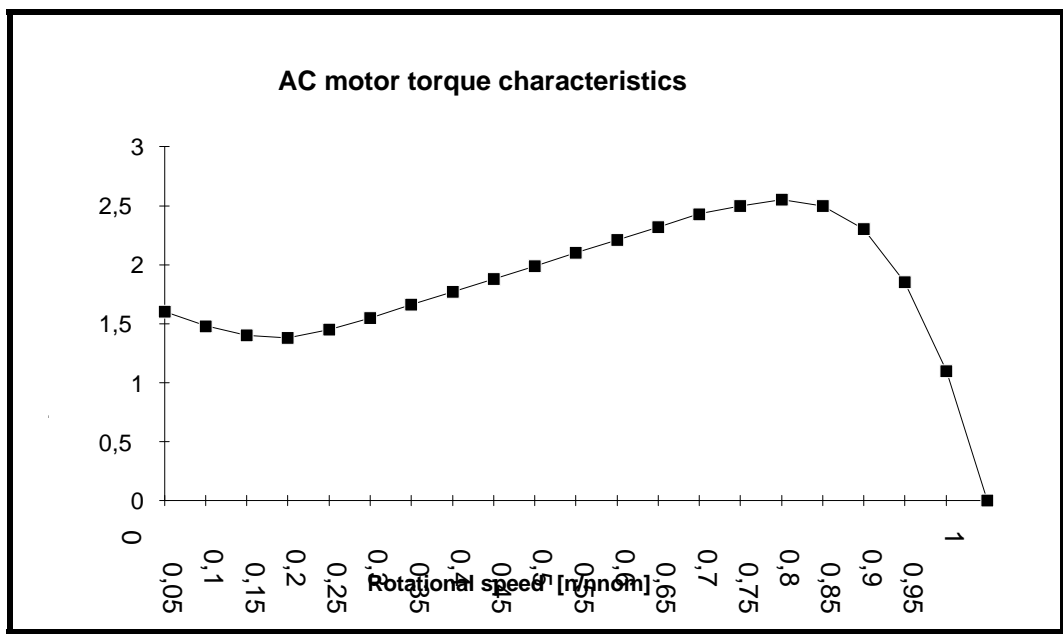


Figure 4. AC asynchronous motor torque as a function of rotational speed.

The AC synchronous motor is suitable, if the power requirement is very high (wood grinding machines, for instance). It has a constant rotational speed and high efficiency especially when the nominal power factor is close to one ($\cos\theta \approx 1$). It is applicable even at low rotational speeds. The synchronous motor rotor follows the rotating magnet field as it was coupled by a torsion spring. It is an active part of the dynamic system, and it can't damp torsional

vibrations. Therefore additional damping will be required. The grinding process itself has good damping properties.

3.2 DC motor operating characteristics

The following motor model represents fairly well a conventional permanent magnet DC motor, as well a brushless DC or synchronous AC servo motor. The electrical relationship of a motor is given by equation 3.2:

$$V = RI + E + L \frac{dI}{dt} \quad (3.2)$$

where V is the input voltage, R and L are the resistance and the inductance of the windings, I is the current, and E is the electromotive force (e.m.f.), which is given by

$$E = K_t \omega \quad (3.3)$$

where K_t is the e.m.f constant or torque constant, and ω is the angular velocity of the motor. The fraction of electrical power, which is converted to mechanical power, is the voltage drop due to the back e.m.f. times the motor current. Thus the amount of power is the same as the mechanical power produced by the motor. The mechanical power is again the angular velocity of the motor multiplied by torque:

$$P = EI = K_t \omega I = T \omega \quad (3.4)$$

Where P is power, ω is angular velocity of the motor and T is torque. From (3.4) we get:

$$T = K_t I \quad (3.5)$$

thus the motor torque is torque constant multiplied by current. We also see, that the torque constant is the same as back e.m.f. constant in (3.3). The equations (3.3) and (3.5) represent the most important characteristics of electric motors: voltage depends on angular speed and torque depends on motor current.

The constant K_t can be derived from the torque of a single current circuit that is the product of current, circuit area and magnet field strength from which follows:

$$K_t = \frac{T}{I} = \frac{N \int_{-\pi/2}^{\pi/2} IBA \cos q d\theta}{Ip} = \frac{2NBA}{p} \quad (3.6)$$

where

N = number of loops in windings

T = torque of the motor

B = strength of magnet field [Vs/m²]

A = area of windings loops

θ = rotor angle of rotation

The constant factor is the multiple for average area of the winding loop during motor rotation. See figure 5.

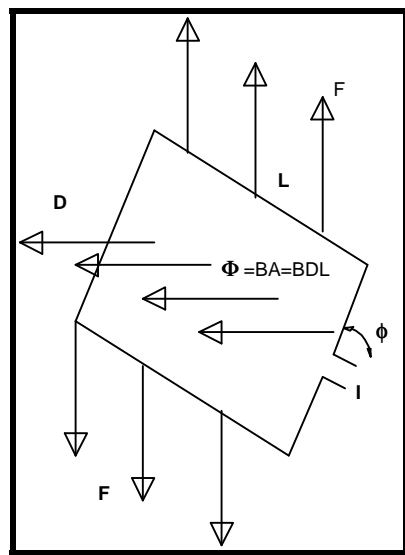


Fig 5. Torque exertion in rotor windings.

The approximation (3.6) is not accurate. The torque constant K_t varies with the rotor position and air gap. This causes fluctuations in the output torque. These fluctuations cause torque ripple, which is the ratio of the torque deviation to the average output torque. The torque ripple is an important parameter of merit, since torque ripple prevents smooth motion, particularly at low speeds, and degrades control accuracy.

To minimise the torque ripple, the rotor windings are divided into a number of coil partitions that are connected to the same number of commutator segments. The current is then switched from one coil to another more smoothly. The number of stator poles is also increased in order to smoothen the magnetic field.

Another important performance figure is concerned with the power performance necessary for exerting torque. Let us consider a stall condition in which the motor does not rotate while

exerting torque. Since the windings don't move, the current in windings is restricted only by input voltage and winding resistance, so that

$$T = K_t I = K_t \sqrt{\frac{P}{R}} = K_m \sqrt{P} \quad (3.7)$$

where the constant K_m accounts for the efficiency of the torque motor in terms of the transformation of electric power to mechanical torque at zero speed. The higher the constant is, the larger the exerted torque becomes, and the lower the power consumed. This constant is referred to as the motor constant - another characteristic parameter for a DC motor. For a direct drive motor it should be high while for a high speed motor it should be low.

Let us now derive the torque characteristics as a function of angular velocity. From (3.2), (3.3) and (3.4) we can derive the torque equation:

$$T = K_t \frac{V}{R} - \frac{K_t^2}{R} \omega = K_t \frac{V}{R} - K_m^2 \omega \quad (3.8)$$

and the power is

$$P = T\omega = (K_t \frac{V}{R} - K_m^2 \omega)\omega \quad (3.9)$$

The torque is linearly decreasing when the angular speed increases. The torque and power characteristics are shown in figure 6.

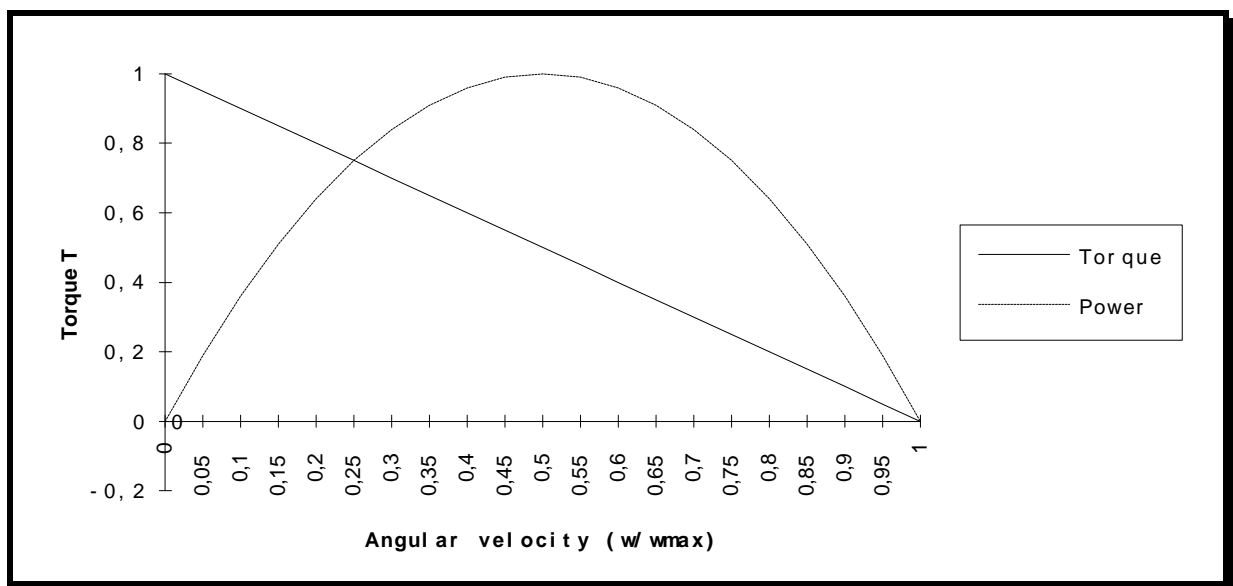


Fig 6. Torque and power vs. speed characteristics for a direct current motor.

The maximum power is obtained when the speed of the motor is half of maximum speed and when the torque is half of the maximum torque. This provides the optimum operating condition, in which the motor can exert its maximum power.

Finally we shall discuss time constants of electric motors, which also are important measures of motor performance. The *electric time constant* of a DC motor is defined from the ratio of windings inductance and resistance. It affects the control system stability, since it describes the response time and controllability of motor torque. The *electric time constant* is given by eq. 3.10:

$$t_e = \frac{L}{R} \quad (3.10)$$

The *mechanical time constant* is the relation between maximum torque T_{max} divided by the product of motor inertia J and maximum rotational speed ω_{max} . It is the time, which would be needed for the motor to achieve 63% of the maximum velocity, if a constant torque T_{max} would be applied. It is given by eq. (3.12):

$$t_m = \frac{J_m \omega_{max}}{T_{max}} \quad (3.11)$$

The mechanical time constant is a practical performance measure in motor selection. According to a rough dimensioning rule, the "decade dimensioning", the motor should have as a minimum acceleration time ten times it's mechanical time constant.

The temperature time constant of an electric motor is restricting the cooling of motor. Usually these constants are quite long, about 30 - 120 min. The "iron-free" motor structures (plate rotor motors, for instance) are an exception, their time constants are much shorter. When the work cycle of a servo application is much shorter than the temperature time constant of a motor, the mean power loss in motor windings is derived from (3.2) and (3.5) and given by eq. 3.12:

$$P_{mean} = \frac{R \int_0^t I^2(t)dt}{t} = \frac{R \int_0^t T^2(t)dt}{t K_t^2} \quad (3.12)$$

Where R is the resistance of windings, $I(t)$ is the current through windings during work cycle τ , and $T(t)$ is the torque during the work cycle. From (3.12) we can now derive a simplified equation of the equivalent torque in a constant acceleration - speed - deceleration - rest cycle.

$$T_e = \frac{\sqrt{(T_a^2 t_a + T_v^2 t_v + T_d^2 t_v + T_r^2 t_r)}}{t_a + t_v + t_d + t_r} \quad (3.13)$$

Where

T = Torque

t = Time the torque load lasts, and the indexes are:

a = acceleration,

v = constant speed,

d = deceleration,

r = rest period.

The equivalent torque represents the torque, which would generate the same temperature if it was continuously applied on the motor. Following points should however be noticed:

- When the ambient temperature rises, the load should be decreased.
- If the control system has "tight dimensioning" i.e. large correcting currents are continuously applied, the equivalent torque should be decreased.
- At high altitudes loads should be decreased.

When the motor type is selected, it is also good to keep in mind the basic differences in operational characteristics of different motors. For instance, in applications, where the motor has to give large stall torque continuously, it is advantageous to select a brushless model, since a brush model would require significant over dimensioning due to stall current.

4. Transmission optimisation considering servo motor self-inertia

The optimisation of transmission speed reduction ratio is vital to get a balanced performance of the system. The self-inertia of a servo motor increases the servo systems inertia, and thus reduces the acceleration performance of the system. The higher the maximum speed of the system, the lower is the acceleration performance. Therefore the designer should know what is the optimum transmission gear reduction. Here we will derive the value of optimum transmission by introducing a transmission radius r , which is the relation between the linear speed of the moving payload mass and the angular velocity of the motor, which can be used as a parameter to define the right transmission ratio. Thus we get eq. 4.1:

$$v_{\max} = \frac{J}{J + mr^2} r \quad (4.1)$$

Figure 7. shows an idealisation of a servo system. The mass m is accelerated by a motor with transmission radius r . The motor has the self-inertia J .

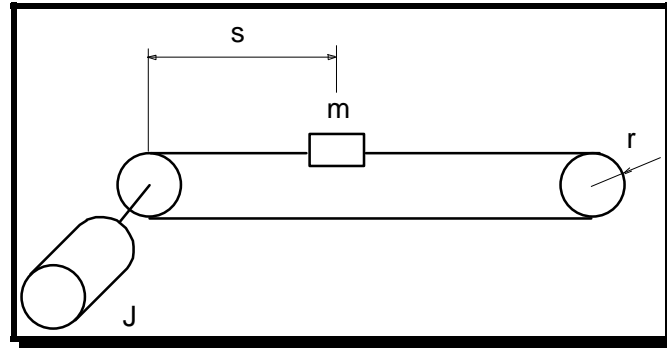


Fig 7. Servo motor motion mechanism

The torque balance in the servo mechanism is given by eq 4.2:

$$T = J\ddot{\theta} + mar = J\ddot{\theta} + mr^2\ddot{\theta} \quad (4.2)$$

The acceleration is then

$$a = \ddot{\theta}r = \frac{Tr}{J + mr^2} \quad (4.3)$$

From (4.3) we can derive the acceleration efficiency of the servo system:

$$h = \frac{T_{netto}}{T} = \frac{Jmr^2}{J(J + mr^2)} = \frac{1}{1 + \frac{J}{mr^2}} \quad (4.4)$$

Let's now derive the optimum reduction speed assuming, that the speed profile is the same as in figure 1. The acceleration time is maximum speed divided by acceleration given in eq. (4.5)

$$t_a = \frac{\dot{\theta}}{\ddot{\theta}} = \frac{(J + mr^2)}{T} \quad (4.5)$$

From eq. (2.3) we derive the total motion time

$$t = \frac{s}{v} + t_a \quad (4.6)$$

which is to be optimised. We substitute to (4.6) the equations of speed (4.1) and acceleration time (4.5) to get the eq. (4.7):

$$t = \frac{s}{v} + t_a = \frac{s}{r\ddot{\kappa}} + \frac{\ddot{\kappa}(J + mr^2)}{T} \quad (4.7)$$

The optimum transmission radius could be obtained by derivation of (4.7) with respect to radius r and the derivative put to zero:

$$\frac{dt}{dr} = \frac{d}{dr} \left(\frac{s}{r\ddot{\kappa}} + \frac{\ddot{\kappa}(J + mr^2)}{T} \right) = -\frac{s}{r^2\ddot{\kappa}} + \frac{2\ddot{\kappa}mr}{T} = 0 \quad (4.8)$$

The optimum radius will then be (4.8):

$$r = \sqrt[3]{\frac{sT}{2\ddot{\kappa}^2 m}} \quad (4.9)$$

It is interesting to observe, that the motors self-inertia will not affect the optimum transmission radius. The acceleration time/total time ratio, will, however, be affected. In (4.10) we derive the acceleration time/total time - relation:

$$\frac{t_a}{t} = \frac{\frac{t_a}{s}}{\frac{s}{v} + t_a} = \frac{\frac{\ddot{\kappa}(J + mr^2)}{T}}{\frac{s}{r\ddot{\kappa}} + \frac{\ddot{\kappa}(J + mr^2)}{T}} = \frac{1}{1 + \frac{sT}{r\ddot{\kappa}^2(J + mr^2)}} \quad (4.10)$$

5. Mechanism

A successful design of a servo system is not just a question of optimum design of the transmission. The minimisation of the time required for moving masses with transmission optimisation contributes to the accuracy, speed and ease of control; an other important factor affecting accuracy is the performance and properties of the mechanism in a servo system.

Backslash and flexibility of the transmission and mechanism decreases the positioning accuracy of the system. The control of backslash clearance is extremely difficult, thus clearance defines the minimum boundary for position accuracy. The dynamic effects of

backslash and flexibility are more difficult to foresee. They cause force variation in the servo system as a function of the input force frequency. It follows that stable operation of a control circuit is possible to achieve only by restricting the gain at certain frequencies, which decreases the accuracy and stiffness of control.

To obtain the required kinematic functions from the servo mechanism, the designer has to ensure, that the kinematic movements don't excite unwanted vibrations in the mechanism, i.e. that the characteristic frequency of kinematic movements of the servo mechanism doesn't resonate with any natural frequency of the mechanism. A rough dimensioning rule is, that the natural frequency of the mechanism should be ten times the characteristic frequency of servo motions.

Lower natural frequencies in the servo mechanism cause remarkable decrease in the servo accuracy of path control or increase in the set-up time in positioning applications. In large structures it is often difficult to achieve high natural frequencies in the mechanism. To achieve high performance in such applications, operation must take place at frequencies more near to natural frequencies. Better performance can be achieved by adding a controlled amount of friction or viscosity damping to the system. The principle for rough dimensioning of suitable damping can be obtained from the theory of second order differential equations: The gain and phase shift can be calculated from equation (5.1)

$$G(s) = \frac{\omega_0^2}{s^2 + 2\zeta\omega_0 s + \omega_0^2} \quad (5.1)$$

where $G(s)$ = Laplace transfer function

ω = excitation frequency

ω_0 = resonance frequency

ζ = damping coefficient

By adjusting the friction to suitable level, the resonance gain can be decreased and the accuracy increased. Large increase in friction requires however increased motor torque, and thus decreases the overall performance.

By tuning up the servo circuit gains, the accuracy can be optimised without the loss of stability. Especially in microcomputer controlled applications, the gains could be readjusted in the different motor speed or mechanism positions, so that optimum performance can be achieved in different operational states. Without an explicit mathematical control model of

the mechanism the tune-up must be based on manual work with empirical measurements on the final installation.

6. Control system

6.1 Amplifier

The selection of feedback control amplifier is closely related to the selection of the motor, and it should be taken into consideration when dimensioning the motor. The performance of the amplifier must be in balance with the motor performance. It shouldn't be less than the motor's performance. On the other hand, too high performance is also waste of resources.

The dimensioning of a feedback amplifier is related to the dimensioning of servo motor. An amplifier has, however, some non-compatible properties, which cause some special dimensioning rules.

The torque of a servo motor is direct proportional to the current supplied by the amplifier. The ratio between motor torque and current is the torque constant, derived in equation (3.5). As for the motor, the amplifier tolerates a given maximum continuous current, and a given maximum peak current. In a motor the ratio between maximum peak current and maximum continuous current is 5 - 10, while for an amplifier it is only 2 - 3. Also the temperature time constant for an amplifier is 0.5 - 5 s, while for a motor it is hundreds or thousands of seconds. Thus, the amplifier must be over dimensioned in periodic load. In some amplifier models, the current is restricted by an I^2dt integrator.

The amplifier must also be capable of creating the required motor voltage. The voltage is proportional to the angular speed of the motor (generator voltage BEMF). To this voltage must be added the resistive loss at maximum torque load, without the inductive loss at stationary load. Thus we get from (3.2) and (3.3):

$$V_s = RI + K_t \omega + L \frac{dI}{dt} \quad (6.1)$$

Where V_s is the voltage capacity required from the amplifier.

One characterising feature in servo amplifiers is the handling of brake energy. As DC servo amplifiers can't feed the braking current back to mains, they need a resistor, which must be dimensioned according braking requirements. For instance, a 10 s cycle, where a 200 kg mass is decelerated from the speed of 10 m/s requires a power dissipation of (6.2):

$$P = \frac{200 * 10^2}{2 \cdot 10} = 1000[\text{W}] \quad (6.2)$$

Friction and other losses might reduce the requirement for resistive braking power dissipation.

6.2 Control device

6.2.1 Position control

The simplest control strategy is position control. The control circuit includes at least a position transducer, an amplifier and the motor. Figure 8 shows a position control circuit with conventional Laplace operators

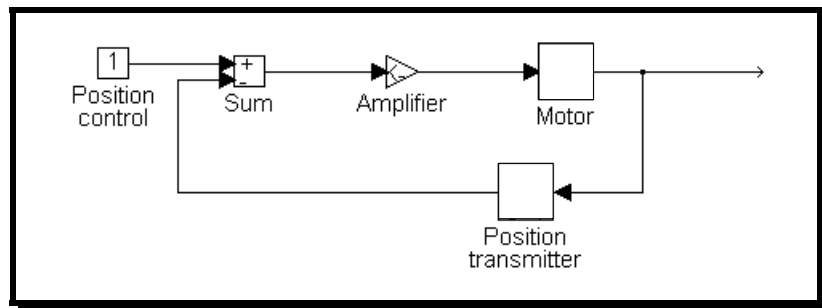


Fig 8. Position control circuit.

This kind of circuit has been traditionally used with analog position transducers. Also digital position servo circuits a similar structure is used, which is called digital position servo control. The control of a mechanisms position and velocity with mass inertia properties require least PD, or preferably of PID type regulator. In typical drive applications, the band width should be at least a few hundred Hz. For further improved performance, control stiffness in excess of 1 kHz will be required.

6.2.2 Position-velocity cascade control

A position-velocity cascade control circuit uses a fast velocity feed-back loop, which is controlled by a position feed-back loop. The velocity feed-back loop is usually installed in the servo amplifier. The velocity transmitter is a DC tacho generator in DC-servos and a brushless tacho or resolver or synchro in brushless motors. In figure 9. a schematic Simulink model of the control system is presented.

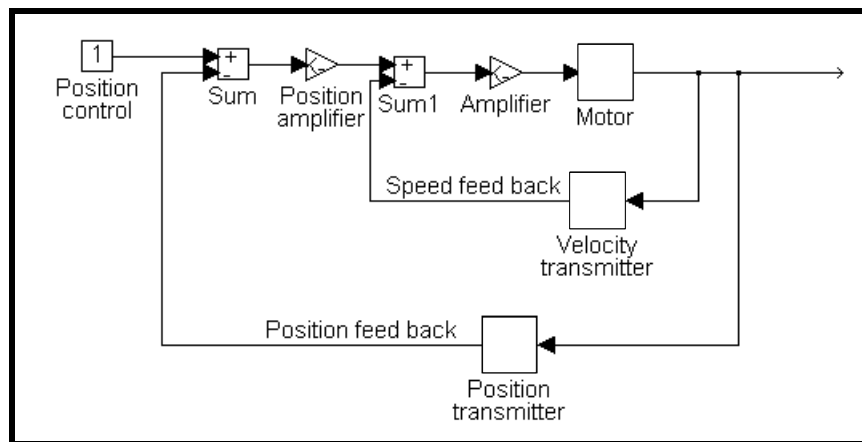


Fig 9. Position-velocity cascade control circuit.

The velocity transmitters are installed at the motor shaft. Thus a high stiffness and band width is achieved. The velocity feed-back loop can be controlled with a simple position feed back loop and still adequate position accuracy and stability is achieved. With higher loads derivation and enlarged band width is however required. Integration should not be used, since the velocity feedback circuit usually includes an integrator.

One drawback in position-velocity cascade control circuits is position-time creep, which is proportional to the speed of movement. Due to creep the execution time in point-to-point control increases and the accuracy of path control decreases.

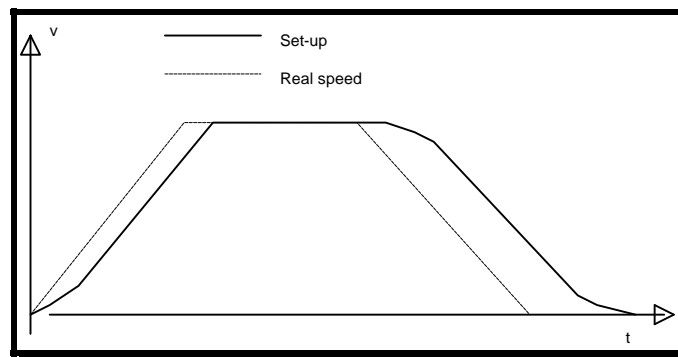


Fig 10. Creep in speed profile.

To eliminate creep *velocity feed forward (velocity compensation)* can be used. The creep is compensated by adding to the velocity set up a factor which is dependent on the position set up. Velocity compensation enables optimal performance ratio between execution speed and stabilisation. The position transmitter can be installed also far from the motor and nearer to

the mechanism. The stabilisation speed decreases, but the absolute accuracy in position increases. This kind of positioning is used much in machine tools, which have position reaction from linear transmitters.

6.2.3 Force control

Force control requires modifications in the control circuit. Most motion control circuits have a primary feedback loop for current or motor torque. If position control is applied in this kind of amplifier, maximum torque can be controlled. The torque can be controlled either by using a real physical force transmitter or a compensation model of the motor.

6.3 Instrumentation

The position transducer produces usually discrete position values for a digital controller, at least after A/D-conversion. The most common position transducer is the two channel pulse transducer. The resolution affects not only the measuring accuracy, but also the dynamic functioning of the system. If position's time derivate is used, accuracy must be increased according to velocity accuracy and bandwidth requirements. In positioning the accuracy should be at least 2 - 10 times higher than the requirements.

The physical installation place should also be considered. The dynamics is usually better if the transducer is close to the motor. In contrary, the positioning accuracy is better near the mechanism. In the latter case it is better to use velocity feedback near the motor. Backslash and mechanical flexibility should be minimised.

7. Control system simulator

7.1 Simulation software

To test the behaviour of a servo control system, a simulation model of the system presented in this paper was built. The software which was used to build up the simulation system was Simulink ver. 1.3 running in Matlab ver 4.2. No Simulink or Matlab Toolbox packages were used.

7.2 Simulation model

The system includes three separate sub-models: control system model, DC-motor model, and mechanism model. The control system model is based on the position-velocity cascade model presented in section 6.2.3. The motor model is a DC-motor model according the theory presented in chapter 4. The mechanism model is a simple mechanism, modelling the robot axis mechanism presented in chapter 3. The sub model structure is presented in figure 11.

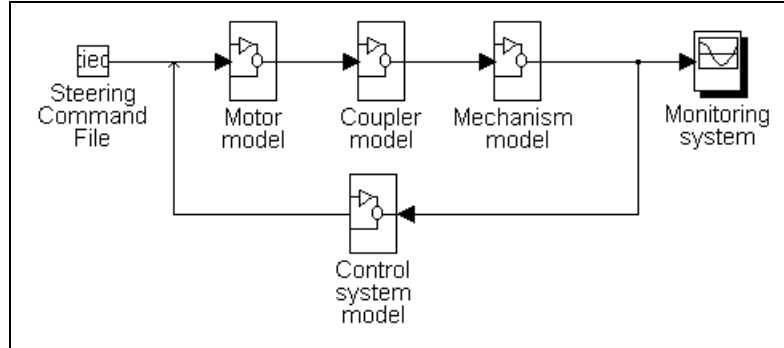


Fig 11. The sub model structure of the simulation system.

The structure of the simulation system is modular and any module can easily be replaced by a more detailed one. Equally, the simulation system could be linearised and exported to other CAE simulation software, like ADAMS, for instance.

The dynamic equations for the simulation model are presented in figure 12. The motor model includes the electromotive force, self-inertia, coil inductance and resistance, self-inertia and electromotive voltage. The spring (elastic coupling) model simulates the elasticity of the mechanical system. The mechanism model includes inertia, friction and gear ratio of the mechanism. The control system model is a cascade control system. This simple simulation model enables fast and efficient simulation of the total servo system.

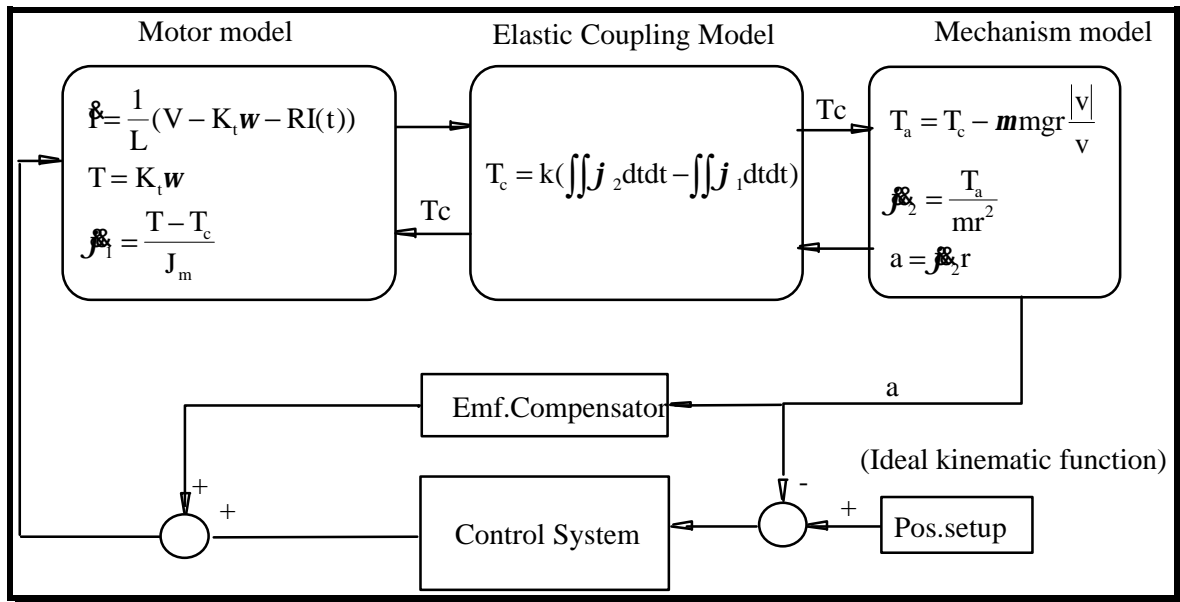


Fig 12. Mathematical sub model structure of the simulation system.

In figure 13. the Simulink simulation system is shown. The results are fed to a result file, which is read by a Matlab-program.

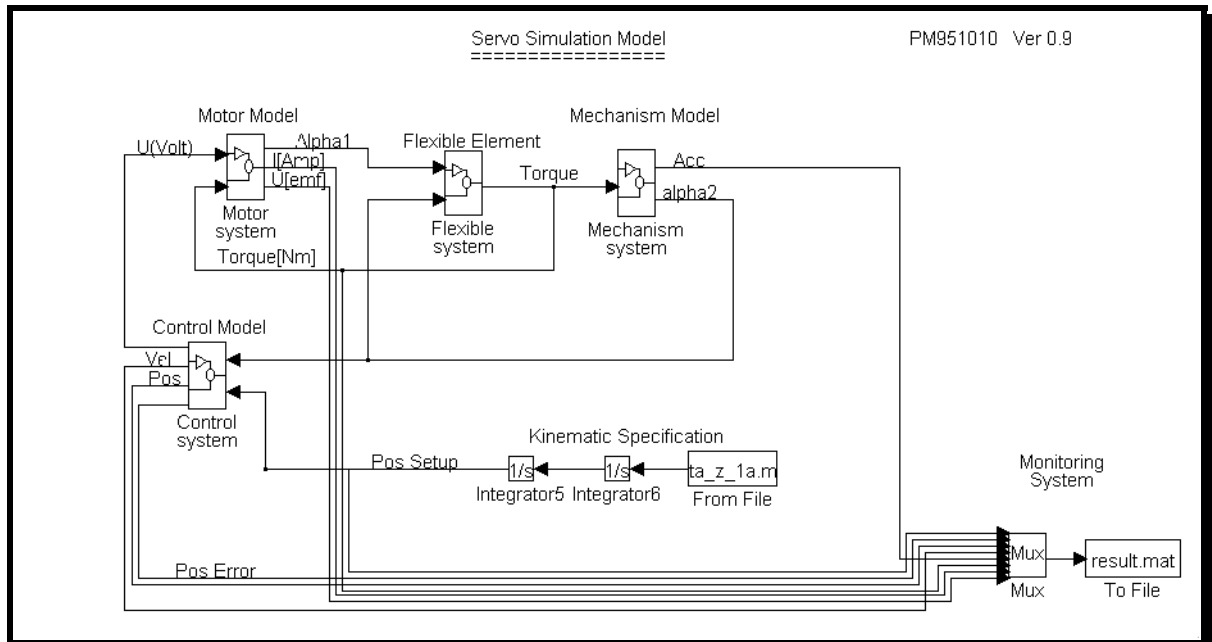


Fig 13. Simulink main model of the servo system.

7.3 Motor model

The motor model is an idealised DC-permanent magnet motor simulating the electromotive force, self-inertia and coil inductance and resistance. In figure 14. a Simulink model of the motor is shown.

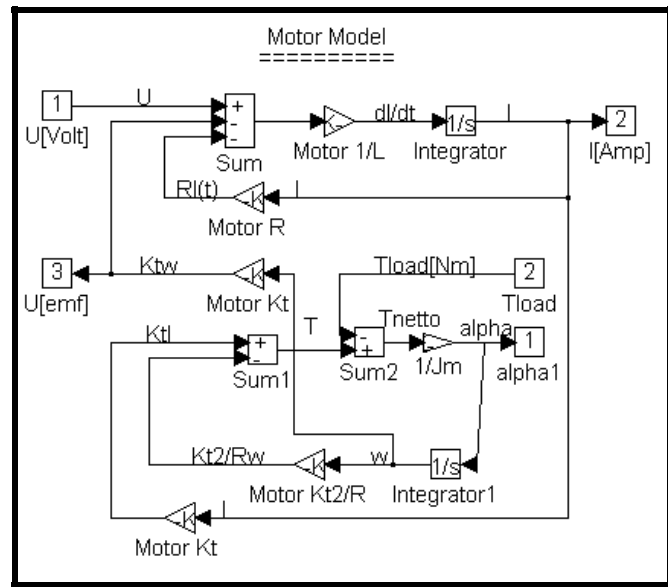


Fig. 14. A Simulink model of DC permanent magnet motor.

7.4 Mechanism model

The mechanism model includes the transmission radius r , Coulomb friction, and inertia. The friction is modelled against motion direction causing hysteresis. Figure 15. shows the mechanism model.

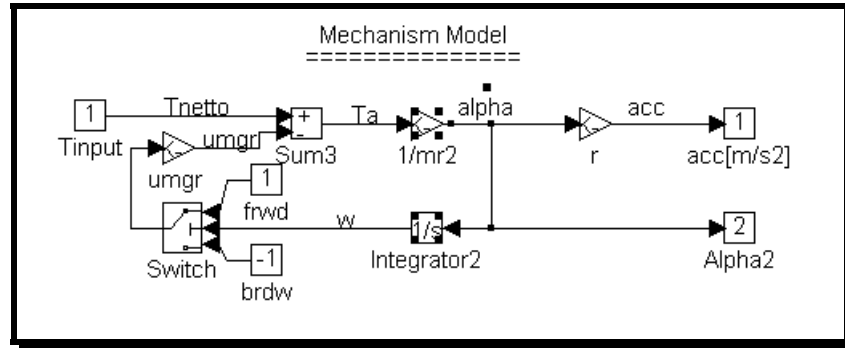


Fig. 15. A Simulink model of the mechanism.

7.5 Spring model

Mechanical time constants are the largest time constants. They should be modelled as accurate as possible. Therefore a model of the transmission elasticity was included in the system, as a spring module. Figure 16 shows the principle.

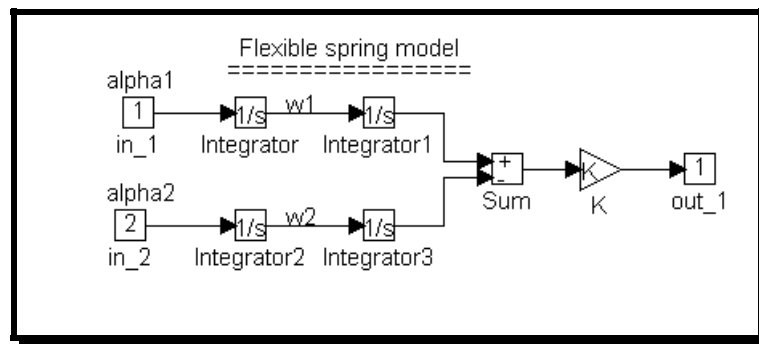


Fig 16. Mechanical transmission as a flexible element.

7.6 Control system

During this project several principle solutions for the control system have been tried and trimmed. The simplest system tried was a position control system with PID-regulator, which controlled directly the input voltage of the motor. The second system tried was a position-velocity cascade control system, which also controlled the motor input voltage directly. Both

in velocity and position loop a PID-regulator was used. In the latter control system problems occurred shortly after the start. The velocity feedback loop was slower than the position feedback loop, which created an unstable system. The performance with simple position feed back was satisfactory high. The only problem was unstable operation of voltage control. The cause was traced back to the electromotive voltage of the motor, which had to be compensated. From the basic equations of the DC-motor a voltage-torque compensator was designed and added to the control loop. To control and restrict the maximum allowed jerk and acceleration, acceleration and jerk restrictors were also added to the system. The final control system version is shown in figure 17.

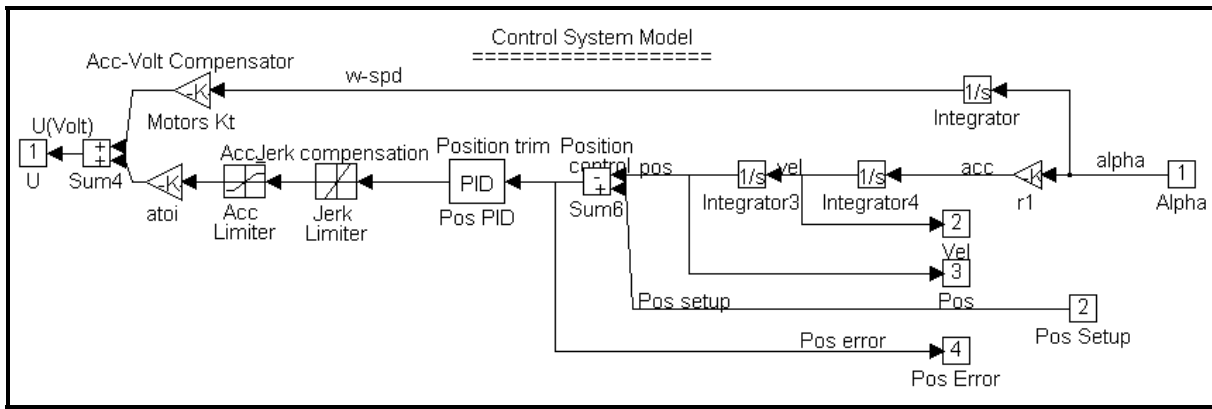


Fig. 17. The final control system together with motor model and mechanism model.

7.7 Compensator

A compensator was designed to transform the acceleration set-up to control motor torque. The control variable was motor input voltage. Thus, the compensator changed the acceleration set-up value to a motor input voltage that would create a motor current corresponding to the required motor torque. The interferences must also be taken care of. The input voltage interferes with the electromotive voltage. The compensator therefore has a compensation feed-back loop from motor angular velocity, which adds the electromotive voltage to input voltage and thus compensates the error. In figure 18. the compensation principle is shown.

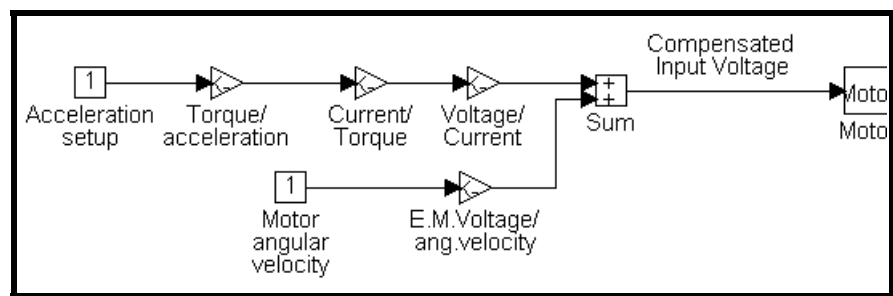


Fig. 18. Compensation principle.

8. Measurements

8.1 Tune up

Several simulations were performed. First the control system was trimmed by transient analysis: System performance was identified by ramp response. The system was first tuned up by using ramp response of 1 m/s. After the system was manually tuned up, the stability of tune up was checked by rising the ramp to 2 m/s. The motivation to identify by ramp response was, that the integration lag could also be trimmed. Step response could not identify integration lag. The third phase of tune up was trimming against acceleration response, which was done against 5 m/s² acceleration. A comprehensive list of the parameter change during the tune up is presented in table 2.

Table 2. Parameter set-up history during the control system trim.

Setup phase	P-Gain	I-Gain	D-Gain	Comments
Ramp 1 m/s	10 000	20 000	50	vibrating, divergent
	10 000	20 000	500	period time t = 0.4 s
	10 000	5 000	5 000	vibrating, period, t = 0.38 s
	1 000	0	0	vibrating, period, t = 0.20 s
	1 250	0	0	t = 0.19 s, divergent
	1 000	0	200	t = 0.16 s, damped t=0.55 s
	1 000	0	50	time con. = 0.17 s, full crit. damp
Ramp 2 m/s	1 000	10	50	divergent
	700	10	50	t = 0.23 s, damped t = 0.21 s
Acceleration 2 m/s	700	50	25	stabile, leave 20 m/m
	700	1 400	50	divergent after 3 s.
ABB PDV profile.	1 000	50	10	stabile, t = 0.11 s

8.2 Simulation of ABB Production Development robot axis behaviour

ABB Production Development produce two gantry robot models: Porta 100 and Porta 160. Both robots have the same kind of basic configuration. The simulation and servo system optimisation problem presented in this paper is based on design problems, from one customised configuration of model 100.

The kinematical path of TCP was specified [1] for each axis as a function of time. The work cycle was a 3 m long sequence path in a conveyor station. A comprehensive specification is given in table 3.

Table 3. Initial ABB specification: a) Path sequence b) Kinematics

Path sequence:	Kinematics:
<ul style="list-style-type: none"> • Pick up a box, mass=10 kg • Lift Z-axis 200 mm • Move Y-axis 1000 mm • Lower Z-axis 800 mm • Deliver box • Return stroke 	<ul style="list-style-type: none"> • Positioning tolerance: 1 - 3 mm • Cycle time: max: 2.5 s • Acceleration max: 20 m/s² • Jerk max: 400 m/s³ • DOF: 3D, orthogonal

According to this specification, transmission and kinematics were to be dimensioned and motor size selected. The kinematical optimisation was done together with ABB's design team, and kinematical simulations were performed and reported in [16, 17]. The simulation of kinematics was executed with ADAMS multi body systems simulations software. The simulations showed clearly, that the kinematical specification had to be changed, but generally it was possible to achieve a 2.5 s cycle time within acceleration and jerk restrictions.

Since the specification could be kinematically achieved, the next thing was to ensure, that the complete servo system (control, mechanism, and motor system) could also fulfil the required performance. The selected simulation concept was to model the mechanism and control system separately for each axis and simulate them one-by-one. The combined kinematics can then be animated in ADAMS, after the real path behaviour is analysed. The assumptions for this kind of simulation is of course completely independent axis system. Since the axis system is orthogonal for gantry robots, and the only common component is the power unit, which is dimensioned large enough, this kind of approach should be justified.

The kinematical path was manually coded from ABB's original customer specification. The path was coded as acceleration set-up value as function of time. The set-up value was then integrated twice to give the position set-up for the servo system. During the coding, the

original specification was found to be mathematically inconsistent. The specification was manually trimmed so, that consistent kinematics could be achieved.

8.3 Results

The simulation system was verified by testing at first the Z-axis operations of the ABB robot. The acceleration, velocity and position as a function of time is shown in figure 19.

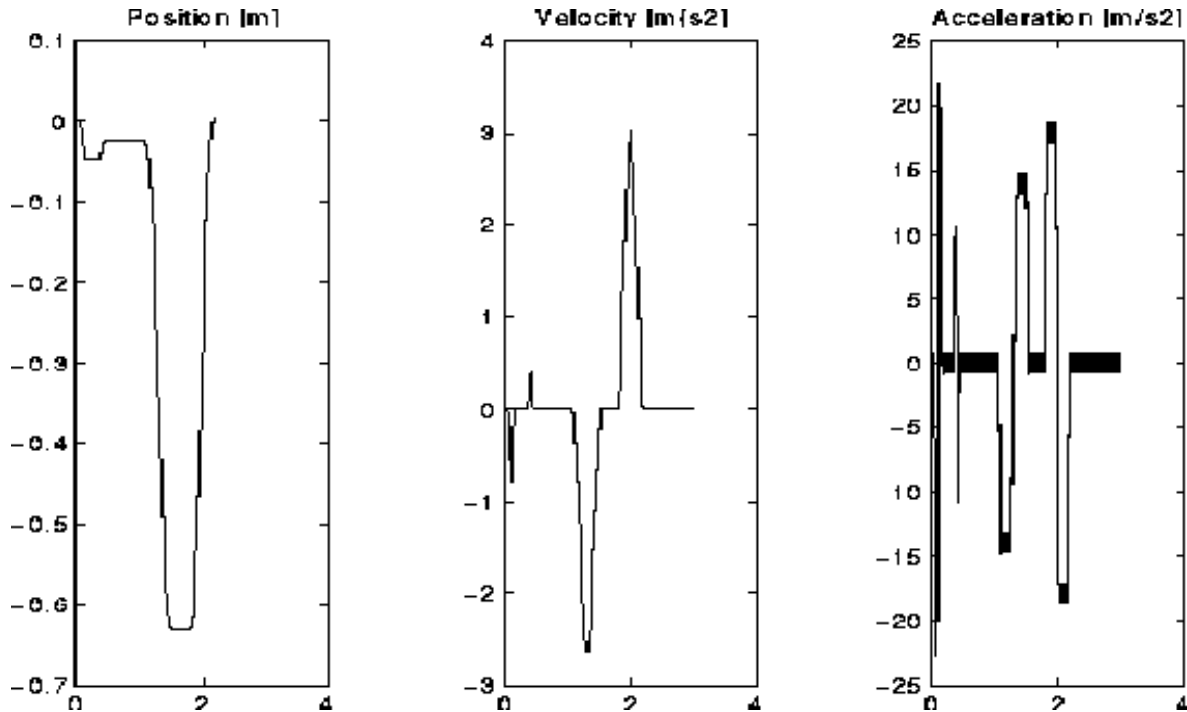


Fig 19. Position, velocity and acceleration profiles of the servo system.

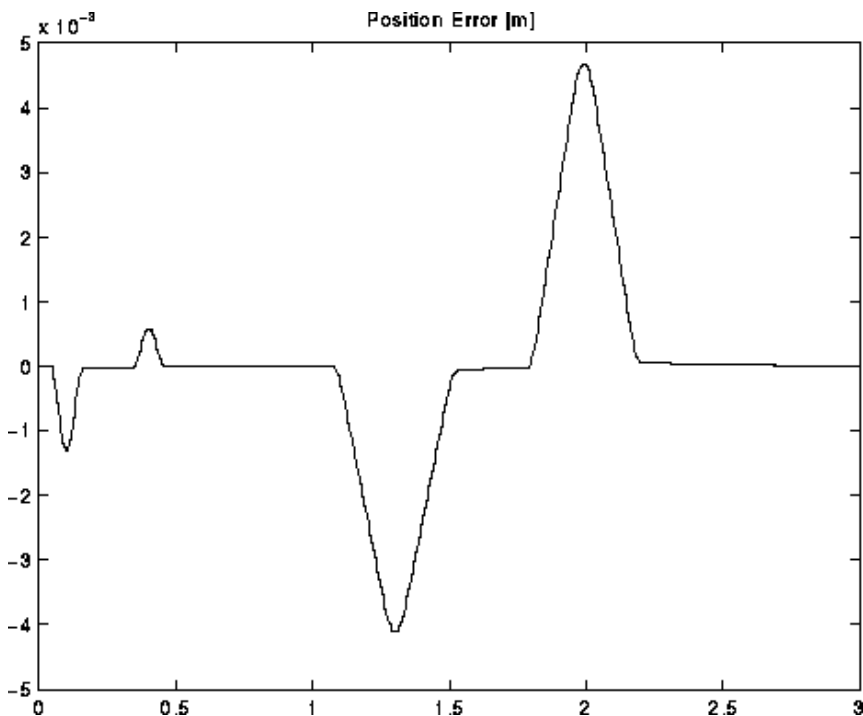


Fig 20. The position error between set-up and real position as a function of time.

It showed possible to achieve the kinematical performance required in specification. The second operation was to check the position accuracy during the operation and the set-up times. In figure 20, a plot of the position accuracy is presented. It should be noticed, that the largest errors (15 mm) are achieved in the middle of the path, while the required position accuracy is tightest at creeping. Thus the required accuracy 1mm is obtained.

The third point of interest in servo systems function verification is the electrical load of the motors. In figure 21. voltage, current and torque load on the motor is presented.

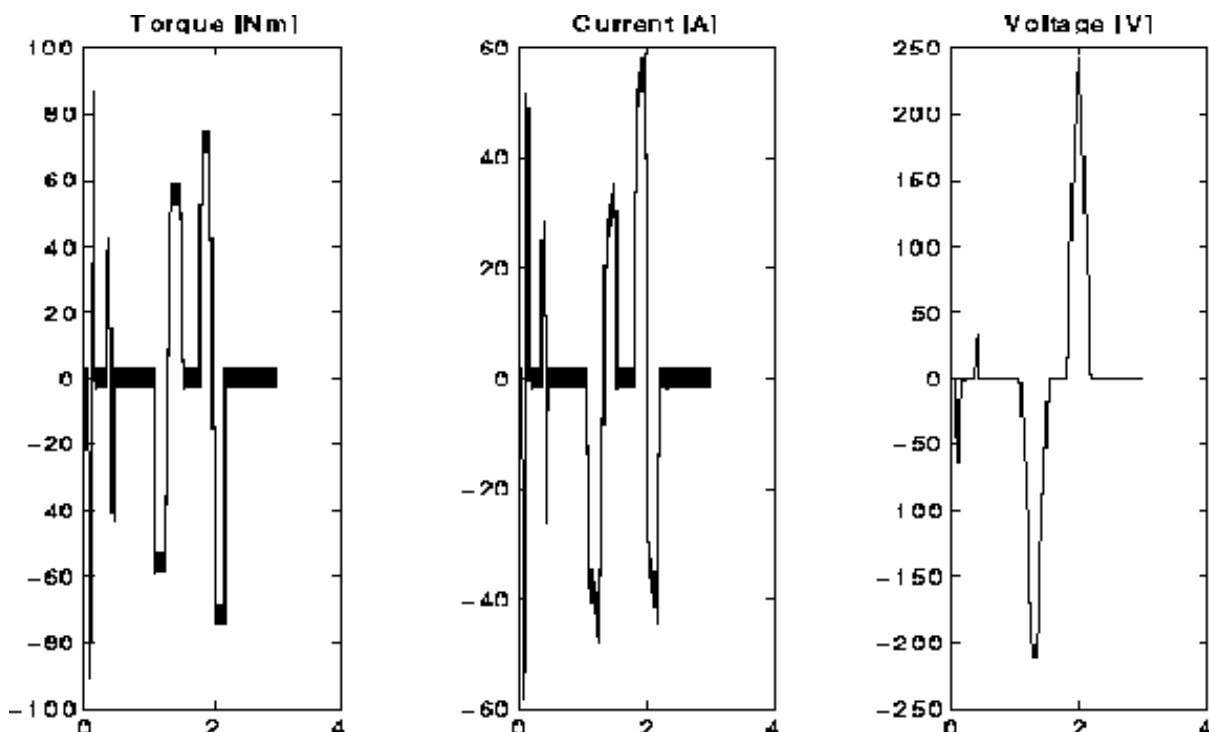


Fig. 21. Voltage, current and torque load of servo motor.

8.4 Tailored Matlab program

When new methods for function simulation in product design are developed, a question to be answered is, which is the complexity level of user interface a designer can manage in an industrial project, where fastness, reliability and ease of use are required. In this paper it is assumed, that concepts and solution principles are rather invariant in a product family. For instance, the main robot products of ABB Production Developments are gantry robots models 100 and 160. The number refers to the dimension of the variant, while the concept is basically the same. Therefore, with one simulation model, most of variants are modelled with parameter changes.

Since the development of the simulation model requires quite much experience of modern tools, a reasonable approach is, that the simulation model is developed by a specialist, who also develops an easy to use interface for the product. This kind of approach has become very popular in automotive industry, for dynamic simulations [23].

The solution in this project was to import the Simulink model into Matlab. The user interface was written as Matlab code, which read the input parameters and calculated the system parameters. Then the Simulink motor system was evaluated with specified path data and a linearisation of the state matrices was calculated to produce a pole plot. In figure 22. a schematic figure of the software is given.

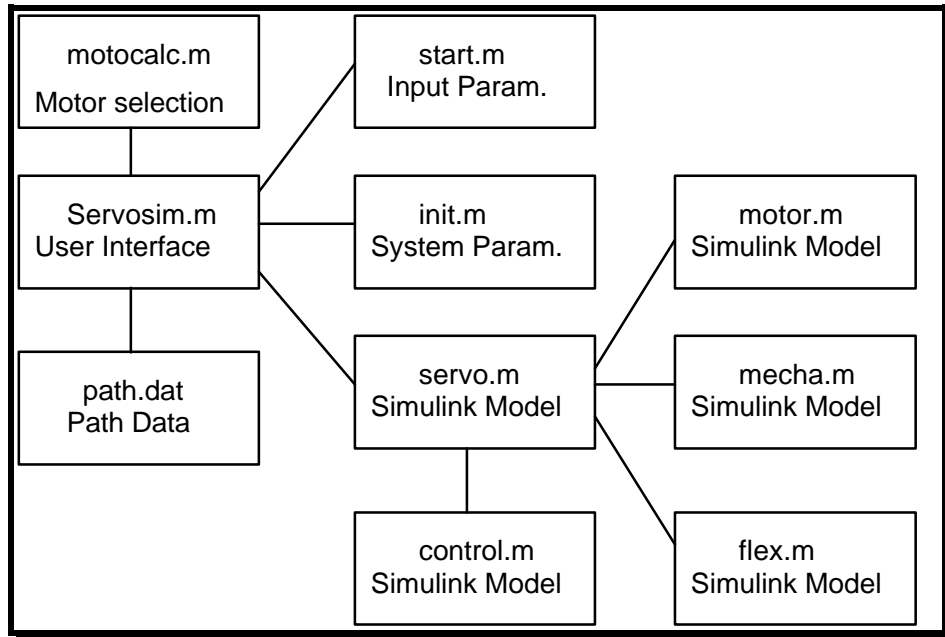


Fig 22. Matlab software for servo system simulation.

8.5 Motor selection program

A separate program for motor selection was written to assist the designer in choosing a suitable motor for a specific robot configuration. The program asks the user of maximum allowed acceleration and jerk, and maximum needed linear position change. According to the specification, the system calculates how fast each possible motor could perform this task, and the corresponding motor load. The program first lists the initial parameters of the motor and mechanism, and calculates the motor's electrical power, efficiency and input voltages, which makes servo amplifier selection easier. The performance is calculated from two assumptions:

firstly, acceleration restricted, that is, what should the transmission radius be, if the system is configured so that the motor can achieve maximum required acceleration in the specified speed range. With this radius, the maximum speed and maximum stroke is calculated, which can be achieved with maximum required acceleration. The second transmission radius is calculated so, that the specified stroke travel length can be achieved in optimum time according to the motors acceleration performance. If the maximum optimal stroke is shorter than the required stroke, the motor is not sufficient for optimal kinematics. In table 4. output of one possible motor from the motor database is shown.

Table 4. Output from motor selection program.

```
*****
* ANALYSIS OF ELECTRIC MOTOR NO:      752330    RESULTS.          *
* Acceleration restricts optimisation with this configuration.   *
*****
Motor Const. Resist. Induct. Inertia rev.[rad/s] Torque Mass
Kt        R       L        Jm      nm      Tm      m
1.60     30.00  0.07030  0.00110  314.16  2.1000  200.000
-----
Inp.Eff   Mech.Eff Resis.Eff Current Amplif. Motor Resist.
Pinp[W]   Pmec.[W] Pres[W]   I [A]   Uamp[V] Umot[V] Ures[V]
711.41    659.73   51.68     1.31    542.03  502.65  39.375
-----
Analysis of Acceleration restricted design potentials:
acc[m/s2] vel[m/s] stroke[m] time [s] mech.eta ropt
91.087    3.292    0.542     0.33    95.23   0.0105
-----
Analysis of Stroke restricted design potentials:
acc[m/s2] vel[m/s] stroke[m] time [s] mech.eta ropt
255.222   1.876    0.176     0.19    86.63   0.0060
-----
```

8.6 Discussion

This work has been concentrated to three important aspects in gantry robot simulation and dimensioning: analysis and optimisation of kinematics, transmission optimisation and motor and servo system modelling. The theoretical background for the simulation, i.e. models and equations required, have been derived and reported.

In this modelling, a *modular approach* has been one important requirement. The need for conceptual changes during design and simulation requires, that the elements of concepts are

modelled, and that they can be easily changed and a new concept topology can be built and simulated.

The modelling of components has been performed by using *graphical tools*. This makes the model easier to develop and understand for a human. On the other hand, analytic Matlab functions can be used, if this is a more suitable way to describe the problem.

From the end user point of view, a *problem oriented user interface* is important. The designer should be able to easily couple a new configuration, test it with a user interface, which contributes to the optimisation of kinematics and selection of electric motors. The change in design concept should not change the simulation specification or interfaces of the software. This can be called the requirement of *problem oriented modularity*.

The *manufacturing* and *product family history* creates inertia in a company and in design solutions. This should not be considered only as a negative phenomena. Instead, it enables long production series and decreases costs. On the other hand, conceptual changes and customer tailoring can be offered by right modularisation of the product family. Simulation modelling can be used effectively for each order to ensure both customer and supplier, that the new installation is an optimal configuration for the customer and it meets the functional requirements. Thus, one *simulation master model* with *modular component models* for one *product family*, should be developed, to be combined for specific customised applications.

8.7 Summary of conclusions

According to the experiences of this research, a simulation model for performance simulation of modular product family customisation, should:

1. Have a modular model structure.
2. It also should have modules that are easy to establish, preferably graphically.
3. Problem oriented user interface, which gives answers to questions on performance and functionality independent of the product concept.
4. One master simulation model for one product family.

9. References

1. ABB Packaging., *Functional Specification FCP Top Loading Gantry*, ABB Production Development, internal report dated 02/05/95.
2. Andersson, K., *A Design Language Based on Engineering Terminology*, PhD Thesis, Dept of Machine Design, Royal Institute of Technology, 1993, Stockholm.
3. Andersson, K, Makkonen P., *CANDLE anpassad för konstruktion av mekanismer*, (CANDLE applied for design of mechanisms), Produktmodeller 1995, Linköping.
4. Andersson. S., *Utvecklingsmetodik: ett system- och flödestekniskt angreppssätt*, (Development methodology: a system and flow technical approach), Department of Machine Elements, Royal Institute of Technology, 1992, Stockholm, Sweden.
5. Asada, H., Youcef-Toumi, K., Direct Drive Robots Theory and practice, MIT Press Cambridge, Massachusetts, 1988, London, England.
6. Electro-Craft Corporation., *DC Motors, Speed Controls, Servo systems: an engineering handbook*. Expanded 3. ed., Pergamon Press, 1977, New York.
7. Eschenaus, Koski, Osycka., *Multicriteria Design Optimisation - Procedures and applications*. Springer-Verlag, 1990, Berlin, Heidelberg.
8. Glad, T., Ljung, L., *Reglerteknik, Grundläggande teori*, (Control system theory, basics), Studentlitteratur, 1981, Lund.
9. Glad, T., Ljung, L., *Modellbygge och Simulering*, (Modelling and simulation), 1991, Studentlitteratur, Lund.
10. Hubka, V., *Principles of Engineering Design, WDK - Workshop Design-Konstruktion*. Butterworth & Co (publisher) Ltd, 1982.
11. Hughes, A., *Electric motors and drives: fundamentals, types and applications*. Oxford: Butterworth-Heinemann, 2nd ed., 1993, Oxford.
12. Lind, H., *A distributed implementation of dynamic control on a direct-drive robot system*. Doctoral Thesis, TRITA-MAE-1993:3, ISSN 0282-0048, ISRN KTH/MAE/R--93/3-SE, 1993, Stockholm, Sweden.
13. Kenji, Tak., *Electric motors and their controls: an introduction*, Oxford University Press, 1991.
14. Makkonen P., *PLASMA - Mechanism Synthesis Program*, MSc Thesis, Dept of Machine Design, Helsinki University of Technology, 1993, Stockholm, Sweden.
15. Makkonen P., Persson J-G. (1993) *Methods for Structural and Dimensional Synthesis for mechanical systems: an application to planar mechanisms*. 44 th CIRP General Assembly, 1994 Singapore.
16. Makkonen, P., *Integrated CAD methodology for Simulation Driven Product Development Process*, OST-95 Symposium in Machine Design, University of Oulu, 1995, Oulu, Finland.
17. Makkonen, P., *Konceptstudie och analys av plockmanipulatorer*, (Concept study and analysis of gantry manipulators), Intern rapport 95/2, Institutionen för maskinkonstruktion, Produktutveckling och konstruktion, KTH, 1995, Stockholm, Sweden.

-
18. Malmquist, J., *Towards Computational Design Methods for Conceptual and Parametric Design*, Doctoral Thesis, Chalmers University of Technology, 1993, Göteborg, Sweden,.
 19. Mathworks Inc., *MATLAB - Reference Guide*, Mathworks Inc., 1993, Natick, Mass.
 20. Mathworks Inc., *Simulink - Reference Guide*, Mathworks Inc., 1993, Natick, Mass.
 21. Mechanical Dynamics Inc: *ADAMS/View reference Manual, Version 8.0*, Mechanical Dynamics Inc., 1994, Ann Arbor, Michigan.
 22. Mechanical Dynamics Inc: *ADAMS/Solver reference Manual, Version 8.0*, Mechanical Dynamics Inc., 1994, Ann Arbor, Michigan.
 23. Dynamic Dimensions, MDI Newsletter., *Integrated automotive simulation system*. Vol 6, no 4. Mechanical Dynamics, Inc., 1995 Ann Arbor, Michigan.
 24. Neelamkavil, F., *Computer Simulation and Modelling*, John Wiley & Sons, 1987.
 25. Rask, I, Sunnersjö, S., *Optimering vid mekaniskt konstruktion*, (Optimisation in mechanical design) Sveriges Verkstadsindustrier, Fakta Rapport Konstruktion Nr. 1, April 1993, V020001, Stockholm.
 26. Sunnersjö, S., *Förberedd Konstruktion*, (Prepared Design) Sveriges Verkstadsindustrier, Fakta Rapport Konstruktion Nr. 6, April 1993, V020006, Stockholm.
 27. Svendsen, K.-H., *Diskretoptimering af sammansatte maskinsystemer - Et bidrag til en "Designer's Workbench"*, (Optimisation of Composite Mechanical Systems) Instituttet for Konstruktionsteknik, Danmarks Tekniske Universitet
 28. Traisfer, John., *Complete Handbook of Electric motor controls*, Prentice-Hall, 1986, Eaglewood Cliffs, New York.
 29. Yamamura, Sakae., *AC Motors for High-Performance Applications: Analysis and Control*, Marcel Dekker Inc., 1986, New York.

Product Development and Performance Optimisation of Rock Drill Boomers

Petri Makkonen
petri@damek.kth.se

Department of Machine Design
Engineering Design
Royal Institute of Technology
S-100 44 STOCKHOLM

1. Background

In March 1996, within a NUTEK funded research program co-operation was initialised between Atlas Copco Rock Drills, ABB Production Development and ABB Robotics Products and KTH Machine Design, Engineering Design. A pilot project was started in each company, to introduce and implement *Simulation Driven Product Development*¹. This paper discusses the project and defines the modelling process used. The characteristics of different modelling techniques are defined and exemplified from the viewpoint of drill boomer development.

At Atlas Copco Rock Drills Simulation Driven Design is used in the development of a new rock drilling rig for a tunnel drilling machine. A major part of the product development is performed using a product model, enabling *virtual prototyping*².

2. Rock Drilling Rig

The tunnelling and mining technology is often divided to tunnelling and production drilling. *Drill boomer*s are used in horizontal tunnelling, to drill a 5-10 m long parallel hole pattern for blasting. The *production drills* are used for large spherically formed hole patterns, being up to 30 m of radius, for blasting of thousands of tons of rock.

¹ *Simulation driven product development* (the original term was introduced by U.Sellgren, but redefined here) is defined as a product development method, where a major part of product development is performed using simulation models.

² *Virtual Prototyping* (the term is introduced by Mechanical Dynamics Inc., developing a Multi Body Systems simulation software ADAMS) is defined as a product development method, which enables function simulation with 3D geometry representation, integrated to CAD software.



Fig. 1a 3-Rig Drill Boomer H170



Fig. 1b. Production Drill, Simba H300

In soft rock (compressive strength less than 150 MPa), the most rapid excavation is achieved using a Tunnel Boring Machine (TBM), executing a continuous crushing (by rotary cutting) and stone transportation process. A TBM is usually manufactured for one project only. Thus its use is a very large investment (60...120 MSEK).

In hard rock, tunnelling is performed with tunnel drilling machines by repetitive a sequence of drilling, explosives charge, rock blasting, ventilation of gases and transportation. The drilling is usually performed by manually operated boomer, which drill the blast hole pattern. In figure 1. a typical hole pattern is shown:

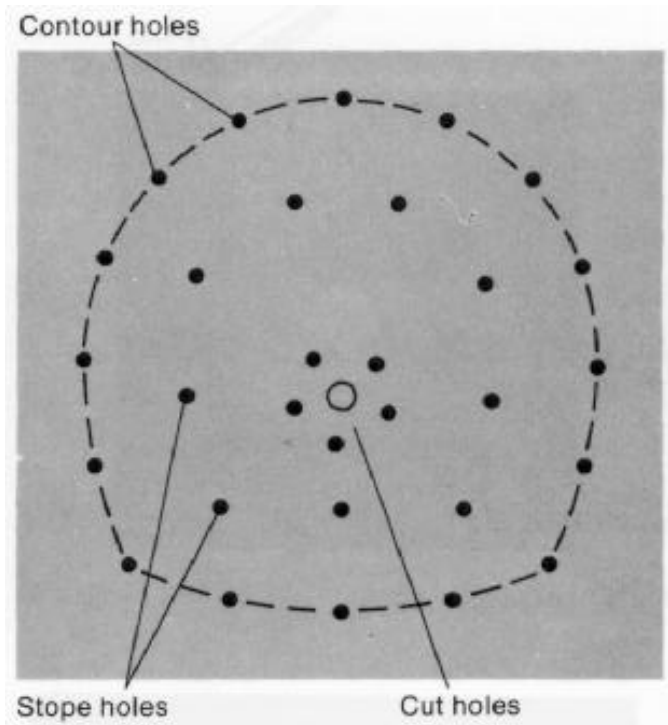


Fig. 2. Blast hole pattern in a tunnel section.

A typical blast hole group is up to 4-5 m long while the co-linearity must be better than ± 50 mm. The positioning accuracy is most critical near the center hole, where the detonation sequence begins. The boomer's function is to position and fix the drill so, that:

- The drill hole groups can be produced fast.
- Parallel holding requirements are fulfilled.
- The design of kinematics enables manual as well as computer control.

Table 1. Typical data for an existing boomer rig.

Kinematic capacity:	Performance:
Boom swing: $\pm 20^\circ$	Max tunnel cross section area: 8 m^2
Boom extension: 1500 mm	Max rock drill weight: 400 kg
Boom rotation: 360°	Sweep radius: 5000 mm
Feed dump: $+30^\circ..-90^\circ$	Coverage, length: 4400 mm
Feed extension: 1500 mm	Coverage, width: 6200 mm

3. ISS-Simulation System

3.1 Simulation Tools and Process

The introduction of general 3D CSG³ based integrated CAD tools⁴ having interfaces to several applications like simulation, tolerancing, drafting, NC-coding, rapid prototyping etc. have now been wide spread accepted in industry. The introduction of these tools in industry has often not been problem free; research is needed. Some typical problems experienced by the participating companies have been:

- Draft-oriented designers have difficulties in direct 3D solid modelling, while 3D projective modelling application is easier to adopt.
- Model parametrisation is complex due to the fact, that parametrisation requires that the designer identifies and models parameter interrelated consistency rules in a parametrised object. E.g. number of cooling flanges in a electric motor house changes the mould geometry in a complex way.
- Model idealisation requires considerations on modelling of feature hierarchy order.

At KTH Machine Design, a collection Mechanical Computer Aided Engineering (MCAE) software have been licensed, comprising 3D CSG software I-DEAS Full Simulation Package, multi body systems software ADAMS, FEA analysis ANSYS and control system tools MATLAB/Simulink. In the author's licentiate thesis, a multiple view simulation environment for mechanical systems simulation and design verification has been sketched, based on the use of these tools. Some applications for these software have been created, e.g. real time kinematic control of MBS-system with FORTRAN.

³ CSG (Constructive Solid Geometry) is a modelling method for 3D geometry generation, where the geometry is defined with combinatoric Boolean logic operations from geometric primitives. The technique is suitable for modelling manufacturing features and in the idealisation of geometry for simulation purposes.

⁴ CAD softwares using a parametrised 3D CSG are currently e.g. I-DEAS, Mechanica, Pro/Engineer and Unigraphics

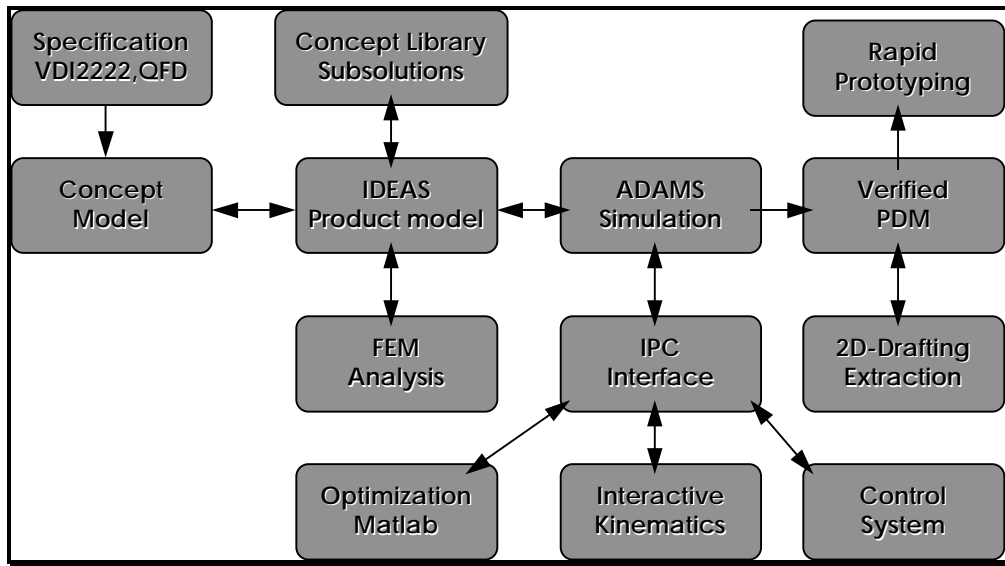


Fig 3. Integrated Simulation System.

A product modelling methodology is developed, specific for each participating company. The research will be based on analysis and experiences of the pilot projects, during the development of product models for some of product families.

Besides analysis, a theory based prescriptive synthesis approach is used. A frame for a product development process for simulation driven design is proposed in the authors licentiate thesis, based on the Theory of Domains and the Chromosome Theory by Andreasen [3] (figure 4.). The design process starts from the customer requirements and manufacturing potentials. These requirements steer the design team's mental patterns during conceptual design [2]. The process is divided vertically in time and horizontally in activity qualities, contributing team work of different domain specialists.

In the figure 4, *QFD* is added to the begining of the design process, mapping the customer requirements to product characteristics. The customer requirements should be breaked down to functional and performance requirements. The functional requirements specify the organ structure of the product, while the performance requirements define the performance measures, which should be identified by the simulation. A parallel research for development of QFD integration to CAE tools is currently going on at KTH Machine Design, named CANDLE by Andersson [1]. Also, the *product model data base* is added for reuse of design models and solutions. A suitable organisation for such data base is presented in the CAD application CADLETTI®⁵.

⁵ CADLETTI® is an add-on package for the Finnish CAD system VERTEX®, by Lujuustekniikka Oy, written by the author in 1990. It is an icon based component standard catalogue including several hundreds of different components, machine elements, and other calculation programs. The catalogue uses a selection tablet based disposition mechanism , using a taxonomy familiar from machine-element handbooks.

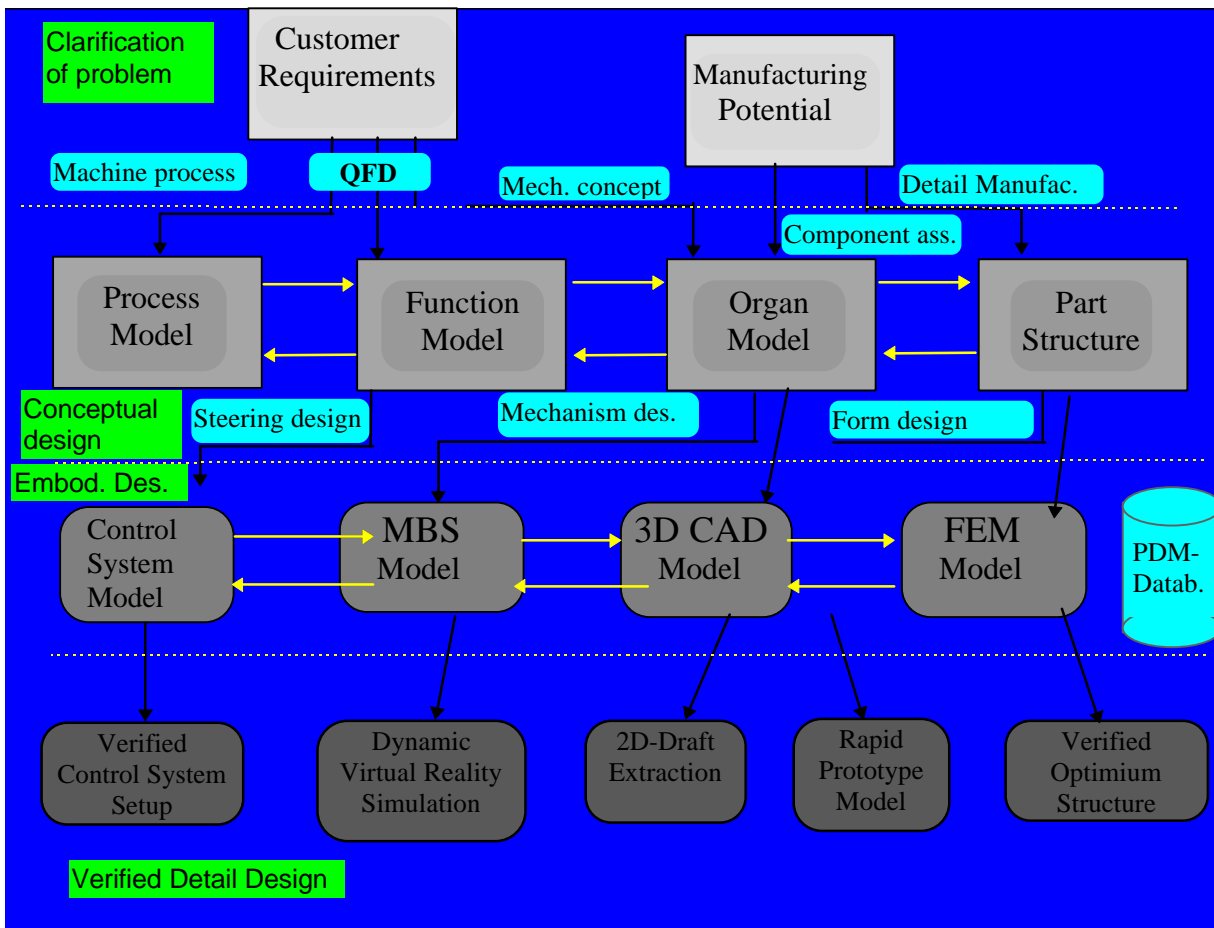


Fig. 4. Integrated Simulation Driven Design Process (ISDDP).

3.2 Properties and Characteristics of ISS-Model

Andreasen [6] distinguishes a products properties between the defining attributes, (characteristics) and behaviour related attributes (properties). In design, only the characteristics can be manipulated directly, while the properties are results of the design. In figure 5. the characteristics of a mechanical system are mainly defined in the geometry model, while the properties are analysed on the top level model.

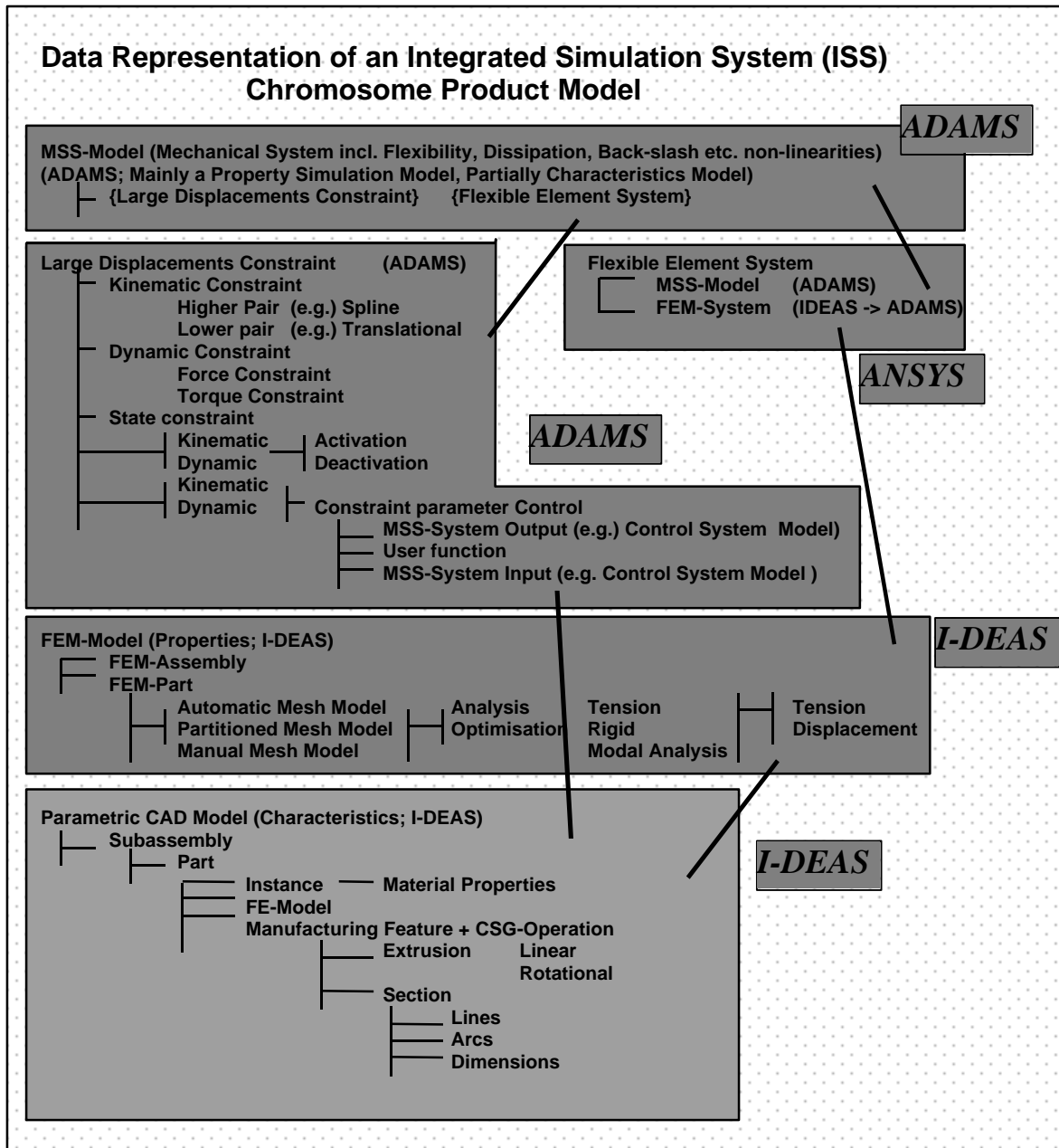


Fig. 5. The taxonomy of Design Properties and Characteristics in ISS-Model

3.3 Geometry modelling

The product modelling begins by defining the geometry models characteristics: features, dimensions and parameter hierarchy. The main dimensions of a part are defined by organ boundaries; i.e. hole distances, function planes etc. Consequently, the secondary dimensions should be parametrized so, that the *design of a part maintains consistency*. The changes in secondary dimensions shouldn't require updating of main dimensions. Otherwise interrelated consistency rules must be added to the model and preparation for optimisation, for instance, becomes more complex

Designers, experienced to design by drafting, may have difficulties adopting 3D solid modelling. The problem isn't that designers wouldn't be used to think in 3D, but in the fact, that in feature based modelling a complex section hierarchy is used, while in

drafting usually only three main projections are used to define the geometry. Thus, using 3D CSG application, a hierarchical model is produced, while projective geometry leads to monolithic structures. This leads to models being difficult to edit, change or idealise. But, after getting used to the “feature based way to thinking”, features are soon used as manufacturing features.

Discipline is required to maintain consistency in CSG-geometry modelling. The FE- and MBS-analyst must be able to *idealise* the geometry [9], without the loss of consistency in the model. This restricts the variation of a feature’s dimensions in relation to other features.

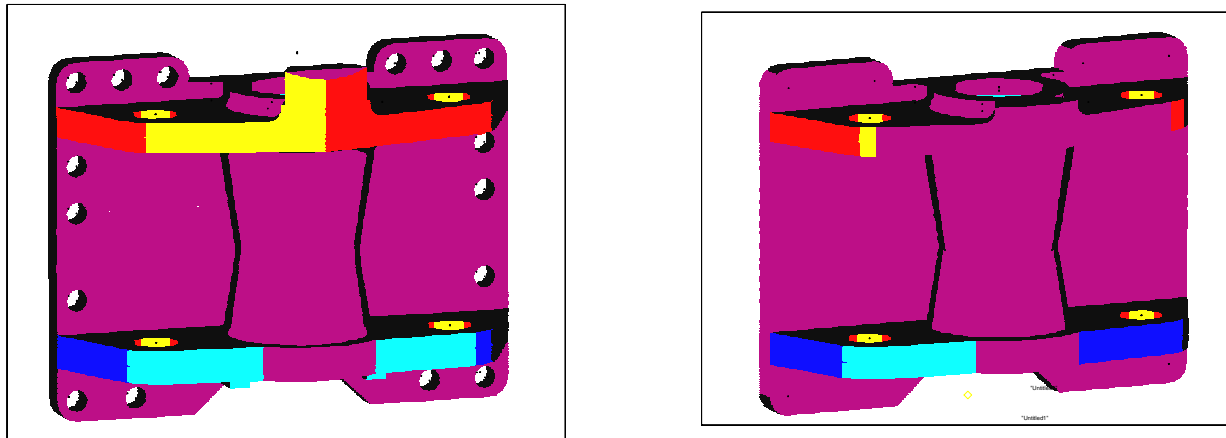


Fig. 6. Model idealisation of a boomer mounting plate.

Currently, a geometry based simulation model, enabling successive and reversible idealisation of geometry, like CSG-technique, seems to be most applicable to avoid FE-model errors when automatic mesh generation algorithms are used. Otherwise, FEM-mesh errors like incompleteness, ambiguousness, ghost geometries, fragmentations and topological errors are created. In a MBS-model, geometries are idealised to solid centroids. Due to this strong discretisation, idealisation might be required only for animation purposes.

4. Model export from CAD to MBS

MBS modelling could currently be performed in two ways in the ADAMS system: either, the dynamical model is written as a text file using Automatic Date Set language (.adl-file), or by using a graphical interface. Recently, several CAD suppliers have created an ADAMS/Solver-preprocessor, or have integrated it as a part of their CAD-code.⁶ However, none of these preprocessors are comprehensive. Advanced MBS-simulation requires model refinement in ADAMS. The support for graphics, for instance, is weak. In fig 7., the model exchange process is shown.

⁶ Currently, preprocessors for ADAMS are available at least from the following CAD suppliers: SDRC (I-DEAS), PTC (Pro/Engineer), EDS (Unigraphics)

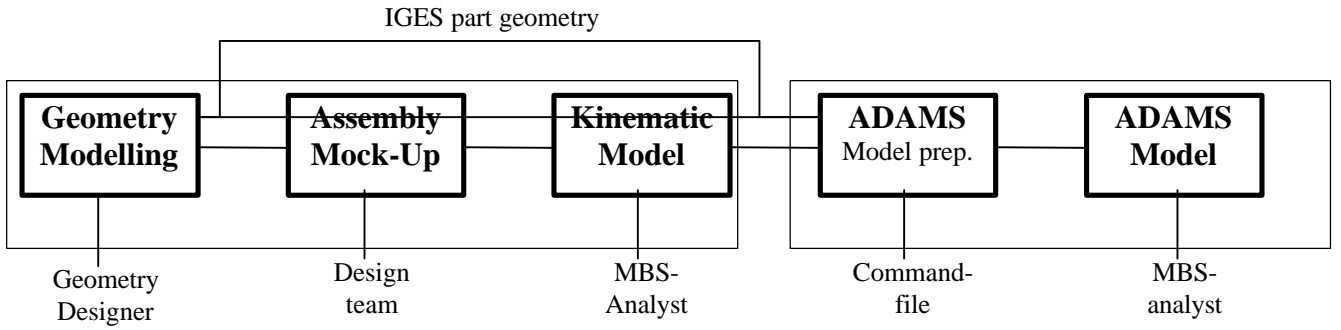


Fig. 7. The export of model from CAD to MBS.

5. Integration of FEM and MBS

In ADAMS, FEA substructures are represented by single NFORCE-statement, defining a single superelement stiffness and damping matrix between multiple coordinate system reference frame (FRF). The FRF is fixed to the substructure, and it moves with the individual rigid substructure. The differences can be illustrated considering a simple cantilever beam structure:

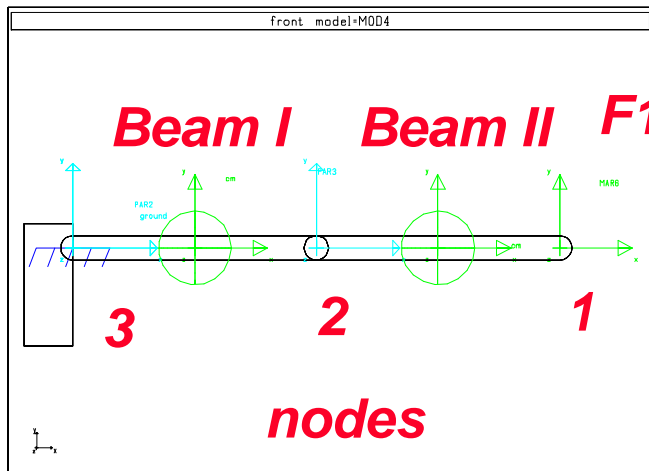


Fig. 8. ADAMS/Solver idealisation of a beam using two substructures.

Mass and damping will not be considered, thus the FEA equation is reduced to the static elastic relation:

$$\{F_{sys}\} = [K_{sys}]\{x\} \quad (1)$$

In the FEA model the system could be discretised into three nodes and two elements, thus resulting in:

$$\begin{bmatrix} F_1 \\ F_2 \\ F_3 \end{bmatrix} = \begin{bmatrix} K_{11}^I & K_{12}^I & 0 \\ K_{21}^I & K_{22}^I + K_{22}^{II} & K_{23}^{II} \\ 0 & K_{32}^{II} & K_{33}^{II} \end{bmatrix} \begin{bmatrix} x_1 \\ x_2 \\ x_3 \end{bmatrix} \quad (2)$$

By fixation of the beam to the ground, the system will be reduced to

$$\begin{Bmatrix} F_1 \\ F_2 \end{Bmatrix} = \begin{bmatrix} K_{11}^I & K_{12}^I \\ K_{21}^I & K_{22}^I + K_{22}^{II} \end{bmatrix} \begin{Bmatrix} x_1 \\ x_2 \end{Bmatrix} \quad (3)$$

If the system is subject to large displacements, the $[K_{sys}]$ and $\{F_{sys}\}$ would be needed to update incrementally. Many FEA programs allow time series analysis by inverting the $[K_{sys}]$ matrix only once, and then multiply it with $\{F_{sys}(t)\}$ several times. In mechanism simulation, the $[K_{sys}]$ matrix would need to be generated several times which makes the simulation ineffective.

The MBS approach in ADAMS solves the beam flexibility several times iterating the spatial variables $\{x\}$ rather than iterating on $[K_{sys}]$ and $\{F_{sys}\}$. The displacements in MBS are calculated locally (relatively FRF), rather than globally as in FEA. Thus the system (2) would instead be divided into two subsystems, one for each FRF. For beam I:

$$\begin{Bmatrix} F_1^e \\ F_2^e \end{Bmatrix} = \begin{bmatrix} K_{11}^I & K_{12}^I \\ K_{21}^I & K_{22}^I \end{bmatrix} \begin{Bmatrix} x_1 \\ x_2 \end{Bmatrix} \quad (4)$$

and for beam II:

$$\begin{Bmatrix} F_2^e \\ F_3^e \end{Bmatrix} = \begin{bmatrix} K_{22}^{II} & K_{23}^{II} \\ K_{32}^{II} & K_{33}^{II} \end{bmatrix} \begin{Bmatrix} x_2 \\ 0 \end{Bmatrix} \quad (5)$$

where $\{F^e\}$ are the element nodal forces.

The displacements and forces in equations (4) and (5) are not consistent, since each is referring to different co-ordinate systems, following the FRF. To solve the system, a common reference frame is selected as ground, here the node 3. The displacements are calculated in relation to the global reference frame as in FEA. The equation (4) will then be modified:

$$\begin{Bmatrix} F_1^e \\ F_2^e \end{Bmatrix}_3 = \begin{bmatrix} K_{11}^I & K_{12}^I \\ K_{21}^I & K_{22}^I \end{bmatrix} \begin{Bmatrix} x_1 - x_2 \\ x_2 \end{Bmatrix}_3 \quad (6)$$

while eq. (5) remains unchanged, since it is already represented in the node 3 coordinate system. The difference between equations (6) and (3) is the term $x_1 - x_2$. It converts the relative displacement of co-ordinate systems of beam I to beam II, while the elasticity matrixes remain constant. Thus, instead of using one system stiffness matrix, MBS analysis uses a group of smaller matrixes. The deflections in each FRF are small, while with a relatively small number of FRFs in a chain a large non-linear deflection can be modelled.

6. The integration of FEM and MBS simulation

A FMBS (Flexible Multi Body System) is created by integrating FEM to MBS modelling. The FEA model is generated from the CAD model, with FEM pre-processor,

using manual and automatic mesh generation. The FEA-constraints are fixed only on the geometry, not on the mesh, to enable FEA-optimisation. FEA-optimisation is done separately for parts, according to mass minimisation and modal frequency requirements. The export of a FE-mesh can be done in two ways: *Modal flexibility discretisation* is used in high frequency analysis. The mass distribution and internal force dynamics effects are neglected. In the lower frequency domain, *superelement mass and elasticity discretisation* is used. Due to less amount of FRFs, high frequency behaviour can't be analysed, while the *non-linear deflection behaviour* can be modelled very accurate. In this project, the non-linear low frequency performance is more important, and it is thus imported to the MBS-model, while the eigenvalue analysis will be performed in the geometry model FEM (I-DEAS), to study individual part stiffness and modal frequency optimisation, importing the dynamic load history from MBS-analysis.

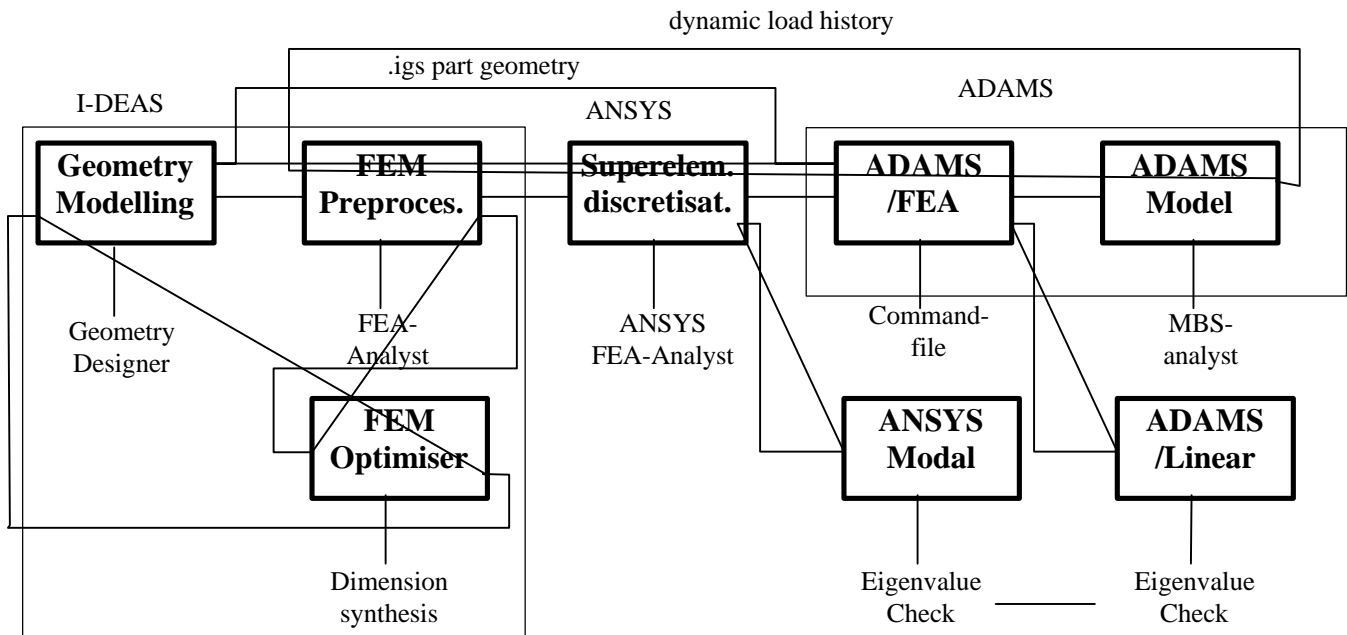


Fig. 9. Integration of FEM and MBS to form a FMBS.

7. Conclusions

The simulation project was started recently, and is now focused on modelling. The selected tools are supporting the modelling process efficiently, and no major conceptual problems have occurred. Some practical conclusions could still be done:

- CAD modelling requires discipline. For instance, a parts co-ordinate systems origo is defined here. The designer must take advantage of CSG-modelling, build the main structures first, and parametrise from functional dimensions. Concept first, manufacturing drafts then.
- The products kinematic parameters (dimensions) should be defined in the assembly phase. Only in this way the results for kinematic synthesis can be updated to the master model. With current software, MBS model geometries can't be exported to CAD
- The fastest way to create a CAD-MBS transformer is to use macro recorder during

the first manual assembly, and to run the macro for updates.

6. References

1. Andersson, K. *Computer Support for Early Design Work*, OST-'96 conference on Machine Design in Stockholm May 1996, Department of Machine Design, University of Oulu, Oulu 1996.
2. Andreasen, M.M. *Syntesemetoder på systemgrundlag, - Bidrag til en Konstruktionsteori* (in Danish), Dissertation, Institutionen för Maskinkonstruktion, Lunds Tekniska Högskola, Sweden 1980.
3. Andreasen, M.M. *Theory of Domains*, Technical Report, Instituttet for Konstruktionsteknik, University of Technology in Denmark, IK-nr.:88.46-B, Lyngby 1988.
4. Korpela, T. *Object oriented classification of data in shaft design*, OST-95' Conference on Machine Design in Oulu, May 1995, Department of Machine design, University of Oulu, Oulu 1995.
5. Makkonen, P., *PLASMA - A Mechanism Synthesis Program*, Masters Thesis, Department of Machine Design, Helsinki University of Technology, Helsinki 1993.
6. Makkonen, P., *User-adapted and Efficient Modelling and Simulation in Product Design*, Licentiate Thesis, Royal Institute of Technology, KTH, Department of Machine Design, 1995.
7. Mechanical Dynamics Inc, *ADAMS/Finite Element Analysis Reference Manual version 8.0*, Mechanical Dynamics, Inc., Ann Arbor, Michigan, 1994.
8. Mortensen, N.H. *Linking Product Life Modelling to design theory*, Produktmodeller '95, 25-26 April, Linköping, ISBN 91-7871-541-5
9. Sellgren, U., *Simulation Driven Design- A Functional view of the design process*, Licentiate Thesis, Department of Machine design, Royal Institute of Technology, KTH, Stockholm 1995.

Configuration and dimensional synthesis in mechanical design: an application for planar mechanisms

**Petri Makkonen, Jan-Gunnar Persson (2);
Department of Machine Design/Engineering Design, Royal Institute of Technology, Stockholm.**

Summary:

An approach to synthesis of mechanical systems in the conceptual and dimensional phase is done by combining topological and dimensional design with graph theory. The topological synthesis is done in two parts. First, part and joint number synthesis is done from the Grübler equation. The synthesis is continued by a grammatical approach. The theory of generative grammar has been applied to mechanisms, and by using this approach, a "grammar of mechanisms" has been formulated. The level of grammar is specified and grammatical rules have been derived from the constraint equations. An example of topological synthesis of mechanisms utilising the developed grammar is presented. Finally, the dimensional synthesis of the mechanism topologies is done utilising non-linear programming (the gradient method) with addition of a penalty-function to avoid discontinuities.

Keywords: Design, synthesis, mechanism optimisation

1. Introduction

In almost every field of machine design the most important design decisions are made during the conceptual phase of design. At this conceptual stage, the selection of solution principles has a great influence on the characteristic properties of the product, like product performance, material cost, manufacturability and the product over-all economy, while actual design costs are still low.

Important design decisions are hence made early. However, at this early stage the designer normally cannot sufficiently consider the effects of his decisions. Performance analysis can be made with current CAE tools only after a fairly detailed geometry model has been developed. Then already several important decisions have been made, e.g. concerning the topology of the product.

This problem has been recognised by researchers and designers. The need for CAD tools for early design has influenced several research projects. A variety of design methodologies, like Pahl & Beitz (8), German guidelines VDI 2222 (10), Axiomatic Design (9), etc. have been developed. These methods have proven to be powerful

particularly for mapping from the customer domain to the functional domain and then to the solution domain, with transformations of customer requirements to functional requirements and to design parameters. These methods support parsing and classification of the design configuration. However, for a rational design decision, product performance must be evaluated. There is a need not only to generate design solutions, but also to analyse the performance of a proposed solution. Furthermore, there is a need for more or less direct generation of design solutions, straight from the functional requirements.

In general, the reversed process of direct synthesis is a very difficult task. In synthesis, information has to be created, as opposed to analysis, characterised by data reduction (3). However, in many cases a complex chain of causal relations exists. These relations could be mapped and a causal model for the generation of solution concepts from the specified requirements could be created. In this paper the application of planar mechanism design has been studied. Mechanisms can easily be represented mathematically, but nevertheless non-continuous functions and the loops of kinematic chains make the design of mechanisms a creative engineering problem.

In this paper, a completely new approach to the design of planar mechanisms is presented. The current methods (2), (4), (5) for search of possible topological alternatives of planar mechanisms and methods for dimensional optimisation have been combined with graph theory and a new grammatical approach to mechanism design is introduced by means of generative grammar.

2. Part and joint number synthesis

The global degree of freedom of a planar mechanism system is given by the Grubler equation (1). All parts have primarily three degrees of freedom, the ground part is fixed, and the systems degree of freedom is restricted by first and second degree of freedom joints.

$$F = 3(P - 1) - 2n_1 - n_2 \quad (1)$$

where F = mechanism global degree-of-freedom,
 P = number of parts (ground included),
 n_1 = number of kinematic pairs of 1st degree (rotation or translation only),
 n_2 = number of kinematic pairs of 2nd degree (combined rotation and translation).

There are three kinds of possible joints in a plane system: rotation and translation joints restrict two degrees and prismatic joints one degree of freedom. In fig. 1 schematic figures of rotation, translation and prismatic joints are shown:



Fig. 1. a) Rotation joint b) Translation joint c) Prismatic joint.

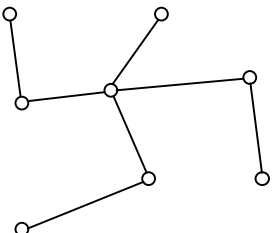
We now use graph theory with application of the three following statements:

- * A *circuit* is a closed path, in which each vertex is traversed exactly once.
- * Two or more graphs are *isomorphic* if there is a one-to-one correspondence between their edges and vertices which preserves incidence.

* A tree is a sub graph of a connected graph containing all of its vertices and no circuits.

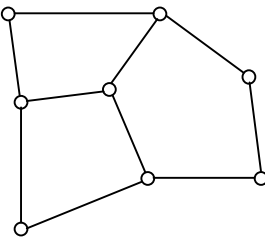
A clarifying picture of the statements above is given in figure 2:

$v: 8$
 $e: 7$
 $L: 0$



a)

$v: 8$
 $e: 10$
 $L: 3$



b)

Fig. 2. a) Tree graph.

b) Graph with three loops.

From the statements above we can now derive the basic equations of graph theory to be applied to mechanism synthesis: For any graph, let

$$\begin{aligned} e &= \text{number of edges}, \\ v &= \text{number of vertices}, \\ L &= \text{number of independent loops}, \\ v_i &= \text{number of vertices of degree } i. \end{aligned}$$

Then from the statements and from fig. 2 we obtain:

$$e_{\text{tree}} = v - 1 \quad (2)$$

$$L = e - v + 1 \quad (3)$$

$$2 \cdot e = \sum i \cdot v_i \quad (4)$$

Moreover, all planar graphs fulfil the Euler equation where a is the number of areas:

$$v - e + a = 2 \quad (5)$$

Any planar mechanism can then be topologically represented as a graph as follows:

The *topological graph* of a mechanism is a graph where vertices correspond to links (or parts) and the edge connections correspond to the joint connection of links.

From the basic structural equations of graphs, eq. (2) - (4), and from the Grübler equation (1), when putting the system global degree-of-freedom to one, we obtain:

$$L = j - l + 1 \quad (6)$$

$$2 \cdot j = \sum i \cdot l_i \quad (7)$$

where

j = number of joints in the mechanism ($j=n_1+n_2$),

l = number of links ($l=P$),

l_i = number of links with i joints.

For a mechanism, when we then put $F = 1$ in equation (1), we get:

$$3P - 4 - 2n_1 - n_2 = 0 \quad (8)$$

Equation (6) could also be written:

$$L = n_1 + n_2 - P + 1 \quad (9)$$

Equation (9) gives the quantity of loops in a planar mechanism with one degree of freedom. By using integer programming of equation (8) and the subsidiary condition all parameters non-negative, we can calculate the following component number combinations for planar mechanisms:

L	n_1	n_2	P	
1	4	0	4	
1	2	1	3	(10)
2	7	0	6	
2	5	1	5	
...	

3. Grammatical manipulation of mechanism topology

Topological variants of mechanisms can be generated in many ways. In this section there has been created a method to develop mechanism topologies, that is based on the American linguist Noam Chomsky's theory of generative grammar, presented in (1). It is based on the idea that languages have grammatical rules. A rule is defined as follows: Let graph $G=(V,E)$ be a finite undirected graph of n vertices (V = set of vertices, E = set of edges). Each string is derived from a distinguished initial symbol according to a set of rewriting rules P . A rewriting rule is a

relation of the form

$$A \rightarrow B \quad (11)$$

where A and B are strings of symbols from V. The relation (11) is to be interpreted that if the device generates a string A it generates also a string B.

Example: Consider the tree in figure 3. By identifying vertex a as an initial one we obtain the string S=*abcbdefedb* as a boundary of the tree. It should be noted, that the string is closed and forms a boundary to the tree, and it can be rotated (cyclically permuted) without any change in the structure.

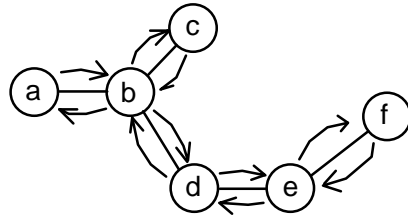


Fig. 3. A graph of a tree.

We can now define a trivial rule on how all trees can grow by adding new branches. To grow the tree using strings, we need two "growth" rules. First we must plant the tree, utilising rule 1:

$$\text{Rule 1: } T \rightarrow ab \quad (\text{initial rule}) \quad (12)$$

Then any new branch or leaf can grow on the tree according to:

$$\text{Rule 2: } x \rightarrow xyx \quad (13)$$

where x is any symbol in the string and y is a new symbol.

We go back to the formal description of generative grammar. The grammar and the language that it generates can be produced by production rules of the form (11) to be a system (14):

$$G=(S, T, N, P)$$

(14)

where S = the set of initial symbols of the language,
 T = the set of end symbols (terminals) of the language,
 N = the set of intermediate symbols of the language,
 P = the set of production rules of the language applied to produce the language.

The set of production rules P are called a grammar, and the set of all possible sentences that can be produced by it, is called a language. The rules are applied recursively as in mathematical induction formulas. To classify the language systematically, it is necessary to take care of all possible choices and if necessary, go back to the previous choices, until no rule can be applied. This procedure is called a *recursive cataloguing* or enumeration. For example, a grammar

$$S \rightarrow aAb, A \rightarrow bAb, A \rightarrow a \quad (15)$$

is generating (or tuning) an infinite language:

$$aab, ababb, abbabbb, \dots \quad (16)$$

Generative grammars can be categorised in four classes by the form of the production rules. The classes are listed in table 1 below in rising order of expression capacity:

Table 1. The classes of formal grammars.

Characterising form	Grammar class
$A \rightarrow aA, A \rightarrow Ab$	Formal languages.
$A \rightarrow aAb$	Context free grammars.
$aAb \rightarrow B$	Context sensitive grammars.
	Generalised languages. (All other possible rule forms)

Grammars can be characterised also in another way. In the example of tree graph string manipulation, mentioned previously, we have used principles of generative grammar to formulate a simple grammar for planting and growing of trees. Trees are nevertheless sub graphs of normal connected graphs, and therefore we can use a simple first level grammar to describe and manipulate them. To manipulate more

complex graph systems we need more sophisticated grammars. In table 2 a list of graph grammars and their area of application is shown:

Table 2. Level of grammars.

Level of Gr.	Manipulation level	Application area
1	strings	Trees
2	words	Connected graphs, forests of trees
3	sentences	Forests of connected graphs

We need a second level grammar to examine topologies of single mechanisms. We outline the grammar of mechanisms in two phases as in the tree example by at first describing the structure of the grammar for mechanisms and secondly by defining grammatical rules derived from mechanism theory.

In a topological graph of a mechanism, parts are represented by vertexes and joints by edges. This graph is a complete description of the topology of a mechanism. All this information can be transformed into a group of strings by the following rules:

1. The number of strings (in the following: topology words) are equal to the number of regions a , i.e. one more than the number of circuits. This can be verified utilising equations (3) and (5):

$$a = L + 1 \quad (17)$$

2. The words are formed by taking in clockwise direction all vertices and edges boundary to the region.
3. The first word is formed from the outer region boundary vertices and edges.

As an example we transform a Watt II mechanism topology into a topology sentence:

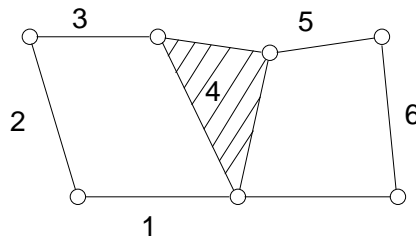


Fig. 4. Watt II mechanism

The words W1, W2 and W3 will then be:

$$\begin{aligned} W1 &= 1r2r3r4r5r6r \\ W2 &= 1r2r3r4r \\ W3 &= 1r4r5r6r \end{aligned} \quad (18)$$

where

1,2,3,4,5,6 are the part numbers
r is the type of joint (rotation)

A practical way to represent the structure is to use a LISP-like notation. Each vertex and edge symbol is an *atom*. Each circuit is a list of atoms, and the whole mechanism sentence is a list of simple lists. The Watt II mechanism in figure 4 will have the following LISP-representation:

$$\begin{aligned} &((1\ r\ 2\ r\ 3\ r\ 4\ r\ 5\ r\ 6\ r) \\ &(1\ r\ 2\ r\ 3\ r\ 4\ r) \\ &(1\ r\ 4\ r\ 5\ r\ 6\ r)) \end{aligned} \quad (19)$$

The sentence above is a complete description of the mechanism topology containing the complete connection information and the types of joints. Thus the *structure rules* for a mechanism topology grammar are:

1. A Mechanism sentence is a list of circuit (word) lists
 $S = (W_1, W_2, \dots, W_n)$.
2. A word list is a list of form $W = (P_1, P_2, \dots, P_n)$ where
 $P_j = X, j$, where X is a part symbol and j is a joint type symbol, where j can be r for rotation, t for translation, g for gear and p for rotational prism.

We have now described the complete *structure rules* for a grammar of planar mechanism topology. The next thing is to develop *production rules* for the grammar, so that new topologies can be generated. The production rules can be formulated from two principles:

1. All complex mechanisms can be constructed by superposition of simple mechanisms in a certain sequence.
2. A simple mechanism has only one loop.

10

The first principle states that complex mechanisms are a sum of simple *sub mechanisms*. Sub mechanisms have only one loop, so they can be found very easily from the Grübler equation (1), where the quantity of loops is put equal to one. From eq. (10) we find the only number combinations that have exactly one loop:

L	n_1	n_2	P	
1	2	1	3	(20)
1	4	0	4	

The first one is a piston-crank-mechanism. The second one is a fourbar mechanism. However, in both cases, it is not necessary that the joint type n_1 is always a rotation joint. It can also be a translation joint, so a fourbar mechanism could in principle be composed also from translation joints.

Now we can define two rules for initialising a mechanism topology by first planting the seed sub mechanism. It can be either

$$\text{Rule 1: } M \rightarrow ((1 \ k \ 2 \ k \ 3 \ p) \\ (1 \ k \ 2 \ k \ 3 \ p)) \quad (21)$$

where k is a first degree of freedom joint, a rotation (r) or translation (t) joint and p is second degree of freedom joint, a rotation prism, or

$$\text{Rule 2: } M \rightarrow ((1 \ k \ 2 \ k \ 3 \ k \ 4 \ k) \\ (1 \ k \ 2 \ k \ 3 \ k \ 4 \ k)) \quad (22)$$

By using these two rules the basic sub mechanism is installed. Then further developing goes on by recursively applying the growth rules 3 and 4 in the basic mechanism structure.

$$\text{Rule 3: } (\dots(\dots X \ j_1 \ p_1 \ j_2 \ p_2 \ \dots \ j_n \ Y \ \dots) \rightarrow \\ (\dots(\dots X \ r \ Q \ p \ Y \ \dots) \dots \\ (\dots Y \ j_n \ \dots \ p_2 \ j_2 \ p_1 \ j_1 \ X \ r \ Q \ p \ \dots)) \quad (23)$$

where

- X = Part from the new chain starts,
- Y = part where to the new chain ends,
- p_i = parts between X and Y in the old chain,
- j_i = joints between X and Y in the old chain,
- Q = new part number,

and

$$\text{Rule 4: } \dots(\dots X j_1 p_1 j_2 p_2 \dots \dots j_n Y \dots) \Rightarrow \dots(\dots X k Q_1 k Q_2 k Y \dots) \dots \\ (\dots Y j_n \dots \dots p_2 j_2 p_1 j_1 X k Q_1 k Q_2 k \dots) \dots \quad (24)$$

where

Q_1 = 1st new part,
 Q_2 = 2nd new part,
 k = rotation or translation joint.

Example. To develop a more complex topology we add a piston-crank-mechanism to a simple fourbar mechanism given by rule 2 (22). We also define that all joints in the fourbar mechanism are of rotation type. Then, we apply rule 3 by adding the piston-crank topology between the parts 3 and 4 in the fourbar topology. The transformation operation is then:

$$((1 r 2 r 3 r 4 r) \quad \Rightarrow \quad ((1 r 2 r 3 r 5 p 4 r) \\ (1 r 2 r 3 r 4 r)) \quad (4 r 3 r 5 p) \quad (1 r 2 r 3 r 4 r)) \quad (25)$$

In graphical representation the transformation operation is described in fig. 5:

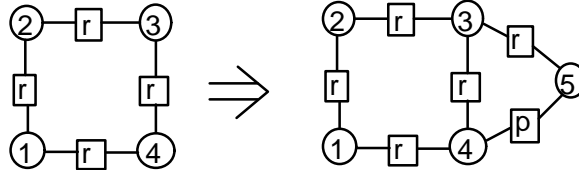


Fig. 5. The grammatical addition of a piston-crank-mechanism into a fourbar mechanism.

5. Nonlinear programming

For dimensioning of a mechanism, optimisation utilising the gradient method, has been used. The least square error function to be minimised during optimisation, is given in eq (26). For a more detailed description of the penalty function, used to handle subsidiary conditions, e.g. concerning acceleration (inertia force), it is referred to (6).

$$f(\bar{x}) = \sum_{i=1}^m \Theta |\bar{p}_o \cdot \bar{b}g - \bar{p}_t(i)|^2 + b \mathbf{G}_o(i) - \mathbf{a}_t \cdot \bar{b}g \mathbf{j} \quad (26)$$

where

\bar{p}_t = trial path point,

\bar{p}_o = object path point,

α_t = trial path angle for the tool,

α_o = object path angle for the tool,

a = path deviation weight (zero in function optimisation),

b = tool angle deviation weight (zero in path optimisation),

m = number of path points.

The function is written in a kinematically bounded form. This leads to the synchronised bounded optimization for the path, i.e. the optimisation path should also get dynamically as close as possible. Normally, only the form of the path is optimized, which is done by calculating the angle and distance difference with the nearest point method. To the error function f , a penalty function should be added to handle subsidiary conditions, i.e. positive dimensions only, limited acceleration (inertia forces) etc.

$$g(\bar{x}) > 0 \quad (27)$$

so, that the complete objective function to be minimized will be:

$$F(\bar{x}) = f(\bar{x}) + p(\bar{x}) \quad (28)$$

The penalty function can for example be of the following form:

$$p(\bar{x}) = k \ln \frac{1}{g(\bar{x})} \quad (29)$$

Now the optimization is done in a classical way by utilizing the gradient method:

$$\bar{x}_{i+1} = \bar{x}_i - k \nabla F(\bar{x}_i) \quad (30)$$

6. Theoretical results

The aim has been to develop a new concept, that should contribute to automatic topological synthesis and analysis of planar mechanisms. This objective has been reached in several respects. Firstly, the possible number combinations for topological structures can be generated, by utilising a known method for number synthesis (2). Then, by utilising graph theory and the theory of generative grammar the main result, a new grammar, -"the grammar of planar mechanisms"- has been developed. The rules of this grammar has been derived from the

Grübler equation and from graph equations. Examples of the use of the rules are also given. The developed grammar has been classified to be *context sensitive* and it is a *second level graph grammar*.

7. Experimental results

The concept presented in this paper has been verified by means of two computer programs. A simple BASIC program was first developed, for dimensional synthesis and optimisation of fourbar mechanisms with eight variables. A comprehensive FORTRAN program (named PLASMA — Planar Link Synthesis and Analysis of Mechanisms Automata) for analysis of arbitrary mechanism configurations was then developed. The sentence of strings which describes the mechanism topology, can be transformed to a Link Adjacency Matrix (LAM), which is used as input to PLASMA. PLASMA then calculates feasible initial values of the mechanism dimensions. PLASMA is linked to a commercial MSA (Mechanical Systems Analysis) program for iterative kinematic analysis of the mechanism during optimisation. PLASMA generates an input file for the MSA program, including part and joint structure and dimensions. The postprocessor part of PLASMA, for evaluation of the objective function and the path error gradient from the MSA result file, is still under development.

In fig. 5, a graphical output of a fourbar mechanism optimisation is presented. The program minimises the square sum error of the difference vectors between object path and actual path. After 68 iterations the average path deviation, based on the square sum error is reduced to 1.8 % of the path length.

	Value	Gradient
X:		
Y:		
Frame:		
Crank:		
Coupler:		
Follower:		
TCP-u		
TCP-v		

(5a)

X:
Y:
Frame:
Crank:
Coupler:
Follower:
TCP-u
TCP-v

(5b)

Fig. 5. Optimisation of a fourbar mechanism, written in BASIC.
(x,y) are crank center global coordinates, TCP=Tool Center Point, (u,v) are TCP local coupler coordinates.

Below, an output example from the FORTRAN program PLASMA is presented. PLASMA reads the Link Adjacency Matrix of a Tsebytsev mechanism and starts to configure the mechanism:

```
Dimension Synthesis Preprocessor LAM- matrix:  

Parts: 6 Joints: 7  

Preprocessor has constructed Joint Data Structure:  

  Jnt  Prt1  Prt2  Mar1  Mar2  Jtyp      X:      Y:      F:  

    1      1      2     101    201     11      0.      0.      0.  

    2      1      2     101    201     11      1.      0.      0.  

    ...      ....      ....
```

After initial configuration the MSA-program Data Set File is created:

```
Joint/01, REVOLUTE, I=0101, J=0201  

MARKER/0101, PART=01, QP=      0.      ,      0.      , 0.0  

MARKER/0101, PART=01, QP=      0.      ,      0.      , 0.0  

    ...      ....
```

Coupler path calculated by and read from the MSA program:

PNT	Time	PosX	PosY	VelM	VelX	VelY	AccM	AccX
1	.00	.00	.00	.63	.57	-.26	.78	-.13
3
.....	23	.13	.13	.08	.71	.54	1.00	-.09
50	..23	.13	.13	.08	.71	.54	1.00	-.09

8. Discussion

The grammatical approach is very suitable for systems that can be represented by graphs. The more restricting design equations can be found, the more grammatical rules can be derived and added to the design grammar.

The grammatical approach presented here should be useful also in many other domains of design. Previously this approach has been used in plant layout problems (7). In mechanical engineering this approach for topological synthesis should be applicable also for a number of other applications, e.g. for transmissions and robots.

9. References:

- (1) Andersson, K., 1993, *A Design Language Based on Engineering Terminology*, PhD thesis, Dept of Machine Design, Royal Institute of Technology, Stockholm.
- (2) Freudenstein, F., Vucina D., 1991, *An Application of Graph Theory and Nonlinear Programming to the kinematic synthesis of Mechanisms*, The Journal of Mechanisms and Machines Theory, Vol 26, pp 553-563.
- (3) van Griethuysen, J.-P., 1992, *The 'Constructive-Deductive' Design Approach - Application to Power Transmissions*, CIRP Annals, Manufacturing Technology, Vol 41/1, pp 169-172.
- (4) Hsu, C-H., 1992, *Generalization of mechanical devices with any number of general constraints.*, The Journal of Mechanisms and Machines Theory, Vol 27, pp 189-199.

- (5) Hwang, W., Hwang, Y., 1992, *Computer aided structural synthesis of planar kinematic chains with simple joints.*, The Journal of Mechanisms and Machines Theory, Vol 27, pp 189-199.
- (6) Makkonen, P., 1993, *PLASMA - A Mechanism Synthesis Program*, Masters Thesis, Helsinki University of Technology.
- (7) Moore, J., Seppänen, J.: 1975, *String processing algorithms for plant layout problems*, 6. Int. Journal prod. res., Vol 13. No3, p.239-254.
- (8) Pahl, G., Beitz, W., 1998, *Engineering Design - A Systematic Approach*, The Design Council & Springer-Verlag, London.
- (9) Suh, N.P., 1990, *The Principles of Design*, Oxford University Press, Oxford, England.
- (10) VDI 2222, 1977, *VDI-Richtlinien, Konstruktionsmetodik - Konzipieren technischer Produkte*, Verein Deutsche Ingenieure, Düsseldorf, Germany.

Rests of the mechanisinsinasodjasoijd

```

0 1 0 2 0 3
0 0 4 0 0 0
0 0 0 5 6 0
0 0 0 0 0 0

```

Dimension Synthesis Preprocessor LAM- matrix:
 Parts: 6 Joints: 7

Preprocessor has constructed Joint Data Structure:

Jnt	Prt1	Prt2	Mar1	Mar2	Jtyp	X:	Y:	F:
1	1	2	101	201	11	0.	0.	0.
2	1	2	101	201	11	1.	0.	0.
3	1	2	101	201	11	2.	0.	0.
4	1	2	101	201	11	.2042	.4564.	0.
....						

Joint/01, REVOLUTE, I=0101, J=0201

MARKER/0101, PART=01, QP= 0. , 0. , 0.0
 MARKER/0101, PART=01, QP= 0. , 0. , 0.0

Coupler path read from MSA program:

PNT	Time	PosX	PosY	VelM	VelX	VelY	AccM	AccX	..
1	.00	.00	.00	.63	.57	-.26	.78	-.13	
..2	.00	.00	.00	.63	.57	-.26	.78	-.13	
3
.....	.23	.13	.13	.08	.71	.54	1.00	-.09	
49	..23	.13	.13	.08	.71	.54	1.00	-.09	
50	..23	.13	.13	.08	.71	.54	1.00	-.09	

Penalty accelerations of joints are read from MSA program::

PNT	Jnt1	Jnt2	
1	.76	.60	.68
2	.77	
60	.68
50	.76	.60	.68

Derivation of the stiffness matrix for beam elements in MBS models

Petri Makkonen, Jan-Gunnar Persson
Department of Machine Design
Engineering Design
Royal Institute of Technology - KTH
Stockholm, Sweden

1. Elasticity and dynamics in MBS models

The dynamic characteristics of a robot system will be dependent of the dynamics of the mechanical structure, of the dynamics of the drive train (motors, actuators, transmissions) and of the dynamics of the control system. For dynamic analysis of the mechanical system, elasticity as well as inertia must be included in the model. In modelling of parallel robots, all elasticity could be represented by elastic beam elements and by elasticity in gear transmissions. With beam representation of structural parts, mass and inertia will be discretised and lumped in the MBS model while elasticity is modelled as a continuos property over the beam structure. An elastic structural part will be represented by a number of beam elements, between lumped masses. The beam elements are then considered massless. Large elastic deflections of the structure will then automatically be accounted for, despite linear elastic properties of each beam element, as each beam element is defined in its local frame and relative motion between the element frames are handled by the MBS model, Makkonen (1996).

2. Modelling elastic properties of beams

2.1 Beam model

For the beam elements, the Timoshenko beam theory is applied as presented by Natrayanaswami (1974), i.e. shear deformation due to lateral force is accounted for. Shear deformation is often negligible, but could be significant for short beams, for thin-walled cross sections and for composite and sandwich structures. The beam elements are considered to meet the following basic assumptions:

- The cross sections remain undeformed and plane under load (Euler-Bernoulli hypothesis)
- Uniform cross section
- Linear elastic beam material, thus Hooke's law is applicable
- Forces and moments at the beam end points (i.e. at the MBS-element markers) are considered linearly dependent on the relative displacement and velocities between the beam end points
- All six flexibility degrees of freedom are considered, i.e: neutral axis tension/compression; torsion; transverse displacement in two directions; angular displacement with respect to two transverse directions
- Mass and inertia are lumped to the frame (the beam element reference frame) and the beam element is considered massless
- The elastic and inertial properties of each element remain time invariant
- All deformations of the elastic structure are represented as a discrete chain of multi body frames with elastic beam elements. Large elastic deflections of the structure will then be automatically accounted for, due to the MBS approach with movable local frames (movable local coordinate systems for each beam element)
- All damping effects of the beam vibrations can be represented by equivalent linear viscous damping, acting between frame (element) pairs

In FEM (Finite Element Modelling), the elasticity of a full, six nodal d.o.f., 3D beam is usually represented by a 12×12 stiffness matrix. The 12×12 matrix gives the relation between each of the six force and moment components at the two beam end points and the six displacement components at the two end points. However, for elastic beam elements in an MBS model, a 6×6 stiffness matrix representation is used instead. This 6×6 matrix gives the relation between each of the six forces and moments at beam end point i with respect to the six displacement components at beam end point i . The opposite beam end point j is located at the origo of the beam element frame. The x-axis of the beam element frame fixed to beam end point j , defines the centroidal axis of the undeformed beam. The y-axis and z-axis of the j frame represent the principal cross section axes of the undeformed beam (Figure 1). All deformation components at end point i are expressed in the j -frame which is fixed to and moving with the beam end point j . All deflection components at beam end point j are then equal to zero, expressed in frame j .

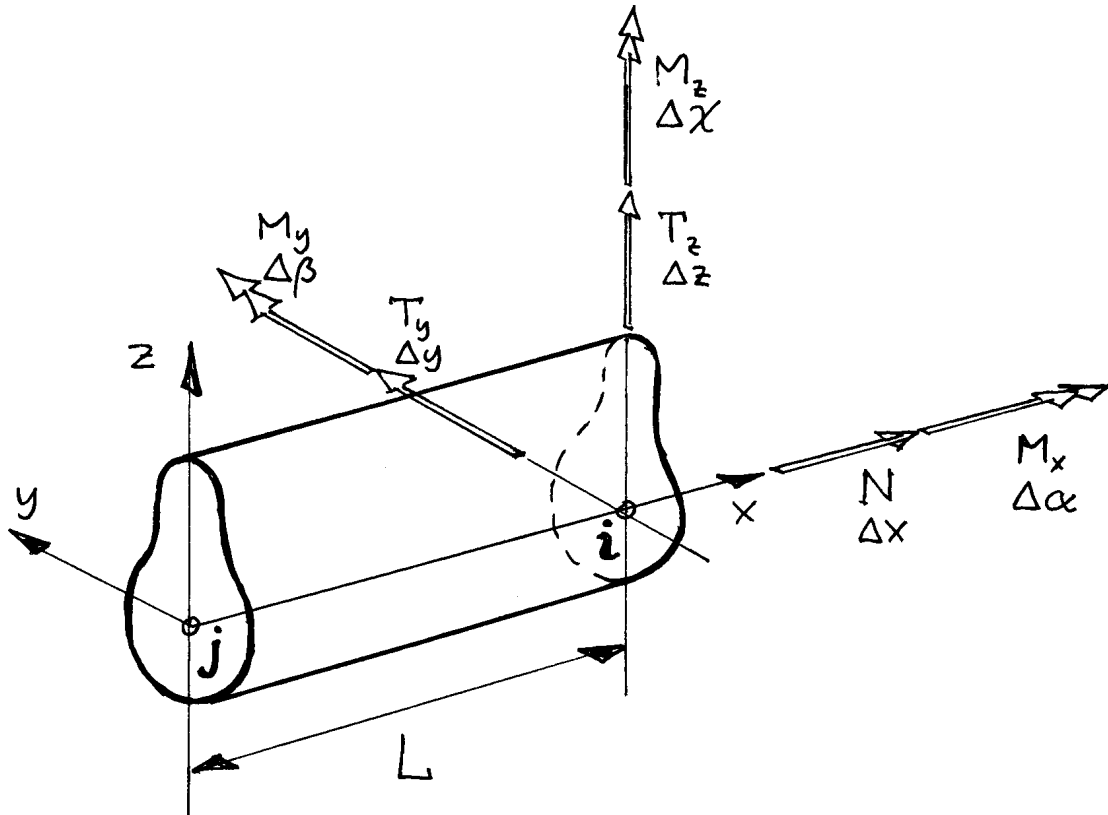


Fig. 1. Beam element with definitions of j -frame, i -forces and i -displacements.

The six force and moment components at end point j can be calculated from force components at end point i , by applying force and moment equilibrium over the beam element.

The 6×6 beam stiffness matrix will then be as follows:

$$\begin{bmatrix} N \\ T_y \\ T_z \\ M_x \\ M_y \\ M_z \end{bmatrix} = K \begin{bmatrix} \Delta x \\ \Delta y \\ \Delta z \\ \Delta a \\ \Delta b \\ \Delta c \end{bmatrix} \quad (1)$$

Stiffness matrix elements corresponding to bending could be obtained by integration of the differential equation for the beam elastic line. The integration is carried out for each separate unit deflection component at beam end point i while keeping all other deflection components equal to zero. Correction for the shear deflection is used, according to the Timoshenko theory.

2.2 Shear stress asymmetric correction factor

The asymmetric correction factors, accounting for uneven shear stress over the beam cross section are expressed by the following general expressions, Handboken Bygg (1983):

$$V_y = \frac{A}{A_{shear,y}} = \frac{A}{I_z^2} \int \frac{S_z^2(y)}{A l_z^2(y)} dA \quad (2)$$

where $A_{shear,y}$ is the effective shear area considering shear force T_y .

$S_z(y)$ is the static moment with respect to the z -axis, for the part of the cross section above location y .

$l_z(y)$ is the local width of the profile at location y .

$$S_z(y) = \int_y^{y_{max}} y \cdot l_z(h) \cdot dh \quad (3)$$

For lateral force in the z direction, the asymmetric shear correction factor is defined correspondingly:

$$V_z = \frac{A}{A_{shear,z}} = \frac{A}{I_y^2} \int \frac{S_y^2(z)}{A l_y^2(z)} dA \quad (4)$$

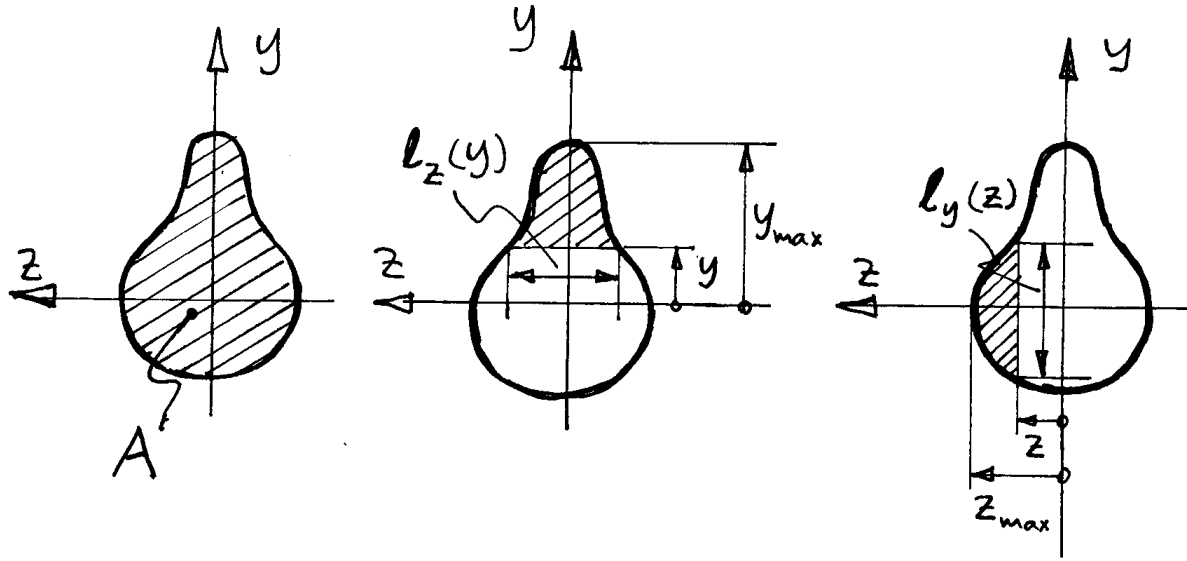


Fig.2. Beam cross sectional properties.

For a solid rectangular section the asymmetric correction factor is $V = 6/5 = 1.2$. For a solid circular profile, $V = 10/9 = 1.11$. For a thin-walled circular pipe, $V = 2$ and for an ordinary H-, I-, or U-profile, $V = A / A_{web}$.

3 Timoshenko beam deflection with adjustment for shear deformation

The matrix elements corresponding to bending are obtained from the differential equation for the beam elastic line. The shear force and bending moments with respect to one principal axis are defined according to figure 3. The angular displacements \mathbf{y} at the beam ends are defined by the first derivative of the lateral displacement w_b due to bending only:

$$\mathbf{y}_j = w'_b(0); \quad \mathbf{y}_i = w'_b(L); \quad (5)$$

The total lateral displacement w is the sum of the displacements due to bending w_b and shear w_s respectively:

$$w(x) = w_b(x) + w_s(x) \quad (6)$$

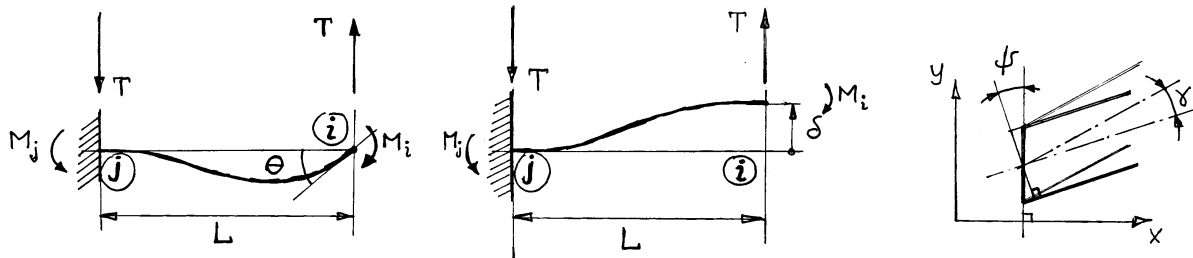


Figure 3. Bending angular and lateral displacements; Shear deformation.

3.1 Beam deflection due to bending

As there is no distributed lateral load, the shear force T is constant over the beam element and the third derivative of the displacement will be obtained immediately:

$$EIw_b''' = -T \quad (7)$$

Integration gives:

$$EIw_b'' = -Tx + C_1 \quad (8)$$

Bending moment boundary condition at point i gives the integration constant C_1 :

$$EIw_b''(L) = -M_i \quad \Rightarrow \quad C_1 = TL - M_i \quad (9)$$

Further integration gives:

$$EIw_b' = -\frac{Tx^2}{2} + (TL - M_i)x + C_2 \quad (10)$$

With boundary condition for angular displacement at point j , the integration constant C_2 can be solved:

$$\mathbf{y}_j = w'_b(0) = 0 \quad \Rightarrow \quad C_2 = 0 \quad (11)$$

Further integration gives the lateral displacement due to bending:

$$EIw_b = -\frac{Tx^3}{6} + (TL - M_i)\frac{x^2}{2} + C_3 \quad (12)$$

Boundary condition for lateral displacement at point j :

$$w(0) = w_b(0) = 0 \quad \Rightarrow \quad C_3 = 0 \quad (13)$$

3.2 Beam deflection due to shear

The shear deformation (shear angle θ) is given by:

$$\theta = w_s' = \frac{Vt}{GA} \quad (14)$$

and hence:

$$EIw_s' = \frac{VEI}{GA} T \quad (15)$$

integration gives the lateral beam displacement due to shear force:

$$EIw_s = \frac{VEI}{GA} Tx \quad (16)$$

3.3 Equation for total beam deflection due to bending and shear

Now, the total lateral beam displacement is the sum of bending and shear:

$$EIw = EIw_b + EIw_s = -\frac{Tx^3}{6} + (TL - M_i) \frac{x^2}{2} + \frac{VEI}{GA} Tx \quad (17)$$

4. Beam stiffness matrix

4.1 Stiffness matrix coefficients for axial tension and torsion

Stiffness matrix elements corresponding to pure tension and pure torsion respectively are easily calculated, as there is no coupling:

$$\Delta x / L = \frac{N}{EA} \quad \Rightarrow \quad K_{11} = \frac{N}{\Delta x} = \frac{EA}{L} \quad (18)$$

$$\Delta a / L = \frac{M_x}{GI_x} \quad \Rightarrow \quad K_{44} = \frac{M_x}{\Delta a} = \frac{GI_x}{L} \quad (19)$$

4.2 Stiffness matrix coefficients for lateral displacement

For the case of lateral displacement d at beam end point i , with all other deformation components equal to zero, we use eq. (17). The boundary condition for angular displacement equal to zero at point i gives:

$$y_i = w_b'(L) = 0 \quad \Rightarrow \quad M_i = \frac{TL}{2} \quad (20)$$

and the boundary condition for lateral displacement at point i :

$$w_b(L) = \mathbf{d} \Rightarrow T = \frac{12EI}{L^3(1+k)} \mathbf{d} \quad (21)$$

where the factor k accounts for shear deformation:

$$k = \frac{12V EI}{GA}; \quad k_y = \frac{12V_y EI_z}{GA}; \quad k_z = \frac{12V_z EI_y}{GA} \quad (22)$$

The stiffness matrix elements for shear force versus lateral displacement can then be taken directly from eq. (21):

$$K_{22} = T_y/\Delta y = \frac{12EI_z}{L^3(1+k_y)} \quad (23)$$

$$K_{33} = T_z/\Delta z = \frac{12EI_y}{L^3(1+k_z)} \quad (24)$$

Insertion of eq. (20) in eq. (21) gives:

$$M_i = \frac{6EI}{L^2(1+k)} \mathbf{d} \quad (25)$$

and hence the matrix elements for bending moment versus lateral displacement, considering appropriate signs according to figure 1 and figure 3:

$$K_{53} = M_y/\Delta z = \frac{6EI_y}{L^2(1+k_z)} \quad (26)$$

$$K_{62} = M_z/\Delta y = -\frac{6EI_z}{L^2(1+k_y)} \quad (27)$$

4.3 Stiffness matrix coefficients for end plane rotation

For the case of angular displacement \mathbf{Q} at beam end point i , with all other deformation components equal to zero, we again use eq. (17). Boundary condition for zero lateral displacement at point i gives:

$$w(L) = 0 \Rightarrow M_i = 2TL \left[\frac{1}{3} + \frac{V EI}{GAL^2} \right] = \frac{TL}{6}(4+k) ; \quad (28)$$

and the boundary condition for angular displacement Θ at point i :

$$\mathbf{y}_i = w'_b(L) = \Theta \Rightarrow T = -\frac{6EI}{L^2(1+k)} \Theta ; \quad (29)$$

The stiffness matrix elements for shear force versus angular displacement can then be taken directly from eq. (29):

$$K_{26} = T_y / \Delta c = -\frac{6EI_z}{L^2(1+k_y)} \quad (30)$$

$$K_{35} = T_z / \Delta b = \frac{6EI_y}{L^2(1+k_z)} \quad (31)$$

Insertion of eq. (28) in (29) gives:

$$M_i = \frac{EI}{L} \frac{(4+k)}{(1+k)} \Theta \quad (32)$$

and hence the matrix elements for bending moment versus angular displacement, considering appropriate signs according to figure 1 and figure 3:

$$K_{55} = M_y / \Delta b = \frac{EI_y(4+k_z)}{L(1+k_z)} \quad (33)$$

$$K_{66} = M_z / \Delta c = \frac{EI_z(4+k_y)}{L(1+k_y)} \quad (34)$$

4.4 Beam element stiffness matrix

The complete Timoshenko beam stiffness matrix then takes the form:

$$K = \begin{bmatrix} \frac{EA}{L} & 0 & 0 & 0 & 0 & 0 \\ 0 & \frac{12EI_z}{L^3(1+k_y)} & 0 & 0 & 0 & -\frac{6EI_z}{L^2(1+k_y)} \\ 0 & 0 & \frac{12EI_y}{L^3(1+k_z)} & 0 & \frac{6EI_y}{L^2(1+k_z)} & 0 \\ 0 & 0 & 0 & \frac{GI_x}{L} & 0 & 0 \\ 0 & 0 & \frac{6EI_y}{L^2(1+k_z)} & 0 & \frac{EI_y(4+k_z)}{(1+k_z)} & 0 \\ 0 & -\frac{6EI_z}{L^2(1+k_y)} & 0 & 0 & 0 & \frac{EI_z(4+k_y)}{(1+k_y)} \end{bmatrix} \quad (35)$$

This is the same form of the beam stiffness matrix that is used in ADAMS/Solver, (1994).

5. Forces at beam end point j

The joint force vector at beam end point j can be calculated from force and moment equilibrium:

$$\overset{\omega}{T}_j = -\overset{\omega}{T}_i \quad (36)$$

$$\overset{\omega}{M}_j = -\overset{\omega}{M}_i - \overset{\omega}{L} \times \overset{\nu}{T}_i \quad (37)$$

where \times denotes vector cross product and $\overset{\omega}{L}$ is the undeformed beam length vector:

$$\overset{\omega}{L} = [L, 0, 0] \quad (38)$$

6. References

Makkonen, P., 1996. *Product Development and Performance Optimisation of Rock Drill Boomers*, PhD Paper E,
OST 96, Machine Design, KTH.

Natrayanaswami, R., Adelman, H. M., 1974. *Inclusion of Transverse Shear Deformation in Finite Element Displacement Formulations*, AIAA Jnl, Vol 12, No 11, 1974, pp 1613-1614.

Handboken Bygg - Allmänna grunder, 1983. Liber Förlag, Stockholm, ISBN 91-38-06075-2.

ADAMS/Solver, 1994. *ADAMS/Solver Reference Manual*. Version 8.0, Mechanical Dynamics, Inc. Ann Arbor, Michigan.